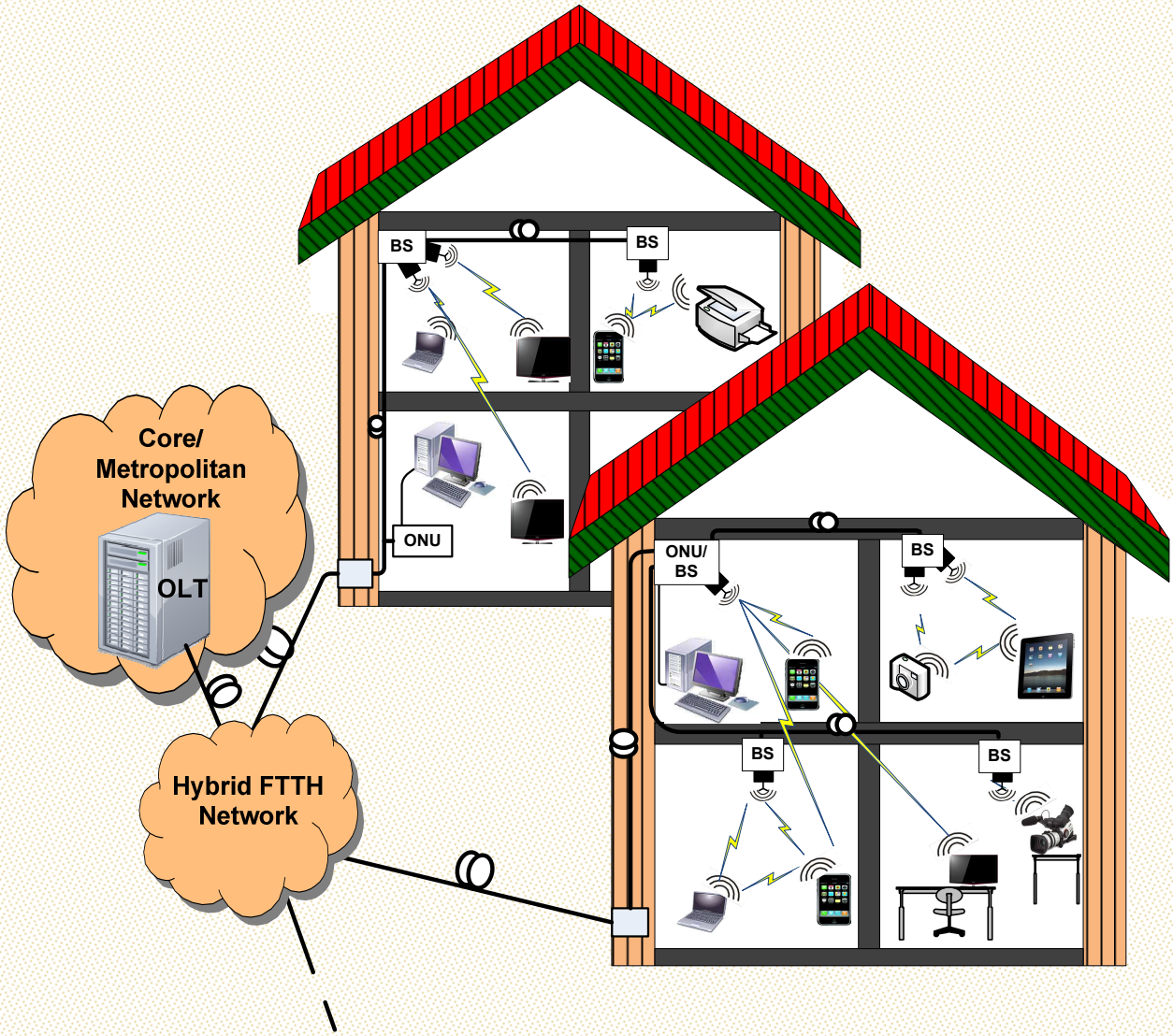

Paulo Alexandre Ferreirinha de Almeida

Radio over Fiber Systems with Support for Wired and Wireless Services

Tese de Doutoramento em Engenharia Electrotécnica e de Computadores, ramo de especialização em Telecomunicações, orientada pelo Doutor Henrique José Almeida da Silva da FCTUC/IT, e apresentada ao Departamento de Engenharia Electrotécnica e de Computadores da Faculdade de Ciências e Tecnologia da Universidade de Coimbra.

Fevereiro 2014

· U C ·

UNIVERSIDADE DE COIMBRA

"*When you have exhausted all possibilities, remember this: you haven't"*

Thomas Edison

Abstract

Wired and wireless access networks are two separate access networks that were designed to carry different types of information independently. From the point of view of an operator, the management and maintenance of these two separate networks implies high costs. Thus, the operators are looking for network architectures capable of integrating these two separate networks into a single shared access network.

The wired access networks mainly based on coaxial cable and digital subscriber line technologies have enabled the access to the triple-play service (telephone, television and Internet), reaching a significant portion of the population worldwide. Nevertheless, due to the increasing demand for broadband services, the operators have been compelled to replace the copper cable based networks by optical fiber access networks. Fiber-to-the-home (FTTH) is already a reality worldwide, and is the future-proof access technology that enables the provision of Gbit/s data rates per user.

On the other hand, during the last years there was an increasing demand for broadband wireless access, due to the advantages of the end-users having wireless connectivity simultaneously with mobility. The evolution from voice and text based services to video based interactive and multimedia services in mobile communications systems, mainly due to the constant evolution in the processing capabilities of consumer devices for handling rich multi-media content, has contributed to the demand for broadband services such as high definition video. Thanks to the growth of mobile broadband services, broadband mobile connectivity is now a necessity, which also leads to the need of increased capacity in the backhaul of mobile and wireless access networks. In order to provide broadband backhaul to the antennas of each cell, radio-over-fiber (RoF) technology has emerged as an affordable solution to distribute broadband radio frequency (RF) signals through optical fiber to base stations antennas. Therefore, with the worldwide deployment of FTTH networks to carry wired services, the integration of RoF technology into FTTH networks to carry broadband wireless signals combined with a wired signal has gained momentum in the last years, as a solution for a smooth integration of the two networks.

In this thesis, a wavelength-division-multiplexing (WDM)-RoF-passive-optical-network (PON) (WDM-RoF-PON) is considered to carry at least a 1 Gbit/s wired signal and several wireless signals per wavelength to each customer's premises. The transport over fiber of RF signals or orthogonal frequency division multiplexing (OFDM) signals

with high order constellations is significantly affected by chromatic dispersion, and eventually the RoF system may not operate at some fiber lengths if intensity-modulation direct-detection (IMDD) systems are used. To overcome this impairment, optical single sideband (OSSB) modulation and optical tandem single sideband (OTSSB) modulation based on the phase-shift method or the modulation chirp of a dual electrode Mach-Zehnder modulator (DE-MZM) are considered along the thesis.

Electro-optic modulation schemes capable of modulating an optical carrier with a wired signal combined with several wireless signals to be radiated at the customer's premises in separate bands are investigated. An optical transmitter scheme based on a z-cut dual-parallel Mach-Zehnder modulator (DP-MZM) capable of providing, on a single wavelength, different wireless services at the microwave band and at the 60 GHz millimeter-wave band, in coexistence with a digital non-return-to-zero (NRZ) signal, is proposed.

OSSB transmission over a 130 km long-reach WDM-PON of a wired signal in coexistence with wireless signals based on OFDM, using the optical filtering method, is demonstrated by numerical simulation. As modulating OFDM signals, a 1 GHz OFDM signal with 16-quadrature amplitude modulation (16-QAM), carrying Gigabit Ethernet data (OFDM-GbE), a 64-QAM long term evolution (LTE) signal with 20 MHz bandwidth, complying with release 8 of the respective standard, and three quadrature phase-shift keying (QPSK) OFDM ultra-wideband (OFDM-UWB) signals, are considered. To obtain successful transmission, optimization of the modulation efficiency and also of the electrical powers that drive the DE-MZM was found to be required.

For mitigation of the power fading of OFDM signals, induced by chromatic dispersion, a method based on the modulation chirp of a DE-MZM is proposed. Performance improvement in the IMDD transmission of a 16-QAM OFDM-GbE signal, a 16-QAM LTE signal, and an OFDM-UWB signal over a long-reach PON is demonstrated by numerical simulation, even when the optical carrier is reduced to improve the modulation efficiency.

Keyworks: Next-generation passive optical network, convergence of wired and wireless access networks, fiber-to-the-home, Mach-Zehnder modulator, modulation chirp, chromatic dispersion.

Resumo

As redes de acesso sem fios e por cabo são duas redes de acesso separadas projetadas para transportar diferentes tipos de informação independentemente. Do ponto de vista de um operador, a gestão e manutenção destas duas redes separadas implica elevados custos. Portanto, os operadores estão à procura de arquiteturas de rede capazes de integrar estas duas redes numa única rede de acesso partilhada.

As redes por cabo principalmente baseadas em cabo coaxial e tecnologia de linha de assinante digital possibilitaram o acesso ao serviço triple-play (telefone, televisão e internet) a uma fração significativa da população, no mundo inteiro. Contudo, devido à procura crescente por serviços de banda larga, os operadores têm sido obrigados a substituir a rede de acesso em cabos de cobre por uma rede de acesso em fibra ótica. Redes de fibra-até-casa (FTTH) já são uma realidade no mundo inteiro, e é uma tecnologia de acesso "à prova de futuro" que permite oferecer taxas de transmissão da ordem de Gbit/s por utilizador.

Por outro lado, nos últimos anos existiu uma procura crescente por serviços de banda larga sem fios, devido às vantagens do utilizador final em ter conectividade sem fios e simultaneamente mobilidade. A evolução de serviços de voz e texto para serviços interactivos de vídeo e multimédia em sistemas de comunicações móveis é devida principalmente à evolução constante das capacidades de processamento dos dispositivos electrónicos dos utilizadores para manipular conteúdos ricos em multimédia. Devido ao crescimento dos serviços banda-larga móvel, a conectividade móvel e de acesso sem fios de banda larga é agora uma necessidade. Para aumentar a capacidade das redes para as antenas de cada célula, a tecnologia de rádio sobre fibra (RoF) emergiu como uma solução acessível para distribuir sinais de rádio frequência (RF) de banda larga através de fibra ótica até às antenas das estações de base. Deste modo, com a instalação de redes FTTH no mundo inteiro para transportar serviços por cabo, a integração da tecnologia RoF nas redes FTTH para transportar sinais sem fios combinados com um sinal de cabo tem ganho força nos últimos anos como uma solução para a integração suave das duas redes.

Nesta tese, uma arquitectura de rede baseada em multiplexação por divisão do comprimento de onda (WDM) de sinais de RoF transmitidos sobre uma rede ótica passiva (PON) é considerada para transportar, em cada comprimento de onda, um sinal de cabo com taxa de transmissão de pelo menos 1 Gbit/s e sinais sem fios, para as

instalações do cliente. O transporte sobre fibra de sinais de RF e sinais com modulação ortogonal por divisão de frequência (OFDM) com constelações de ordem elevada são afectados pela dispersão cromática se forem usados sistemas com modulação intensidade e detecção directa (IMDD). Para superar este problema, a modulação ótica em banda lateral única (OSSB) e a modulação ótica tandem em banda lateral única, baseadas no método do desfasamento ou o desvio dinâmico de frequência (*chirp*) de modulação gerado por um modulador de Mach-Zehnder de dois eléctrodos (DE-MZM), são consideradas ao longo da tese.

São investigados esquemas de modulação electro-óticos capazes de modular uma portadora ótica com um sinal de cabo combinado com vários sinais sem fios para difusão em bandas separadas, nas instalações do cliente. É proposto um esquema de um transmissor ótico baseado em dois moduladores de Mach-Zehnder *z-cut* em paralelo, capazes de fornecer, num único comprimento de onda, diferentes sinais sem fios nas bandas de microondas e de ondas milimétricas na região de 60 GHz, conjuntamente com um sinal digital sem retorno a zero.

É demonstrada por simulação numérica a transmissão OSSB de um sinal de cabo combinado com sinais sem fios baseados em OFDM, usando o método da filtragem ótica, através de uma WDM-PON com 130km de extensão. Como sinais modulantes são considerados: um sinal OFDM com largura de banda de 1 GHz, modulação de amplitude em quadratura com 16 estados de sinalização (16-QAM), transportando dados da tecnologia *Gigabit Ethernet* (OFDM-GbE); um sinal *Long Term Evolution* (LTE) com largura de banda de 20 MHz e modulação 64-QAM satisfazendo a release 8 da norma; e três sinais OFDM de largura de banda ultra ampla (OFDM-UWB) largura de banda de 528 MHz e modulação em quadratura de fase (QPSK). Para conseguir transmissão bem-sucedida foi necessária a optimização da eficiência de modulação e também das potências eléctricas dos sinais que comandam o modulador.

Para mitigar o desvanecimento da potência dos sinais OFDM, induzido pela dispersão cromática, é proposto um método baseado no desvio dinâmico de frequência (*chirp*) do sinal gerado por um DE-MZM. O melhoramento do desempenho conseguido na transmissão com IMDD de um sinal 16-QAM OFDM-GbE, um sinal 16-QAM LTE e um sinal OFDM-UWB, sobre uma PON de grande alcance, é demonstrado por simulação numérica, mesmo quando a portadora ótica é reduzida para melhorar a eficiência de modulação.

Palavras-chave: Rede ótica de próxima geração, convergência das redes por cabo e sem fios, fibra-até-casa, modulador de Mach-Zehnder, *chirp* de modulação, dispersão cromática.

Acknowledgments

During the last years in the entire journey of my PhD, I have had the opportunity to grow up in all dimensions either personal as professional. This journey and results obtained would not have been possible without the help of a number of people.

First of all, I would like to express my gratitude to my supervisor of this work, Prof. Dr. Henrique Silva, for the freedom, the confidence, and guidance to think and overcome the difficulties found along the work, which allow me growing up as a researcher.

A special thanks to Eng. Filipe Ferreira (soon Doctor) for their friendship and stimulating discussions on a variety of subjects in telecommunications. I would like to thank all of my labmates during this period of time Eng. Filipe Bugalho, Eng. Celestino Martins, Eng. Filipa Lopes, Tatiana Chantre, for the company, support and the good times spent in the lab.

I would like to thank my family for their friendship and support along the years of studies of my life by always being the first people to believe in my abilities and determination to achieve the goals established by myself. Among them, I would like to highlight Eng. Pedro Ferreirinha by always be present when I needed.

I would like to thank all my friends in special doctor Filipe Pinheiro for their friendship and support along the years, first at high school and after at University of Coimbra.

Finally, I would like to fully acknowledge the technical and financial support of Instituto de Telecomunicações – Pólo de Coimbra as well as the financial support during four years of research of the Fundação para a Ciência e Tecnologia under the PhD grant SFRH/BD/62647/2009.

Thank you all those I might forget. This thesis is dedicated to those who have influenced my life.

Thank you all!

List of Acronyms

AON	Active Optical Networks
APON	ATM-PON
ARN	Active Remote Node
ASE	Amplified Spontaneous Emission
ATM	Asynchronous Transfer Mode
AWG	Arrayed Waveguide Grating
2G	Second Generation
3DTV	Three Dimensional Television
3G	Third Generation
4G	Fourth Generation
5G	Fifth Generation
10G-EPON	10 Gbit/s EPON
10G-GPON	10 Gbit/s GPON
BB	Baseband
B2B	Back-to-Back
BER	Bit Error Rate
BI-SMF	Bending insensitive-SMF
BPON	Broadband PON
BPSK	Binary phase shift keying
BS	Base Station
CAPEX	Capital Expenditure
CO	Central Office
CP	Cyclic Prefix
CW	Continuous Wave
EAM	Electro-Absorption Modulator
EDFA	Erbium-Doped Fiber Amplifier
EHS	Electrical Hybrid Signal
EVM	Error Vector Magnitude
DE-MZM	Dual-Electrode MZM
DFT	Discrete Fourier Transform
D-RoF	Digital Radio-over-Fiber
DSL	Digital Subscriber Line
DVB-T	Digital Video Broadcasting - Terrestrial
DC	Direct Current
DFB	Distributed Feedback
DP-MZM	Dual-Parallel Mach-Zehnder Modulator
DPSK	Differential Phase Shift Keying
EPON	Ethernet PON
ER	Extinction Ratio
EU	European Union

EVMBR	EVM Bias Ratio
FDD	Frequency Division Duplex
FDM	Frequency Division Multiplexing
FEC	Forward Error Correction
FFT	Fast Fourier Transform
FP7	Framework Programme Seven
FSAN	Full-Service Access Network
FBG	Fiber Bragg Grating
FT	Fourier Transform
FTTB	Fiber to the Building
FTTC	Fiber to the Curb
FTTH	Fiber to the Home
FTTN	Fiber to the Node
FWHM	Full Width at Half Maximum
GbE	Gigabit Ethernet
GPON	Gigabit PON
GSM	Global System for Mobile Communications
ICI	Inter-Carrier Interference
IFFT	Inverse Fast Fourier Transform
IMDD	Intensity-Modulation and Direct-Detection
IMD2	Second-order Intermodulation Distortion
IMD3	Third-order Intermodulation Distortion
ISI	Inter-Symbol Interference
ITU-T	International Telecommunication Union for Telecommunication Standardization Sector
MIMO	Multiple Input Multiple Output
MMW	Millimeter-Wave
MW	Microwave
MZM	Mach-Zehnder modulator
NG	Next-Generation
NGOAN	Next generation of optical access network
NG-PON	Next-Generation-PON
NG-PON1	Next-Generation PON1
NG-PON2	Next-Generation PON2
NRZ	Non-Return-to-Zero
R-EAM	Reflective-EAM
RMS	Root Mean Square
RN	Remote Node
RSOA	Reflective Semiconductor Optical Amplifier
ODN	Optical Distribution Network
ODSB	Optical Double Sideband

ODSB-SC	ODSB - Suppressed Carrier
ODSB-RC	ODSB - Reduce Carrier
OF	Optical Filter
OFDM	Orthogonal Frequency Division Multiplexing
OFDMA	Orthogonal Frequency Division Multiple Access
OLT	Optical Line Terminal
ONU	Optical Network Unit
OOK	On-Off-Keying
OPEX	Operation Expenditure
OSNR	Optical Signal-to-Noise Ratio
OHS	Optical Hybrid Signal
OTSSB	Optical Tandem Single Sideband
OSSB	Optical Single Sideband
OSSB-RC	OSSB - Reduced Carrier
LASER	Light Amplification by Stimulated Emission of Radiation
LPF	Low Pass Filter
LTE	Long Term Evolution
LTE-A	LTE-Advanced
LO	Local Oscillator
$LiNbO_3$	Lithium Niobate
LR-PON	Long-Reach-PON
RBS	Remote Base Station
RF	Radio Frequency
RoF	Radio over Fiber
ROSNR	Required OSNR
SCM	Subcarrier Multiplexing
SEMZM	Single Electrode-MZM
SMF	Single Mode Fiber
SSMF	Standard SMF
SNR	Signal-to-Noise
P2P	Point-to-Point
P2MP	Point-to-Multipoint
PMD	Polarization Mode Dispersion
PSD	Power Spectral Density
PAPR	Peak-to-Average Power Ratio
PIN	Positive-Intrinsic-Negative
PON	Passive Optical Network
QP	Quadrature Point
QPSK	Quadrature Phase-Shift-Keying
TDM	Time division multiplex
TDMA	Time division multiple access
TFC	Time Frequency Code

TWDM	Time and Wavelength Division Multiplexing
UHDTV	Ultra-High Definition Television
UHD3DTV	Ultra-High-Definition Three Dimensional Television
UMTS	Universal Mobile Telecommunications System
UWB	Ultra-Wideband
VCSEL	Vertical Cavity Surface Emitting Laser
VEA	Variable Electrical Attenuator
VOA	Variable Optical Attenuator
VoD	Video on Demand
WDM	Wavelength Division Multiplexing
WLANs	Wireless Local Area Networks
WMANs	Wireless Metropolitan Area Networks
WiMAX	Worldwide Interoperability for Microwave Access
WPAN	Wireless Personal Area Network

List of Symbols

α	Chirp parameter
α_{DS}	Chirp parameter due to drive signals of a DE-MZM
α_{ER}	Chirp parameter due to finite extinction of a DE-MZM
α_f	Optical fiber attenuation coefficient
$\beta(\omega)$	Dispersion propagation constant of the dispersive fiber
β_0	Constant phase shit
β_1	Group delay per unit length unit
β_2	Second-order group delay dispersion
B_g	Guard bandwidth
B_{OFDM}	Total OFDM signal Bandwidth
B_T	Two-sided 3-dB linewidth of the Lorentzian PSD
B_{GbE}	OFDM-GbE signal Bandwidth
B_{LTE}	LTE signal Bandwidth
B_{UWB}	OFDM-UWB signal Bandwidth
c	Speed of light in vacuum
Cn	Complex data symbols
Δf	Subcarrier frequency spacing
$\Delta v(t)$	Instantaneous optical frequency offset
D	Chromatic dispersion
D_t	Total accumulated chromatic dispersion
$EVMBR$	EVM bias ratio
ε	Extinction ratio of a MZM
$E_{in}(t)$	Input electrical field of a MZM
$E_{in}(f)$	Fourier transform of the $E_{in}(t)$
$E_{LO}(t)$	LO electric field
E_{LO}	Amplitude of the LO electric field
$E_{out}(t)$	Output electrical field of a MZM
$E_{out}(f)$	Fourier transform of the $E_{out}(t)$
$E_{PIN}(t)$	Electric field at the input of the PIN photodiode
$E_{PIN}(f)$	Fourier transform of the $E_{PIN}(t)$
$E_{PM}(t)$	Output electric field of a phase modulator
f_s	Sampling frequency
f_{rf}	RF frequency
γ	Scaling factor related to ε
$i(t)$	Photodetected current
i_{DC}	DC current
$i_s(t)$	Signal current
$i_s\text{-}_{MW}(t)$	Signal current located at the MW band

$i_{s\text{-}MMW}(t)$	Signal current located at the MMW band
$i_{IMD2}(t)$	IMD2 current
$i_{LO}(t)$	LO current
$I(t)$	Intensity transfer function of a MZM
$j = \sqrt{-1}$	Pure imaginary number
L	Fiber length
λ_c	Optical carrier wavelength
m	Optical modulation index
N	Number of subcarriers/ FFT size
N_d	Number of data subcarriers
N_g	Number of guard subcarriers
N_p	Number of pilot subcarriers
$Nzps$	Number of zero prefix samples
$\phi(t)$	Instantaneous optical phase of the $E_{out}(t)$
$\phi_i(t)$	Instantaneous optical phase shift of the i-th arm of a DE-MZM, i = 1, 2
$\phi_R(t)$	Instantaneous residual phase of the $E_{out}(t)$ due to finite ER of a DE-MZM
$\phi_{LO}(t)$	Instantaneous optical phase of the RF LO
ϕ_{RF}^{tx}	Phase noise of the transmitter RF carrier
ϕ_{RF}^{rx}	Phase noise of the receiver RF carrier
P	Average power of the CW laser
P_{RF}	RF power
$\Re$	Responsivity
ρ	Amplitude drive voltages ratio of a DE-MZM
R_L	Load resistor
$s_{OFDM}^{k}(t)$	k-th OFDM symbol of an OFDM signal
σ^2	Gaussian variance
σ^2_{xi}	Energy of the in-phase component of a complex signal
σ^2_{xq}	Energy of the quadrature component of a complex signal
t	Time
τ	Time delay
T	IFFT and FFT time period
T_{cp}	Cyclic prefix interval
T_s	Symbol period
$T_E(t)$	Electric field transfer function
V_π	Switching voltage
$V_i(t)$	Electrical drive signal of the i-th arm of a DE-MZM, i = 1, 2
V_i	Maximum amplitude of the drive signal of the arm i of a DE-MZM

V_{bias}	Bias voltage of a DE-MZM
$V_{\text{bias}i}$	Bias voltage of the arm i of a DE-MZM
V_{RF}^{tx}	Amplitude of the transmitter RF carrier
V_{RF}^{rx}	Amplitude of the receiver RF carrier
$\nu(t)$	Instantaneous optical frequency
ν_{c}	Optical carrier frequency
ω	Angular frequency
ω_{c}	Optical carrier angular frequency
ω_{LO}	LO angular frequency
ω_{rf}	RF signal angular frequency
$x(t)$	Modulating signal
$X(f)$	Fourier transform of the $x(t)$
$x_i(t)$	In-phase component of a complex signal
$x_q(t)$	Quadrature component of a complex signal
$x_{\text{a}}(t)$	Analytic signal
$x_{\text{h}}(t)$	Hilbert transform of $x(t)$

Contents

List of Figures

List of Tables

1

Introduction

1.1 Motivation and contextualization of the thesis

Telecommunications networks grew from the needs of voice carriers to provide connectivity between subscribers. This old paradigm has been changed within the last twenty years. The growing demand for broadband data connectivity mainly for internet access is currently a significant driver in the development of global communications networks at every level. Due to the drastic improvement of the performance of digital electronics and desktop computers, the demand for multimedia services has experienced a large increase. Nowadays, internet access has become an extension of the traditional utilities: water, electricity and gas. Billions of people are engaged in social networks, which have often facilitated communication and exchange of ideas. Remote house monitoring and e-health applications improve the living standards of living of people. Video conferencing can reduce commuting and business traveling and allow more flexibility between professional and personal life. Finally, entertainment activities such as listening to music or playing video games have increasingly become more based on internet and social networks.

The traffic carried over internet protocol networks has increased exponentially and the zettabyte threshold will be reached by the end of 2015, and Cisco estimates that it will reach 1.4 zettabytes per year by 2017 [1]. Video will be the main driver for the traffic increase. The sum of all forms of internet protocol television, video on demand (VoD), and peer to peer) will be in the range of 80 to 90 percent of the global consumer traffic by 2017. The effect of increasing video traffic over networks has been described

by the terms “data tsunami” and “exaflood” [2], and will require changes of the operators in terms of capacity of their networks and business models.

The wired access networks based on copper, mainly based on cable and digital subscriber line (DSL) technologies, have enabled this digital revolution to reach a significant portion of the population, but are reaching their bandwidth limits, especially when the distance between the local exchange and the end-user is longer than a few kilometers, and have become the so-called last-mile bottleneck. To enable the continued growth of bandwidth demand, access networks based on fiber optics are the only ‘future-proof’ solution. Fiber-optic networks are therefore gaining momentum in ’last-mile’ networks, and fiber-to-the-home (FTTH) or fiber-to-the-curb (FTTC) technology is already deployed on a significant scale. FTTC may be seen as one of the migration scenarios to FTTH in the delivery of broadband services to the customers. FTTH networks have become a reality, with a significant deployment in several countries. Since December of 2010 more than 6 million subscribers now use direct fiber optic connections to the home or building in the United States, more than 17 million in Japan, 3.9 million in Europe, 4.2 million in Russia, 10 million in Korea, and almost 42 million worldwide [3], [4], and the number of subscribers continues growing at a fast rate. FTTH is widely recognized as the optimal solution for providing broadband to new and existing communities.

In parallel with the evolution of fixed access networks, during the last years there was an increasing demand for broadband wireless and mobile access, due to the possibility of the end-users having connectivity simultaneously with mobility. Furthermore, mobile networks have been exposed to challenges in recent years, due to the broadband evolution from voice and text based services to video based interactive and multimedia services, mainly due to the constant evolution and innovations in the processing capabilities of consumer devices for handling rich multi-media content. Since 2010, mobile data traffic has surpassed the voice traffic. Mobile data traffic is expected to grow around 12 times between 2012 and the end of 2018, driven mainly by video and web browsing [5]. The increasing number of wireless devices that are accessing mobile networks worldwide is one of the primary contributors to traffic growth. According to the global mobile data traffic forecast of Cisco [6], by the end of 2013, the number of mobile-connected devices may have exceeded the number of people on earth, and by 2017 there will be nearly 1.4 mobile devices per capita. Today, laptops generate a great amount of traffic, but smartphones and newer device categories

such as tablets and machine-to-machine nodes will begin to account for a more significant portion of the traffic by 2017. By the end of 2017, the smartphones, laptops, and tablets will be responsible for 67.5%, 14% and 5.1% respectively, of all the global mobile traffic. The mobile video percentage estimated for 2017 is 66.5% of the 11.2 exabytes per month, whereas mobile web data is estimated to be 24.9%. Thanks to the mobile broadband growth, broadband mobile connectivity is now a necessity, which also leads to the need of increased capacity in the backhaul of mobile and wireless access networks.

To provide access to broadband services, the Universal Mobile Telecommunications System (UMTS) Long Term Evolution (LTE) was introduced in the 3rd Generation Partnership Project (3GPP), Release 8 [7]. The objective is to develop a high data rate, low latency and packet optimized radio access technology. LTE is also referred as Evolved UMTS Terrestrial Radio Access. The LTE and LTE-Advanced (LTE-A) fourth generation (4 G) system operate at low frequencies of the microwave (MW) band, characterized by having high spectral congestion. Therefore, in order to increase the wireless transmission capacity it is required to reduce the cell size (small-cells) in order to increase the frequency reuse, along with the employment of multiple-input-multiple-output (MIMO) techniques. However, this solution is not enough for future demand of higher data rate wireless communications services, such as fifth generation (5G) systems for which the requirements are not yet defined [8]. 5 G is also referred to as beyond 2020 mobile communications technologies and, in November 2012, the European (EU) project "Mobile and wireless communications Enablers for the Twenty-twenty Information Society" (METIS) [9] started its activity towards the definition of 5G requirements. To increase the wireless transmission capacity in future 5G systems, a spectral unlicensed band where many GHz of spectrum can be used to offer orders of magnitude higher data rates to mobile users is imperative. Millimeter-waves (MMW) at the frequencies of 28 and 38 GHz have been pointed out from extensive measurements in dense urban environments [10].

To provide backhaul to the antennas of each cell, radio-over-fiber (RoF) has emerged as an affordable solution to distribute broadband radio frequency (RF) signals through optical fiber to base stations (BSs) antennas [11]. It has been shown that RoF technology can provide the required feeder network, as it is best suited to deal with the demands of small-cell wireless networks [12]. Furthermore, RoF technology allows the transmission of signals in different bands, including the baseband (BB) [13].

Much mobile data activity takes place within the users premises. A survey conducted by Cisco's Internet Business Solutions Group indicates that the percentage of mobile Internet at home is approximately 40 % of the total mobile data use, on average. The amount of mobile data use that is "on the move" is approximately 35 %, while the remaining 25 % of mobile Internet use occurs at work, which is usually an indoor environment. The relatively high percentage of indoor-based mobile data use suggests that operators may be able to offload traffic onto a fixed network, through the deployment of femtocell technology. Femtocells allow service providers to extend service coverage at home for both voice and data, especially where access would otherwise be limited or unavailable. Femtocell technology is featured by the use of simplified and low power BSs (or Node B network elements), which substantially increases the battery autonomy of mobile devices, and at a lower cost than the outdoor service. Currently, the femtocells are backhaul connected using standard broadband DSL or cable service into the mobile network of operators, but with the deployment of FTTH networks the mobile backhaul to femtocells can be provided through a hybrid optical access network integrating RoF networks for backhaul of wireless services and FTTH networks for wired services [13]. When these heterogeneous access networks converge to a highly integrated network via a common optical feeder network, network operators can reap the benefits of lowering the operating costs of their access networks and meeting the capital costs of future upgrades more easily. In addition, the converged access network will facilitate greater sharing of a common network infrastructure between multiple network operators. Furthermore, the Full-Service Access Network (FSAN) group [14], formed by telecom operators and equipment vendors, is considering the convergence of wired and mobile networks for the next-generation passive optical network (PON), or NG-PON2.

In this thesis, the integration of RoF networks for backhaul of wireless services provided to the customers with the FTTH networks for wired services will be addressed, considering as reference architecture the wavelength division multiplexing (WDM) – PONs (WDM-PONs).

1.2 Radio over fiber communication systems

RoF technology has been envisioned as a promising technology for realizing broadband mobile and wireless access networks [11]. It involves the merging of wireless and

mobile networks into a fiber backbone which is often based on WDM [15], [16]. RoF uses analogue optical transmission through optical fiber, which is typically characterized by being transparent to the modulation format of the RF signals, taking into account some limitations caused by additional noise and distortion. The optical fiber has low attenuation and a huge bandwidth, which allows transmitting and delivering RF signals of broad bandwidth to the antennas, to be radiated. The possibility of delivering broadband wireless signals to the end-user enables the provision of broadband services, such as ultra-high definition television (UHDTV), VoD, three dimensional television (3DTV), which will be supported in the future by smartphones, laptops, tablets, etc.

However, more wireless transmission bandwidth leads to spectral congestion at the lower MW bands used in current wireless access networks. MMW systems have the potential to resolve the scarcity of bandwidth and the spectral congestion. Nevertheless, in this spectral region the propagation of RF signals suffers high atmospheric attenuation, which leads to the reduction in the size of the system cells, known as small-cells, picocells. This allows greater frequency reuse, which enhances network capacity but, since each cell requires a BS, many more BSs are required to cover a given service area. Minimization of the BS cost is therefore a vital condition that has to be satisfied for the successful deployment of such RoF systems. Therefore, as much hardware as possible should be moved from the BSs to a central point of the network, which is the central office (CO). Then, all the hardware required to perform the modulation and up-conversion of RF signals should be placed at the CO, in order to share its cost among the BSs. In this way, only photodetection, filtering and amplification are performed in the BSs, before the radiation of the signals to the end- users.

1.2.1 Intensity-modulation direct-detection systems

The simplest manner to modulate a RF signal and transmit it through the optical fiber is based on intensity-modulation and direct-detection (IMDD). Intensity-modulation of light can be achieved either through direct modulation of a laser diode or by using a modulator to externally modulate light from a continuous wave (CW) laser [17], as sketched in Fig. 1.1. External modulation is preferred in high-performance applications, whereas the advantage of direct-modulation is low cost, especially when uncooled laser diodes are used. Direct modulation of a laser (sketched in Fig. 1.1 a)) simply means

driving it with a time-varying current, which results in the radiation intensity (i.e. optical power) tracking the changes in the current. Direct-modulation up to about 30 GHz is possible, but one inconvenience of this scheme is frequency chirp, because the optical frequency is also modulated [18]. This can be overcome by operating the laser in CW mode and using an external modulator instead. There are several possible devices to perform external intensity modulation, but the most widely used external modulators are the Mach-Zehnder modulator (MZM) and the electro-absorption modulator (EAM) [17], between which the MZM is the preferred one. MZMs are voltage-driven devices and have larger modulation bandwidths. An added advantage of these devices is that, in addition to intensity modulation, they can also provide phase and frequency modulation. In Fig. 1.1 b) a sketch of a RoF link employing external modulation is shown.

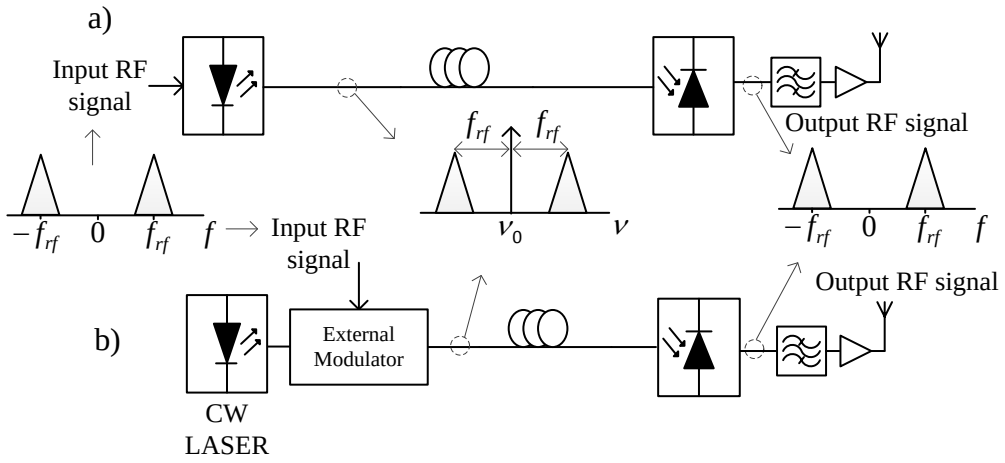

Figure 1.1 – RoF link employing intensity-modulation and direct-detection with: (a) A directly modulated laser; (b) An external modulator.

MZMs are based on the use of the electro-optic effect to change the phase of the input optical field and on the use of a Mach-Zehnder Interferometer to convert the phase change into an intensity variation [17].

Once modulation has been applied, it will be transmitted through the optical fiber. At the fiber output, a photodetector is used to recover the original modulating signal. The first stage in a photodetector is a photodiode; this is a square-law device that produces a photocurrent which is directly proportional to the square of the electric field magnitude. This quantity is proportional to the radiation intensity (W/sr) which in turn is proportional to the received optical power. A photodiode can therefore only directly detect intensity modulation, hence the term direct detection.

However, in conventional intensity-modulation the optical carrier is modulated to generate an optical field with the carrier and two sidebands, known as optical double-sideband (ODSB) modulation. At the photodetector, each sideband beats with the optical carrier, generating two beat signals which constructively interfere to produce a single component at the RF frequency. When the signal is transmitted over fiber, chromatic dispersion causes the sidebands to experience different phase shifts, depending on the fiber link distance, modulation frequency, and dispersion parameter of the fiber. These phase shifts result in relative phase differences between the carrier and each sideband, and produce a phase difference between the two beat signals at the RF frequency, which results in a power degradation of the resulting RF signal [19]. When the phase difference is π, complete cancellation of the RF signal occurs.

It has been shown that an optical wave centered at wavelength λ_c and ideally modulated at an RF frequency f_{rf}, propagating along a length L of optical fiber with dispersion parameter D and detected with an ideal positive-intrinsic-negative (PIN) photodiode, produces an RF signal at the frequency f_{rf} and the RF generated power will vary approximately [19], [20] as:

$$P_{RF} \propto \cos\left(\frac{\pi LD}{c}\lambda_c^2 f_{rf}^2\right) \tag{1.1}$$

where c denotes the speed of light in vacuum. The power fading as a function of fiber length at a given frequency has a periodic profile. The RF power degradation associated with standard single mode fiber (SSMF) transmission was evaluated for three RF frequencies, and is presented in Fig. 1.2 for a fiber length of up to 100 km. The figure shows the fading effect as a function of fiber length for 2 GHz, 5 GHz, and 20 GHz RF signals.

As the RF frequency increases, the effect of dispersion is more pronounced and the fiber-link length is severely limited. Figure 1.2 indicates the feasibility of implementing IMDD techniques for backhaul of wireless RF signals up to 100 km, for carrier frequencies up to 5 GHz. Thus, for transmission of mobile phone signals around 2 GHz, such as those used in Global System for Mobile Communications (GSM), UMTS and LTE, the dispersion penalty is not a major impairment in IMDD systems.

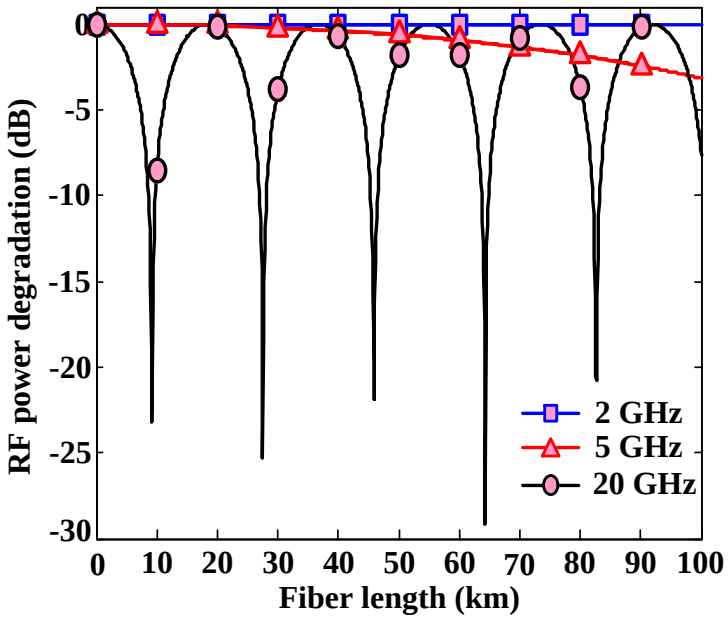

Figure 1.2 - RF power degradation as a function of fiber length for IMDD of an RF signal over SSMF (D = 17 ps/(km.nm)) for subcarrier frequencies of 2 GHz, 5 GHz, and 20 GHz.

As the RF frequency increases, the effect of dispersion is more pronounced and the fiber-link length is severely limited. Figure 1.2 indicates the feasibility of implementing IMDD techniques for backhaul of wireless RF signals up to 100 km, for carrier frequencies up to 5 GHz. Thus, for transmission of mobile phone signals around 2 GHz, such as those used in GSM, UMTS and LTE, the dispersion penalty is not a major impairment in IMDD systems. This indicates also that the wireless local and metropolitan area networks (WLANs and WMANs) may be supported by an IMDD RoF backhaul. Such technologies include WiFi (IEEE 802.11a/b/g/n) at 2.4 GHz and 5 GHz, and mobile Worldwide Interoperability for Microwave Access (WiMAX) at 3.5 GHz.

The transport over fiber of higher frequency RF signals will be significantly affected by dispersion, and eventually the RoF system does not work at some fiber lengths if IMDD systems are used. To overcome this impairment, optical single sideband (OSSB) modulation was proposed and has been used to remove this cause of power fading [20]. However, when OSSB is used 6 dB of RF power is lost due to the suppression of one of the two sidebands, compared to ODSB. Several other approaches were proposed to compensate the dispersion-induced power fading in conventional ODSB analog photonic transmission, including modulation chirp in a dual-electrode MZM (DE-MZM) [20] and linearly chirped fiber Bragg gratings (FBGs) [21], only to cite the most used techniques.

In this thesis, two techniques used to mitigate the chromatic dispersion will be evaluated: modulation chirp of a DE-MZM and OSSB modulation based on phase shift and filtering methods.

1.3 Main contributions

The main contributions of this thesis are listed below:

- An optical transmitter scheme based on a z-cut dual-parallel Mach-Zehnder modulator (DP-MZM), capable to deliver different wireless services at the MW band and at the 60 GHz MMW band in coexistence with a digital non-return-to-zero (NRZ) signal on a single wavelength;
- Method to overcome the intermodulation distortion of orthogonal frequency division multiplexing (OFDM) signals more impaired by intermodulation distortion resulting from beating between OFDM signals upon photodetection, after OSSB transmission with modulation efficiency improved biasing a DE-MZM below the quadrature point is demonstrated by numerical simulation.
- Decomposition of the α chirp parameter of a DE-MZM with finite extinction ratio (ER) as a sum of two chirp parameters: a chirp parameter exclusively due to the drive signals and another chirp parameter due only to extinction ratio;
- Drive voltages suitable to control the chirp at the output of a DE-MZM, as a function of the ER of the DE-MZM, the bias voltages and the modulation index;
- Demonstration of chromatic dispersion mitigation of an optical signal externally intensity modulated by various subcarrier multiplexed OFDM signals based on modulation chirp of a DE-MZM;
- Derivation of a general expression for the photodetected current of an OFDM band-pass signal and respective RF power in a RoF system, in the presence of modulation chirp of a DE-MZM;
- Demonstration that the modulation chirp can be useful to reduce the chromatic dispersion penalty, even when the optical carrier is reduced to improve the modulation efficiency of the IMDD systems.

1.4 Structure of the thesis

The thesis is structured as follows. In **Chapter 2**, an overview of optical access networks is presented. The main hybrid optical access network architectures proposed in

European projects in the least four years are reviewed, following a discussion about the advantages and disadvantages of each architecture considered by FSAN to meet NG-PON2 requirements. The chapter is concluded with a presentation of the architecture considered in this thesis. In **Chapter 3**, the operation principle of a lithium niobate ($LiNbO_3$) z-cut DEMZM is presented along with its intensity transfer function, as a basis for presenting the $LiNbO_3$ z-cut DP-MZM and its intensity transfer function. Afterwards, a mathematical description for small-signal operation of OSSB modulation and optical tandem single sideband (OTSSB) modulation, both based on the phase shift method, is presented. In **Chapter 4**, a literature review of the different optical transmitter schemes based on directly modulated lasers and on external modulation to generate an optical hybrid signal (OHS) composed by multi-bands, namely BB, MW band, and MMW band, is carried out. Afterwards, simulation results of two optical transmitter schemes to generate a multiband OHS based on a $LiNbO_3$ z-cut DP-MZM are presented. In **Chapter 5**, OSSB - reduced carrier (OSSB-RC) transmission based on the filtering method of OFDM signals following different standards is analyzed. To transmit successfully an OSSB signal composed by an OFDM signal carrying Gigabit Ethernet (GbE) data (OFDM-GbE), an LTE signal, and three independent OFDM ultra-wideband (UWB) (OFDM-UWB) signals with different constellations and order up to 64, through a long-reach-PON (LR-PON), the modulation efficiency of the OSSB signal must be improved. The modulation efficiency is improved by biasing the DE-MZM below the quadrature point (QP) of its intensity transfer function, which increases the intermodulation distortion after direct-detection. To overcome the intermodulation distortion, it is proposed to increase the electrical power of the OFDM signals more impaired at the input of the DE-MZM. Thus, in Chapter 5 results of optimization of the bias voltage of the DE-MZM to improve the modulation efficiency and the electrical power of the OFDM signals more impaired by intermodulation distortion are presented and discussed. In **Chapter 6**, the modulation chirp generated by a DE-MZM and its influence on the transmission of signals based on OFDM is studied in detail. Firstly, the decomposition of the chirp parameter as a sum of the chirp parameter due uniquely to the drive signals and the chirp parameter due only to finite ER is derived. Then, closed form expressions for the voltage amplitudes of the drive signals used to control the modulation chirp at the output of a DE-MZM are derived. Secondly, based on these voltage amplitudes of the drive signals, the effect of modulation chirp on the received band-pass OFDM signal and on the 3 dB transmission bandwidth are derived. Finally,

mitigation of power fading induced by chromatic dispersion in the transmission of an OHS modulated in intensity, composed by an OFDM-GbE signal, a LTE signal and an OFDM-UWB signal, is demonstrated by numerical simulation. Furthermore, a comparison of the power penalty incurred by ODSB and ODSB - reduced carrier (ODSB-RC) modulations for an OHS composed by an OFDM-GbE signal and three independent OFDM-UWB signals is carried out. The main conclusions of this thesis are summarized and proposals for the extension of this research work are provided in **Chapter 7**.

2

Hybrid optical access network architectures

2.1 Introduction

The telecommunications networks have been in constant evolution since the deployment of copper cable-based networks for telephony services. The copper cable and DSL technologies have enabled a digital revolution with widespread access to the Internet. However, with the high demand for broadband services and the low product distance-bandwidth of these access technologies in the fixed access network, they have become the last-mile bottleneck of the network. To achieve the high bandwidth required by the emerging services demanded by the end-users, such as triple-play service (television, telephone and internet), the operators have been compelled to replace the copper cable based network by optical fiber access networks, which requires a huge investment. However, FTTH is already a reality with millions of subscribers worldwide, but it is expected that the increasing demand for a wide variety of services, including high-speed Internet access, ultra-high-definition three dimensional television (UHD-3DTV) distribution, interactive multimedia gaming and conferencing, in addition to symmetric bandwidth on- demand services, will not be satisfied by the optical fiber access network based on Ethernet/Gigabit-capable passive optical networks (EPON/GPON) and their successors, 10 Gigabit-EPON (10G-EPON) and 10 Gigabit-PON (10G-PON) also known as NG-PON1. So a new generation of broadband access system will be required. This access system is also referred to as next-generation PON, or NG-PON2 in the FSAN standardization group. NG-PON2 aims to offer broadband

access anywhere and at any time with the seamless integration of broadband wired and wireless access networks, referred to as hybrid optical access network.

In this chapter, an overview of the optical access networks evolution and their standardization is presented. Furthermore, a review of three EU Framework Programme seven (FP7) research projects on hybrid optical access networks undertaken in the last years is provided. Afterwards, a discussion about the advantages and disadvantages of the several possible solutions considered for the implementation of NG-PON2 is presented, followed by the description of the architecture considered in this thesis for integration of broadband wired and wireless access networks.

The remainder of this chapter is organized as follows. In Section 2.2, an overview of optical access networks and the progress of the standardization in this domain is provided. A description of the main hybrid optical access network architectures proposed in EU FP7 research projects in last 4 years, namely ACCORDANCE, SODALES, and FIVER, is presented in Section 2.3. This section ends with a discussion of advantages and disadvantages of the several solutions considered for the evolution to NG-PON2. In Section 2.4, a description of the optical access network architecture considered along the thesis is presented. The chapter is summarized in Section 2.5.

2.2 Optical access networks and standardization

The introduction of optical fiber in the access domain (‘last-mile’) has been under development since the latter half of the 1980’s [22], and allows several network architectures besides the simple point-to-point (P2P) configuration, due to the inherently high bandwidth and low attenuation of the medium. There are basically two kinds of optical access networks, namely passive optical network (PON) and active optical networks (AON). It is designated as PON when there are no active components in the field, otherwise the network is known as AON [23]. PON technology is attracting more and more attention of the telecommunications industry as the “last-mile” solution. PON technology aims to provide an economically-viable point-to-multipoint (P2MP) optical infrastructure for the access network. Its development represents therefore a significant progress towards the realization of a fully-optical broadband communications access network. The nomenclature of optical access networks has been coined in the early PON standards, and the main terms are illustrated in Fig. 2.1. The CO serves as an interface between the optical access network and the core or metropolitan network. The optical

line terminal (OLT) located in the CO performs aggregation and routing functionalities for traffic flows between the high-speed highly-multiplexed core network and the distributed lower-speed access network. The remote node (RN) is the location of the branching device (power splitter/combiner, wavelength multiplexer/demultiplexer). The fiber segment that interconnects the OLT to the RN is usually designated by feeder fiber, and carries the aggregate downstream/upstream data information to/from all end-users. The optical network unit (ONU) contains the optical to electrical interfaces to the various devices in the customer premises. It is located in the user premises in the case of FTTH systems, or at a distance, for FTTX systems, where X describes how closely the optical access network approaches the customer premises. Contemporary variants of FTTX include [24]:

Fiber-to-the-home (FTTH): This option requires an ONU for each customer, placed at the customer premises.

Fiber-to-the-building (FTTB): An ONU is placed within each building, and customers are served for example by twisted pair cables.

Fiber-to-the-curb (FTTC): This is similar to FTTB, although the ONU here serves multiple buildings within a neighborhood.

Fiber-to-the-node (FTTN): The ONU serves multiple users over a wider coverage area, and includes intermediate-range hybrid fiber-coax (HFC) schemes.

The optical distribution network (ODN) includes all the fiber segments used to distribute/aggregate the data information of the users between the RN and the ONU.

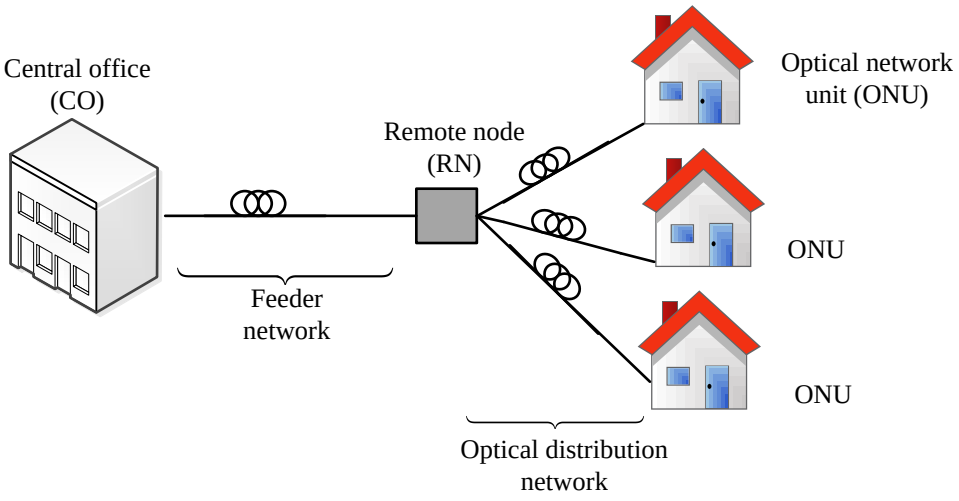

Figure 2.1 – General layout of an optical access network.

To minimize some of the investment risks involved in new access infrastructures, and to ensure interoperability, the leading telecom operators and equipment vendors

formed a group called FSAN [14], aiming to develop optical broadband standards specifications for the International Telecommunication Union for Telecommunications Standardization Sector (ITU-T), Study Group 15 [25]. The first PON standard specified operation of up to 622 Mbit/s downstream and up to 155 Mbit/s upstream, under ITU-T specification G.983, released in 1998 [26]. It was based on the asynchronous transfer mode (ATM) protocol, which was heavily favored by the telecommunications industry at the time, and was called ATM PON (APON). A slightly upgraded version of APON was known as broadband PON (BPON), which was finalized in 2002. Symmetric 2.5 Gbit/s or asymmetric 2.5 Gbit/s downstream with 1.25 Gbit/s upstream operation, designated by Gigabit-capable PON (GPON), was specified in ITU-T recommendation G.984, released in 2005 [27], and is already widely deployed in Europe and North America. The following NG-PON1 was standardized as ITU-T recommendation G.987 in 2010 [28], and is also known as XG-PON1. These systems use simple NRZ modulation, broadcast-and-select for the downstream and time division multiple access (TDMA) in the upstream to enable sharing of the OLT and feeder network among many users. The supported throughputs of XG-PON1 are 10 Gbit/s in the downstream and 2.5 Gbit/s in the upstream. XG-PON1 may be considered as a mid-term upgrade towards a following generation, and thus its main objectives are to allow the coexistence with currently deployed GPON and reuse of the outside plant [29].

Similar activities were undertaken under the umbrella of IEEE, based on the popular Ethernet protocol technologies. 1 Gb/s EPON was standardized as IEEE 802.3ah [30], being mostly adopted in China and Japan. The following generation, known as 10G-EPON and standardized as IEEE 802.3av in September 2009 [31], specifies either symmetrical 10 Gbit/s or asymmetrical 10 Gbit/s downstream and 1.25 Gbit/s upstream bit-rates. This development has led to two different and competing families of standards, a situation which remains unchanged up to now.

Discussions about a following generation capable of offering beyond 10 Gbit/s capacity, known as NG-PON2, have already started at the pre-standardization consortium FSAN that will guide ITU's decisions. NG-PON2 must support at least 40 Gbit/s aggregate capacity per feeder fiber downstream and at least 10 Gbit/s in the upstream. Typically, any NG-PON2 ONU shall be able to support at least 1 Gbit/s service, whereas the actual capability per ONU on the PON will depend on operator requirements concerning split ratio and the applications considered.

Operators may also require the inclusion of mobile backhauling, creating a hybrid optical access network supporting wired and mobile services on the same infrastructure. In this context, fixed access and mobile backhauling, LTE and LTE-A are the relevant mobile network technologies within the FSAN timescales for which NG-PON2 systems must provide backhauling solutions [32].

The convergence of residential and business applications on a common access platform also drives the need for more bandwidth-symmetric systems. For example, mobile backhaul will require sustained and symmetric 1 Gbit/s data rates, while residential customers may be less bandwidth demanding and require the available peak bandwidths for short durations with less symmetry of data rates [32]. Example applications demanding higher data rates are enterprise connectivity and mobile backhaul applications, especially with LTE data rates in the region of up to 300 Mbit/s and increasing to 1 Gbit/s for LTE-A. In addition, mobile operators are looking to reduce capital expenditure (CAPEX) and operation expenditure (OPEX) costs and improve the performance of wireless infrastructures. Regarding reach, the maximum passive fiber reach capability for NG-PON2 should be at least 40 km. However, integration of the metropolitan network into the optical access network has been considered, resulting in the transmission so called LR-PONs. LR-PONs employ optical amplification to extend the reach over 100 km and provide broadband access for a large number of users (>1024), exploiting wavelength multiplexing in an effort to reduce the number of COs in the entire network, as well as CAPEX and OPEX of the operators, and to simplify the network management [33], [34].

The FSAN group has been considering a number of options for NG-PON2. Among the technologies under consideration for NG-PON2, which is expected to deliver the kind of bandwidths that will be required in five years, the following have attracted more interest [32], [35]: WDM-PON; coherent ultra-dense WDM-PON; OFDM-PON; 40 Gbit/s time division multiplexing (TDM)-PON; and time and wavelength division multiplexing (TWDM)-PON, an hybrid system that stacks four 10 G-PONs (XG-PON1) in different wavelengths onto a single fiber to deliver 40 Gbit/s capacity downstream.

In the literature, different architectures based on the technologies considered for NG-PON2 have been analyzed, and performance studies have been carried out to evaluate if those architectures comply with the NG-PON2 requirements. In the last years, there have been research efforts funded by the EU to investigate architectures capable of

offering integration of broadband wired and wireless access networks into a single shared optical fiber network.

2.3 Hybrid optical access network architectures

Several EU FP7 research projects on the convergence of optical fiber and wireless access networks have been undertaken in the last years, which have advanced significantly the state of the art and explored different technologies and network architectures. In the next section the EU projects ACCORDANCE, SODALES and FIVER, based on OFDM-PON, TWDM-AON and WDM-OFDM-RoF-PON, respectively, are described.

2.3.1 OFDM-PON - ACCORDANCE architecture

The use of OFDM in optical access networks has been driven mainly by the necessity of increasing transmission rates without increasing the bandwidth of optoelectronic transceivers, and to provide fine granularity in bandwidth allocation among the users. Furthermore, the main benefit of OFDM is that each of the sub-carriers transmitted in parallel has a much lower bitrate than the aggregate rate, making them less susceptible to impairments like chromatic dispersion, which induces inter-symbol interference (ISI). Consequently, the OFDM signal can travel much longer distances without the need for dispersion compensating modules. As a consequence, several OFDM-PON configurations have been proposed. An extensive review of research efforts in this topic can be found in [36].

The EU FP7 project entitled “A Converged Copper-Optical-Radio OFDMA-based Access Network with high Capacity and Flexibility (ACCORDANCE)” [37], [38] has investigated the introduction of orthogonal frequency division multiple access (OFDMA) into a PON architecture, offering at the same time optical backhauling for wireless and copper-based networks. The converged copper, optical and radio backhaul access network based on OFDMA provides high capacity, flexibility and the interoperability of protocols in the form of distinctive network segments, through the application of OFDMA to provide segment access to and from the network CO. The use of OFDM technology in the optical domain offers the opportunity to facilitate the integration between wireless and OFDM wired networks. As the two transmission systems use the same modulation format, it is possible to allocate different bands inside the frequency spectrum for different applications.

An example of the ACCORDANCE architecture is provided in Fig. 2.2.

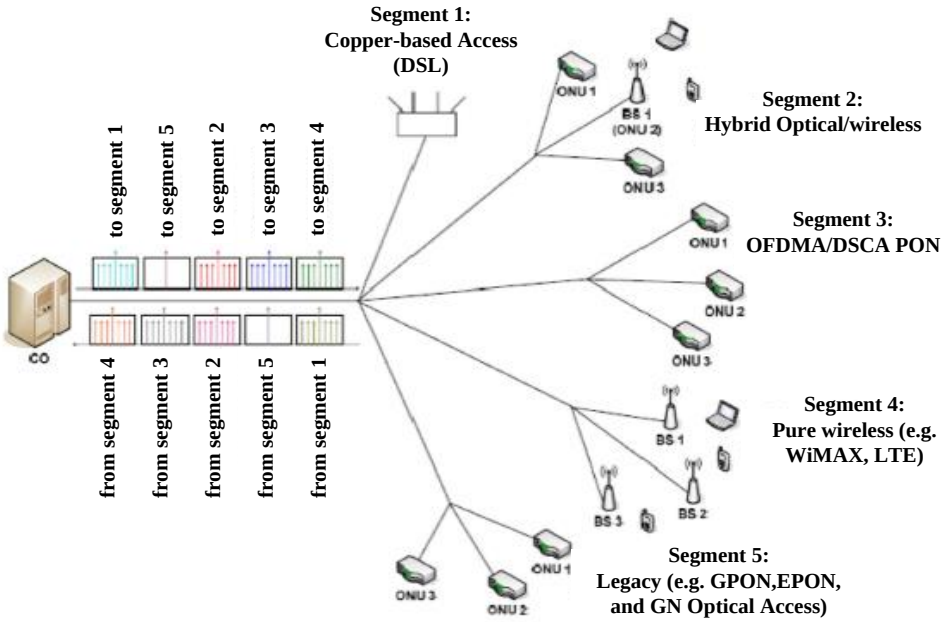

Figure 2.2 – Example of the ACCORDANCE architecture [37].

The P2MP topology of ACCORDANCE architecture consists of the OLT located at the CO and several ONUs located either at the user premises or at BSs that provide connectivity to mobile terminals. One single feeder optical fiber from the OLT is used to carry all upstream and downstream signals up to a power splitter which broadcasts them to multiple network segments. In each segment, further passive splitters are used for FTTH deployments, to broadcast the signals to all ONUs of each segment. Alternatively, some of those fibers can connect directly to the BSs wireless antennas, or switches with DSL interfaces.

In the CO, the OLT is like a normal OLT but combining the additional functionalities of a digital subscriber line access multiplexer. It employs frequency division multiplexing (FDM) of OFDM bands to address different access network segments shown in Fig. 2.2. Each network segment can provide connectivity to a different access technology, and connectivity to an independent operator and then the multiplexing of the different segments can be as shown in Fig. 2.3:

1. *Copper-based Access*: This is achieved by using FDM bands as transparent pipes for transmitting the corresponding discrete multitone modulation signal to/from the DSL users.

2. *Hybrid Optical-Wireless*: This type of access is a mixture of optical wired and wireless access networks, whereby optical and wireless users are allowed to coexist within the same FDM bands.

3. *OFDMA/DSCA PONs*: In these network segments, individual sub-carriers of an FDM band are assigned dynamically. Dynamic sub-carrier allocation (DSCA) to different ONUs of the segment allows multiplexing to take place at the subcarrier granularity.

4. *Pure Wireless*: In this case, a set of subcarriers in an FDM band is dedicated to a group of wireless BSs. Then, RoF or digital radio-over-fiber (D-RoF) techniques can be used to carry the corresponding OFDM wireless signals through the optical infrastructure.

5. *Legacy or Next-Generation Optical Access*: In the case of legacy PON technologies like EPON or GPON, as well as possible updates of the latter (e.g. 10G GPON/EPON) may be employed using OFDM as modulation format.

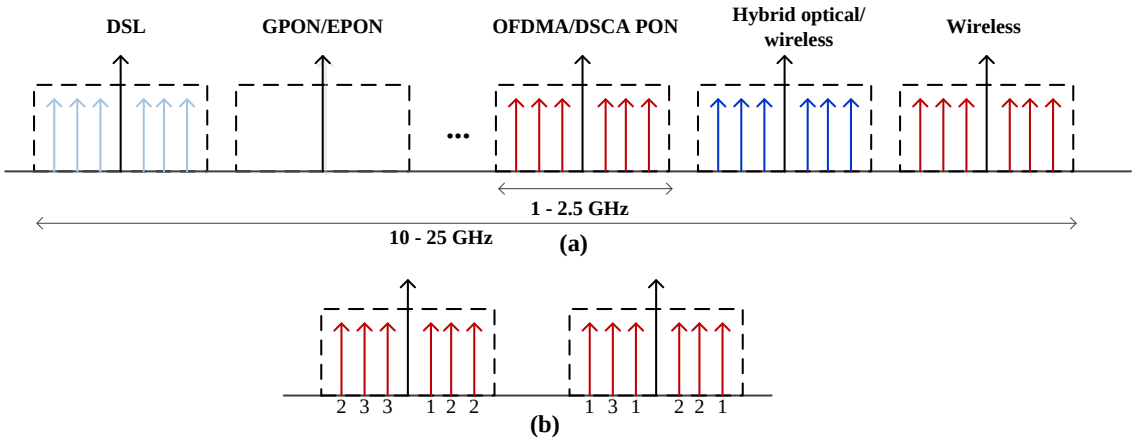

Figure 2.3 – Downstream FDM a) window assignment; b) assignment of individual sub-carriers to different ONUs [39].

The RN located in the first branching point shown in Fig. 2.2 can include either a power splitter or a wavelength demultiplexer (most commonly an arrayed waveguide grating (AWG)) [40]. Using a power splitter in RN allows greater flexibility in the OLT, since FDM of different segments can be of variable width among different services. However, this option introduces a considerable increase in the power budget and the operation bandwidth of every ONU in the network, since all ONUs receive the aggregate band signal, performing the demultiplexing of the desirable subcarriers in the electrical domain. On the other hand, when an AWG is employed in the RN less

flexibility in terms of segment assignment is obtained, since all subcarriers are allocated inside the same FDM band on a static or dynamic wavelength. This option allows reducing the power budget and the speed of the electronics required in the ONUs, reducing the cost per ONU at the expense of less flexibility.

The ACCORDANCE architecture enables a seamless OFDM-based access network where all different services are consolidated, allowing a full coexistence of wired and wireless applications. In addition, it enables convergence of the different access and radio services, namely FTTH, wireless and DSL technologies. It should be clarified that independent operators can coexist, assigned to different segments, and in this way the ACCORDANCE architecture is open to be shared among different operators.

2.3.2 TWDM-AON – SODALES architecture

A WDM-TDM hybrid PON stacks a number of wavelengths, each of which serves a separate TDM-PON, operating at 10 Gbit/s [41]. This allows PON sizes with thousands of users, employing high splitting ratios, large number of wavelengths and high reach, so that they can enable a reduction of the number of required COs. However, high splitting ratios attenuate the optical signal at the RN. To overcome this, high-speed optical switches can be deployed at the RN, increasing further the number of end-users per OLT and the maximum distance between OLT and ONUs [42]. A recent EU FP7 project takes advantage from that characteristic and proposes an optical access network architecture capable to transport transparently services for wired and wireless/mobile applications.

The on-going SODALES (SOftware-Defined Access using Low-Energy Subsystems) project aims to develop an innovative high-bandwidth access network architecture that offers transparent transport services for fixed and mobile applications [43], [44]. The access network architecture proposal will be compatible with existing PON and wireless access solutions: fixed optical and radio access, LTE and beyond, and legacy wired services, namely cable television and DSL technologies. An example of the SODALE architecture is depicted in Fig. 2.4.

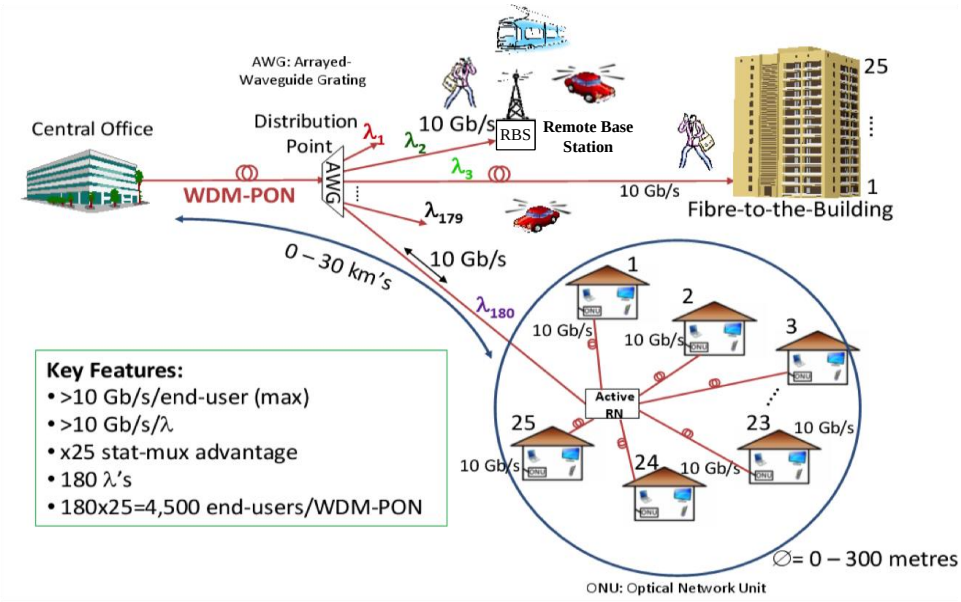

Figure 2.4 – Example of SODALES architecture [43].

The WDM-PON SODALES architecture limits the reach to 30 km, since distances larger than 30 km are not relevant for the vast majority of European deployments [44]. FTTH has been widely accepted as the infrastructure platform that will be able to support present and future applications. The SODALES architecture integrates the following hypotheses for fixed access: WDM-PONs, which are very likely the next generation FTTH networks, able to offer at least 1 Gbit/s and beyond to end-users and suitable for urban areas with high population density, whereas in locations where the deployment of fiber is difficult or economically not feasible, 60 GHz radio fixed access is emerging as the key alternative solution, as defined in ITU-R F.1497 Recommendation [45]. Furthermore, this architecture aims to support 4G (LTE) and beyond mobile radio services, through the fiber mobile backhaul infrastructure.

The SODALES project proposes a novel, converged next generation access network that integrates Layer-2 Ethernet and wireless (LTE, 60 GHz and beyond) over statistical multiplexing and WDM-PON that offers interconnection to fixed and mobile subscribers in a green, simplified, optimized and easy-to-manage access infrastructure. The main novelty is the development of a high-functionality, low-energy active remote node (ARN) offering high-speed switching and statistical-multiplexing features, for maximal exploitation of available network resources, together with radio and legacy systems compatibility. The ARN takes advantage of the required powering at the remote base stations (RBSs). For the downstream case, the FTTH data modulates a wavelength routed through a passive AWG which routes the wavelength/data to the appropriate end-

user over the optical fiber final drop. However, when a wireless final drop is employed, the output port of the AWG routes the data to the ARN, which converts the signal to the electrical domain and transmits it over the 60 GHz band to the end-user. On the other hand, the mobile data are routed through the AWG to the RBS, where the mobile data, after being converted to the electrical domain, are retransmitted to the final mobile-user over a wireless final drop. These three different forms of access are identified in the scheme shown in Fig. 2.5. It should be noted that an ARN and a RBS can be consolidated into a single node, to provide both wireless fixed access and wireless mobile access.

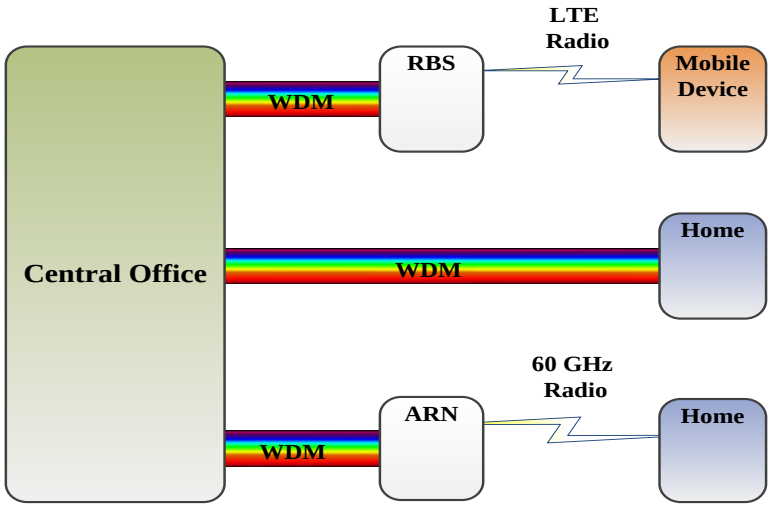

Figure 2.5 - Schematic overview of the unified, ultra-broadband SODALES access platform [44].

This architecture aims to provide 1 Gbit/s peak data (10 Gbit/s in future upgrades) to up to 4,500 (25×180) end-users, using 180 wavelengths in the C and L bands. Each wavelength is routed to 1 of 180 active RNs via a single or a cascade of wavelength-groomed passive AWGs. At the ARN location, an Ethernet-based interconnection device serves up to 25 end-users located up to 300 m away, via 60 GHz wireless or optical fiber drops. Details about the ARN are presented in [46].

2.3.3 WDM-OFDM-RoF-PON – FIVER architecture

Delivering quad-play services (mobile phone, telephone, internet, and television) through the fiber being deployed in the FTTH networks is gaining considerable interest around the world, in order to improve the mobile phone coverage and provide broadband services to the customers at home.

Various service providers are now seeking for ways to bundle not just triple-play or quad-play services but also security and control of homes, which is being called the

quintuple-play service. Service providers now want to offer to the customers the possibility to control their homes and perform remote monitoring or security actions, sometimes referred to as MSA (monitoring, security, and automation). RoF is one of the promising technologies for integration of broadband wireless and wired services, and enables a flexible access network infrastructure capable of offering broadband connectivity for a range of wireless services and applications. RoF technology can be used in MW mobile networks, such as second generation (2 G), third generation (3 G), 4 G and future generation systems [47], as well as in WLANs operating at both MW and MMW frequencies [48].

In EU FP7 project called FIVER (Fully-converged quintuple-play integrated optical-wireless access architectures) [49], a novel integrated access network architecture based on RoF, employing only OFDM signals for the provision of quintuple-play services, is proposed. In the scope of this project, the integrated FTTH optical access network, the in-home optical distribution network, and the final radio link are evaluated. FIVER services are fully converged: a custom OFDM signal for gigabit-Ethernet provision (OFDM-GbE) and the standardized wireless OFDM signals, including LTE, WiMAX, UWB and digital video broadcasting - terrestrial (DVB-T) are transmitted in their native format through the FTTH network, the in-building network and wirelessly at the customer's premises. The FIVER project architecture is shown in Fig. 2.6.

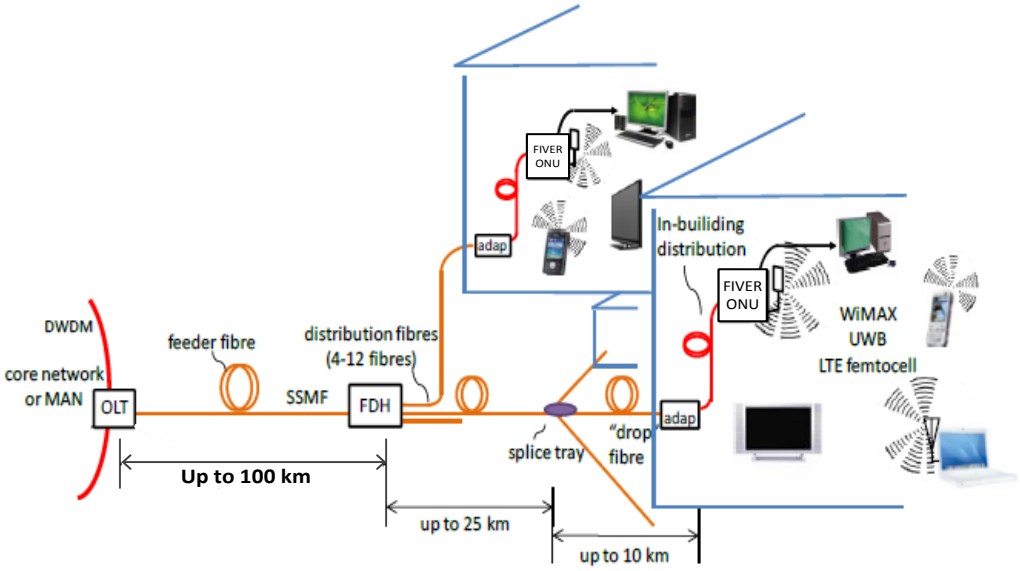

Figure 2.6 - FIVER architecture integrating FTTH and in-building optical and radio transmission [50].

The services supported by the FIVER integrated network are transmitted using a bundle of OFDM signals comprising DVB-T, custom OFDM-GbE, LTE, WiMAX and UWB in their native format. The multiplexing technique used in the OLT to multiplex

the different wireless OFDM signals is subcarrier multiplexing (SCM) and is not restricted to these wireless standards, and thus may be deployed with more signals, limited only by bandwidth availability. The electric spectrum of the bundle of OFDM signals after SCM is sketched in Fig. 2.7.

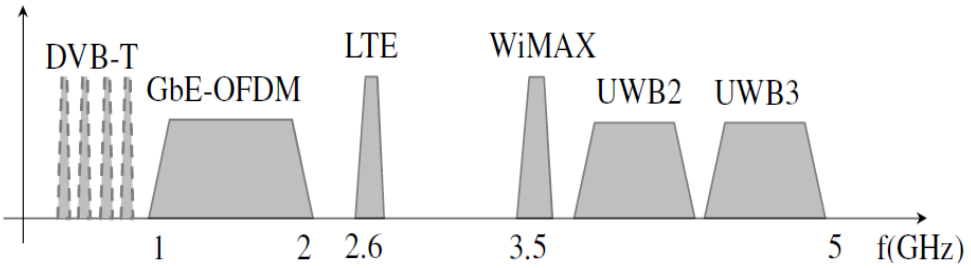

Figure 2.7 – Sketch of the electric spectrum of the OFDM signal transmitted in the downlink [51].

In the CO, the optical signal is generated by a laser, either directly modulated or externally modulated by a MZM, and transmitted through SSMF to a fiber distribution hub (FDH), from which different drop fibers provide access to a user or a group of users. The FDH includes filtering and splicing. At the customer's premises, the optical signal is photodetected and then needs to be demodulated to provide the Internet, audio and video services. At the entrance of the building is where the operator leaves the optical fiber, and after this point the customer is responsible for the wireless connectivity or the in-building distribution.

The proposed architecture complies with the FSAN specification for NG-PON2, with the capability of smooth migration for future generations with the reuse of the legacy fiber plant. Two different architectures are evaluated in the FIVER project: Pure WDM-PON and "colorless" WDM-PON. In the pure WDM architecture two different wavelengths are used, one for downstream and another for upstream, whereas in the "colorless" WDM architecture a single wavelength is used for downstream and upstream with a reflective electro-absorption modulator (R-EAM) deployed at the ONU to avoid the necessity of expensive lasers at users' homes. The first architecture uses a MZM in the 1550 nm wavelength window and could be used to implement LR-PONs with more than 100 km SSMF reach, whereas the second architecture with a REAM in the ONU could be used to implement PONs with 20 km of SSMF reach [52].

Since all modulating signals are OFDM signals, the FIVER network enables a cost-effective fully centralized architecture where centralized management and compensation of the wireless and optical transmission impairments are located in the OLT.

In order to perform centralized transmission impairment compensation at the OLT, a channel sounding technique is proposed [51]. This technique consists in adding extra RF-pilots at the edges of the spectrum of each OFDM signal considered to be transmitted, as shown in Fig. 2.8, to collect information about the channel transmission impairments and compensate them by employing pre-compensation at the OLT.

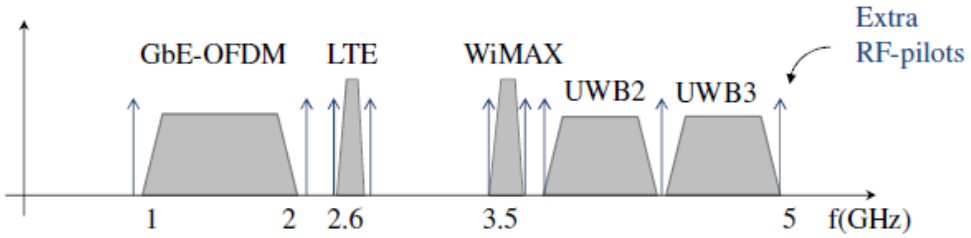

Figure 2.8 - Sketch of the electric spectra of the OFDM signals with extra RF-pilots inserted [51].

In the OFDM transmission, the high frequency subcarriers of the received signal are attenuated due to the limited frequency response of devices (electro-optic modulators, filters,..) and the power fading induced by chromatic dispersion, which degrades the signal-to-noise (SNR) of each subcarrier. Therefore, the extra RF-pilots experience the same attenuation and, as both input extra RF pilots and degraded output extra RF pilots are known at the OLT, the degradation introduced by the channel is known using the channel sounding technique. The proof-of-concept was demonstrated in [53], and it has been concluded that the power level of the higher frequency signals should be increased. Furthermore, in order to keep the same modulation index, the power increase for the higher frequency OFDM signals is obtained at the expense of decreasing the power level of the lower frequency signals.

Finally, [54] describes a successfully demonstrated multi-user 4-wavelength OFDM WDM-PON providing quintuple-play based on OFDM signals DVB-T, LTE, WiMAX, UWB and custom OFDM with GbE capabilities, in a real on-the-field FTTH network of the Towercom operator in Bratislava (Slovakia), providing 1.45 Gbit/s per user. The experimental results confirm the successful service provision with 60.8 km optical reach, including integrated optical and electrical in-building distribution of 100 m bending insensitive-SMF (BI-SMF) and 20 m coaxial cable from legacy DVB-T in-home distribution.

2.3.4 Pros and cons of the different solutions for NG-PON2

The vast majority of deployed PONs worldwide are TDM-PONs. The most straightforward way to upgrade the TDM-PON to the requirements of the NG-PON2 architecture is to employ 40 Gbit/s on-off-keying (OOK) modulation, but there are issues such as expensive 40 GHz electronics and photonics, and low receiver sensitivity, that make it unfeasible for access networks.

The combination of WDM and TDM, TWDM-PON technology has been chosen as the primary solution for NG-PON2 architecture [55], thanks to its capacity to stack a number of wavelengths, each of which serves a separate TDM-PON, usually operated at 10 Gbit/s to reuse the transceivers specified in the XG-PON1 standard. Such systems tend to have high splitting ratios, large number of wavelengths to increase the number of users and high reach, so that they can enable a reduction of the number of required COs. Furthermore, the costs of reach extenders and additional wavelength-selective components in the field are shared by more users, improving cost-efficiency. The company Huawei has developed the world's first full 40 Gbit/s TWDM-PON system prototype, and the tests performed have verified that the TWDM-PON is achievable through the reuse and integration of commercial devices and components [55]. On the other hand, the problem of wavelength selectivity in the ONU or RN appears also in WDM-PONs. Another issue is that the 10 Gbit/s data rate is shared by all users allocated at one wavelength. Then, as the splitting ratio goes up the bit rate for each user decreases, and thus demanding applications such as 3DTV cannot be offered. Therefore, while such networks are suitable for achieving node consolidation and metro-access convergence, an upgrade of the bit rate to support broadband services raises serious issues.

OFDM-PONs are an interesting option for next-generation-PONs (NG-PONs), as it has been explained for the ACCORDANCE project, since OFDM allows efficient spectrum utilization and fine granularity in bandwidth allocation among the users. As a consequence, several OFDM-PON configurations have been investigated [36]. If a low-cost direct-detection scheme is implemented in the ONU, the transmission is limited by the low receiver sensitivity and therefore low splitting ratios are allowed. The sensitivity can be improved if coherent detection is employed. In that case, however, the complexity of the receiver will be similar to the case of coherent WDM-PON in terms of components per ONU. For the upstream channel, additional challenges are created

due to the decorrelation of the optical subcarriers from the different ONUs. The upstream OFDM signal in a OFDMA-PON with k ONUs is a superposition of k components, which pass through optical channels of different lengths from ONU to the OLT (different path delays) modulated from different lasers (different phase noises and optical wavelength drifts). As a result, the correction of timing and frequency offsets of each user in case of a common discrete Fourier transform (DFT) cannot be accomplished at the OLT receiver, since correction for one user would misalign all other users. This decorrelation will cause inter-carrier interference (ICI) and ISI and can result in serious performance degradations [56]. This problem can be avoided if WDM techniques are employed. The introduction of WDM will complicate the system design, since colorless operation will have to be achieved to ensure cost-efficient operation.

In the direct-detection OFDM-PON, a frequency shift of subcarriers to create a guard band in the form of empty subcarriers is required to avoid intermodulation products that degrade the system performance upon detection. However, the inclusion of the guard bands reduces the spectral efficiency of the system which reduces the total number of ONUs that can be served in a single-wavelength OFDM-PON. Another issue is the power consumption of such high-speed digital signal processing - intensive transceivers, both in the OLT and the ONUs. For these reasons, it appears that OFDM-PONs may not be the ultimate candidate for the NG-PON2.

From the above discussion, it is evident that WDM-PONs are a future-proof technology for the next generation of optical access networks (NGOAs), since they offer logical P2P connections, flexible bit rates per user, long-reach and simple management. In this architecture, each ONU receives only its data on its own wavelength, in contrast with the TDM-PON system. Hence, WDM-PON systems have an advantage over other solutions in terms of privacy. The higher cost of colored ONUs (designed to operate at a specific wavelength) is a disadvantage of WDM-PON systems. However, WDM-PONs have been extensively researched to solve key challenges, such as colorless operation, which is crucial to the commercial success of this scheme. A number of solutions have been studied to remove the need for colored components. One option is a WDM-PON in which each ONU is equipped with a tunable laser [57], but this is not a low-cost option at the moment. The second option is a seeded WDM-PON, where the upstream wavelengths for all ONUs are generated at the OLT or RN. The wavelengths are then reflected and modulated with data at the ONUs. In this option, reflective semiconductor optical amplifiers (RSOAs) [58] and R-EAM [52], [59] are

typically used. However, the reach of reflective WDM-PONs is limited, mainly due to the interference between the seed signal and the upstream signal, both propagating in the same fiber, resulting from Rayleigh backscattering.

Furthermore, WDM-PON allows the transparent transmission of wireless/mobile RF modulated signals in their native format for BSs, in coexistence with transmission of wired signals for ONUs. The transmission of wireless signals in their native format is a great advantage, since it allows simplifying the hardware required in BSs or in customer premises equipment.

2.4 WDM-RoF-PON - Architecture considered

In a RoF network, multiple BSs are connected to the CO through WDM of the RF optical signals. The CO centralizes all data routing and processing of the network in order to allow the sharing of equipment at the CO, and to enable a simple radio distribution architecture and low complexity BSs. Multiple BSs are connected to RNs in a tree architecture topology, whereas the RNs are connected to the CO in a star architecture topology. Each BS communicates with the CO through the RN on a separate wavelength [60]. Each wavelength can transport multiple RF modulated signals allocated on different frequencies multiplexed using SCM. A direct relation can be established between WDM-PONs and WDM-RoF networks, where the BSs in the RoF networks are replaced by ONUs in WDM-PONs. In this way, the integration of these two different networks becomes direct using SCM to multiplex multiple RF modulated signals on different bands along with a BB signal. Thus, a single wavelength carries both wired services of PONs and mobile services of RoF networks.

In the receiver side, the wired and wireless services can be recovered together in the same receiver, that is, in a hybrid ONU/BS (lowest-cost option) or separately with the wired service signal in an ONU and the wireless services recovered in a BS. These two possibilities are illustrated in Fig. 2.9. Figure 2.9 shows an overall scenario of integration of a WDM-RoF network into a WDM-PON to support wired and wireless services to customer's premises. The architecture considered in this thesis, illustrated in Fig. 2.9, is similar to the FIVER architecture above described.

In this thesis the end-user is always considered at home or inside a building because, such as was mentioned in Chapter 1, 65 % of mobile traffic originates inside a home or building, these being the places with worse coverage.

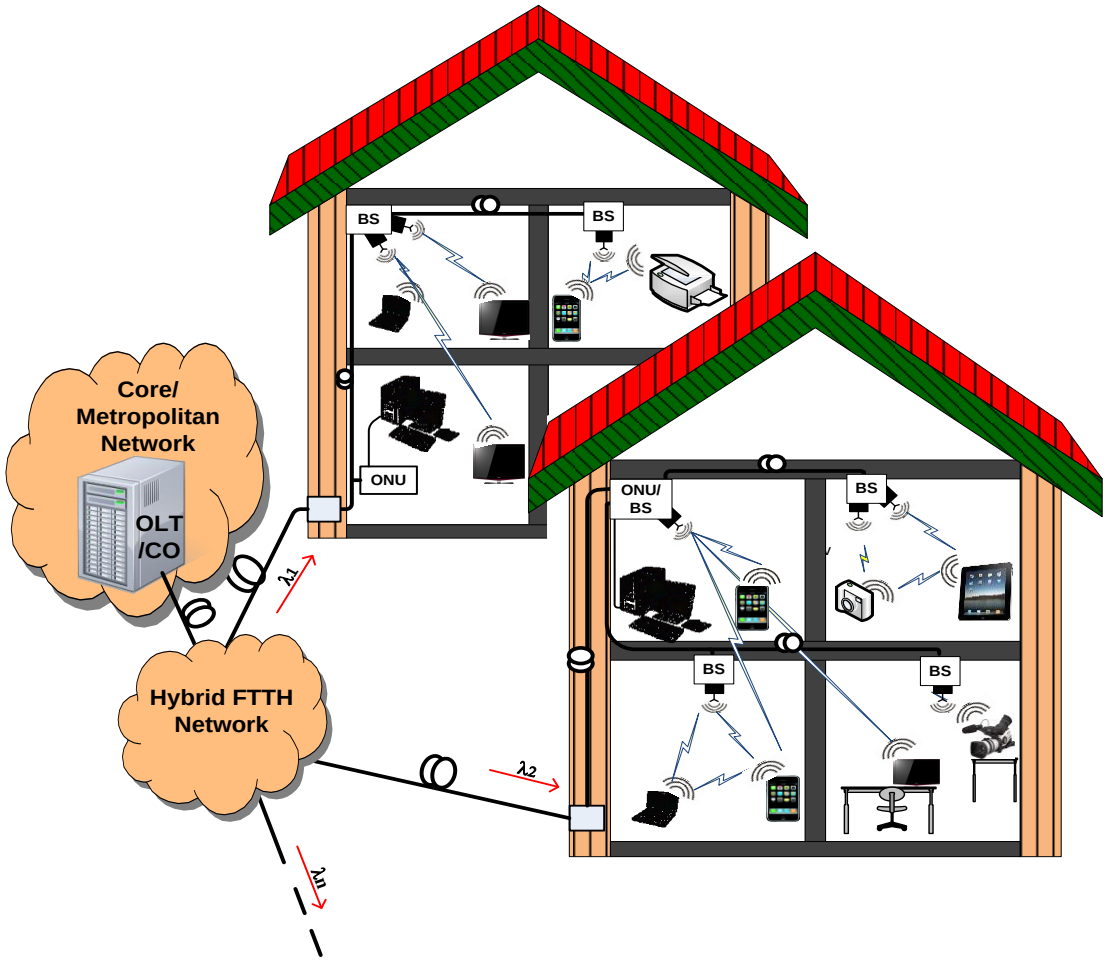

Figure 2.9 – WDM-RoF-FTTH architecture scenario integrating RoF networks into FTTH networks to provide wired services and wireless services to the customer's premises.

Therefore, the delivery of wired and wireless services considering a FTTH network is of great importance in the coming years, due to the dramatic increase in mobile traffic expected, mainly based on video.

Figure 2.9 shows an OLT located in the CO of the network operator, where wireless and wired services modulate simultaneously an optical carrier. Then, the optical hybrid signal (OHS) containing the quad-play/quintuple-play service is distributed through a SSMF-based FTTH network to an ONU and BS or hybrid ONU/BS located at each customer premises. As shown in Fig. 2.9 a FTTH network that supports wired and wireless services are here referred to as hybrid FTTH network.

In this thesis, the signals considered to be modulated simultaneously on an optical carrier will be: a BB signal based on OOK modulation or OFDM modulation providing at least 1 Gbit/s per user, whereas the wireless signals will be: an LTE signal and OFDM-UWB signals. The LTE signal is considered to provide access to mobile networks through the femtocells, and OFDM-UWB signals are considered to provide wireless access to multimedia services such as UHDTV and 3DTV.

Unlike to the FIVER architecture above described, the WiMAX service will not be considered, since WiMAX is a competitor of the LTE technology and, according to the WiMAX Forum website, WiMAX has been most deployed in Africa, CALA (Caribbean and Latin America Region) and mainly in Asia-Pacific. The high deployment in these countries, compared with the deployments in Eastern Europe, Western Europe and North America, might be due to the fact that, in those countries, most households do not have broadband Internet at their homes via DSL or cable [61]. Furthermore, since mid-2010, deployments appear to have somewhat stagnated, product certification rate is slightly declining and session attendance is low.

2.5 Summary

The wired and wireless access networks have been in constant evolution driven by the demand of the end-user. Currently, both wired optical access networks and wireless/mobile access networks are in a transformation process from separate networks to a single shared optical network, in order to provide broadband access anywhere, anytime and anyone at low CAPEX and OPEX.

In this chapter, an overview of existing optical access networks and the main requirements for the NGOANs was presented. Furthermore, the main EU FP7 projects that allow providing seamless integration of wired and wireless services were reviewed. Afterwards, a discussion about the pros and cons of each solution considered for NG-PON2 is presented based on which it is concluded that WDM-PON is a ‘future proof’ solution for NGOANs. The architecture considered for the thesis is presented at the end of the chapter.

3

Optical Single Sideband Modulation based on Mach-Zehnder Modulators

3.1 Introduction

Lithium niobate MZMs have been widely used for high bit-rate signal transmission and broadband RoF systems [62]. Unlike direct modulation of a laser diode, LiNbO3 MZMs allow zero-chirp or adjustable-chirp operation and advanced modulation formats such as OSSB modulation and high quality signal generation [63].

In this chapter, the operation principle of a z-cut DE-MZM is presented along with its intensity transfer function, as a basis for presenting the z-cut DP-MZM and its output electric field. Afterwards, a mathematical description for small-signal operation of OSSB modulation and OTSSB modulation is demonstrated.

The remainder of this chapter is structured as follows. In sub-Section 3.2.1 the operation principle for a z-cut DE-MZM is presented. Furthermore, the intensity transfer function of the DE-MZM is derived and the main points used to bias it are studied. In the following sub-Section 3.2.2 the output electro-optic field for the z-cut DP-MZM is derived. In Section 3.3, a mathematical description for small-signal operation of OSSB modulation and OTSSB modulation based on the phase-shift method is derived. Finally, a summary of the chapter is presented.

3.2 Mach-Zehnder modulators

In all simulations presented in this thesis, an external modulator based on a MZM is used as electro-optic modulator. Therefore, the in depth study of the MZM has paramount importance.

3.2.1 Dual electrode Mach-Zehnder modulator

A MZM is an electro-optic device based on the operation principle of the Mach-Zehnder interferometer. In Fig. 3.1 a) the top view of the basic structure of a z-cut DE-MZM is shown, whereas in Fig. 3.1 b) the cross-section view of the z-cut DE-MZM is schematized.

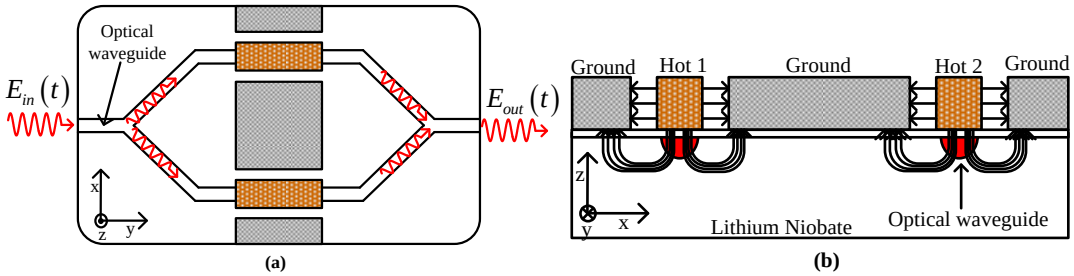

Figure 3.1 - Z-cut dual electrode Mach-Zehnder Modulator; a) Top view and b) Cross-section view.

An integrated MZM consists of two parallel phase modulators between two Y-junctions, one at the input and other at the output, interconnected through a planar waveguide structure deposited on the substrate. The LiNbO3 substrate has been the material of choice for the fabrication of electro-optic modulators due to its high electro-optic coefficients in a broad wavelength range near the infrared band used for telecommunications systems [64]. The most advanced technology for fabricating waveguides is Ti:LiNbO3. An embedded strip waveguide is fabricated by diffusing titanium (Ti) into a LiNbO3 substrate to increase its refractive index in the region of the strip. Besides LiNbO3, III/V compound semiconductors are also used, such as Indium phosphide (InP) [65] and Gallium arsenide (GaAs) / Aluminium gallium arsenide (AlGaAs) [66]. Other materials for the substrate such as polymers [67], and silicon [68] have been employed in the fabrication of electro-optic MZMs.

The input optical signal, $E_{in}(t)$, is split into two arms through the input Y-junction, where the resulting optical signals suffer a phase shift in the phase modulators controlled by the strength of an electric field across the waveguide. The phase modulators make use of the Pockels effect in the optical waveguide to create the phase

shift in each arm. The nature of this effect is that the refractive index of the waveguide changes linearly with the applied electric field. Careful driving of the electrical signals applied to each arm of the modulator allows controlling the type of interference at the output of the Y-junction combiner, resulting in the output signal $E_{out}(t)$. When the differential phase shift between the arms equals ± π, destructive interference occurs at the output Y-junction and no optical signal exists at the output of the DE-MZM. Otherwise, with no differential phase shift maximum amplitude of the output signal occurs. Therefore, through the interferometric configuration of waveguides, the MZM converts a phase modulation into intensity modulation.

3.2.1.1 Z-cut DE-MZM intensity transfer function

In the fabrication process of a MZM, due to construction limitations, a symmetrical optical waveguide interferometer is a challenge, since the splitting ratio of the Y-junctions is not exactly 50/50, and the loss in each arm is different. To model this unbalanced splitting/combining ratio between the arms of the MZM, Walklin and Conradi introduced the scaling factor γ in one arm, taking values between 0 and 1. For balanced MZMs this scaling factor is 1. The electric field at the output of the DE-MZM is given by [69]:

$$E_{out}(t) = \frac{E_{in}(t)}{2}\left\{e^{j(\phi_{01}+\phi_1(t))} + \gamma e^{j(\phi_{02}+\phi_2(t))}\right\} \tag{3.1}$$

where t denotes time, $E_{in}(t)$ is the electric field at the input of the DE-MZM, often assumed to be a CW signal, and γ is related to the optical ER, ε, defined as the ratio between maximum and minimum output intensities, by the relation $\gamma = \sqrt{\varepsilon} - 1 / \sqrt{\varepsilon} + 1$ [69]. ϕ_{01} and ϕ_{02} are constant phase shifts due to propagation through the optical waveguide length in the upper and lower arms of the DE-MZM, respectively. As these phase shift are constant, and $|\phi_{01}-\phi_{02}|$ is small, they are often ignored in order to simply the transfer function.

The input-output electric transfer function of each optical phase modulator, when neglecting the constant phase shift and insertion losses, is given by:

$$\frac{E_{out}(t)}{E_{in}(t)} = e^{j\phi(t)} \tag{3.2}$$

and the time-varying phase shifts $\phi_1(t)$ and $\phi_2(t)$ in (3.1) can be expressed as:

$$\phi_1(t) = \frac{\pi}{V_\pi} V_1(t) \tag{3.3}$$

$$\phi_2(t) = \frac{\pi}{V_\pi} V_2(t) \tag{3.4}$$

where $V_1(t)$ and $V_2(t)$ are the drive voltages of the DE-MZM, V_π is the switching voltage of the modulator, which is the voltage required to produce a phase shift equal to ± π, also designated in the literature as half-wave voltage. The phase shifts in (3.3) and (3.4) are directly proportional to the amplitudes of the voltages applied to the electrodes of the phase modulators.

Dividing (3.1) by $E_{in}(t)$ results in the transfer function in terms of the electric field, expressed as:

$$T_E(t) = \frac{E_{out}(t)}{E_{in}(t)} = \frac{1}{2}\left\{e^{j\phi_1(t)} + \gamma e^{j\phi_2(t)}\right\}. \tag{3.5}$$

The transfer characteristic in term of intensity (power), usually called transmittance, is obtained by taking the square of the magnitude of (3.5), obtaining:

$$I(t) = T_E(t)T_E(t)^* = \frac{P_{out}(t)}{P_{in}(t)} = \frac{1}{4}\left\{1+\gamma^2+2\gamma\cos\left(\frac{\pi}{V_\pi}\left(V_1(t)-V_2(t)\right)\right)\right\} \tag{3.6}$$

In Fig. 3.2, the transmittance of a DE-MZM with a direct current (DC) ER of 25 dB ($\gamma = 0.89$), given by (3.6), is shown as a function of the differential drive voltage normalized by the switching voltage.

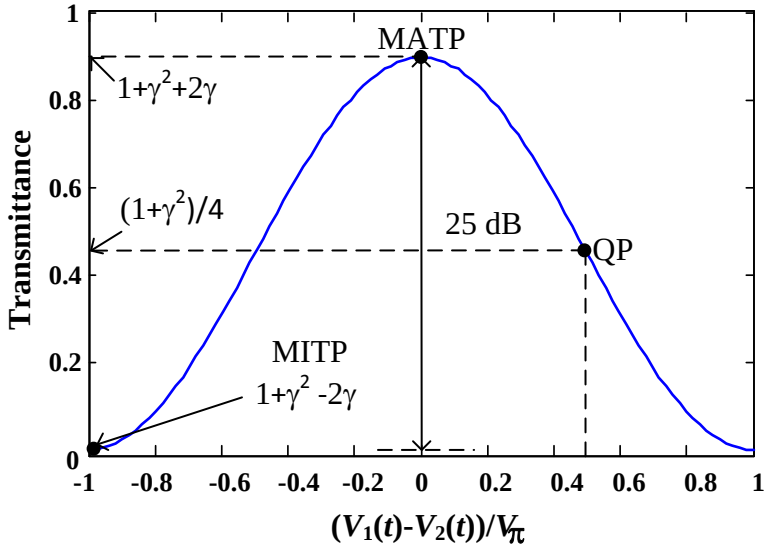

Figure 3.2- Transmitance of a DE-MZM with DC ER = 25dB as a function of the differential drive voltage normalized by the switching voltage.

The region where the DE-MZM transmittance is more linear is around the inflection point, determined by the differential voltage $V = V_1(t)\text{-}V_2(t)$ for which $d^2I/dV^2 = 0$. The operator d^2/dV^2 denotes the second derivative relative to *V*. From (3.6),

$$\frac{d^2I(V)}{dV^2} = \frac{-2\gamma}{4}\left(\frac{\pi}{V_\pi}\right)^2 \cos\left(\frac{\pi}{V_\pi}V\right) = 0 \Rightarrow V = \frac{V_\pi}{2} \tag{3.7}$$

Thus, a DE-MZM with a finite ER keeps unchanged the differential voltages required to be biased at the QP, at the minimum transmition point (MITP), and at the maximum transmission point (MATP). However, the corresponding values of transmittance change depending on the DC finite ER. For example, at the QP the transmittance is $(1+\gamma^2)/4$, instead of 0.5 for the case of an ideal MZM. The exact values of the transmittance at the different bias points are shown in Fig. 3.2 as a function of γ, related with the ER.

3.2.2 Z-cut dual-parallel Mach-Zehnder modulator

The z-cut DP-MZM, schematized in Fig. 3.3, is composed by two sub-MZMs A and B, in each arm of the main MZM C, integrated into a single-chip using a z-cut $LiNbO_3$ substrate [63]. The $LiNbO_3$ DP-MZM modulator has been used for generation of various advanced modulation formats at 40 Gbit/s and 80 Gbit/s, including return-to-zero OOK, differential quadrature phase-shift-keying, quadrature amplitude modulation (QAM), wideband frequency-shift keying, and OSSB modulation [63], to improve the spectral efficiency of the transmission and increase the system robustness against chromatic dispersion. Consequently, this modulator has been called versatile lightwave modulator.

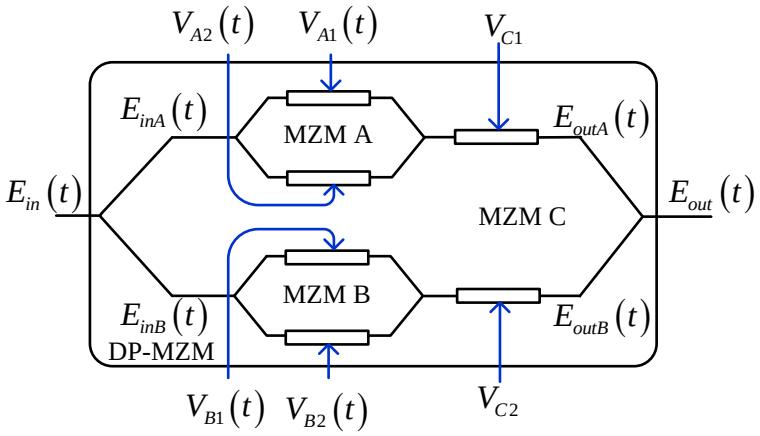

Figure 3.3 - Structure of a z-cut dual-parallel Mach-Zehnder modulator.

Based on the analysis previously presented for the z-cut DE-MZM, the electro-optic field at the output of the DP-MZM will be derived. The electro-optic field components at the output of the input Y-junction are given by:

$$E_{inA}(t) = \frac{E_{in}(t)}{\sqrt{2}} \tag{3.8}$$

$$E_{inB}(t) = \sqrt{\frac{\gamma_C}{2}} E_{in}(t) \tag{3.9}$$

In the upper arm of the main MZM (MZM C), the electro-optic field at the output of the cascade of the MZM A and the phase modulator of MZM C is expressed by:

$$\begin{aligned} E_{outA}(t) &= E_{inA}(t) T_{EA}(t) e^{j\phi_{C1}} \\ &= \frac{E_{in}(t)}{\sqrt{2}} \left(e^{j\phi_{A1}(t)} + \gamma_A e^{j\phi_{A2}(t)} \right) e^{j\phi_{C1}}, \end{aligned} \tag{3.10}$$

where $T_{EA}(t)$ is the electric field transfer function of the sub-MZM A, expressed by (3.5). Similarly, for the lower arm of the main MZM, the electric field at the output of sub-MZM A is given by:

$$\begin{aligned} E_{outB}(t) &= E_{inB}(t) T_{EB}(t) e^{j\phi_{C2}} \\ &= \sqrt{\frac{\gamma_C}{2}} E_{in}(t) \left(e^{j\phi_{B1}(t)} + \gamma_B e^{j\phi_{B2}(t)} \right) e^{j\phi_{C2}}. \end{aligned} \tag{3.11}$$

where $T_{EB}(t)$ is the electric field transfer function of the sub-MZM B. The resulting output electric filed of the DP-MZM is given as:

$$\begin{aligned} E_{out}(t) &= \frac{E_{outA}(t)}{\sqrt{2}} + \sqrt{\frac{\gamma_C}{2}} E_{outB}(t) \\ &= \frac{E_{in}(t)}{2} \left\{ \left(e^{j\phi_{A1}(t)} + \gamma_A e^{j\phi_{A2}(t)} \right) e^{j\phi_{C1}} + \gamma_C \left(e^{j\phi_{B1}(t)} + \gamma_B e^{j\phi_{B2}(t)} \right) e^{j\phi_{C2}} \right\} \end{aligned} \tag{3.12}$$

where γ_A, γ_B, and γ_C are the scaling factors of the sub-MZMs A and B and of the main MZM C, respectively. The phase shifts ϕ_{C1} and ϕ_{C2}, induced by the DC voltages V_{C1} and V_{C2}, are used to control the differential phase shift at the input of the output Y-junction. In OSSB modulation through the phase shifting method, $|\phi_{C1}-\phi_{C2}| = \pi/2$ [63] in order to generate two ODSB signals in quadrature.

To simplify the model of either z-cut or x-cut DP-MZM, it is common to consider the half-wave voltages of each sub-MZM equal, that is $V_{\pi,A} = V_{\pi,B} = V_{\pi,C} = V_\pi$, since in practice the voltage difference is small [63]. Furthermore, in analysis it is also common

to consider $\gamma_A = \gamma_B = \gamma_C = \gamma$, and thus the electric field at the output of the DP-MZM, given by (3.12), is simplified to:

$$\begin{aligned} E_{out}(t) &= \frac{E_{outA}(t)}{\sqrt{2}} + \sqrt{\frac{\gamma}{2}} E_{outB}(t) \\ &= \frac{E_{in}(t)}{2}\left\{\left(e^{j\phi_{A1}(t)} + \gamma e^{j\phi_{A2}(t)}\right)e^{j\phi_{C1}} + \gamma\left(e^{j\phi_{B1}(t)} + \gamma e^{j\phi_{B2}(t)}\right)e^{j\phi_{C2}}\right\} \end{aligned} \tag{3.13}$$

with $\phi_{k1}(t) = \pi/V_\pi \, V_{k1}(t)$ and $\phi_{k2}(t) = \pi/V_\pi \, V_{k2}(t)$, for k = A, B.

3.3 OSSB modulation

OSSB modulation was initially proposed in RoF systems to overcome the power fading induced by chromatic dispersion [20], [70]. However, OSSB modulation has been intensively investigated for baseband long-haul and ultra-long-haul WDM transmission, as a solution to increase the spectral efficiency of signal formats in order to increase the transmission capacity. Besides that, OSSB modulation has been demonstrated to be more tolerant to group velocity dispersion [71], [72].

OSSB modulation for RF signals transmission can be obtained through conversion of ODSB modulated signals into OSSB using phase modulation in an optical phase modulator [71]. The forward method is through filtering method [70], which an optical sideband is rejected by optical filtering. Using the phase-shift method, an OSSB signal can be obtained from the modulating signal through electro-optic modulation [20], [71], [72]. The study all of these methods are beyond the scope of this thesis. In this thesis the filtering method and phase-shift method are applied to overcome the power fading induced by chromatic dispersion, and then a brief description of each method is presented.

In Fig. 3.4, the scheme of an OSSB transmitter based on the filtering method is presented.

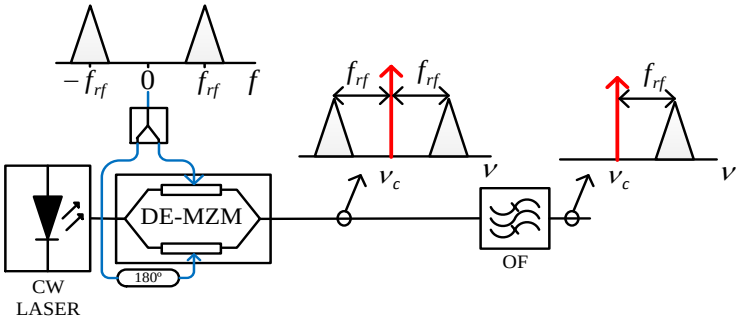

Figure 3.4 – Scheme of OSSB generation based on filtering method.

The optical sinal emitted by a CW laser is externally modulated by a DE-MZM operated in push-pull in order to minimize modulation chirp on the ODSB modulated signal at its output. This ODSB modulated signal is applied to an optical filter (OF) tuned to remove an optical sideband. Rejection of the lower sideband is represented in Fig. 3.4. The filtering method is the simplest method to generate an OSSB signal, but it presents the drawback of half the power of the ODSB signal being rejected, in contrast with the phase-shift method, with which the power of the suppressed sideband is transferred to the other sideband.

The generation of OSSB signals through the phase shift method uses a DE-MZM [70], [71], [72], as represented schematically in Fig. 3.5. The RF modulating signal is applied to a 3 dB 90º hybrid coupler that divides the applied input signal in two equal output signals with a 90º phase shift. The function of the 90º hybrid coupler is to perform the Hilbert transform, generating at its output a signal similar to the input but with a 90º phase shift in all spectral components. The two output signals drive different electrodes of the DE-MZM. The DE-MZM is biased at the QP by a DC voltage equal to $V_\pi/2$, and modulates the CW signal from the laser in OSSB with carrier.

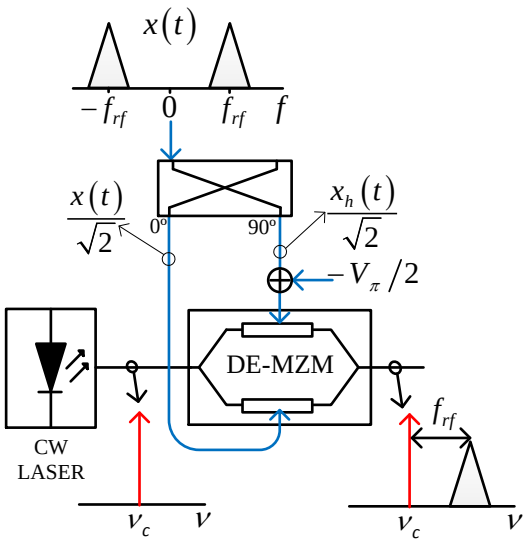

Figure 3.5 – Scheme of OSSB modulation based on the phase-shift method, using a DE-MZM.

The derivation of the electric field of an OSSB modulated signal using the phase-shift method based on a DE-MZM, assuming the small-signal regime [73], is presented in the next sub-section, following the derivation of the optical tandem single sideband (OTSSB) modulated signal. The mathematical description for the signal generated with the filtering method is not presented, since it is easily obtained from the ODSB modulated signal eliminating all spectral components of the unwanted sideband.

3.3.1 Small-signal mathematical description of OSSB modulation

Considering a balanced DE-MZM ($\gamma = 1$), without insertion losses and biased at the QP, the electric field at the output of the DE-MZM is expressed as:

$$E_{out}(t) = E_{in}(t) e^{j\frac{\pi}{2V_\pi}(V_1(t)+V_2(t))} \cos\left(\frac{\pi}{2V_\pi}\left(V_1(t)-V_2(t)\right)\right), \tag{3.14}$$

considering the drive signals given by:

$$\begin{aligned} V_1(t) &= x(t) - \frac{V_\pi}{2}, \\ V_2(t) &= x_h(t) \end{aligned} \tag{3.15}$$

where $x(t)$ is the modulating signal and $x_h(t)$ is the Hilbert transform of $x(t)$ obtained with a 3 dB 90º hybrid coupler. The electric field can then be simplified to:

$$\begin{aligned} E_{out}(t) = E_{in}(t) e^{j\frac{\pi}{2V_\pi}(x(t)+x_h(t))} \frac{e^{-j\frac{\pi}{4}}}{\sqrt{2}} \Bigg[& \cos\left(\frac{\pi}{2V_\pi}\left(x(t)-x_h(t)\right)\right) \\ & + \sin\left(\frac{\pi}{2V_\pi}\left(x(t)-x_h(t)\right)\right)\Bigg]. \end{aligned} \tag{3.16}$$

Assuming the small-signal regime ($|x(t) - x_h(t)| \ll 1$), and taking into account that $\cos(x) \approx 1$, $\sin(x) \approx x$, $e^x \approx 1+x$ for $|x| \ll 1$, and neglecting the terms $x(t)^2$, $x_h(t)^2$ and $x(t)x_h(t)$ (distorted terms), then, after some algebraic manipulations, the electro-optic field is simplified to:

$$E_{out}(t) \approx \underbrace{\frac{E_{in}(t)}{2}(1-j)}_{\substack{\text{Un-modulated} \\ \text{optical carrier}}} + \underbrace{\frac{\pi E_{in}(t)}{2V_\pi}\left(x(t)+jx_h(t)\right)}_{\text{Modulated upper-sideband}} \tag{3.17}$$

This is the expression of the small-signal approximation of the electric field of an OSSB more carrier modulated signal, which includes two terms, one for the un-modulated optical carrier and the other for the un-suppressed optical sideband. The signal $x_a(t) = x(t)+jx_h(t)$ is designated by analytic signal and has the property of single sideband spectrum [74]:

$$FT\{x_a(t)\} = X_a(f) = \begin{cases} 2X(f), & f \geq 0 \\ 0, & f < 0 \end{cases} \tag{3.18}$$

where the operator $FT\{.\}$ is the Fourier transform, and $X(f) = FT\{x(t)\}$. The simplest example of an analytic signal is $x_a(t) = e^{jwt} = \cos(wt) + j\sin(wt)$, which presents an upper

single sideband spectrum. Thus, the electric field expression (3.17) corresponds to an upper-single sideband spectrum.

In some applications for RoF systems it is desirable to generate simultaneously two OSSB modulated signals in both sides of the optical carrier, in order to overcome the effects of fiber chromatic dispersion for transporting RF signals over the fiber and improve the spectral efficiency around the optical carrier. Optical tandem single side band (OTSSB) improves the spectral efficiency of OSSB by doubling the bandwidth usage [75]. In the next sub-section, a mathematical derivation of the small-signal approximation of the electric field of an OTSSB modulated signal is presented.

3.3.2 Small-signal mathematical description of OTSSB modulation

Considering again a balanced DE-MZM ($\gamma = 1$), without insertion losses, and two different RF modulating signals $x_1(t)$ and $x_2(t)$ to be OTSSB modulated. The two RF signals are applied to different input ports of a 3 dB 90º hybrid coupler. The configuration required to drive the DE-MZM in order to obtain at the output an OTSSB modulated signal is schematically shown in Fig. 3.6.

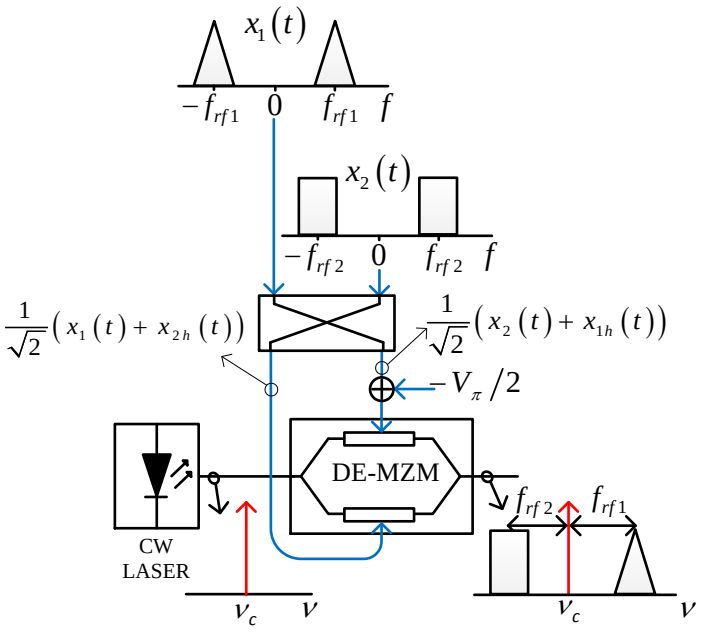

Figure 3.6 – OTSSB modulation scheme.

At each output port of the 3 dB 90º hybrid coupler is obtained a modulating signal and the Hilbert transform of the other modulating signal, applied at different input ports,

as shown in Fig. 3.6. The drive signals applied to the electrodes of the DE-MZM are expressed by

$$\begin{aligned} V_1(t) &= x_2(t) + x_{1h}(t) - \frac{V_\pi}{2} \\ V_2(t) &= x_1(t) + x_{2h}(t) \end{aligned} \tag{3.19}$$

Applying these drive signals in (3.14), assuming small-signal regime, and neglecting the distortion terms $x_1(t)^2$, $x_1(t)x_{1h}(t)$, $x_1(t)x_2(t)$, $x_1(t)x_{2h}(t)$, $x_2(t)^2$, $x_2(t)x_{2h}(t)$, the electric field of the OTSSB modulated signal is approximated by:

$$E_{out}(t) \approx \underbrace{\frac{E_{in}(t)}{2}}_{\substack{\text{Un-modulated} \\ \text{optical carrier}}} + \underbrace{\frac{\pi E_{in}(t)}{2V_\pi}\left(x_2(t) - jx_{2h}(t)\right)}_{\text{Modulated lower-sideband}} + \underbrace{\frac{\pi E_{in}(t)}{2V_\pi}\left(x_1(t) + jx_{1h}(t)\right)}_{\text{Modulated upper-sideband}} \tag{3.20}$$

Three different terms can be observed in this expression: one for the un-modulated optical carrier, one for the optical modulated lower-sideband, and one for the optical modulated upper-sideband. Therefore, OTSSB modulation is a spectral efficient way to perform OSSB modulation of two different RF signals simultaneously.

3.4 Summary

The MZMs are the most promising electro-optical modulators to meet the future optical access networks requirements, due to their characteristics, such as modulation bandwidth and zero-chirp or adjustable-chirp operation. The $LiNbO_3$ MZM is the type of MZM more widely used, due to its high electro-optic coefficients in a large wavelength range of the near infrared band used for telecommunications systems.

In this chapter, the $LiNbO_3$ z-cut DE-MZM and the z-cut DP-MZM were analyzed, and their output electric fields were derived. Finally, OSSB modulation based on filtering and phase-shift methods are described. Afterwards, the output electric field for OSSB and OTSSB signals based on the phase-shift method are derived.

4

Multiband optical hybrid signal generation schemes

4.1 Introduction

The high data rate demands of wireless and wired networks have rapidly increased in the recent years. RoF and FTTH systems are promising candidates for wireless and wired access networks, respectively. To simplify the costs of separated wireless and wired networks, the integration of these two networks into a single shared optical infrastructure becomes essential. The primary concern is to transmit a BB signal in coexistence with wireless signals on a single wavelength along a WDM-PON in a cost-effective way with acceptable performance. In the last years, progress in direct-modulation of a laser has been reported and several schemes based on external modulation to generate a multiband OHS have also been demonstrated.

In this chapter, a literature review of the different schemes to generate an OHS composed by multi-bands such as a BB, a MW band, and a MMW band is carried out. Afterwards, two schemes to generate a multiband OHS based on a $LiNbO_3$ z-cut DP-MZM are presented in detail, along with performance results obtained by numerical simulation.

The remainder of this chapter is organized as follows. In Section 4.2 a literature review about generation of an OHS is provided, starting with directly-modulated lasers, followed by the latest schemes using external modulation proposed in the literature, mainly based on $LiNbO_3$ MZMs. An optical transmitter scheme based on a z-cut DP-MZM capable to deliver a BB signal and two wireless services in three separated bands is evaluated by numerical simulation in Section 4.3.1. Furthermore, a modified scheme based on the same optical transmitter is evaluated in Section 4.3.2 through numerical simulation, and is shown to be capable of delivering to the end-user three different services: a BB signal, three different signals at MW band, and a signal at MMW band. At the end of the chapter, the main conclusions of this study are summarized.

4.2 Multi-band OHS generation schemes – Literature review

Optical multi-band signal generation schemes are optical transmitter schemes capable of generating an optical signal composed by multi-bands carried over a single wavelength.

4.2.1 Based on direct modulation of a laser

Direct-modulation is the simplest and cheapest technique to modulate the intensity of an optical carrier. In the direct intensity modulation by multiple services, SCM is used a priori to multiplex different services, including a baseband signal, in the frequency domain and then the subcarrier multiplexed signal modulate directly the optical carrier emitted by a laser. In the last years, the employment of direct modulation of a laser in hybrid optical access networks has been demonstrated [76]-[79].

In [76], a comparative study between a vertical-cavity surface-emitting laser (VCSEL) and a distributed feedback (DFB) laser has been experimentally performed in the transmission over a 26 km SMF PON of narrowband wired and wireless services. The performance of all services confirmed the viability of VCSELs as power-efficient optical sources for converged optical access networks.

In [77], transmission of a BB OFDM signal and three OFDM-UWB wireless signals along a SSMF LR-PON using a directly modulated laser with 4 GHz -3 dB bandwidth is experimentally demonstrated. Successful 100 km SSMF reach for all signals was demonstrated, when common forward error correction (FEC) algorithms, whose bit

error rate (BER) threshold is 10^{-3}, is used. The performance of the four signals was limited mainly due to intermodulation distortion over the BB signal upon direct photodetection, and to degradation introduced on the OFDM-UWB signal of higher frequency due to reduced electro-optic modulation bandwidth of the laser. To overcome the reduced modulation bandwidth of a laser in order to increase the capacity to multiplex more wireless signals in the frequency domain, in [78] the channel sounding technique is employed. In the channel sounding technique, extra RF-pilots are inserted at the edges of each OFDM signal in the frequency domain, to estimate the attenuation introduced by the channel and pre-compensate the attenuation with amplification in the OLT. Transmission of a bundle composed by five different OFDM signals with a bandwidth between 1 GHz and 4.8 GHz, offering quintuple-play services to each user along a LR-PON with reach up to 125 km, is demonstrated in [78] employing a directly modulated laser with 4 GHz bandwidth.

In all of these reported works, the positive chirp degrades the transmitted signals due to the noise distortion generated by the interaction of positive chirp with fiber dispersion and consequent reduction of the transmission bandwidth. Since the electro-optic bandwidth of lasers directly modulated by broadband signals is reduced, the positive chirp of the lasers can become a problem to transmit this type of services. In [79], the authors demonstrated that the transmission bandwidth can be increased in transmission systems employing directly modulated lasers by controlling the residual dispersion at the RN with a dispersion compensation module.

The direct modulation of a laser with four and five broadband OFDM signals [78], [79] and their successful transmission was possible because the BB OFDM signals have a confined spectrum with higher spectral efficiency than binary BB modulation formats such as NRZ signal. However, when employing a binary modulation format in BB for GbE provision, higher crosstalk degradation on the wireless OFDM signals is expected, thereby degrading the performance and reducing the transmission reach.

The utilization of direct modulation of lasers in hybrid access networks is limited to the low frequency signals, due to the reduced bandwidth of commercialized lasers and to the small transmission distance achievable due to interaction of the chromatic dispersion of the fiber with the positive chirp of lasers diodes. To overcome these limitations, several schemes to transmit the RF signals by using external modulation based on $LiNbO_3$ MZMs have been investigated. Furthermore, optical transmitter schemes based on $LiNbO_3$ MZMs adequate to generate signals at three distinct bands,

namely BB, MW band, and MMW band, using components of reduced bandwidth, have been extensively investigated [80]. In the next sub-section, the most recent methods proposed in the literature, mainly based on $LiNbO_3$ MZMs, are presented.

4.2.2 Based on external modulation

A cost-effective multi-services hybrid access network has been intensively investigated where external modulation is employed to integrate wired and wireless services at the CO over a single wavelength. In the last years, several schemes based on external modulation have been proposed. A comparison between three configurations of external optical modulation employing a DE-MZM to realize OSSB modulation based on the phase-shift method, for simultaneous broadband data transmission at BB and MMW, allowing the coexistence of optically fed wired and wireless access networks, is carried out by simulation in [81].

The scheme proposed in [82] is based on SCM of three signals to accomplish simultaneous modulation by baseband, MW and 60 GHz band signals using a single electro-absorption modulator (EAM). The EAM is the key device for electrical-to-optical conversion over a wide range from DC to the 60 GHz band. However, the signal performance is limited by the EAM nonlinearity, residual chirp, and crosstalk among the three signals. Additionally, the method requires a high-frequency local oscillator (LO) and is severely limited by RF power fading induced by chromatic dispersion, due to the high frequency subcarriers employed.

A new approach for simultaneous multiband generation and high-dispersion-tolerant transmission was demonstrated in [83]. The block diagram of the scheme considered is shown in Fig. 4.1. However, this scheme requires the cascade of two single-electrode Mach-Zehnder modulators (SE-MZMs) and an OF between them, for generation of OSSB from the ODSB signal at the output of the first MZM. The second MZM is biased at MITP to suppress the optical carrier, and thus accomplishes optical up-conversion without spectrum overlapping.

At the receiver, the different bands of OHS are separated by optical filtering. The 60 GHz signal is recovered in the MMW receiver, and the remainder optical signal is split between the MW and BB receivers.

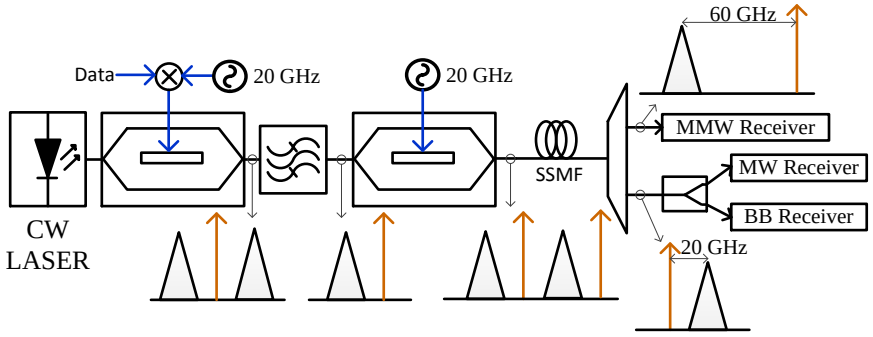

Figure 4.1 – Multiband OHS generation scheme based on the cascade of two SE-MZMs with and optical filter between them [83].

Another optical transmitter scheme capable of generating simultaneously a 1.25 Gbit/s OOK BB signal and a 20 GHz 622 Mbit/s OOK-ASK RF signal after photodetection, using a single x-cut DP-MZM, is demonstrated in [84]. The optical transmitter scheme is shown in Fig. 4.2. The BB and the RF signals are used to modulate independently the optical signals in different x-cut sub-MZMs, which are added optically at the output of the main Y-junction of the DP-MZM, adjusting the bias voltage, V_{bias}. After optical transmission towards the end-user, the optical BB signal is separated from the optical RF sidebands through a FBG along with an optical circulator. After the optical BB signal is reflected by the FBG, it is detected by a low-speed photodetector, while the remainder optical signal becomes an optical double sideband-suppressed carrier (ODSB-SC) signal, which results in frequency doubling after photodetection.

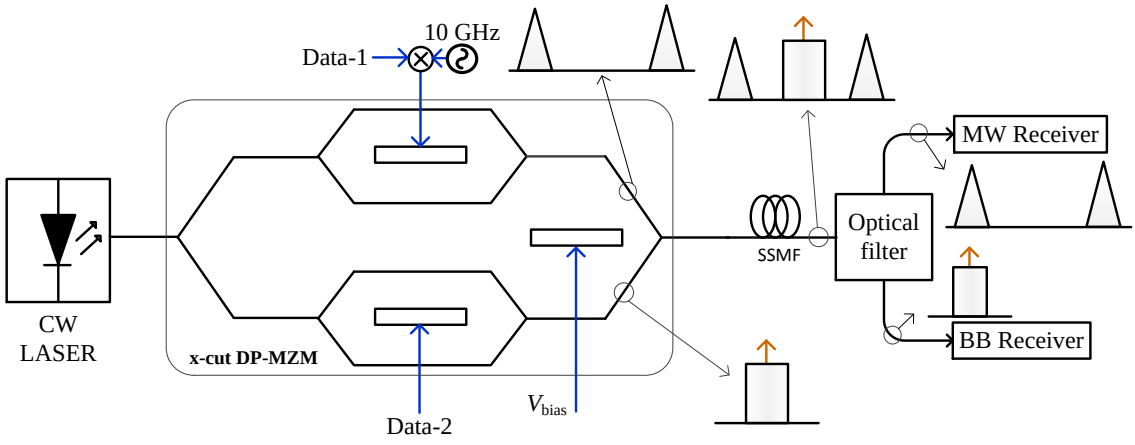

Figure 4.2 –Multiband OHS generation scheme based on x-cut DP-MZM [84].

In this scheme, an OOK-ASK signal is delivered centered at 20 GHz using an oscillator at half the frequency of the transmitter, due to the generation of an ODSB-SC signal at the input of the MW receiver.

In [85], an optical transmitter scheme based on an x-cut DP-MZM followed by a SE-MZM is implemented, to accomplish optical up-conversion. The block diagram of this scheme is shown in Fig. 4.3. This optical transmitter generates an OHS capable of generating three different band signals after photodetection: BB, MW and MMW signals. The RF signals are obtained from ODSB-SC signals, which results in doubling and quadrupling the frequency of the signals.

In the DP-MZM, the upper sub-MZM optical signal is modulated by a 1.25 Gbit/s OOK-ASK RF signal, using bias at the MITP to suppress the optical carrier, whereas the lower sub-MZM optical signal is modulated a 1.25 Gbit/s differential phase shift keying (DPSK) signal. After up-conversion, the OHS is transmitted towards the end-user. After transmission, two FBGs with optical circulators are used to separate the two optical bands, which are detected using separate receivers. The optical MW signal is split into two signals, one is detected by an MW receiver, and the other is filtered to obtain one sideband, which is remodulated by the upstream OOK signal.

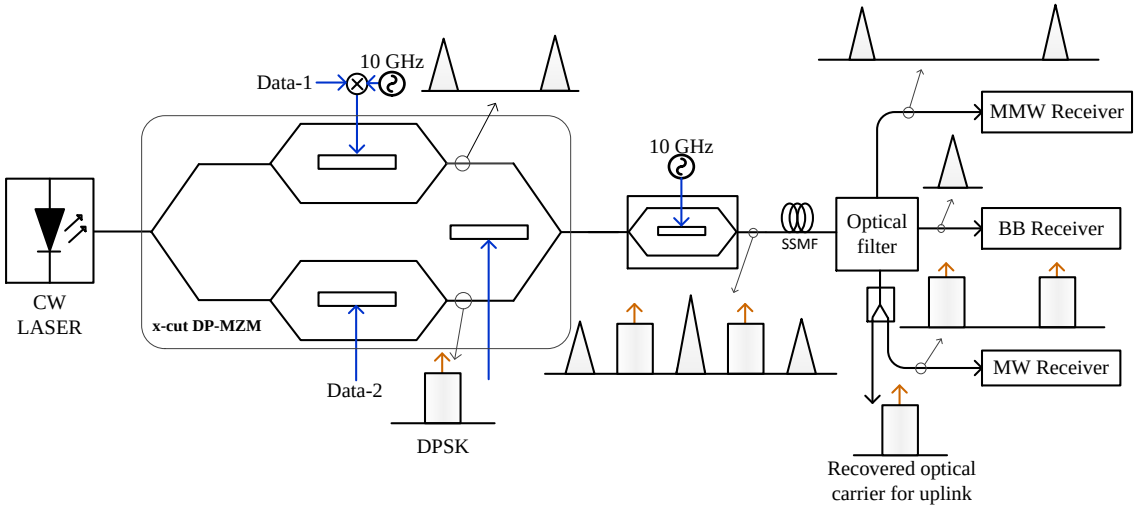

Figure 4.3 - Multiband OHS generation scheme based on the cascade of an x-cut DP-MZM and a SE-MZM [85].

Upstream symmetric data transmission is obtained through re-modulation of the downstream DPSK signal. Therefore, the architecture configuration shown in Fig. 4.3 is a configuration of reduced cost, since no additional light source and wavelength management are required at the end-user premises equipment.

A new scheme for generation of an OHS based on a DP-MZM, with new approach to demultiplex the different signals at the end-user side, has been demonstrated in [86]. A simplified block diagram of this scheme is depicted in Fig. 4.4. Unlike the previous

configurations, in this configuration all signals are jointly recovered and separated in the electrical domain by electrical filtering. The RF signal is separated from the BB signal in the MW receiver through electrical filtering. This configuration has the advantage of making the receivers independent of the wavelength, since it does not require any optical filter.

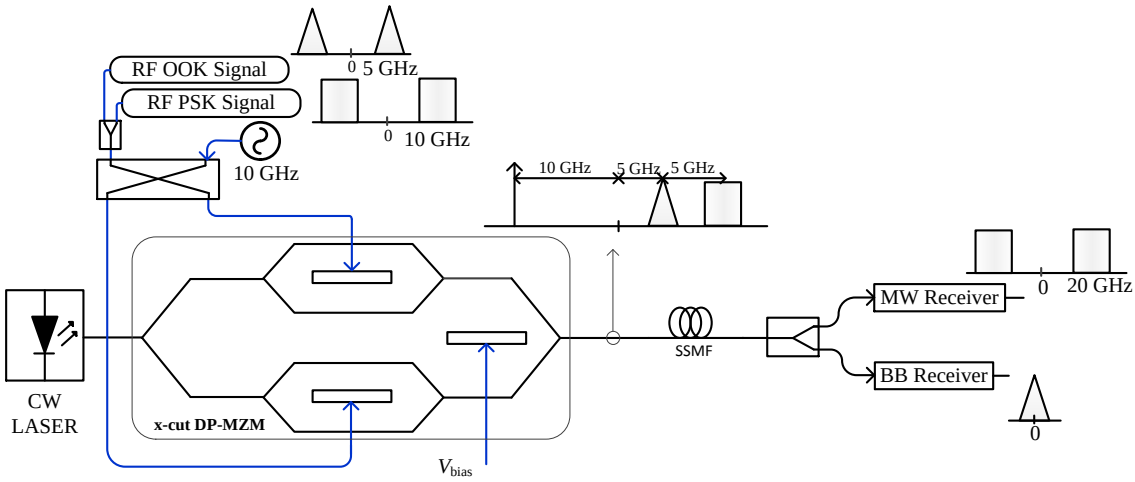

Figure 4.4 – OTSSB modulation of two different signals using an x-cut DP-MZM [86].

In [86], a 5 GHz 1.25 Gbit/s OOK RF signal, a 10 GHz 312.5 MSymbol/s quadrature phase-shift-keying (QPSK) modulated signal, and a 10 GHz sinusoidal signal are combined to modulate a single wavelength in OTSSB, using a DP-MZM.

To recover the wired BB signal, only a low-speed photodetector is required. Furthermore, there is no RF power fading issue because an OTSSB modulation with suppressed carrier is used in the proposed system. Moreover, a frequency doubling for optical RF signal generation is achieved, thereby reducing the bandwidth requirement of the RF transmitter, which is very important for RoF systems with MMW band signals.

Recently, an optical transmitter configuration based on the cascade of two MZMs inside an interferometric structure has been demonstrated [87]. The interferometric Mach-Zehnder structure of the optical transmitter is shown in Fig. 4.5.

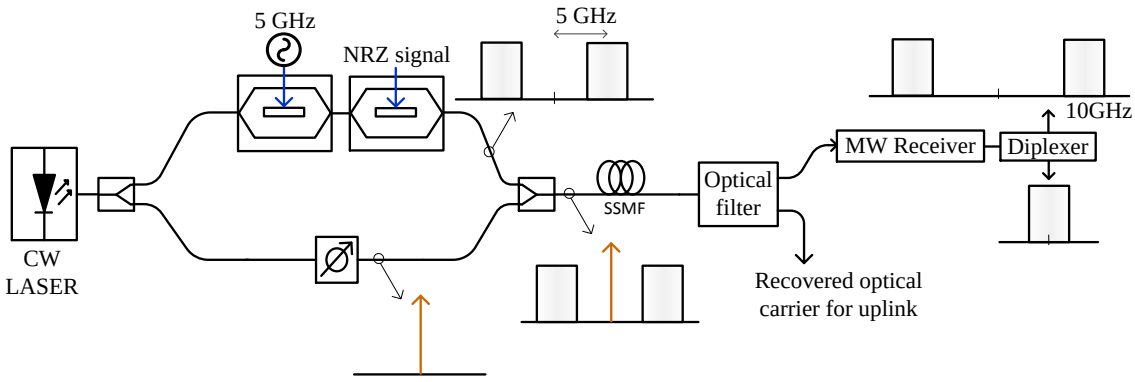

Figure 4.5 – Optical transmitter based on the cascade of two SE-MZMs in one arm of a Mach-Zehnder interferometric structure [87].

A CW signal is first divided into two paths by a 3-dB directional coupler. In the upper path, the first MZM is biased at the MITP and is driven by a 5 GHz sinusoidal signal to produce two coherent optical tones with a frequency separation of 10 GHz [88]. Then, in the second MZM, the two phase-locked optical tones are modulated by a 5 Gbit/s NRZ signal, generating an ODSB-SC signal. In the lower path, the power of the un-modulated CW signal is adjusted by a variable optical attenuator (VOA) and recombined with the optical signal from the upper path.

The resulting optical signal is transmitted through optical fiber towards the final user. At the end-user side, an optical filter based on a passive optical interferometer with a differential delay of 100 ps (free spectral range of 10 GHz) is used to optically demultiplex the distributed CW and the RoF signals. An ODSB-SC modulated signal is obtained at the input of the MW receiver, whereas the CW signal is used as optical carrier for uplink transmission. The coherent beating between the two modulated tones generates the RF signal at two times the frequency of the LO used in the transmitter, while the self-beating of the NRZ signal produces the BB detected signal. The BB signal and the MW signal are separated by electrical filtering in the diplexer.

In the same year, an evolution of the optical transmitter presented before has been proposed to support a BB signal different from the wireless signal [89]. The transmitter scheme is shown in Fig. 4.6. To achieve that goal, an MZM is added in the lower optical path of Fig. 4.5, after the VOA.

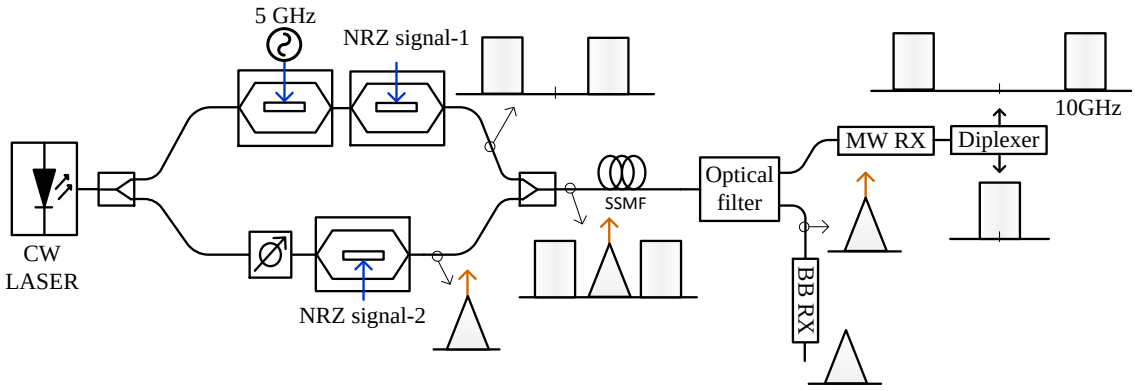

Figure 4.6 - Optical transmitter based on the cascade of two SE-MZMs in one arm and a single SE-MZM in the other arm of a Mach-Zehnder interferometric structure [89].

The operation principle of the transmitter scheme depicted in Fig. 4.6 is identical to that of the scheme shown in Fig. 4.5, with the exception of an extra MZM (MZM in the lower path) added to enable modulation of the optical carrier by a BB signal. The operation principle to recover the different signals is different from that used in the scheme shown in Fig. 4.5, because the optical filter based on a passive optical delay interferometer with free spectral range equal to 10 GHz demultiplexes the different optical bands to different receivers. At the upper output of the optical filter an ODSB-SC signal is obtained which generates an RF modulated signal centered at 10 GHz, after photodetection. The RF signal can then be directly radiated by an antenna. The self-beating of the sidebands generates a BB signal with the same information that is contained in the MW wireless signal. At the lower output of the optical delay interferometer, an optical carrier modulated by the BB signal is obtained. In order to recover that BB signal, a low-speed photodetector is required.

To reduce the bandwidth required for the components used in the optical transmitters, to deliver MW and MMW modulated signals, and simultaneously overcome the chromatic dispersion effect, ODSB-SC modulation has been demonstrated to be more effective, compared with ODSB modulation. ODSB-SC modulation reduces the bandwidth required for the components to one half, because the signal generated after photodetection is located at the frequency equal to the optical sideband frequency separation. Furthermore, ODSB-SC modulation is tolerant to chromatic dispersion, since a single beating occurs in the photodetection, and thus destructive interference does not occur.

However, in most optical schemes previously presented the RF modulated signal delivered in the MW or MMW band contains the same information of the signal

delivered at BB. In the next section, two optical transmitter schemes capable of delivering a BB signal and wireless signals carrying independent information are presented.

4.3 Transmitter schemes based on a z-cut DPMZM

In this section, the performance of two optical transmitter schemes adequate to generate an OHS capable of delivering simultaneously to the end-user services in three separated bands, namely BB, MW band and MMW band, on a single optical carrier, using a single external modulator, will be discussed and evaluated. The external modulator considered is a z-cut DP-MZM [63].

4.3.1 Generation of three-wireless bands and one baseband signal

An optical transmitter scheme capable of generating an OHS composed by a wired signal in coexistence with two different wireless signals (service 1 and service 2) [90], [91] is presented in this section. The OHS at the receiver side, by self-heterodyning in a high-speed photodiode, generates the two different wireless services in three separate bands: 3.1 to 10.6 GHz, 57 to 64 GHz, and 41 to 48 GHz, using an optical filter to separate the wired signal from the wireless signals of the OHS at the input of the receiver.

4.3.1.1 Operating principle of the transmitter

Figure 4.7 illustrates the conceptual diagram of the proposed optical transmitter. The transmitter employs a single integrated external modulator, a z-cut DP-MZM. This consists of two sub-MZMs A and B, one in each arm of a main MZM structure (MZM C), integrated into a single z-cut LiNbO3 chip, as explained in Chapter 3. Each sub-MZM consists of a z-cut MZM, with two phase modulators per MZM.

The CW signal from a single mode laser is injected into the DP-MZM, and is split equally between the two sub-MZMs. The two sub-MZMs are operated independently. The sub-MZM A is biased at the QP, with the DC voltage - $V_\pi/2$ added to the RF signal in the upper electrode. The electrical signals combined in both outputs of the 90º hybrid coupler drive the two electrodes of the sub-MZM A.

At the output of the sub-MZM A an OTSSB signal is obtained, with the optical spectra of the services 1 and 2 on opposite sides of the optical carrier, with a frequency separation of f_{s1} and f_{s2} from the optical carrier, respectively.

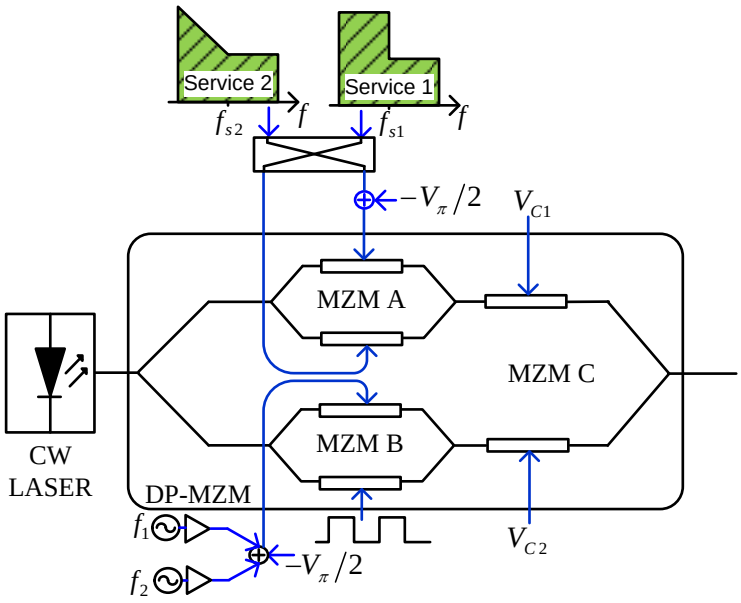

Figure 4.7 - Conceptual diagram of the proposed optical transmitter.

The optical spectrum at the output of sub-MZM A is sketched in Fig. 4.8.

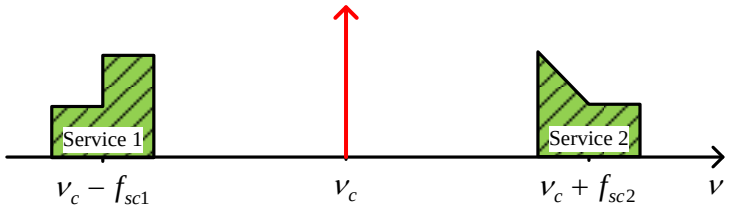

Figure 4.8 - Sketch of the optical spectrum at the output of sub-MZM A.

The sub-MZM B, biased at the QP, is driven as the DE-MZM was driven in [92]. An RF signal composed by two RF sinusoidal signals with frequencies f_1 and f_2 drives the upper electrode, whereas the lower electrode is driven simultaneously by a NRZ BB signal. The spectrum of the resulting optical signal at the output of sub-MZM B is sketched in Fig. 4.9.

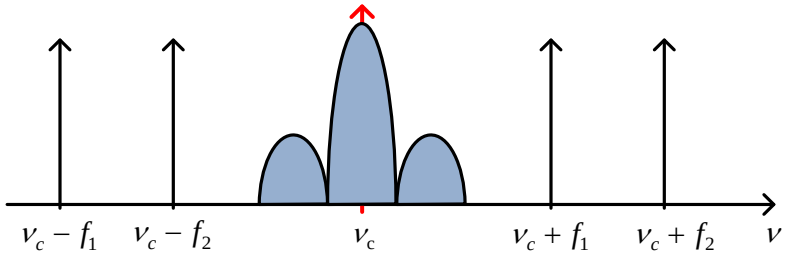

Figure 4.9 - Sketch of the optical spectrum at the output of sub-MZM B.

The optical signals at the output of each sub-MZM are injected into the phase modulators of the main MZM, where the phase shift in each phase modulator should be controlled in order to produce as much as possible a constructive interference at the output of the DP-MZM combiner. The resulting optical signal at the DP-MZM output is sketched in Fig. 4.10. In this figure, neither intermodulation nor harmonic distortion spectral components resulting from nonlinearity of the DP-MZM are considered.

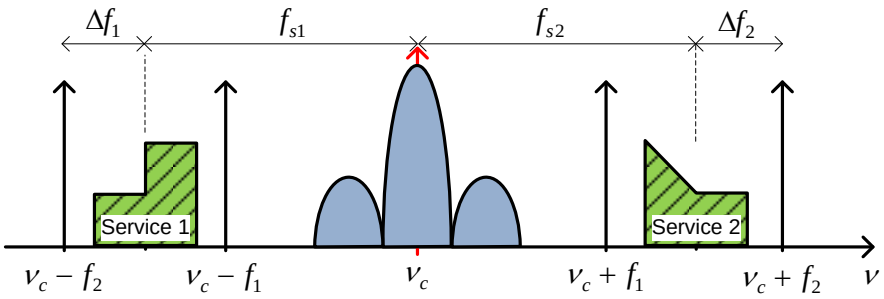

Figure 4.10 - Sketch of the optical spectrum at the DPMZM output.

4.3.1.2 Generation of wireless bands by self-heterodyning

At the receiver side, the OHS is sent to an FBG along with an optical circulator to separate the wired service from the wireless services. Fig. 4.11 depicts in detail the scheme used to demultiplex the wired signal and wireless signals from the OHS, and the generation of the two wireless services in multi-bands based on self-heterodyning in a high-speed photodiode.

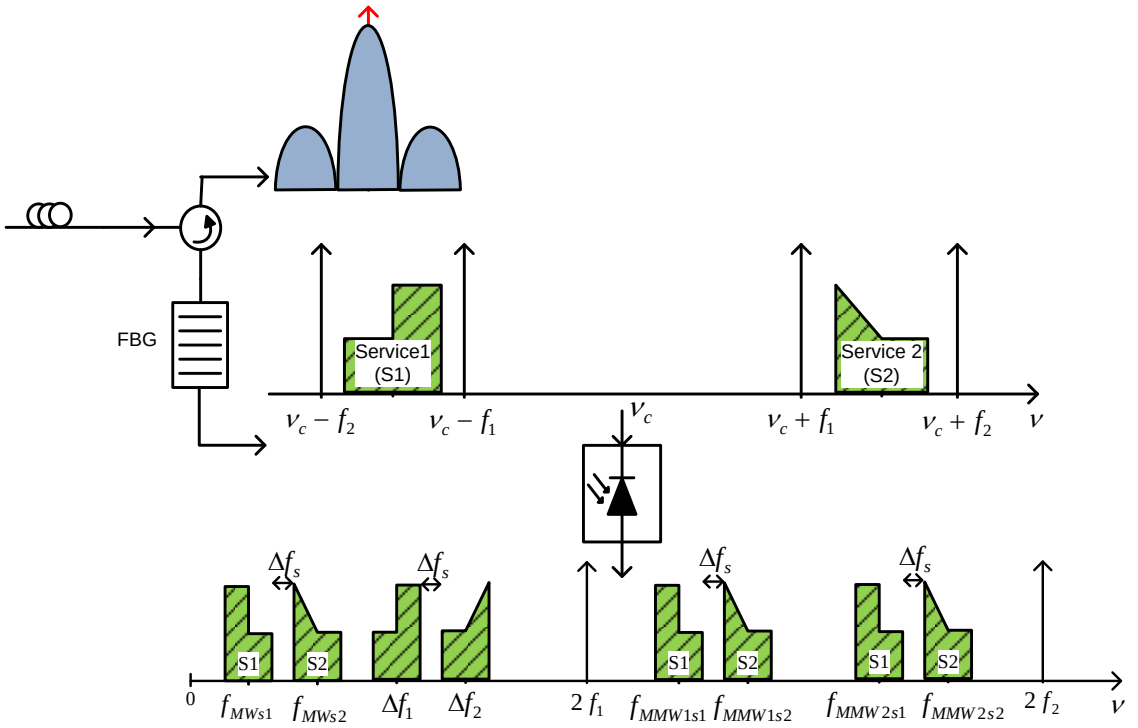

Figure 4.11 - Scheme to demultiplex the wired service and wireless services from the OHS and generation of multi-bands by self-heterodyning in a high-speed photodiode.

The service 1 signal, after self-heterodyning in the photodiode with the optical spectral components at ν_c-f_1, ν_c+f_1, and ν_c+f_2, is located in the MW band at frequency f_{MWs1} and in the MMW band at frequencies f_{MMW1s1} and $f_{MMW2s1,}$ respectively. Simultaneously, the service 2 signal, by self-heterodyning in the photodiode with the optical spectral components at ν_c+f_1, ν_c-f_1, and ν_c-f_2, is located in the MW band at frequency f_{MWs2} and in the MMW band at frequencies f_{MMW1s2} and f_{MMW2s2}. Here Δf_s is the guard band between the service 1 and service 2 signals. The two signals at frequencies Δf_1 and Δf_2 do not correspond to the modulating signals injected in the 90º hybrid coupler, because the service 1 and service 2 signals undergo a frequency reversal (rotation of the spectrum) in the self-heterodyning process with the optical spectral components ν_c-f_2 and ν_c+f_2 respectively.

These signals are undesired, and then the frequencies f_{s1}, f_{s2}, f_1 and f_2 should be chosen in order to avoid that Δf_1 and Δf_2 coincide with the frequencies of the desired bands. From, Fig. 4.10 and Fig. 4.11 the following equations can be derived:

$$f_{MMW2s1} = f_2 + f_{s1} = 2 f_{s1} + \Delta f_1, \tag{4.1}$$

$$f_{MMW2s2} = f_2 + f_{s2} = f_{MMW2s1} + \Delta f_s, \tag{4.2}$$

$$f_{MMW1s1} = f_{s1} + f_1, \tag{4.3}$$

$$f_{MMW1s2} = f_{s2} + f_1, \tag{4.4}$$

$$f_{s2} = f_{s1} + \Delta f_s, \quad (4.5)$$
$$f_2 = f_{s1} + \Delta f_1, \quad (4.6)$$
$$f_{MWs1} = f_{s1} - f_1, \quad (4.7)$$
$$f_{MWs2} = f_{s2} - f_1, \quad (4.8)$$
$$\Delta f_2 = \Delta f_1 - \Delta f_s. \quad (4.9)$$

In order to ensure the delivery of services 1 and 2 in the two separated bands, 3.1 to 10.6 GHz (UWB) and 57 to 64 GHz, the frequencies f_{MMW2s1} = 58 GHz and Δf_1 = 11 GHz, were fixed. Considering Δf_s = 2 GHz, enough to separate the two RF signals in the receiver, (4.1) and (4.5) yield f_{s1} = 23.5 GHz and f_{s2} = 25.5 GHz. With f_{s1} and f_{s2} known, (4.1) or (4.6) yield f_2= 34.5 GHz. Using (4.2), f_{MMW2s2}= 60 GHz is obtained. Fixing f_{MWs1}= 5 GHz, from (4.7) f_1= 18.5 GHz is obtained and (4.3), (4.4) and (4.8) yield f_{MMW1s1}=42 GHz, f_{MMW1s2}=44 GHz, and f_{MWs2}=7 GHz, respectively.

In summary, the wireless service 1 and wireless service 2 signals should be up-converted to the frequencies equal to 23.5 GHz and 25.5 GHz, respectively, whereas the sinusoidal signals that drive the upper electrode of sub-MZM B should have frequencies equal to f_1 = 18.5 GHz and f_2 = 34.5 GHz, in order to generate by self-heterodyning at the output of a high-speed photodiode the wireless service 1 signal at frequencies 5 GHz, 42 GHz, and 58 GHz, and simultaneously the wireless service 2 signal at frequencies 7 GHz, 44 GHz and 60 GHz. The drive signals of the transmitter are adjusted/up-converted to these frequencies and the performance of the transmitter is assessed in the next sub-section.

4.3.1.3 Modeling and optimization of the transmitter

The scheme of the simulation setup used to evaluate the performance of the optical transmitter is presented in Fig. 4.12. The drive signals of the sub-MZM A considered are: service 1 is a 400 Mbit/s 16- QAM OFDM signal up-converted to the central frequency of 23.5 GHz; service 2 is an 800 Mbit/s 16-QAM OFDM signal up-converted to the central frequency of 25.5 GHz. The main parameters of the OFDM services are gathered in Table 4.1.

Table 4.1 - Main parameters of the OFDM modulation for each wireless service.

	Service 1	**Service 2**
Central frequency [GHz]	23.5	25.5

Data rate [Mbit/s]	400	800
Number of subcarriers (N)	256	256
Cyclic prefix (CP)	0 and 1/8 (32 samples)	0 and 1/8

The CW signal is generated by a laser with linewidth of 1 MHz and 10 dBm of power. The DP-MZM is assumed to be balanced ($\gamma_A = \gamma_B = \gamma_C = 1$) and the half-wave voltage V_π of all sub-MZMs is assumed equal to 5 V. Initially, the voltages V_A and V_B are assumed equal to 0 V. The lower electrode of sub-MZM B is driven by a digital signal generated by a 1.6 Gbit/s pseudo-random binary sequence of length 2^{30}-1, NRZ encoded and with DC component blocked, whereas the upper electrode is driven by two sinusoidal signals of equal amplitude.

At the output of the DP-MZM, a 3rd-order super Gaussian OF with bandwidth of 72 GHz (> $2f_2$) centered at 1550 nm is used to suppress all optical spectral components with frequencies above f_2. In practice, the OF can also be used to limit the out-of-band amplified spontaneous emission (ASE) noise power generated by the erbium-doped fiber amplifier (EDFA) used at the output of the DP-MZM to compensate the insertion loss or to boost the level of the OHS to the level desired at the input of the SSMF. However, in a WDM access network the OF can be replaced by the multiplexer.

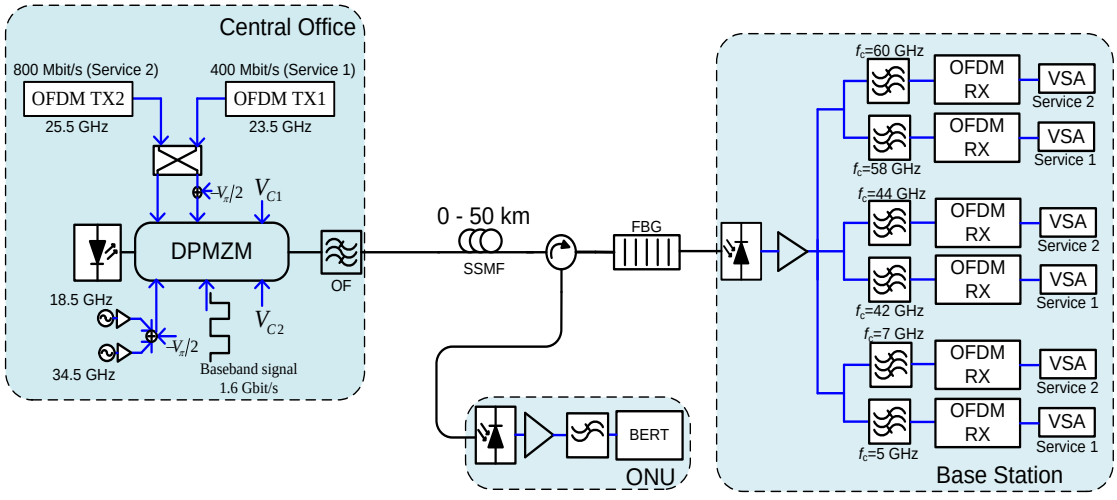

Figure 4.12- Scheme of the simulation setup.

At the input of the ONU/BS, an FBG with a bandwidth of 30 GHz and Gaussian apodization [93] with 100% reflectivity is employed to separate the wired signal from the wireless signals. The optical wired signal reflected by the FBG is sent through an

optical circulator to a low-speed optical receiver, where it is detected by a photodiode (with responsivity of 0.9 A/W, thermal noise spectral density of 2×10^{-11}A/√Hz, and dark current of 2 nA) and the photocurrent is amplified and filtered by a 1.2 GHz (0.75×1.6 GHz) Bessel low-pass filter (LPF) and sent to a BER tester (BERT), which assesses the performance of the wired signal through BER estimation using the Gaussian approximation [94]. The optical signal transmitted through the FBG is converted to the electrical domain using a high-speed PIN photodiode (with responsivity of 0.65 A/W, thermal noise of 2×10^{-11} A/√Hz, and dark current of 2 nA). The RF amplifiers employed have unlimited flattened frequency response, 15 dB gain and current noise spectral density of 2×10^{-12} A/√Hz.

The wireless three-band RF signal, obtained by self-heterodyning, as explained before and illustrated in Fig. 4.11, is amplified and split equally between three arms corresponding to the three separate bands. In each arm, the wireless signal is again split equally into two signals. The two resulting signals in each band are injected in RF Butterworth band pass filters where the desired services are selected. Each service is applied to the respective OFDM receiver (OFDM RX) to perform down-conversion to the BB and OFDM demodulation, including removal of the CP, serial-to-parallel conversion, inverse fast Fourier Transform (IFFT), subcarriers equalization, symbol de-mapping and parallel-to-serial conversion. The performance of the wireless signals is assessed by the root mean square error vector magnitude (EVM) [95], through a vector signal analyzer (VSA).

The simulation results were obtained using VPI TransmissionMaker 8.5^{TM}. In order to evaluate the performance of the optical transmitter, the critical parameters were optimized for an optical back-to-back (B2B) configuration. The performance of the optical transmitter was optimized starting by determining the optimum RF power of the two RF sinusoidal signals, required to drive the sub-MZM B in order to maximize the RF power of service 1 and 2 signals at the input of the OFDM RXs and consequently minimize the EVM. The RF sinusoidal signals in optical domain perform the function of the optical carriers in the photodetection of the wireless signals.

Figure 4.13 shows the RF power for both services in all bands at the input of the OFDM-RXs, as a function of the RF drive power of the sinusoidal signals, considering both sinusoidal signals with equal amplitude and the RF drive power of services 1 and 2 injected into sub-MZM A fixed at 3 dBm. The optical modulation index *m* of the digital

NRZ signal is fixed at 0.2, with V_{pp} representing the peak-to-peak drive voltage of the digital NRZ signal.

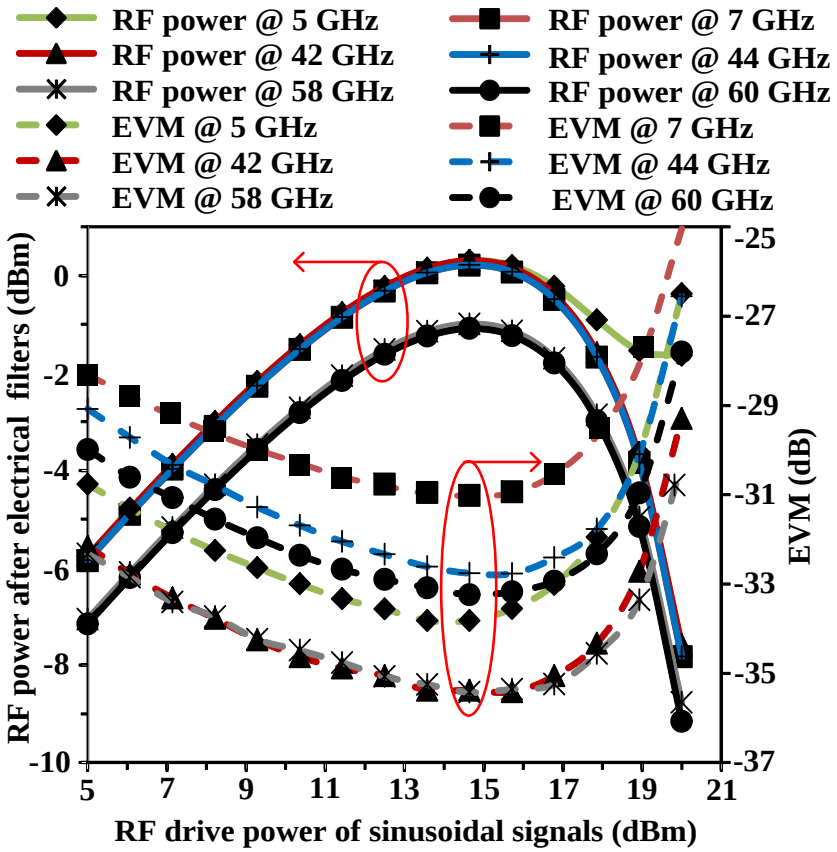

Figure 4.13 - EVM and RF power for the two services in all bands in optical B2B configuration as a function of the RF sinusoidal signals drive power.

The EVM degradation of the wireless signals for low power levels is mainly due to the Gaussian noise but, as the drive power of the sinusoidal signals increases, the EVM improves and the RF power of the services 1 and 2 in any band increases until the drive power of the sinusoidal signals reaches 14.65 dBm. Therefore, the optimal power to drive the sinusoidal signals is 14.65 dBm, which corresponds to the drive power for which the optical tones reach their maximum in the optical domain [91]. The RF power in all bands after photodetection is proportional to the optical power of the optical spectral components located at ν_c-f_1, ν_c+f_1, ν_c-f_2 and ν_c+f_2, and to the drive power of the services 1 and 2 injected in the sub-MZM A.

The optimum DC voltages V_{C1} and V_{C2} to control the phase difference between the two arms at the input of the DP-MZM main combiner are investigated. The power of the two RF sinusoidal signals is fixed at 14.65 dBm and, in order to simplify the

analysis, voltage V_{C2} is considered null ($V_{C2} = 0$). Figure 4.14 shows the BER of the BB signal and the EVM of services 1 and 2 in all bands, as V_{C1} increases from 0 to V_π.

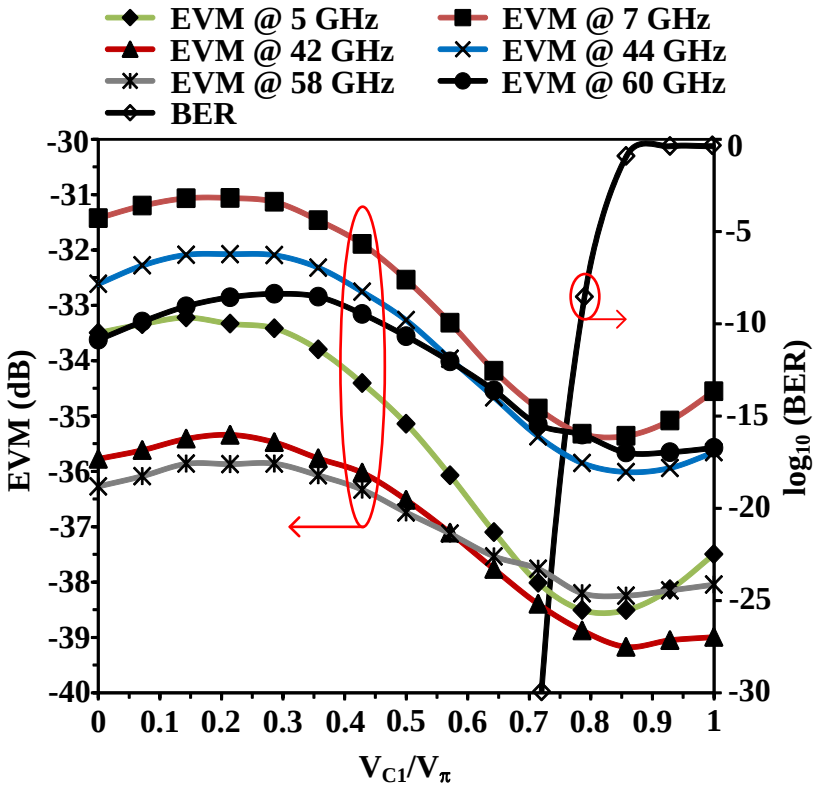

Figure 4.14 - EVM of all wireless services in any band, and BER of the baseband signal as a function of DC voltages V_{C1}, considering $V_{C2} = 0$.

By examination of Fig. 4.14, a trade-off can be observed between the BER of the BB signal and the EVM of the wireless services in all bands, as the DC voltage V_{C1} increases from 0 to V_π.

The BER degradation of the BB signal as V_{C1} increases is due to the type of interference which occurs at the output of the DP-MZM combiner. For values of V_{C1} higher than $0.5V_\pi$, the optical carriers at the output of the sub-MZM A and sub-MZM B begin to interfere destructively, and the power of the resulting optical carrier at the output of the DP-MZM cancels when V_{C1} is near V_π, preventing the recovery of the BB signal at the ONU by direct detection.

Regarding the wireless signals, the phase of the optical spectral components with frequencies ν_c-f_1, ν_c+f_1, ν_c-f_2 and ν_c+f_2 are kept unchanged, whereas the phase of the OTSSB signal suffers a phase shift from 0 to π as the voltage V_{C1} increases from 0 to V_π. Unlike the BB signal, for which interaction of the different optical carriers occurs at the output of the DP-MZM, in the case of the wireless signals the interaction occurs

upon photodetection, since there is no spectral overlap between the OTSSB signals from the sub-MZM A and optical tones from the sub-MZM B. As demonstrated in Appendix D, namely in Section D.2, the phase shift induced by the DC voltage on the phase modulator is translated to the electrical domain, affecting the phase of the subcarriers of the received OFDM signal. Consequently, the QAM data symbols are affected and therefore the EVM of the received OFDM signals vary as V_{C1} increases from 0 to V_{π}, because the OFDM symbols do not contain any pilot subcarriers. Finally, the DC voltage V_{C1} that enables the advantage provided by the EVM variation is $V_{C1} = 0.75V_{\pi}$.

Due to the nonlinear characteristics of the MZMs, when the drive power of the RF signals increases, the second-order intermodulation distortion (IMD2) spectral components fall around the optical carrier [96], [97] and, after photodetection, these spectral components generate third-order intermodulation distortion (IMD3) components difficult or even impossible to remove from the signal by filtering. The IMD2 products at the output of the sub-MZM A, after recombination with the optical signal from the sub-MZM B, degrade the BB signal. Thus, it becomes important to know the maximum drive power of the wireless signals in the sub-MZM A which is tolerated by the BB signal.

Considering, the power of the two RF sinusoidal signals fixed at 14.65 dBm, $V_{C1} = 0.75V_{\pi}$ and $V_{C2} = 0$, the EVM of the wireless signals in all bands and the BER of the BB signal, for different RF drive powers of both wireless services, are evaluated and shown in Fig. 4.15.

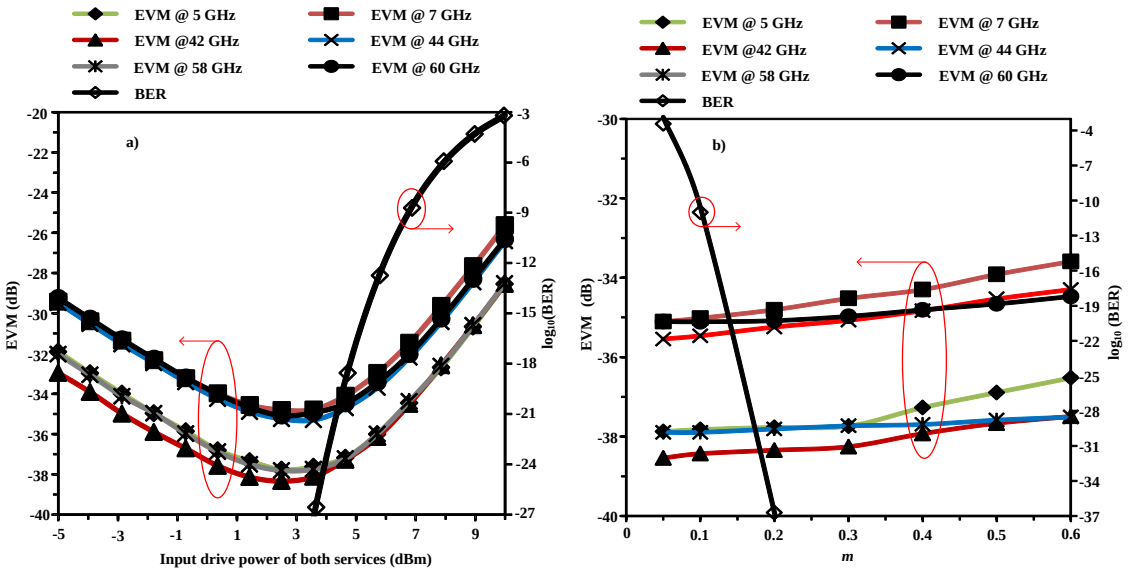

Figure 4.15 – EVM of each service in all bands and BER of the BB signal: a) as a function of the wireless signal drive powers; b) as a function of the modulation index of the BB signal.

From Fig. 4.15 a) it can be concluded that the RF drive power for any service should be lower than 6.79 dBm, in order to keep the BER below 10^{-9}, and the best EVM performance for the wireless signals in any band is obtained for an input wireless drive power equal to 2.5 dBm.

In order to determine the optimum modulation index, *m*, to drive the digital NRZ signal on the sub-MZM B, and to know if increasing the NRZ signal amplitude causes any impact on the wireless signals due to crosstalk, *m* is increased and the BER of the NRZ signal and EVM of the wireless signals in any band are estimated and are shown in Fig. 4.15 b). From Fig. 4.15 b) it can be concluded that *m* should be larger than 0.1 in order to keep the BER lower than 10^{-9}. As *m* increases above 0.1, the wireless services in any band present EVM degradation due to crosstalk of the BB signal on the wireless signals.

4.3.1.4 Tolerance to chromatic dispersion

The tolerance of the modulation scheme to fiber chromatic dispersion is assessed, considering the transmission of the OHS through SSMF characterized by an attenuation coefficient of 0.2 dB/km and a dispersion coefficient of 17 ps/(nm.km), from the CO to the ONU/BS. Fig. 4.16 shows the EVM degradation (EVM values normalized by the EVM values obtained for an optical B2B configuration - Fig. 4.15 b) for all wireless signals in any band, and the BER of the BB signal as a function of the fiber length from the CO to the ONU/BS.

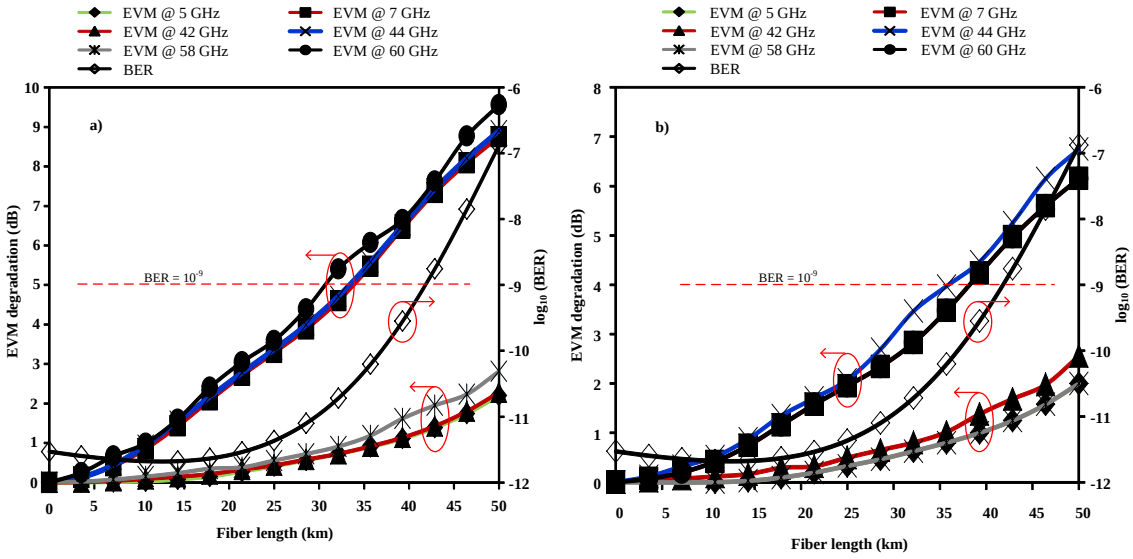

Figure 4.16 - EVM of wireless signals in all bands and BER of the BB signal, for different fiber lengths: a) OFDM signals with CP = 0 and b) OFDM signals with CP = 1/8.

By comparison of the EVM degradation curves shown in Fig. 4.16, it can be observed that the wireless service 2 is more degraded than the wireless service 1, because the data rate of wireless service 2 is higher than the data rate of wireless service 1. A source of degradation in an OFDM transmission system is ISI. The source of the ISI can be chromatic dispersion or polarization mode dispersion (PMD) along the transmission link. The optical fiber simulation model employed considers only the chromatic dispersion. To overcome the ISI, the delay spread due to the chromatic dispersion should not exceed the guard time between the symbols. It has been shown that the minimum CP duration required to eliminate all ISI caused by chromatic dispersion can be expressed as [98]:

$$T_{CP} \geq \frac{c}{\nu_c^2}\left|D_t\right| N\Delta f \tag{4.10}$$

where D_t is the total accumulated chromatic dispersion in ps/pm, N is the number of subcarriers, and Δf the frequency separation between subcarriers.

For the OFDM signals considered, Δf is equal to the inverse of the symbol period. Therefore, as the symbol rate of service 2 is higher than the symbol rate of service 1, the subcarrier frequency separation for service 2 is larger than for service 1. Thus, the minimum CP duration required for service 2 should be larger than for service 1, but in the simulation results shown in Fig. 4.16 they are considered equal, which explain the performance difference between the two services signals observed in Fig. 4.16 a) and in Fig. 4.16 b). It can be concluded that the EVM degradations presented in Fig. 4.16 b) are smaller than the EVM degradations presented in Fig. 4.16 a) due to the presence of the CP in the OFDM symbols, and thus less ISI occurs.

Furthermore, it is observed that the EVM degradation for any case increases with the fiber length. This EVM degradation increase is not due to the power fading induced by chromatic dispersion, since OTSSB is employed, but it is instead due to the fact that the OFDM symbols do not contain pilot subcarriers to perform the linear equalization of phase and amplitude of subcarriers at the receiver.

4.3.2 Generation of two-wireless bands and one baseband signal

The optical transmitter presented in the previous section delivers two different services in three separate wireless bands, and this can be useful because it enables fallback. The

delivery of the same wireless services in separate bands presents however some drawbacks, namely energy and spectrum wasted in the delivery of the same services. In this section, a simplified transmitter scheme capable of delivering different services in different bands is assessed.

The proposed optical transmitter is capable of generating an OHS comprising a 2.5 Gbit/s GPON BB signal, three 200 Mbit/s OFDM channels with frequencies ranging from 3.1 to 4.7 GHz, which corresponds to the 1st group of multi-band OFDM-UWB, and a 397 Mbit/s 58.32 GHz binary phase shift keying (BPSK) signal [99]. Each OFDM signal presents the same characteristics of the OFDM-UWB signals following the ECMA-368 standard [100], except the channel bandwidth. The channel bandwidth does not comply with the specification in the ECMA-368 standard, since Δf = 4.125 MHz is not ensured. More information about modulation and demodulation of multi-band-OFDM-UWB signals following the standard ECMA-368 can be found in Appendix B. To ensure the orthogonality between subcarriers, the minimum Δf of the OFDM signals should be equal to the inverse of the OFDM symbol period [101]. The BPSK signal at the MMW band follows the ECMA-387 standard [102] for the device type A, operating in single carrier block transmission mode A0.

4.3.2.1 Operating principle of transmitter and receiver

The scheme of the proposed optical transmitter is shown in Fig. 4.17. The operating principle of this optical transmitter follows the same principle of the optical transmitter presented in Section 4.3.1, with some differences. The sub-MZM A biased at the QP is now driven with three QPSK-OFDM subcarrier multiplexed signals, up-converted to the frequencies f_1, f_2, f_3, respectively. The three OFDM subcarrier multiplexed signals drive one port of the 90º hybrid coupler, while the other port is driven by an RF BPSK signal up-converted to the frequency f_{sc1} that follows the ECMA-387 standard [102] for the device type A. The sub-MZM B, biased at the QP, is driven by a RF LO signal with frequency f_{LO} and by a NRZ signal, applied to different electrodes [102].

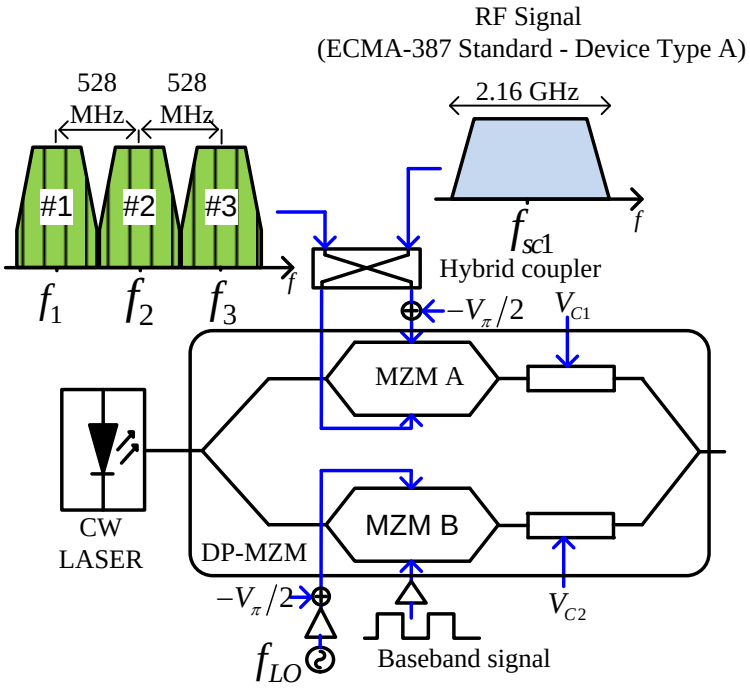

Figure 4.17 - Conceptual diagram of the proposed multiband optical transmitter.

The resulting optical signal at the output of the DP-MZM is sketched in Fig. 4.18 a). In this figure, neither inter-modulation nor harmonic distortion spectral components resulting from nonlinearity of the DP-MZM are considered. Figure 4.18 b) is a sketch of the optical spectrum without the BB signal at the output of the optical filter based on a FBG that separates the wired signal from the wireless signals. In Fig. 4.18 c), a sketch of the electrical spectrum resulting from self-heterodyning in a high-speed photodiode is shown. B_g is the guard band between the optical spectral component at frequency ν_c-f_{LO} and the edge of the closest channel, as sketched in Fig. 4.18 a). In order to ensure that the FBG does not affect the closest wireless channel in the lower sideband, B_g was considered equal to 5 GHz.

The frequencies of the RF signals required to drive the optical transmitter in order to generate, at the output of a high-speed photodiode, three OFDM signals in the MW band (3.1-4.7 GHz) and a MMW wireless personal area network (WPAN) signal at 58.32 GHz, are f_{LO} = 26.16 GHz, f_{sc1} = 32.2 GHz and f_1 = 29.592 GHz (= f_{LO} +3.432 GHz) [99]. The frequencies f_2 and f_3 are easily obtained adding 512 MHz to the frequency f_1.

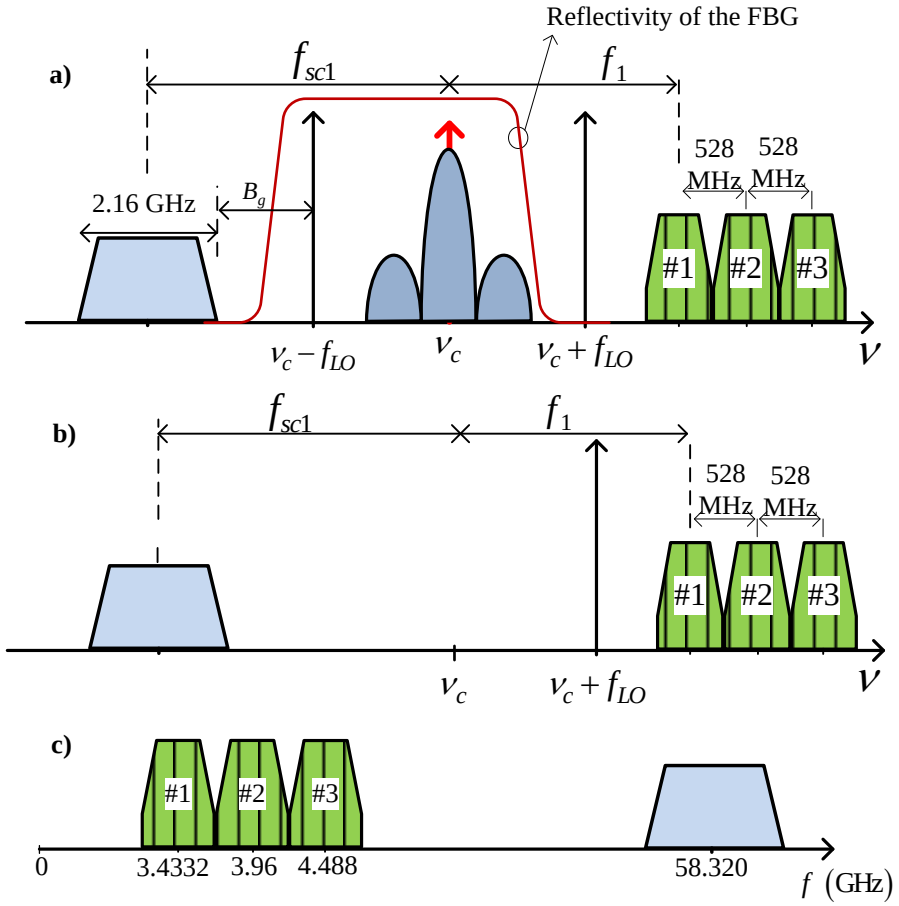

Figure 4.18 - Principle of multiband generation by self-heterodyning in a high-speed photodiode: (a) Spectrum of the optical signal at the output of the DP-MZM; (b) Optical spectrum without the baseband signal and the spectral component at ν_c-f_{LO} at the output of the FBG; (c) Spectrum of the photocurrent at the output of a high-speed photodiode, when the input is the signal illustrated in (b).

4.3.2.2 Simulation setup and transmitter optimization

In Fig. 4.19 is presented the conceptual diagram of the simulated system considered to evaluate the feasibility of the distribution of an OHS generated at the CO over a FTTH network. In the CO, one port of the 90º hybrid coupler is driven by 3 QPSK-OFDM subcarrier multiplexed signals, each of which carries 200 Mbit/s in 128 subcarriers, whereas the other port is driven by a 397 Mbit/s BPSK signal.

The CW signal is generated by the laser with linewidth 1 MHz and 10 dBm of power. The upper arm of sub-MZM B is driven by a RF LO signal with frequency 26.16 GHz, whereas the lower arm is driven by a 2.5 Gbit/s PRBS with a length of 2^{30}-1, NRZ encoded and with the DC component blocked. The DP-MZM is assumed to be balanced, with a half-wave voltage V_π equal to 5 V in all sub-MZMs.

Initially, the voltages V_{C1} and V_{C2} are equal to 0 V. At the output of the DP-MZM, a 3rd order super-Gaussian OF with a bandwidth of 75 GHz, centered at 1550 nm, is used to suppress all optical spectral components with frequencies above ν_c+33.28 GHz.

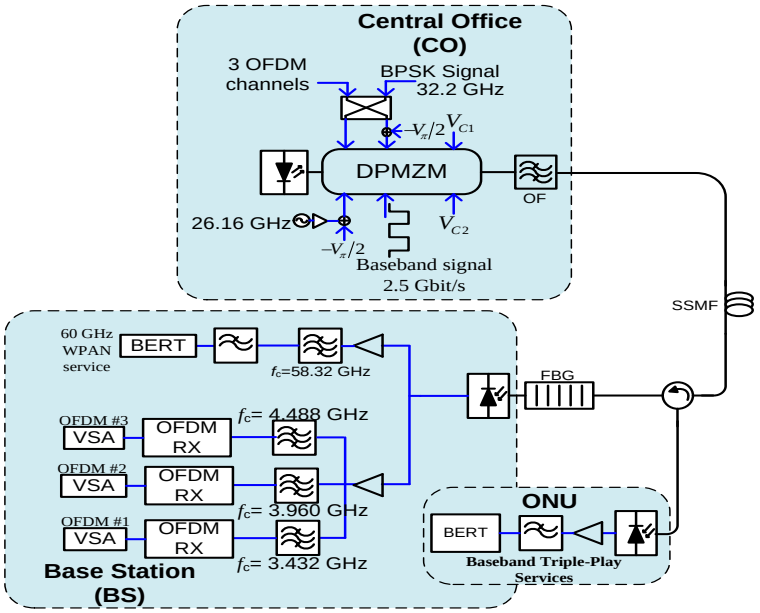

Figure 4.19 - Conceptual diagram of simulated system.

At the input of the BS, a FBG with a bandwidth of 38 GHz and raised-cosine flat-top apodization [93], centered at 1549.9 nm (1550 nm-0.1 nm), with 100% reflectivity is employed to reflect the wired signal to the ONU. In order to study the feasibility of the simultaneous distribution of three OFDM channels and one MMW WPAN signal together with a GPON signal over a hybrid FTTH network, the main critical parameters of the optical transmitter are optimized for an optical B2B configuration.

The drive power for each OFDM signal is fixed at -5 dBm, and the RF drive power of the LO signal is optimized. The best RF drive power that optimizes simultaneously the performance of the OFDM signals at the MW band and the 58.32 GHz BPSK WPAN signal is 12 dBm. The voltages V_{C1} and V_{C2} that drive the phase modulators at the output of each sub-MZM are optimized in order to get the best performance for all signals. The optical modulation index m considered for the digital BB signal is 0.2. Figure 4.20 (a) shows the BER of the GPON signal and the EVM of all OFDM channels, as V_{C2} increases from 0 to V_π, considering V_{C1} = 0 V.

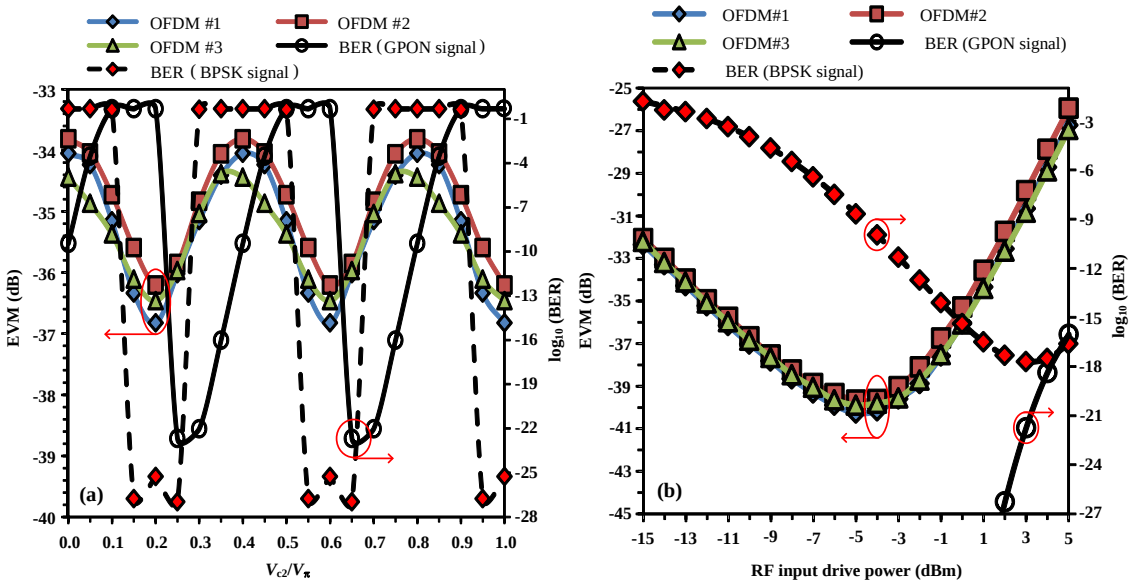

Figure 4.20 - EVM of all OFDM channels and BER of the GPON and BPSK signals, in the optical B2B configuration: (a) for different values of V_{c2} and V_{c1} = 0; (b) for different values of the RF input drive power.

As explained for Fig. 4.14, the optical phase shift generated by the phase modulator with the DC voltage V_{C2} is preserved in the electrical domain, affecting the phase of the subcarriers of the received OFDM signal, as demonstrated in Appendix D, namely in Section D.2. The optical phase shift changes also the phase of the received WPAN BPSK signal, and thus for certain values of V_{C2} the coherent detection are aligned and for others are misaligned. When the phases are aligned, the BER of the BPSK signal reaches its minimum. In the case of the BB GPON signal, the optical carrier at the output of the DP-MZM is canceled for some values of V_{C2} between 0 and V_{π}, preventing the recovery of the BB signal at the ONU by direct detection, which corresponds to the higher BER values. In order to get the best performance for all signals, a minimum value of V_{C2} equal to $0.25V_{\pi}$ is required.

The quality of the RF signals and BB signal is evaluated for different input power levels of the RF signals, for an optical B2B configuration. From Fig. 4.20 (b), it can be concluded that the BER of the GPON signal is negligible for any input RF power level considered and, to keep the BER of the BPSK signal lower than 10^{-9}, the RF power of the BPSK signal should be larger than –5 dBm. Furthermore, it is possible to conclude that the best EVM for all OFDM channels is obtained for an input power equal to - 5 dBm.

4.3.2.3 Study of the chromatic dispersion tolerance

To evaluate the tolerance to fiber chromatic dispersion, transmission of the OHS through SSMF was assumed, considering the linear model for the fiber. At the input of the SSMF, the launched power of the OHS is 3 dBm. Figure 4.21 shows the EVM degradation of the OFDM signal and the BER of the BB 2.5 Gbit/s GPON and 58.32 GHz BPSK signals, for different fiber lengths from the CO to the ONU/BS. The RF drive power of the WPAN BPSK signal is fixed at – 2 dBm, whereas the RF drive power for each OFDM signal is fixed at -5 dBm.

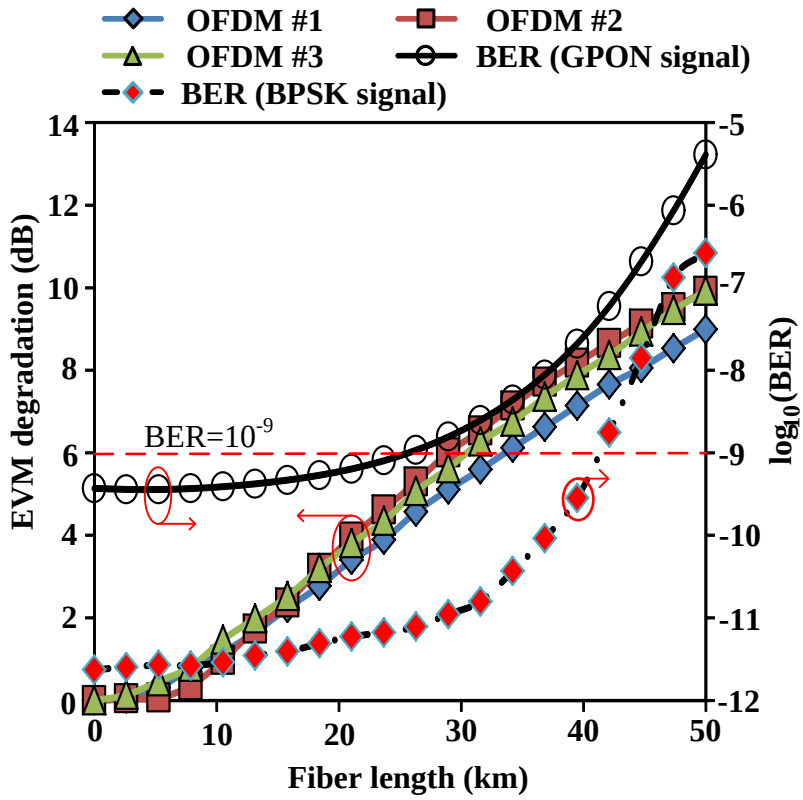

Figure 4.21 - EVM of three OFDM signals and the BER of BPSK signal, for different fiber lengths.

It can be concluded from Fig. 4.21 that the GPON signal can be transmitted through up to 25 km with a BER $\leq 10^{-9}$, whereas the WPAN BPSK signal can be transmitted through up to more than 45 km with a BER $\leq 10^{-9}$. This difference in transmission reach is due to the fact that the WPAN BPSK signal is OSSB modulated, whereas the GPON signal is an ODSB modulated signal. In addition, the GPON signal is strongly affected by chromatic dispersion, once in the electro-optic modulation of the sub-MZM B the chirp cannot be canceled, because the drive signals of each electrode are different. Therefore, even if sub-MZM B is driven in push-pull mode there will be always chirp.

In Fig. 4.21 it is observed that the EVM degradation increases almost linearly with the fiber length, because the OFDM signals do not contain pilot subcarriers to perform linear equalization of the phase and amplitude of each subcarrier at the receiver. The phase of the subcarriers depends on the fiber length because fiber dispersion induces different phase shifts on different subcarriers. This relative phase shift between OFDM subcarriers induces ICI and results in loss of orthogonality [103]. Thus, EVM degradation increases with accumulated dispersion.

4.4 Summary

In any communication system, the transmitter is an essential block of the system, to establish communication between two points with acceptable performance. In this chapter, a study was presented about optical transmitters capable of transmitting a BB signal and wireless signals over a single wavelength through optical fiber.

A review of the recent literature about generation of multiband OHS based on directly modulated lasers and MZM structures was provided. Finally, two transmitter schemes based on a $LiNbO_3$ z-cut DP-MZM, capable of delivering to the costumers a multiband OHS containing signals in the BB and in MW and MMW bands, were presented and studied in detail.

5

OSSB transmission of signals following different standards

5.1 Introduction

Convergence of optical and wireless access networks into a single hybrid optical network has received much attention of the scientific community around the world in the last years, due to the possibility of reducing OPEX of future broadband access networks. LR-PONs allow reducing the OPEX further, since a larger geographic area can be covered with a single CO and without optical-electrical-optical conversions at the middle of the network [13], [33], [53].

In the transmission of multi-services with different quality requirements, several challenges have been raised, namely the transmission of large constellation OFDM signals through at least 100 km with low power penalty. The simplest manner to transmit multi-services is by using IMDD systems, but the ODSB signals transmitted suffer power fading upon photodetection, due to the chromatic dispersion of the fiber. In [53], experimental IMDD of the quintuple-play services based on OFDM over a LR-

WDM-PON employing centralized compensation is discussed, considering the transmission of a custom OFDM-GbE signal carrying Ethernet data and the wireless LTE, WiMAX and OFDM-UWB signals. However, all OFDM signals employed QPSK mapping, and the LTE and WiMAX standardized systems employed dynamic adaptive modulation between 64-QAM, 16-QAM and QPSK mapping [104]. Therefore, demonstration of successful transmission over a WDM-LR-PON should be performed using 64-QAM mapping.

Recently [105], the transmission of 64-QAM LTE signals through an IMDD system resulted in a high power penalty after transmission through 80 km of SSMF, and it was not possible to achieve a reach of at least 100 km due to chromatic dispersion, whereas for 16-QAM and QPSK mapping transmission up to 150 km was numerically demonstrated with reasonable low power penalty. To overcome this problem, OSSB modulation in OFDM direct-detection systems has been used [106]-[109]. OSSB modulation is a spectrally efficient way of reducing the dispersion-induced power fading, at the cost of reducing the transmitted signal power to one half, compared to ODSB modulation.

Due to the nonlinear characteristic of the MZM, both ODSB and OSSB systems must be operated with a small modulation index, in order to avoid harmonic and intermodulation distortion that cause crosstalk between signals. Obviously, a small modulation index means inefficient modulation (less power in optical sidebands) and thus poor receiver sensitivity, because the optical carrier does not carry information. The modulation efficiency is defined by the ratio between the power in the optical sidebands and the total power of the optical signal (sidebands plus optical carrier). In order to increase the modulation efficiency while maintaining reasonably good linearity, ODSB-RC and OSSB-RC modulations have been demonstrated using an optical notch filter [106], [107] in cascade with a MZM or an x-cut DP-MZM [108]. Hui *et al.* [106] used a tunable Fabry-Pérot filter in reflection mode to reduce the optical carrier in high speed OSSB transmission of a subcarrier multiplexed signal, whereas Lim *et al.* [107] used a narrow band FGB to remove a portion of the optical carrier of a millimeter-wave OSSB signal, leaving only a fraction of the optical carrier power for direct-detection at the receiver. However, the optical carrier filtering needs self-tuning when commercial low-cost lasers are employed, due to the wavelength drifts. To overcome this drawback, OSSB-RC modulation with tunable optical carrier to sideband power ratio based on an integrated x-cut DP-MZM has been demonstrated [108]. This approach enables not only

OSSB modulation to overcome the power fading induced by chromatic dispersion, but also adjustable optical carrier reduction to improve the modulation efficiency and consequently the receiver sensitivity. This scheme demonstrates good performance, but the cost of x-cut DP-MZMs is still high. A technique in which the MZM bias voltage is used to tune the optical carrier to sideband power ratio was proposed in [110]. However, this technique only allows obtaining ODSB-RC modulation, and OSSB modulation cannot be obtained without optical filtering. OSSB-RC modulation obtained by optical filtering of an ODSB-RC signal, biasing the MZM below its QP to reduce the power of the optical carrier, has been demonstrated in [111], [112]. This approach is cost-effective, since it does not require an optical notch filter to suppress the optical carrier.

In [109] and [111], [112], OSSB transmission with improved receiver sensitivity was achieved through a trade-off between QPSK OFDM distortion and a bandwidth gap (B_g) between the optical carrier and the data spectrum. A B_g equal to the OFDM signal bandwidth, B_{OFDM}, has been demonstrated to be enough to avoid the second-order intermodulation distortion near the optical carrier, and the intermodulation distortion due to subcarrier-to-subcarrier beating upon photodetection. In radio-over-fiber systems transmitting multi-services based on OFDM signals over multi-bands complying different standards [100], [113], this B_g cannot be ensured since the standardized central frequencies of signals radiated after photodetection should not be changed in the transmitter side, in order to simplify the hardware required in the customer premises equipment.

In this chapter, OSSB-RC transmission along LR-WDM-PON of multi-services based on OFDM signals complying with different standards and different constellation mapping is numerically demonstrated. Furthermore, this chapter addresses the problem of not being possible to ensure a B_g equal to B_{OFDM} in multi-services based on OFDM signals centered at low frequencies of the MW band following different standards, present in the hybrid optical access networks, when the modulation efficiency is enhanced by biasing the MZM near its null intensity point. In this situation, the OFDM signals near DC are strongly affected by intermodulation products which deteriorate their performance. A solution to overcome the intermodulation products is based on driving the different signals with different drive powers. This was demonstrated to be effective to transmit hybrid OSSB-RC signals comprising a custom 1 GHz 16-QAM OFDM-GbE signal, a 20 MHz 64-QAM LTE signal, and three independent OFDM-UWB signals, through a 130 km reach WDM-PON network [114], [115].

This chapter is organized as follows. Section 5.2 describes the modeling of a WDM-PON operating with a single wavelength, and introduces the equivalent block diagram of the system used to evaluate the performance of multi-services based on OFDM. In Section 5.3, the main parameters required to generate each OFDM signal following different standards are presented. Furthermore, simulation results which show an improvement of the modulation efficiency are presented and discussed, following the identification of the optimum drive powers required to overcome the intermodulation distortion of the more impaired signals. Finally, in Section 5.4 a summary of the chapter is presented.

5.2 Modeling the transmission system

FTTH networks are currently based on the PON architecture, and the integration of metropolitan networks into optical access networks has been considered, resulting in the so called LR-PONs [116], [117]. The LR-PONs make use of dense WDM technology, in order to increase the utilization factor of the fiber installed in metropolitan networks, and employ optical amplification to extend the transmission reach. Considering that the separation between adjacent wavelengths is enough to allow neglecting the crosstalk between adjacent channels, one of the dense WDM signals transmitted from the CO to the RN is isolated and the path of the signal through the LR-PON and the equipment required to transmit a single wavelength signal is represented schematically in Fig. 5.1.

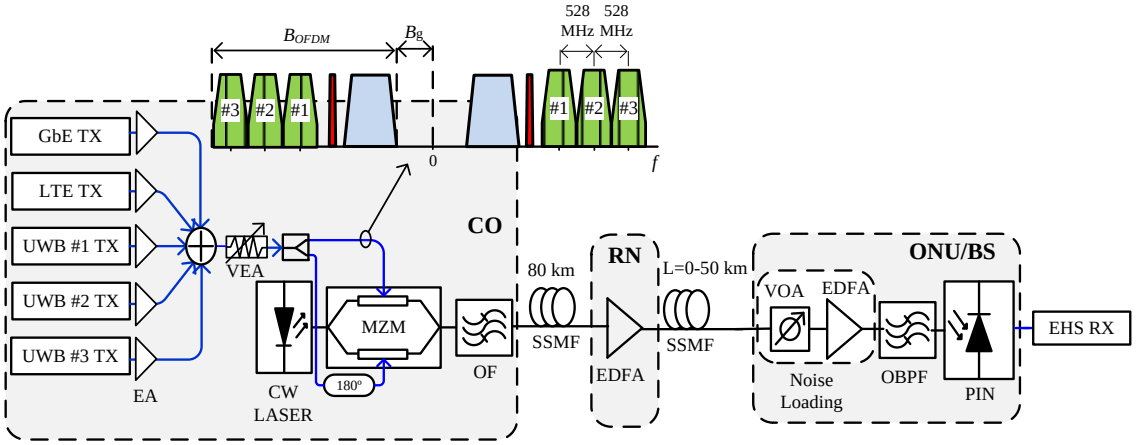

Figure 5.1 - Schematic of the OSSB transmitter based on the filtering method and path of the transmitted signal through the LR-PON.

The work reported here was performed with a simulation setup modelled by Fig. 5.1, which represents schematically an OSSB transmitter based on the filtering method to overcome the undesired dispersion-induced power fading effect. In the CO, an ODSB

signal is generated at the output of a DE-MZM operated in push-pull mode, followed by an OSSB filter to remove a sideband before transmission to the customer's premises.

The electrical hybrid signal (EHS) comprising five OFDM signals amplified separately modulates externally the optical signal emitted by a CW laser with a linewidth of 5 MHz (a conventional DFB laser), emitting at 1550 nm, through a DE-MZM with 25 dB extinction ratio, half-wave voltage V_π = 5 V and 6 dB insertion loss. The phase noise of the laser was modeled as a Wiener–Lévy process with zero mean and Gaussian variance $\sigma^2=2\pi B_T$, where the parameter B_T represents the two-sided 3-dB linewidth of the Lorentzian power spectral density (PSD) of the laser emission [119]. The electro-optic field at the output of the DE-MZM is described by (3.1) and is expressed as:

$$E_{out}(t)=\frac{E_{in}}{2}\left\{e^{j\phi_1(t)}+\gamma e^{j\phi_2(t)}\right\}, \tag{5.1}$$

where t denotes time, E_{in} is the CW electrical field at the input of the DEMZM, $\phi_{1,2}(t) = \pi V_{1,2}(t)/V_\pi$, where $V_1(t)$ an $V_2(t)$ are the driving voltage signals. γ is the scaling factor, between 0 and 1, used to account for the unbalance between the arms of the DE-MZM. For balanced MZMs this scaling factor is 1. A variable electrical attenuator (VEA) is used to adjust the optical modulation index, m, of the ODSB modulation. A third-order super-Gaussian filter [120] with 7 GHz bandwidth was considered as OSSB filter. The resulting OSSB hybrid signal at the output of the OF has 0 dBm and is sent to the customers through the SSMF feeder network. The SSMF is modeled using a low-pass equivalent representation of a linear bandpass system in which the fiber dispersion is accounted for through the quadratic phase of the fiber's transfer function, given by:

$$H(f)=\exp(-\alpha_f L)\exp(j\pi\frac{DL\lambda_c^2 f^2}{c}), \tag{5.2}$$

where c is the free-space speed of light, λ_c is the operating wavelength (1550 nm), α_f = 0.2 dB/km is the attenuation coefficient of the fiber, L is the fiber length, and D = 17 ps/(km.nm) is the first order dispersion coefficient of the fiber. After transmission through 80 km of fiber, the optical signal is amplified in the RN by a noiseless EDFA, to compensate for the losses in the feeder network. The amplified optical signal is then sent through the SSMF distribution network to the hybrid ONU/BS located at the customer's premises, where the optical signals are recovered to the electrical domain. At the input of the hybrid ONU/BS, a VOA along with an EDFA

with a gain of 15 dB and a noise figure of 4 dB are used to adjust the optical signal-to-noise ratio (OSNR) of the system. The ASE noise generated by the EDFA is considered Gaussian, and the OSNR is evaluated considering optical noise over the two perpendicular directions of polarization, in a reference optical bandwidth of 0.1 nm.

In the hybrid ONU/BS, a second-order super-Gaussian optical filter [119] with 12.5 GHz -3dB bandwidth centered at 1550 nm is deployed to reduce the ASE noise power, and a PIN photodetector with a responsivity of 0.9 A/W is considered. The PIN photodetector was modeled as producing a photocurrent proportional to the square of the sum of all optical field components in a given polarization, plus the square of the sum of all optical field components in the perpendicular polarization. The thermal noise of the receiver is not considered, since at the output of the PIN photodetector its effect is insignificant, compared with the signal–ASE beating noise [120]. Therefore, the received EHS is demodulated in the EHS receiver (EHS RX), where the photodetected signal is split among the respective receivers, to perform OFDM demodulation including removal of cyclic prefix, serial-to-parallel conversion, IFFT, subcarriers equalization, symbol de-mapping and parallel-to-serial conversion, and then the BER is evaluated based on the EVM method applied to the received signal constellation at the equalizer output. The performance of the different OFDM signals is assessed in terms of the required OSNR (ROSNR) at the input of the hybrid ONU/BS in order to obtain a BER = 10^{-9}. BER estimation based on the EVM method is explained in Appendix C. A BER = 10^{-9} is enough to ensure that the EVM limits of -14.5 dB for the QPSK OFDM-UWB signal and -18.6 dB for the 16-QAM LTE signal are respected after optical transmission, as is demonstrated in Section C.3 of Appendix C.

5.3 Numerical simulation results

In the CO, the EHS that drives the DE-MZM is generated by SCM of a custom OFDM-GbE signal of bandwidth (B_{GbE}) equal to 1 GHz, a 64-QAM LTE signal with channel bandwidth (B_{LTE}) equal to 20 MHz and normal CP, and three independent OFDM-UWB signals of the first group of the ECMA-368 standard [100], each with 528 MHz bandwidth (B_{UWBs}). The structure of the transmitter and receiver and the main parameters required to perform the modulation and the demodulation of all OFDM signals are described in Appendix B. The three OFDM-UWB #1, -UWB #2 and -UWB #3 signals are filtered by a Bessel LPF of order 6 and -3 dB bandwidth equal to

264 MHz [77], before up-conversion to the central frequencies of 3.432, 3.960 and 4.488 GHz, respectively, in order to reduce the aliasing spectrum. The custom OFDM-GbE signal follows a subcarrier allocation structure similar to that specified in the ECMA-368 standard. The real and imaginary components of the BB custom OFDM-GbE signal are filtered by a Bessel LPF of order 6 and -3dB bandwidth equal to 510 MHz before up-conversion to the central frequency of 1.5 GHz (1.5 x B_{GbE}). The baseband 64-QAM LTE signal complying with release 8 [114] is filtered by a Bessel LPF of 20 MHz [105] before up-conversion to 2.6 GHz (E-UTRA band 7 - downstream 2.62-2.69 GHz) in the transmitter, to be down-converted in the receiver. For any OFDM signal, the bandwidths of the LPFs at the transmitter and at the receiver are equal, such as demonstrated numerically in [105]. The electrical spectrum of the resulting EHS, with the initial frequency allocation for the GbE signal, is shown in Fig. 5.2.

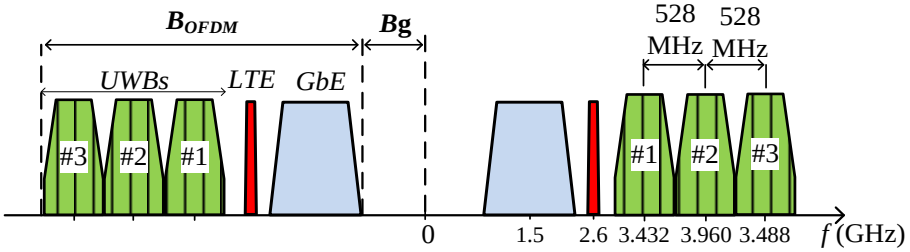

Figure 5.2 – EHS with initial frequency allocation.

The simulation results were obtained with Matlab®, considering 1536 OFDM-UWB symbols, 1584 OFDM-GbE symbols, and 7 LTE symbols. The OSNR was fixed at 35 dB and the DE-MZM was biased at the QP of its intensity transfer function, with the voltage $-0.5V_{\pi}$. The OSSB filter with 7 GHz bandwidth was detuned to 2.9 GHz apart from the optical carrier, in order to reject the lower sideband. Since the electrical OFDM signals have different bandwidths, the electrical power (in a 50 Ohm load) of each signal before being combined in the EHS was adjusted in order to ensure that all signals have the same PSD, equal to -4.24×10^{-8} dBm/Hz. The PSD = -4.2410^{-8} dBm/Hz was selected as the minimum PSD that allows the EVM of the UWB signals to comply with the EVM limit defined in the ECMA-368 standard. Note that the OFDM signals have a spectrum similar to filtered Gaussian noise, and therefore the PSD can be approximated by the ratio between signal power and signal bandwidth. The resulting drive powers for the OFDM signals are gathered in Table 5.1.

Table 5.1 - Powers of the drive OFDM signals.

	GbE	LTE	UWBs
Drive power [dBm]	-19.37	-36.03	-22.38

The optimum *m* to operate the DE-MZM was studied for an optical B2B configuration, and the result obtained is shown in Fig. 5.3 a).

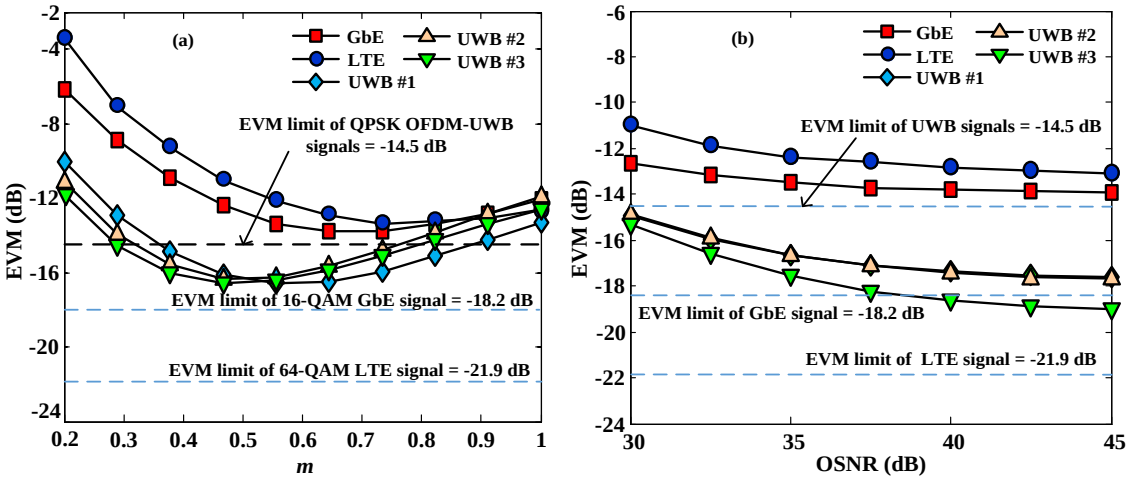

Figure 5.3 - EVM of the different signals for an optical B2B configuration with the DE-MZM biased at – 0.5 V_π, as a function of: a) *m* for an OSNR = 35 dB; (b) the OSNR for *m* = 0.6.

From Fig. 5.3 a) it can be concluded that an OSNR = 35 dB is enough to recover the OFDM-UWB signals with an EVM below the EVM limit. However, this OSNR is insufficient for the signals with larger constellation size, such as the 64-QAM LTE signal and the 16-QAM OFDM-GbE signal. The EVM limits for all signals, as defined in the respective standards [113], [114], are included in the figures. The EVM limit for the GbE signal corresponds to a BER = 10^{-4} that is typically considered, including an operational margin from the state-of-the-art FEC limit, BER = 2×10^{-3}.

From the results shown in Fig. 5.3 a), a simulation study of the EVM for all signals as a function of the OSNR with the DE-MZM biased at – 0.5V_π and operating with an *m* equal to 0.6 was carried out, and the result is shown in Fig. 5.3 b). From this study, it can be concluded that the increase of OSNR above 35 dB has little impact on the performance of the system. The reason for this is that, due to the nonlinearity of the DE-MZM, the DE-MZM must be operated with a low *m*, which leads to inefficient modulation, and therefore the power of the ODSB signal is dominated mainly by the power of the optical carrier. Since an OSSB signal obtained by the filtering method is a version of an ODSB signal without one of the sidebands, the power of an OSSB signal is even more dominated by the power of the optical carrier. To reduce the optical

carrier, ODSB-RC may be implemented by biasing the DE-MZM below the QP. However, the nonlinearity of the DE-MZM increases when biased below the QP, and therefore the B_g should be increased to accommodate all intermodulation products around DC, which is not possible due to the coexistence of wireless signals.

Since the central frequency of the 16-QAM OFDM-GbE signal is not yet standardized, a study of the optimal central frequency to transmit the OFDM-GbE signal together with the other wireless signals through optical fiber was performed, for an optical B2B configuration, preceded by a comparison of the EVM obtained with the DE-MZM biased at QP with that obtained with the DE-MZM biased below the QP, through the EVM bias ratio (EVMBR) defined as:

$$EVMBR(dB) = 20\log_{10}\left(\frac{EVM_{rms}\big|_{QP}}{EVM_{rms}\big|_{Vbias}}\right). \tag{5.3}$$

An EVMBR equal to zero means that the EVM values are equal for both bias points, and then there is no EVM improvement when biasing the DE-MZM below the QP, whereas for EVMBR greater than zero the EVM values obtained with the DE-MZM biased below the QP are better than those obtained with the DE-MZM biased at the QP. The opposite case, an EVMBR lower than zero, means that the EVM is degraded with the DE-MZM biased below the QP.

The DE-MZM was driven with $m = 0.5$, the OSNR was fixed at 35 dB, and the central frequency of the GbE signal was increased from 1 GHz to 2.3 GHz. The standardized central frequency of all other OFDM signals was kept unchanged. To have more insight of the EVMBR variation shown in Fig. 5.4 b), the EVM obtained for all signals when the DE-MZM is biased at the QP and the GbE central frequency increases from 1 GHz to 2.3 GHz is shown in Fig. 5.4 a). The EVMBR was determined for the DE-MZM biased at $-0.7V_\pi$, which is an operating point located in the nonlinear part of the intensity transfer function of the DE-MZM.

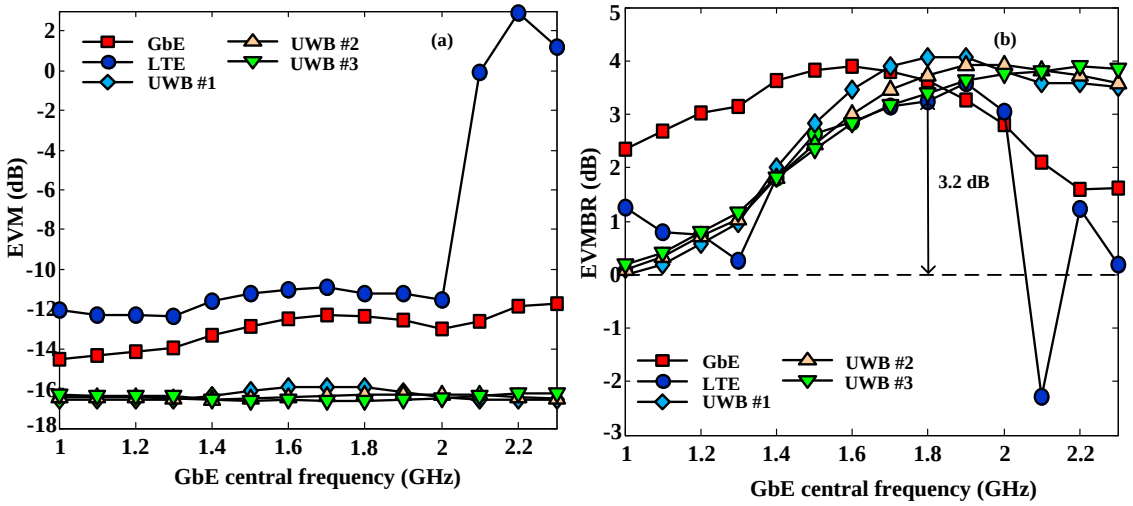

Figure 5.4 - (a) EVM of all signals for an optical B2B configuration with the DE-MZM biased at – 0.5V_π, as a function of the GbE signal central frequency; (b) EVMBR of all OFDM signals, as a function of the GbE central frequency, with the DE-MZM biased at -0.7V_π.

From Fig. 5.4 a) and b) it can observed that, when the GbE signal is up-converted for frequencies higher than 2 GHz, the LTE signal is strongly affected by crosstalk of the GbE signal on the LTE signal. Note that the upper frequency of the GbE signal is equal to the GbE central frequency + 500 MHz, whereas the lower frequency of the LTE signal is equal to 2.590 GHz (2.6 GHz-10MHz). The EVM degradation due to crosstalk imposed by the GbE signal on the LTE signal is stronger than the degradation caused by the LTE signal on the GbE signal, because the constellation size of the LTE signal is larger and consequently the Euclidean distance between QAM symbols is smaller, thereby decreasing the crosstalk tolerance. Furthermore, in Fig. 5.4 a) it can be observed that, when the DE-MZM is biased at the QP, the UWB signals do not suffer any crosstalk as the GbE central frequency is increased from 1 to 2.3 GHz, whereas when the DE-MZM is biased below the QP the UWB signals suffer degradation due to 2-nd harmonic generation of the GbE and LTE signals. In Fig. 5.4 b) it is clear that the best frequency to up-convert the custom baseband complex-valued 16-QAM OFDM-GbE signal is 1.8 GHz, as a trade-off between the EVM values obtained for the GbE and LTE signals, which are the signals with larger constellations.

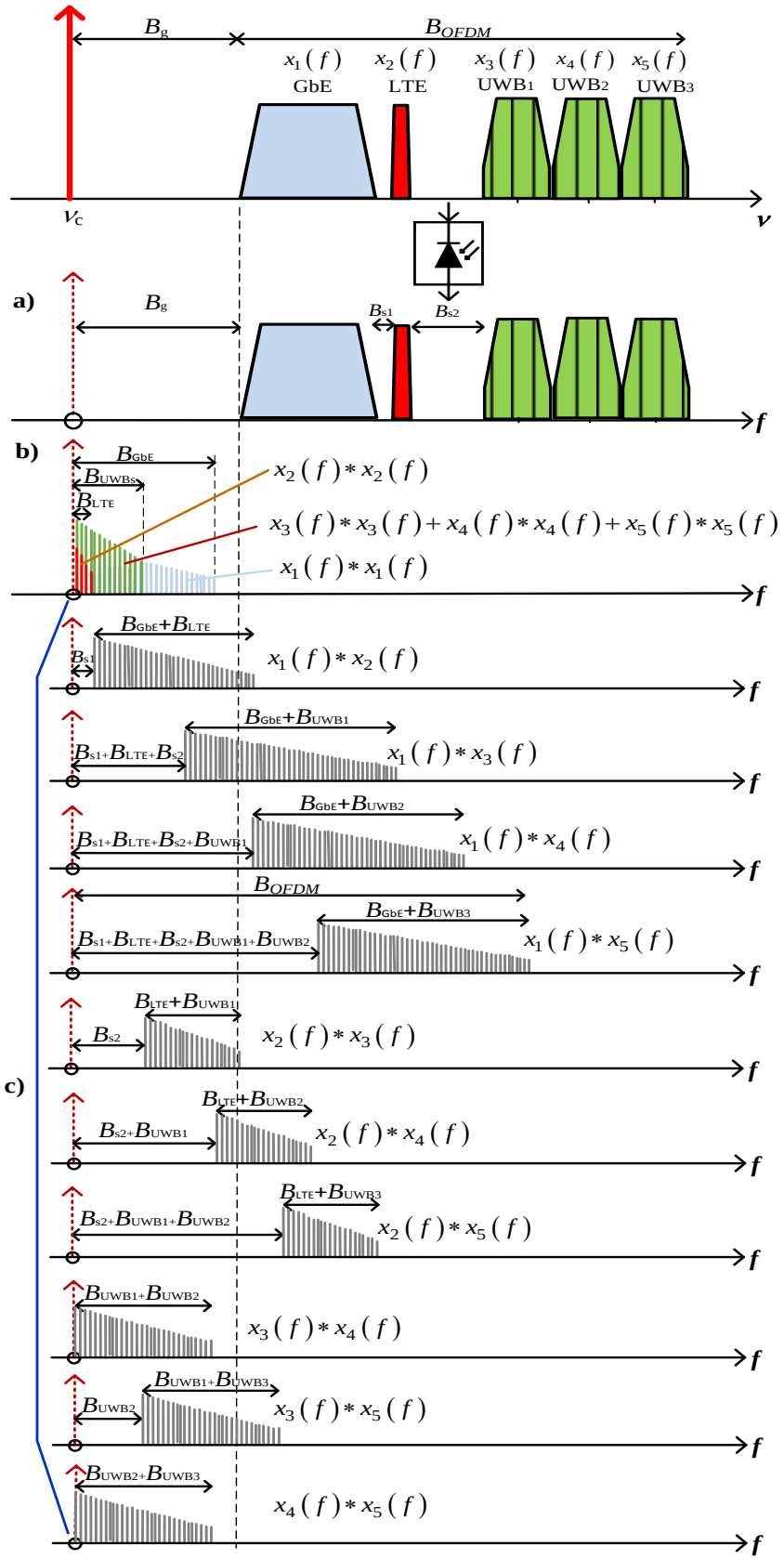

Figure 5.5 - Direct - detection of the OFDM OSSB hybrid signal: (a) Spectrum of the useful received OFDM signals; (b) Spectrum of the intermodulation distortion terms resulting from beating between subcarriers of the same OFDM signal; (c) Spectrum of the intermodulation distortion terms resulting from beating between subcarriers of different OFDM signals;

Fixing the GbE central frequency at 1.8 GHz results in a total OFDM aggregate bandwidth B_{OFDM} = 3.452 GHz and a bandwidth gap B_g = 1.3 GHz, which lead to the ratio B_g/B_{OFDM} = 0.377. B_g is larger than the bandwidth of any OFDM signal, and thus this bandwidth gap is large enough to accommodate all intermodulation distortion terms resulting from the beating between subcarriers of the same OFDM signal, as sketched in Fig. 5.5 b). However, the B_g/B_{OFDM} ratio is lower than 1, and consequently B_g is not sufficient to accommodate the intermodulation distortion terms resulting from the beating between subcarriers of different OFDM signals, as sketched in Fig. 5.5 c). An OSSB OFDM signal and its electrical directly detected components are sketched in Fig. 5.5 a), for the case that the OFDM signal is composed by four independent OFDM wireless signals and an OFDM wired signal. In [121], a sketch is presented for the case of direct-detection of an OSSB signal composed by a non-standardized OFDM wired signal. In this case, intermodulation distortion terms are due only to the beating of subcarriers of the same signal, as sketched in Fig. 5.5 b). Besides that, there is freedom to adjust the central frequency and consequently B_g. In Fig. 5.5 a), the OFDM signal is sketched without any spurious components, whereas the spurious terms are sketched in Fig. 5.5 b) and c). From Fig. 5.5 c) for the beating term $x_1(f)*x_5(f)$, it is evident that, since B_{OFDM} = 3.452 GHz is greater than the central frequency of the UWB #1 signal, half of the UWB #1 signal after photodetection is affected by the intermodulation distortion terms resulting from beating between subcarriers of the different OFDM signals.

5.3.1 Improving the modulation efficiency

Besides the optical power of the OSSB signal being dominated by the optical carrier, the signal is corrupted by the intermodulation distortion terms resulting from beating between subcarriers of the same and different OFDM signals, after direct detection. To overcome the first performance constraint, reduction of the optical carrier power by biasing the DE-MZM below the QP is carried out. The optimal performance is a trade-off between the bias voltage and *m*, since as the bias voltage decreases towards the MITP more nonlinear is the modulation and consequently lower has to be the *m*. In Fig. 5.6, contour plots of the EVM values for the different OFDM signals as a function of *m* and for different DE-MZM bias voltages are shown in an optical B2B configuration, with an OSNR = 35 dB.

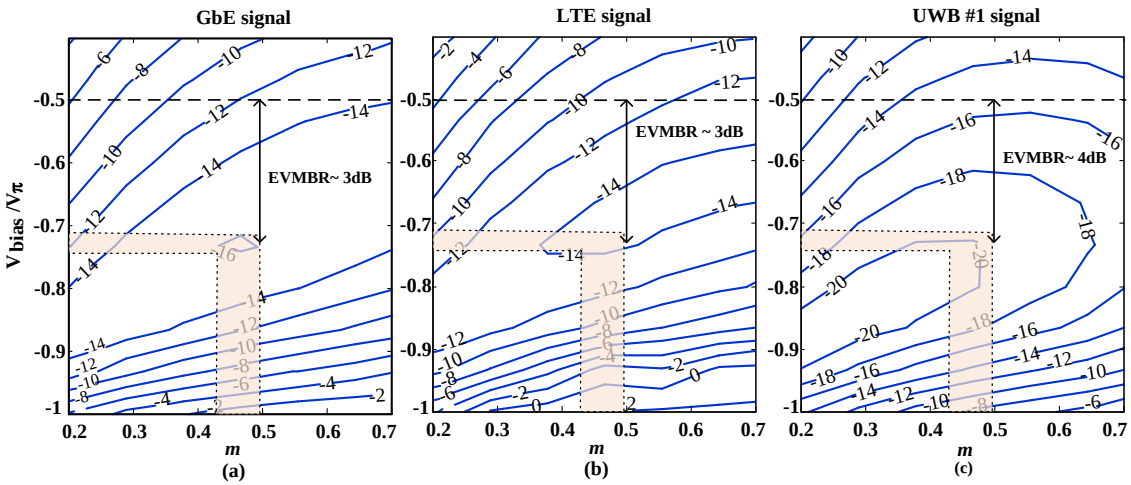

Figure 5.6 - Contour plot of the EVM values, in decibels, as a function of *m* for different DE-MZM bias voltages, for:(a) GbE signal; (b) LTE signal; (c) UWB # 1 signal.

As can be observed in Fig. 5.6, for the same EVM level, when the bias voltage decreases towards $-V_\pi$ the *m* needs to be decreased to keep the same EVM level, otherwise the EVM increases due to generation of intermodulation distortion at the output of the DE-MZM. In Fig. 5.6, the EVM values obtained for the UWB #2 and UWB #3 signals are not shown, because UWB #1 is the signal with the worst performance among all three UWB signals, because it is the UWB signal more degraded by intermodulation distortion, as shown in Fig. 5.5. Therefore, ensuring that UWB #1 complies with the EVM limit is enough to ensure that UWB #2 and UWB #3 also comply with the EVM limit defined in the ECMA-368 standard. In Fig. 5.6, a shaded region defined by the optimal EVM region of the GbE signal is shown, since this signal is more affected by intermodulation distortion than all the others, after photodetection, as shown in Fig. 5.5.

From Fig. 5.6) it can be concluded that the optimal bias voltage is -0.73V_π and is determined by the performance of the GbE and LTE signals. Furthermore, reducing the power of the optical carrier by biasing the DE-MZM at -0.73V_π allowed improving further the EVM values of the UWB signals and improving slightly the EVM values of the GbE and LTE signals, relative to the case of the DE-MZM biased at the QP. Considering an *m* around 0.5, the GbE signal has an EVM equal to -13 and -16 dB when the DE-MZM is biased at the QP and at -0.73 V_π, respectively. Therefore, the EVM improvement given by the EVMBR (5.3) is around -3 dB for the GbE signal. The estimated EVMBR, shown in Fig. 5.4 b), is approximately in accordance with that shown in Fig. 5.6.

5.3.2 Overcoming the intermodulation distortion

The EVM values obtained for the GbE and LTE signals with improved modulation efficiency do not yet comply with the EVM limit defined in the respective standards. To improve further the EVM values of the GbE and LTE signals, it is required to overcome the intermodulation distortion terms that fall on the bands occupied by these signals, as sketched in Fig. 5.5. In order to overcome the intermodulation products over the GbE and LTE bands, it is here proposed to increase the drive power of these signals, keeping unchanged the drive powers of the UWB signals, since their performance has reached the required quality. In order to recover successfully the GbE and LTE signals, the drive powers of these signals were increased asymmetrically. The additional drive power relative to the drive power presented in Table 5.1, is shown in Fig. 5.7 as a function of *m* for an OSNR = 35dB.

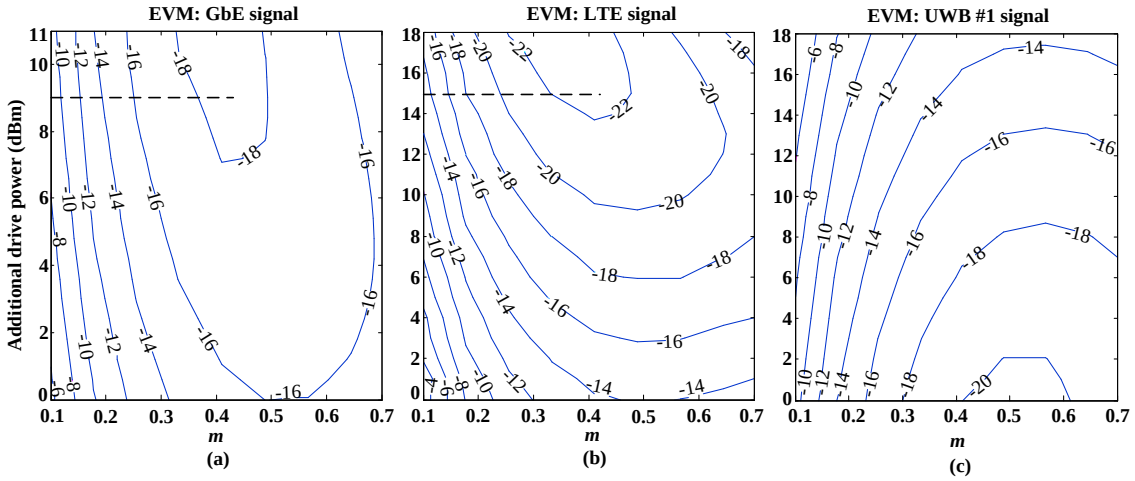

Figure 5.7 - Contour plot of the EVM values as a function of *m* for different additional drive powers, for (a) GbE signal, (b) LTE signal, (c) UWB # 1 signal.

In Fig. 5.7 it can be observed that, as the drive power increases, *m* is required to decrease in order to preserve the same EVM, thereby avoiding the intermodulation distortion power increase. The additional drive powers for the GbE and LTE signals, before being combined in the EHS in the transmitter, were 9 dBm and 15 dBm, respectively. In addition, from Fig. 5.6 c) is can be observed that, as the drive powers of the GbE and LTE signals increase, the EVM for the UWB #1 signal and consequently also for the UWB #2 and UWB #3 signals are degraded. For an *m* around 0.5, the maximum additional drive powers for the GbE and LTE signals are 10 dBm and 16 dBm, in order to recover the UWB #1 signal successfully.

The resulting drive powers and respective PSDs for all drive signals are gathered in Tabel 5.2.

Table 5.2 – Optimal powers of the drive OFDM signals and respective PSDs.

	GbE	LTE	UWBs
Drive powers[dBm]	-10.37	-20.91	-22.38
PSD[dBm/Hz]	$-1.04\text{x}10^{-8}$	$-1.05\text{x}10^{-6}$	$-4.24\text{x}10^{-8}$

The optimum *m* to drive the DE-MZM when it is biased at $-0.73V_{\pi}$ and for an OSNR = 35 dB at the input of the hybrid ONU/BS was studied for the EHS composed by OFDM signals with different PSDs. The EVM values obtained for all signals are shown in Fig. 5.8 as a function of *m*.

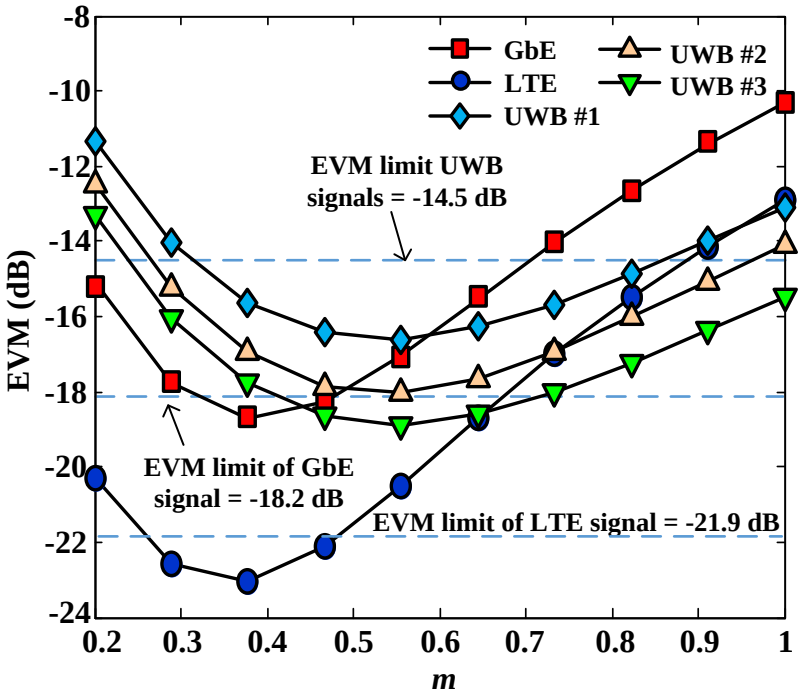

Figure 5.8 - EVM for the different signals as a function of the *m* when the DE-MZM is biased at $-0.73V_{\pi}$.

From Fig. 5.8 it can concluded that the optimal *m* to drive the DE-MZM is 0.38 and that the EVM for the UWB #2 and UWB #3 signals is better than for the UWB #1 signal, as was assumed at the beginning of the transmitter optimization.

Up to here, the performance of the optical transmission system was investigated without optical fiber, that is, without the effect of chromatic dispersion. In order to evaluate the performance after optical transmission through a LR-WDM-PON, the OSSB hybrid signal which optical PSD is shown in Fig. 5.9 is assumed to be transmitted through SSMF up to 130 km.

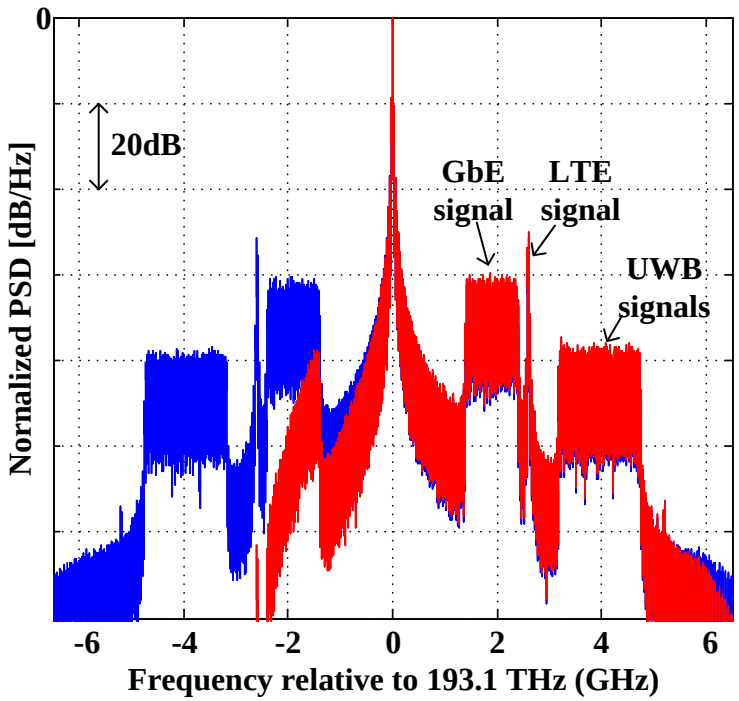

Figure 5.9 - Normalized PSD of the ODSB modulated signal at the output of the DE-MZM (blue) and of the OSSB modulated signal at the output of the OSSB filter (red).

The critical parameters of the optical transmission system were adjusted to the optimal values previously found: the DE-MZM was biased at $-0.73V_{\pi}$, driven with $m = 0.38$, and the OSNR at the input of the hybrid ONU/BS was fixed at 35 dB. The electrical drive powers of the OFDM signals were fixed at the values presented in Table 5.2. In Fig. 5.9, the normalized PSD is shown for the ODSB modulated hybrid signal at the output of the DE-MZM and for the OSSB modulated hybrid signal at the output of the OSSB filter. The OSSB hybrid signal is amplified at the RN for fiber lengths larger than 80 km. Figure 5.10 shows the EVM of all signals for different fiber lengths from the CO to the customer's premises.

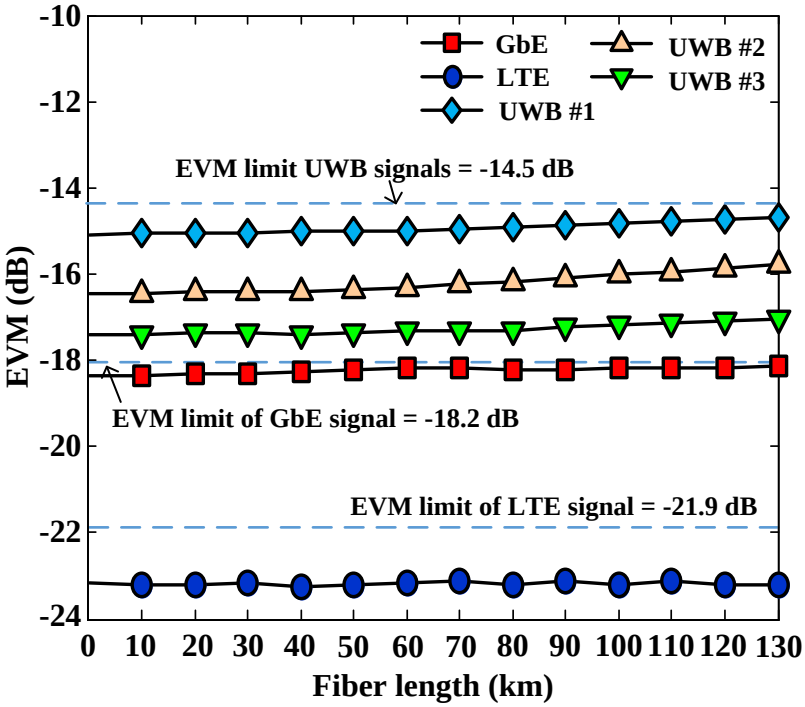

Figure 5.10 - EVM for all signals for different fiber lengths from the CO to the ONU/BS.

In Fig. 5.10 it can be observed that all signals considered could be recovered successfully after transmission through 130 km of SSMF with negligible degradation. Thus, it can be concluded that the modulation efficiency and the drive powers of the OSSB transmitter can be optimized in an optical B2B configuration.

5.4 Summary

In radio-over-fiber systems carrying multi-services OFDM signals over multi-bands and complying with different standards, it is not always possible to ensure that the bandwidth gap between DC and the lowest frequency signal component is greater or equal to the total aggregate OFDM signal bandwidth. This occurs in hybrid optical access networks providing connectivity of wired services and wireless backhaul because the wireless services are carried on low frequencies of the MW band. This fact limits the performance, especially when the modulation efficiency is improved by biasing the DE-MZM below the QP. Since the bandwidth gap required is not ensured, the OFDM signals closer to DC after direct-detection are strongly affected by intermodulation distortion.

In this chapter, this impairment was addressed for transmission of OSSB modulated signals obtained with the filtering method in order to overcome the power fading induced by chromatic dispersion. For this OSSB modulation method, improvement of

the modulation efficiency is required for successful transmission of OFDM signals with high constellation order.

To overcome the intermodulation distortion, in this chapter it was demonstrated through numerical simulation that driving the OFDM signals more affected by intermodulation distortion with higher powers is an effective solution. Furthermore, since the chromatic dispersion has low impact on the performance of the signals after transmission through 130 km of SSMF, the drive power optimization to overcome the intermodulation distortion of the more impaired signals can be performed in a B2B configuration.

6

Modulation chirp of dual-electrode Mach-Zehnder modulators

6.1 Introduction

In optical communication systems, the frequency chirp is an important phenomenon that is known to limit the performance of dispersive lightwave systems and appears in different forms: in electro-optic modulation, designated here by modulation chirp, in non-linear transmission, due to the non-linear effect of self-phase modulation, and the chirp introduced by photonic devices such as optical amplifiers. For optical signals with power level lower than the nonlinear threshold power, the transmission is linear and the self-phase modulation effect can be neglected in single channel optical transmission. Thus, in typical optical communication systems the most important frequency chirp is the modulation chirp generated by a phase modulation in directly modulated lasers [122], and in external modulation by semiconductor optical amplifiers [123], EAMs [124] or MZMs [125].

Intensity modulation in semiconductor lasers or amplifiers is invariably accompanied by undesirable phase modulation, resulting from refractive index variation associated with changes in the carrier density. An effect of the intensity modulation is that the carrier density in the active region of a laser or semiconductor amplifier changes and this leads to time-dependent phase changes, *i.e* to a modulation chirp at the output.

The positive modulation chirp of directly modulated lasers broadens the transmitted signal spectrum beyond the information bandwidth of the modulating signal. This results in a dispersion limited distance of only a few kilometers in systems operating at Gbit/s rates [122]. This limitation occurs because the tolerance to chromatic dispersion decreases with transmission bandwidth in standard fiber operating at 1550 nm. For this reason, the use of external modulation namely based on LiNbO3 DE-MZM in high-speed transmission systems has been considered very attractive, because it is possible to operate the modulator chirpless.

However, it has been demonstrated that the introduction of controlled modulation chirp in external modulation using a DE-MZM can improve the receiver sensitivity and consequently improve the transmission reach [125]-[127]. In a DE-MZM, the amount of chirp and its polarity can be controlled through the drive signals voltage amplitudes applied to each electrode [124]. Depending on the transmission distance, if a correct amount of modulation chirp is applied to the intensity modulated signal, the transmitted signal will be more robust against chromatic dispersion than an un-chirped signal.

In this chapter, the modulation chirp generated by a DE-MZM and its influence on the transmission of signals based on OFDM following different standards is studied in detail. Closed form expressions for the drive signals voltage amplitudes required to control the modulation chirp at the output of a DE-MZM are derived. Based on these drive signals voltage amplitudes, the effect of the modulation chirp on the received OFDM signals and on the SMF transmission -3 dB bandwidth are derived. Finally, the mitigation of chromatic dispersion in the transmission of an OHS composed by an OFDM-GbE signal, an LTE signal and an OFDM-UWB signal is demonstrated by numerical simulation. Furthermore, a performance comparison between ODSB and ODSB-RC modulation of an OHS composed by an OFDM-GbE signal and three OFDM-UWB signals is performed by numerical simulation.

The remainder of this chapter is organized as follow. In Section 6.2, the modulation chirp produced by a CW laser and by a DE-MZM is characterized. In Section 6.3, expressions for the drive signals voltage amplitudes are derived, and the effect of the

modulation chirp on the received narrowband OFDM signal and on the -3dB SMF transmission bandwidth is derived. The mitigation of power fading induced by chromatic dispersion, for an OHS composed by an OFDM-GbE signal, an LTE signal and an OFDM-UWB signal, is demonstrated by numerical simulation in Section 6.4.1. A performance comparison of chromatic dispersion mitigation between ODSB and ODSB-RC modulated signals is achieved by numerical simulation in Section 6.4.2. Finally, in Section 6.5 a summary of the chapter is provided.

6.2 Small-signal chirp parameter for intensity modulation based on a DE-MZM

In Fig. 6.1 the schematic of a general intensity modulation scheme based on external modulation using a DE-MZM is presented.

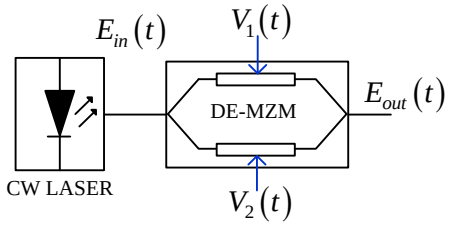

Figure 6.1 – Intensity modulation scheme based on a DE-MZM.

where $E_{\text{in}}(t)$ is the CW signal emitted by a single-mode laser, $V_1(t)$ and $V_2(t)$ are the drive voltage signals applied to the electrodes of the DE-MZM, and $E_{out}(t)$ is the output optical signal.

As discussed above, a directly modulated laser generate chirp at its output. In Section 6.2.1 it is explained why the CW laser employed with external modulation does not generate chirp at its output, and thus in external modulation based on a DE-MZM the chirp generated is only due to the DE-MZM. In Section 6.2.2, the modulation chirp in the intensity modulation using a DE-MZM is characterized.

6.2.1 Modulation chirp of the CW Lasers

In order to evaluate accurately the modulation chirp generated by external intensity modulation based on a DE-MZM, as represented in Fig. 6.1, it is necessary to know the modulation chirp introduced by the CW laser. The relation between the instantaneous frequency $v(t)$ (i.e. the time derivative of the phase modulation) and the instantaneous optical radiation intensity $I(t)$ in a directly modulated laser can be expressed as [128]:

$$\nu(t) = \nu_c + \Delta\nu(t) = \frac{1}{2\pi}\frac{d\phi}{dt} = \frac{\alpha}{4\pi}\left(\frac{1}{I(t)}\frac{dI(t)}{dt} + kI(t)\right) \tag{6.1}$$

where ν_c is the central emission frequency, $\Delta\nu(t)$ is the instantaneous frequency offset, d/dt is the differentiation operator, k is the adiabatic chirp coefficient related with the laser structure, and α is the linewidth enhancement factor of the laser, also known as the Henry parameter. The first term on the right-hand side of (6.1) represents the dynamic/transient chirp in the directly modulated laser. The second term is the adiabatic chirp, which is a function of the steady-state output intensity. The dynamic chirp is negligible when the laser is operated in CW mode, since the output power is constant, and then the first term on the right-hand side in (6.1) is null. In practice, the adiabatic chirp can be estimated varying the amplitude of constant bias current and measuring the frequency shift of the central emission. The adiabatic chirp is typically expressed in MHz/mA and is not an issue when the laser is operated in CW mode.

6.2.2 Modulation chirp of the DE-MZMs

The optical field at the output of a DE-MZM, derived in Chapter 3, is expressed by (3.1) as:

$$E_{out}(t) = \frac{E_{in}(t)}{2}\left\{e^{j\phi_1(t)} + \gamma e^{j\phi_2(t)}\right\} \tag{6.2}$$

considering the amplitude of the complex envelope of the input optical field normalized to unity, the output optical field can be represented in a phasor diagram [129] as shown in Fig. 6.2.

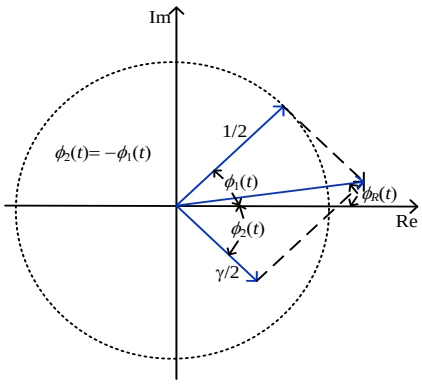

Figure 6.2 – Phasor diagram of the optical field at the output of a DE-MZM.

The phasor diagram shown in Fig. 6.2 is valid for the DE-MZM operated in the push-pull mode, i.e. $\phi_2(t) = -\phi_1(t)$. When $\gamma = 1$ the resultant vector is always along the real

axis, however it has been demonstrated that a DE-MZM with a finite ER ($\gamma < 1$) will always be accompanied by residual chirp, even when driven in the push-pull mode with equal-amplitude signals [67]. In Fig. 6.2 it can be observed that, due to the asymmetry of the DE-MZM, there exists a residual phase, $\phi_R(t)$, in the output optical field related with the DC value of the ER of the DE-MZM. The residual phase, for a DE-MZM operated in balanced push-pull mode, is given by:

$$\phi_R(t) = \arctan\left[\tan\left[\phi_1(t)\right]\frac{(1-\gamma)}{(1+\gamma)}\right]. \tag{6.3}$$

From (6.3) it is easily concluded that for an ideal DE-MZM ($\gamma = 1$) the residual phase $\phi_R(t)$ is null, with the corresponding resultant vector aligned with real axis.

Therefore, it becomes important to know the contributions for the chirp parameter in detail, in order to control and optimize their effects. Thus, simplified expressions are required to quantify separately the chirp parameter components due to finite ER and due to the drive signals.

With this goal in mind, equation (6.2) can be rewritten as the combination of two terms [126], the first term expressing the transfer characteristic of an ideal DE-MZM and the second term introducing an extra phase modulation (correction term), taking the form:

$$E_{out}(t) = E_{in}(t)e^{j\left(\frac{\phi_1(t)+\phi_2(t)}{2}\right)}\cos\left[\frac{1}{2}\left(\phi_1(t)-\phi_2(t)\right)\right] + E_{in}(t)\frac{(\gamma-1)}{2}e^{j\phi_2(t)} \tag{6.4}$$

Two different undesired phase modulations are identified in this equation. The first one, represented by the exponential factor in the first term, is an undesired phase modulation due to the drive signals (DSs) applied to both phase modulators, and the second one, represented by the second term of (6.4), is due to the finite ER of the DE-MZM. These undesired phase modulations originate two distinct chirp sources. It should be noted that for an ideal DE-MZM ($\gamma = 1$) the second term of (6.4) is null.

Likewise in directly modulated lasers, the magnitude and sign of the chirp in a DE-MZM can be uniquely expressed in terms of the α chirp parameter [129] by:

$$\alpha = \frac{2I\dfrac{d\phi(t)}{dt}}{\dfrac{dI(t)}{dt}} \tag{6.5}$$

where $\phi(t)$ is the instantaneous phase of the optical signal at the output of the DE-MZM. Note that (6.5) is in accordance with (6.1). From (6.2), the output optical field of the DE-MZM can be expressed in the polar form:

$$E_{out}(t) = \left|E_{out}(t)\right| e^{j\phi(t)} \tag{6.6}$$

with

$$\phi(t) = \arctan\left(\frac{\sin\phi_1(t) + \gamma\sin\phi_2(t)}{\cos\phi_1(t) + \gamma\cos\phi_2(t)}\right) \tag{6.7}$$

and $|E_{\text{out}}(t)| = (\, I(t)\,)^{½}$, with $I(t)$ given by

$$I(t) = \frac{E_{in}^2}{4}\left(1 + \gamma^2 + 2\gamma\cos\left(\phi_1(t) - \phi_2(t)\right)\right) \tag{6.8}$$

By substituting (6.7) and (6.8) in (6.5), and after some algebraic manipulations, the α chirp parameter of the DE-MZM can be written as the sum of two terms that correspond to different sources of chirp:

$$\begin{aligned}\alpha = &\frac{\frac{d}{dt}\left\{\phi_1(t) + \phi_2(t)\right\}}{-\frac{d}{dt}\left\{\phi_1(t) - \phi_2(t)\right\}}\cot\left(\frac{1}{2}\left(\phi_1(t) - \phi_2(t)\right)\right) \\ &+ \frac{\frac{d}{dt}\left\{\phi_1(t)\left(\frac{1-\gamma}{\gamma}\right) + (\gamma - 1)\phi_2(t)\right\}}{-\frac{d}{dt}\left\{\phi_1(t) - \phi_2(t)\right\}\sin\left(\phi_1(t) - \phi_2(t)\right)} = \alpha_{DS} + \alpha_{ER}\end{aligned} \tag{6.9}$$

Considering both electrodes driven with mathematically similar waveforms, $V_1(t) = V_1\cos(\omega t) + V_{\text{bias}}$ and $V_2(t) = V_2\cos(\omega t)$, and $\phi_i(t) = \frac{\pi}{V_\pi}V_i(t)$, results:

$$\alpha_{DS} = \frac{(V_1 + V_2)}{(V_2 - V_1)}\cot\left(\frac{\pi}{2V_\pi}(V_1 - V_2)\cos(\omega t) + \frac{\pi}{2V_\pi}V_{bias}\right) \tag{6.10}$$

and

$$\alpha_{ER} = \frac{V_1\left(\frac{1-\gamma}{\gamma}\right) + (\gamma - 1)V_2}{(V_2 - V_1)\sin\left(\frac{\pi}{V_\pi}(V_1 - V_2)\cos(\omega t) + \frac{\pi}{V_\pi}V_{bias}\right)} \tag{6.11}$$

where V_{bias} is the DC voltage used to bias the DE-MZM and ω is the angular frequency of the DS. Equation (6.10) is in excellent agreement with equation (3) in [130], experimentally validated. The first term, α_{DS}, results exclusively from the DS, and is adjustable through the voltage amplitudes applied to both electrodes of the modulator.

The second term, α_{ER}, results from finite ER of the DE-MZM, and is null only when the DE-MZM is balanced ($\gamma = 1$).

Considering the DE-MZM operated in the small-signal regime, with (V_1-V_2) $\ll V_\pi$, and driven in unbalanced push-pull mode, such that $V_1 = -\rho V_2$, (6.10) and (6.11) are simplified to:

$$\alpha_{DS} = \frac{(1-\rho)}{(1+\rho)} \cot\left(\frac{\pi}{2V_\pi} V_{bias}\right) \tag{6.12}$$

and

$$\alpha_{ER} = \frac{-\rho\left(\frac{1-\gamma}{\gamma}\right)+(\gamma-1)}{(1+\rho)\sin\left(\frac{\pi}{V_\pi} V_{bias}\right)} \tag{6.13}$$

Equations (6.12) and (6.13) allow concluding that the α chirp parameter in the small-signal regime depends only on the ratio between the voltage amplitudes of the DS, independently of the type of drive signals applied to the DE-MZM. The sign of the α parameter can be controlled through the bias voltages applied to the DE-MZM.

Figure 6.3 shows how the α chirp parameter and its components vary as functions of the drive power ratio, $10\log_{10}(|\rho|^2)$, for a DE-MZM with an ER equal to 20 dB, and biased at the QP with a voltage $-V_\pi/2$.

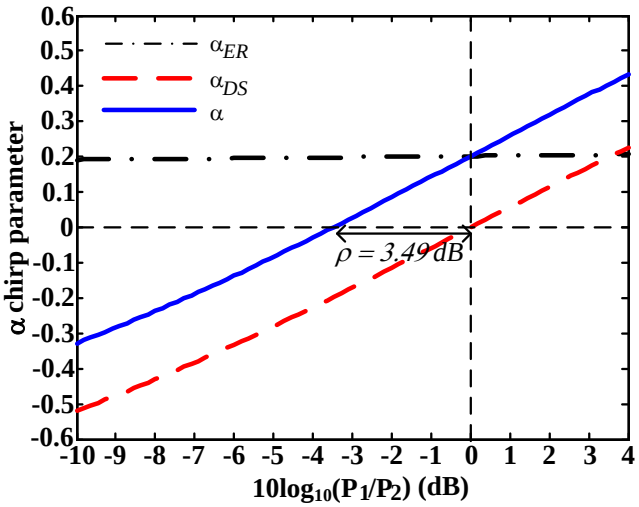

Figure 6.3 - Chirp parameter and its components as functions of the drive power ratio.

The curve of α is in excellent agreement with Fig. 1 in [130], obtained experimentally. Furthermore, α follows the same variation of α_{DS} with an offset equal to α_{ER} in the yy-axis. The variation of α_{ER} as a function of the drive power ratio is

negligible, depending only on the ER of the DE-MZM. If the DE-MZM was ideal, the α parameter would be equal to α_{DS} and the ratio of voltage amplitudes, ρ, required to ensure $\alpha = 0$ at the output of the DE-MZM would be equal to 1. In practice, a DE-MZM has finite ER, then it is required that $\rho = \gamma^2$, which for an ER equal to 20 dB corresponds to 3.49 dB.

In the derivation of the expressions for the α chirp parameter components, (6.10) to (6.13), the drive signals were considered sinusoidal. In practice, the drive signals of a DE-MZM are normally modulated signals. In order to check the applicability of the expressions derived, the α chirp parameter was calculated for different drive signals through numerical simulation and compared with the values obtained for the sinusoidal drive signals. Furthermore, the α chirp parameter is determined for different bias points of the DE-MZM.

The α chirp parameter is numerically calculated from the simulated optical field at the output of the DE-MZM, in accordance with its definition, expressed by (6.5). The operational α parameter is determined as the median of the complete instantaneous α waveform, in order to avoid the discontinuities of divisions by zero [131].

Five different drive signals are considered, a 1 Gbit/s NRZ signal filtered by a 750 MHz Bessel LPF of 5th order, a 3 GHz sinusoidal signal, an OFDM-UWB channel signal centered at 3.960 GHz, a 20 MHz LTE signal, and finally an EHS composed by all previously described drive signals. The main parameters and the description of how the modulated signals are generated can be found in Appendix B.

The DE-MZM is considered with ER = 20 dB, biased at the QP with a voltage $-V_\pi/2$. In Fig. 6.4 the α chirp parameter is shown for different drive signals as a function of the DE-MZM bias voltage, for a m equal to 5% and considering ρ = -3 dB.

The results presented in Fig. 6.4 demonstrate that the α parameter is independent of the drive signals, and agree with (6.12) and (6.13) when the DE-MZM is biased at the QP. However, the same does not occur when the DE-MZM is biased at the MITP or MATP. At theses bias points the value of the chirp parameter is not defined because of singularities, as shown in Fig. 6.4.

We conclude that, for a bias voltage range around the QP, the α parameter for modulated signals is coincident with that obtained with a CW sinusoidal signal, whereas for MITP or MATP the α chirp parameter derived for sinusoidal signals cannot be used

to estimate the α parameter for a different modulating signal, due to singularities present in (6.12) with (6.13) for $V_{bias} = 0$ and $V_{bias} = V_{\pi}$.

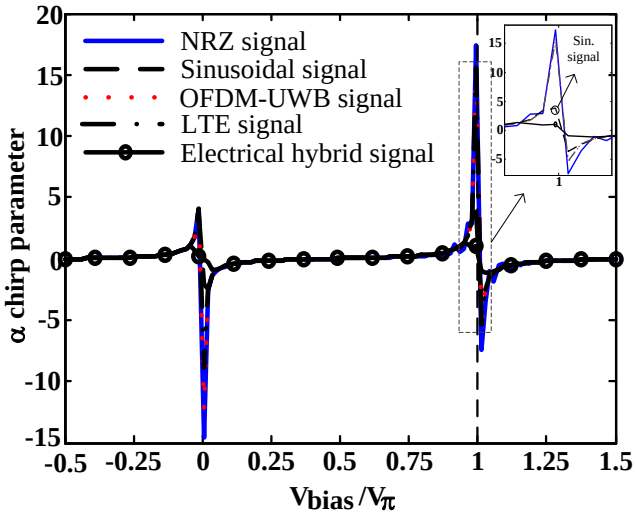

Figure 6.4 – Chirp parameter for different drive signals, as a function of the DE-MZM bias voltage.

At these two bias points the modulation at the output of the DE-MZM is purely in phase, as can be concluded through equations (6.4) and (6.5) as is observed in [132].

6.3 Effect of the modulation chirp of a DE-MZM on the SSMF transmission

6.3.1 Control of the modulation chirp

The modulation chirp of a DE-MZM has been controlled mainly by the chirp due to the drive signals, through the amplitudes of the drive signals, whereas the residual chirp due to finite ER has been controlled by selecting a DE-MZM with a determined ER to set its magnitude. The polarity of the modulation chirp has been set changing the bias voltage by $\pm V_{\pi}$ [130]. Thus, whenever a chirpless modulation optical transmission system is required, a high ER DE-MZM should be selected, which is expensive.

Gnauck *et al.* [125] derived an expression for the chirp parameter, defined only in terms of the peak-to-peak amplitudes, not including the effect of residual chirp due to finite ER of the DE-MZM.

A technique that allows controlling the total modulation chirp ($\alpha_{DS}+\alpha_{ER}$) with accuracy for any DE-MZM in a simple manner is desirable. This can be found assuming the time dependent drive signals [71]:

$$\begin{aligned} V_1(t) &= V_1 x(t) - V_{bias1} \\ V_2(t) &= V_2 x(t) + V_{bias2}, \end{aligned} \tag{6.14}$$

where $x(t)$ is the modulating signal with DC component removed, such that $-1 \leq x(t) \leq 1$ and V_{bias1} and V_{bias2} are DC voltages applied to different electrodes to bias the DE-MZM.

In [111], expressions for the amplitude of the drive signals were derived in order to control the total modulation chirp desired at the output of the DE-MZM. The α chirp parameter for the small-signal regime is equal to the sum of (6.10) and (6.11) and is expressed by:

$$\alpha = \frac{\gamma(V_1 + V_2)\cos(\pi V_{bias}/V_\pi) + V_1 + \gamma^2 V_2}{\gamma(V_2 - V_1)\sin(\pi V_{bias}/V_\pi)}. \tag{6.15}$$

The modulation index is given by $m = (V_1\text{-}V_2)/(2V_\pi)$. Therefore, the following linear system of equations can be written:

$$\begin{cases} V_1 - V_2 = 2mV_\pi \\ \gamma(V_1 + V_2)\cos(\pi V_{bias}/V_\pi) + V_1 + \gamma^2 V_2 = \alpha\gamma(V_2 - V_1)\sin(\pi V_{bias}/V_\pi) \end{cases} \tag{6.16}$$

with $V_{bias} = -(V_{bias1}+V_{bias2})$. Solving (6.16) for V_1 and V_2, the amplitudes of the drive voltages as functions of the modulation chirp parameter, α, unbalance DE-MZM scaling factor, γ, and bias voltage V_{bias}, for any optical modulation index, m, are expressed by [111]:

$$\begin{aligned} V_1 &= 2\frac{\gamma\cos(\pi V_{bias}/V_\pi) + \gamma^2 - \alpha\gamma\sin(\pi V_{bias}/V_\pi)}{2\gamma\cos(\pi V_{bias}/V_\pi) + 1 + \gamma^2} mV_\pi \\ V_2 &= -2\frac{\gamma\cos(\pi V_{bias}/V_\pi) + 1 + \alpha\gamma\sin(\pi V_{bias}/V_\pi)}{2\gamma\cos(\pi V_{bias}/V_\pi) + 1 + \gamma^2} mV_\pi \end{aligned} \tag{6.17}$$

It should be noted that, for an ideal DE-MZM, $\gamma = 1$, biased at the QP and performing chirpless modulation ($\alpha = 0$), the amplitudes are $V_1 = mV\pi$ and $V_2 = -mV\pi$, which is in accordance with the amplitudes of the drive signals proposed in [71] to generate a chirpless ODSB signal.

6.3.2 Effect of modulation chirp of a DE-MZM on the received signal

As well known, the negative pre-chirping can mitigate the power fading induced by chromatic dispersion [125]. A theoretical analysis of the effect of modulation chirp of a

DE-MZM on the received passband OFDM signal, when transmitted along dispersive single mode fiber, is discussed in this section.

A complex-valued baseband OFDM signal, up-converted to the central frequency f_{rf} ($\omega_{rf} = 2\pi f_{rf}$), can be expressed by:

$$x(t) = x_i(t)\cos(\omega_{rf} t) - x_q(t)\sin(\omega_{rf} t) \tag{6.18}$$

where $x_i(t)$ and $x_q(t)$ are the baseband in-phase and quadrature components of the OFDM signal, with zero mean and energies σ^2_{xi} and σ^2_{xq}, respectively, at the output of the OFDM modulator, before the RF up-converter. Driving the DE-MZM with the drive signals given by (6.14), the optical field at the output of the LiNbO3 DE-MZM with finite ER can be expressed by:

$$E_{out}(t) = \frac{\sqrt{2P}e^{j\omega_c t}}{2}\left\{ e^{j\frac{\pi}{V_\pi}(V_1 x(t) - V_{bias1})} + \gamma e^{j\frac{\pi}{V_\pi}(V_2 x(t) + V_{bias2})} \right\}, \tag{6.19}$$

where $-1 \le x(t) \le 1$ and the amplitudes of the drive signals, V_1 and V_2, are given by (6.17), with $V_{bias} = -(V_{bias1} + V_{bias2})$, and P is the average power of the CW laser emitting at the frequency ν_c ($\omega_c = 2\pi\nu_c$) fed into the optical input of the DE-MZM. Under small-signal modulation conditions ($m \ll 1$), the higher order sidebands are small and can be ignored, and thus the optical field signal given by equation (6.19) can be simplified to:

$$E_{out}(t) \cong \frac{\sqrt{2P}}{2}\left\{ E_- e^{j(\omega_c - \omega_{rf})t} + E_0 e^{j\omega_c t} + E_+ e^{j(\omega_c + \omega_{rf})t} \right\}, \tag{6.20}$$

with

$$\begin{aligned} E_- &= -\left[\Gamma_1 \Lambda_1^* + \gamma \Gamma_2 \Lambda_2^* \right] \\ E_0 &= \left[\Gamma_1 A_1 + \gamma \Gamma_2 A_2 \right] \\ E_+ &= \left[\Gamma_1 \Lambda_1 + \gamma \Gamma_2 \Lambda_2 \right] \end{aligned} \tag{6.21}$$

where $\Gamma_1 = \exp(-j\pi V_{bias1}/V_\pi)$, $\Gamma_2 = \exp(j\pi V_{bias2}/V_\pi)$, $\Lambda_k = J_1(\theta_{kq}(t)) + jJ_1(\theta_{ki}(t))$, $A_k = J_0(\theta_{ki}(t)) + J_0(\theta_{kq}(t))$, with $J_n(\cdot)$ the Bessel function of the first kind of order n ($n = 0,1$), and $\theta_{ki}(t) = \pi V_k x_i(t)/V_\pi$, $\theta_{kq}(t) = -\pi V_k x_q(t)/V_\pi$ are the modulation phase shifts of the baseband in-phase and quadrature components, respectively, when applied to the electrode k = 1, 2. The superscript * denotes the complex conjugate and $j = \sqrt{-1}$ is a pure imaginary number. When this optical signal is transmitted over a dispersive single mode fiber, a phase shift to each optical sideband relative to optical carrier is induced. The

Taylor's expansion of the dispersion propagation constant of the dispersive fiber can be expressed as [133]:

$$\beta(\omega) \approx \beta_0 + \beta_1(\omega - \omega_c) + \beta_2/2(\omega - \omega_c)^2, \quad (6.22)$$

where $\beta_m = d^m\beta(\omega)/d\omega^m|_{\omega=\omega_c}$. The effect of high order fiber dispersion at 1550 nm is neglected. For the sideband centered at the frequency $\omega_c \pm \omega_{rf}$, the dispersion propagation constant is given by:

$$\beta(\omega_c \pm \omega_{rf}) = \beta_{\pm} = \beta_0 \pm \beta_1\omega_{rf} + \beta_2/2\,\omega_{rf}{}^2. \quad (6.23)$$

After transmission over a length L of SSMF, the optical field at the PIN photodiode input can be written as:

$$E_{PIN}(t,L) \cong \frac{\sqrt{2P}}{2}\left\{E_{-}e^{-j\beta_{-}L}e^{j(\omega_c-\omega_{rf})t} + E_0e^{-j\beta_0 L}e^{j\omega_c t} + E_{+}e^{-j\beta_{+}L}e^{j(\omega_c+\omega_{rf})t}\right\}, \quad (6.24)$$

Considering a limited bandwidth PIN photodiode with responsivity $\Re$, the photocurrent can be expressed as:

$$i(t) = \Re\left\{E_{PIN}(t,L)\,E_{PIN}(t,L)^*\right\} = i_{DC} + i_s(t) \quad (6.25)$$

where i_{DC} is the DC photocurrent and $i_s(t)$ the signal photocurrent. For small-signal approximation, $J_n(x) \approx 1/n!(x/2)^n$, and the signal photocurrent as a function of the system parameters is given by:

$$i_s(t) \approx 2\Re P\pi\gamma m F_{bias}\sqrt{1+\alpha^2}\cos\left(\frac{\pi D\lambda_c^2 f_{rf}^2 L}{c} + \arctan(\alpha)\right)\left[x_i(t) + jx_q(t)\right]\cos\left(\omega_{rf}(t-\tau)\right) \quad (6.26)$$

where $F_{\text{bias}} = \sin(\pi(V_{\text{bias1}}+V_{\text{bias2}})/V_\pi)$, D is the dispersion parameter, λ_c is the carrier wavelength, and $\tau = \beta_1 L$ is the time delay suffered by the optical signal propagating a distance L through optical fiber with group delay per unit length, β_1. In the derivation of Eq. (6.26), a very narrow-bandwidth OFDM signal was assumed, such that the amplitude factor cos(·) present in Eq. (6.26) for the central frequency f_{rf} can be assumed constant over all the signal bandwidth. It should be noted that, in the case of a real-valued OFDM signal, expression (6.26) continues valid, with $x_q(t) = 0$.

The average power of the photodetected signal can be approximated by:

$$P_{RF} = \langle i_s(t)^2\rangle R_L \approx 2R_L\left(\Re P\pi\gamma m\right)^2 F_{bias}^2\left(\sigma_{xi}^2 + \sigma_{xq}^2\right)\left(1+\alpha^2\right)\cos\left(\frac{\pi D\lambda_c^2 f_{rf}^2 L}{c} + \arctan(\alpha)\right)^2 \quad (6.27)$$

where $\langle\cdot\rangle$ denotes the averaging operator in time domain and R_L is the load resistor where the RF power is measured. The RF power given by (6.27) is in accordance with equation (1) in [134], when normalized by the RF power in optical B2B configuration, considering as modulating signal a real sinusoidal signal ($x_q(t) = 0$). Thus, (6.27) is the general expression of the RF power after photodetection, in the presence of the modulation chirp. From (6.27) it can be concluded that:

1) When the DE-MZM is biased at its null intensity point, (V_{bias1} and V_{bias2} equal to $V_\pi/2$) there is no signal photocurrent located at the frequency $\omega_{rf.}$ This is clear, since in this case only odd-order harmonics of ω_{rf} are present at the output of the DE-MZM, and there is no optical carrier to beat with the 1st order harmonics to generate the photocurrent signal at ω_{rf}.
2) The negative values of the chirp parameter factor arctan(α), within the argument of the cosine function, have the effect of generating a phase shift opposite to that caused by the cumulative dispersion along the fiber. Thus, the first null occurs for a greater fiber length in the presence of negative chirp, allowing mitigation of the power fading induced by chromatic dispersion for a given distance.
3) The chirp parameter has also impact on the maximum received power, through the factor ($1+\alpha^2$).

In order to validate (6.27), Fig. 6.5 depicts the RF power of the received signal normalized by its maximum obtained analytically, with (6.26), and from numerical simulation of a OFDM-UWB signal following the ECMA-386 standard [100], centered at the frequency f_{rf} = 3.960 GHz, which correspond to the 1st of 14 channels. The DE - MZM is biased at the QP. More details about the OFDM-UWB signal are presented in Appendix B.

From Fig. 6.5 it is concluded that the analytical model derived for the signal photocurrent and its RF power shows excellent agreement with the numerical simulated results obtained, with a small discrepancy. This small discrepancy between the curves can be due to the high peak-to-average power ratio (PAPR) of the components $x_i(t)$ and xq(t). Hence, the approximation of the Bessel functions in Eq. (6.26) may not be

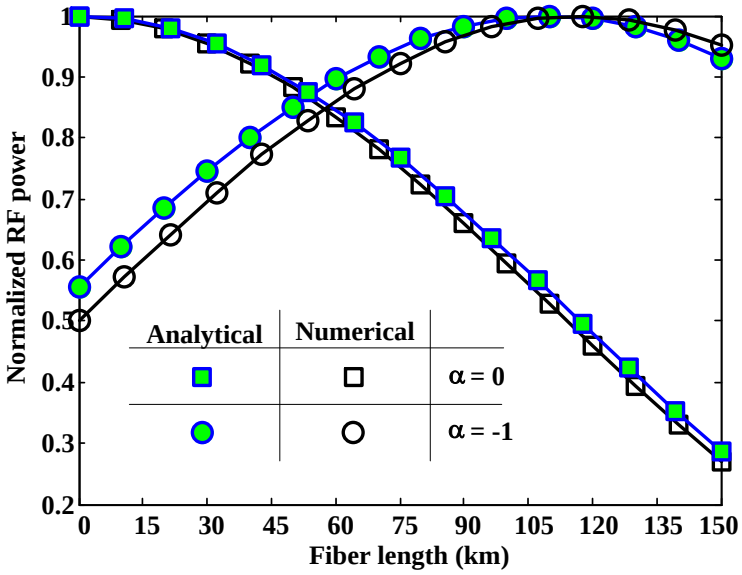

Figure 6.5 – Normalized RF powers as a function of fiber length, for an OFDM signal centered at 3.96 GHz.

accurate, since $x_i(t)$ and $x_q(t)$ have high-peaks at some points. Furthermore, it is observed that the first null for $\alpha = -1$ occurs for a fiber length larger than for $\alpha = 0$.

6.3.3 Effect of modulation chirp of a DE-MZM on the transmission bandwidth

The modulation chirp has impact on the bandwidth-distance product of a SMF [129] and consequently on the SMF transmission bandwidth. The analysis of the transmission bandwidth of the linear dispersive SMF is carried out for a DE-MZM., in a way similar to [135]. First of all, the frequency response of the total transmission system, *i.e.* cascade of transmitter, optical fiber and receiver, is determined. This is then normalized by the frequency response of the system for an optical B2B configuration, in order to exclude the effect of the frequency response of the transmitter and the receiver. The transmission system, whose frequency response is analyzed, is schematically shown in Fig. 6.6. Furthermore, in Fig. 6.6 the main variables used in the analysis along the transmission system are presented, taking into account the time-frequency duality of the Fourier transform (FT).

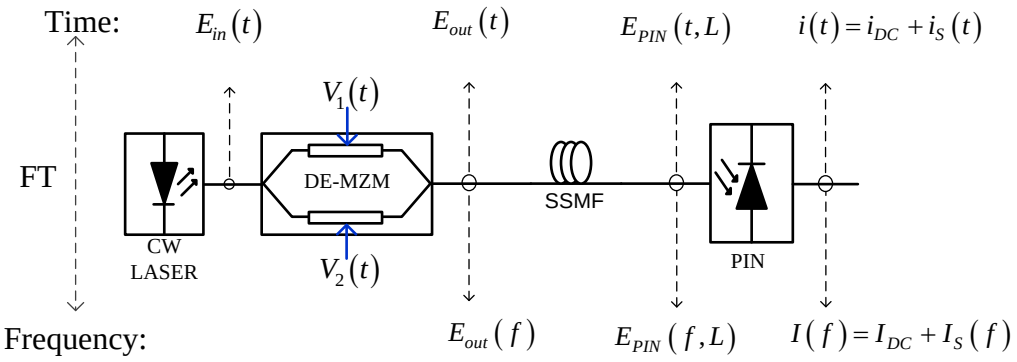

Figure 6.6 – Schematic representation of the time-frequency duality of the variables along the transmission system.

The DE-MZM is driven assuming $x(t) = \cos(\omega_{rf} t)$ in (6.14), and then the optical field at the output of the DE-MZM is expressed by:

$$E_{out}(t) = \frac{\sqrt{2P}e^{jw_c t}}{2}\left[e^{-j\frac{\pi}{V_\pi}V_{bias1}} e^{j\frac{\pi}{V_\pi}V_1\cos(w_{rf}t)} + \gamma e^{j\frac{\pi}{V_\pi}V_{bias2}} e^{j\frac{\pi}{V_\pi}V_2\cos(w_{rf}t)} \right], \quad (6.28)$$

where V_1 and V_2 are given by (6.17) and, for small-signal regime ($m \ll 1$), the optical field in (6.28) can be rewritten as:

$$E_{out}(t) \cong \frac{\sqrt{2P}}{2}\left[E_1 e^{j(w_c - w_{rf})t} + E_0 e^{jw_c t} + E_1 e^{j(w_c + w_{rf})t} \right], \quad (6.29)$$

where:

$$\begin{aligned} E_0 &= \left[\Gamma_1 J_0\left(\frac{\pi}{V_\pi}V_1\right) + \gamma\Gamma_2 J_0\left(\frac{\pi}{V_\pi}V_2\right) \right] \\ E_1 &= j\left[\Gamma_1 J_1\left(\frac{\pi}{V_\pi}V_1\right) + \gamma\Gamma_2 J_1\left(\frac{\pi}{V_\pi}V_2\right) \right]. \end{aligned} \quad (6.30)$$

and Γ_1 and Γ_2 were defined in the previous sub-section. Applying the FT to (6.29), the electric field in the frequency domain is expressed by:

$$E_{out}(f) \cong \frac{\sqrt{2P}}{2}\left[E_1\delta\left(f - \left(\nu_c - f_{rf}\right)\right) + E_0\delta(f - \nu_c) + E_1\delta\left(f - \left(\nu_c + f_{rf}\right)\right) \right], \quad (6.31)$$

where $\delta(f)$ is the Dirac delta function in the frequency domain. After transmission through a length L of dispersive single mode fiber, the electric field in the frequency domain can be expressed by:

$$E_{PIN}(f,L) \cong \frac{\sqrt{2P}}{2} e^{-\alpha_f L}\left[E_1 e^{-j\beta_- L}\delta\left(f-\left(\nu_c - f_{rf}\right)\right)\right. \\ + E_0 e^{-j\beta_0 L}\delta\left(f-\nu_c\right) \\ \left. + E_1 e^{-j\beta_+ L}\delta\left(f-\left(\nu_c + f_{rf}\right)\right)\right] \tag{6.32}$$

where $\beta\pm$ is given by (6.23), and α_f is the attenuation coefficient of the fiber. The photocurrent at the output of a broadband PIN photodiode, in the frequency domain, is then expressed by:

$$\begin{aligned} I(f) &= \Re E_{PIN}(f,L) * E_{PIN}^*(-f,L) \\ &\cong \Re\left(\frac{\sqrt{2P}e^{-\alpha_f L}}{2}\right)^2 \left\{\left(|E_0|^2 + |E_1|^2 + |E_1|^2\right)\delta(f)\right. \\ &\quad + \left[E_0 E_1^* e^{j(\beta_+ - \beta_0)L} + E_1 E_0^* e^{j(\beta_0 - \beta_-)L}\right]\delta\left(f + f_{rf}\right) \\ &\quad \left. + \left[E_0 E_1^* e^{j(\beta_- - \beta_0)L} + E_1 E_0^* e^{j(\beta_0 - \beta_+)L}\right]\delta\left(f - f_{rf}\right)\right\} \end{aligned} \tag{6.33}$$

and the signal photocurrent in the frequency domain is expressed by:

$$\begin{aligned} I_S(f) \cong \Re\left(\frac{\sqrt{2P}}{2} e^{-\alpha_f L}\right)^2 &\left\{\left[E_0 E_1^* e^{j(\beta_+ - \beta_0)L} + E_1 E_0^* e^{j(\beta_0 - \beta_-)L}\right]\delta\left(f + f_{rf}\right)\right. \\ &\left. + \left[E_0 E_1^* e^{j(\beta_- - \beta_0)L} + E_1 E_0^* e^{j(\beta_0 - \beta_+)L}\right]\delta\left(f - f_{rf}\right)\right\}. \end{aligned} \tag{6.34}$$

For small-signal approximation, $J_n(x) \approx 1/n!(x/2)^n$ and, after some algebraic manipulation, the resulting transmission frequency response is expressed by:

$$H(f) = \frac{I_S(f)}{I_S(f)\big|_{z=0}} \cong 2e^{-2\alpha_f L}\sqrt{1+\alpha^2}\left[\cos\left(\frac{\pi D\lambda_c^2 f^2 L}{c} + \arctan(\alpha)\right)\right]. \tag{6.35}$$

Accordingly, the -3-dB bandwidth of the transmission system can be expressed by:

$$f_{3dB}^2 = \frac{c}{\lambda_c^2}\frac{\arctan\left(\sqrt{1+2\alpha^2}\right) - \arctan(\alpha)}{\pi DL}, \tag{6.36}$$

and is similar to the expression of the -3 dB bandwidth of the transmission system using an EAM, derived in [124]. In Fig. 6.7, the variation of bandwidth of an SSMF transmission system as a function of the α chirp parameter is shown, for different fiber lengths, considering a chromatic dispersion parameter D = 17 ps/(km.nm).

It is clear from Fig. 6.7 that the bandwidth of an SMF transmission system is curtailed for positive chirp values. Furthermore, as expected, the bandwidth of an SMF

transmission system is smaller for larger fiber lengths. Nevertheless, the bandwidth difference for different fiber lengths becomes smaller for higher positive α values.

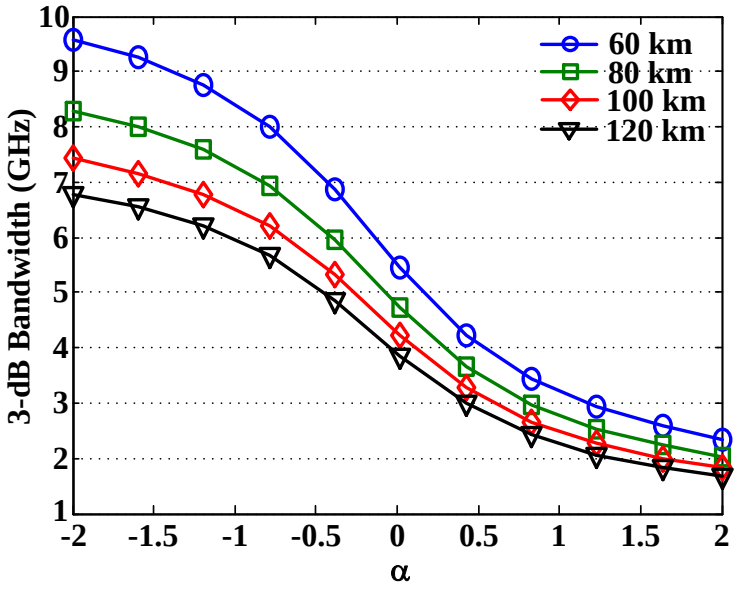

Figure 6.7 - 3-dB bandwidth of an SMF transmission system as a function of the α chirp parameter, for different fiber lengths.

Since the bandwidth is not the only concern for signal performance, in the following section a multi-service OFDM transmission system is presented, to evaluate the transmission performance in long-reach FTTH networks.

6.4 Chromatic dispersion penalty mitigation using modulation chirp

6.4.1 IMDD transmission systems

In Fig. 6.8, a schematic of the simulation setup used to simulate the OHS transmission through an LR-FTTH is presented, similar to that used in [53]. Fig. 6.8 represents the downstream direction between the OLT located at the CO and the hybrid ONU/BS located at the customer premises.

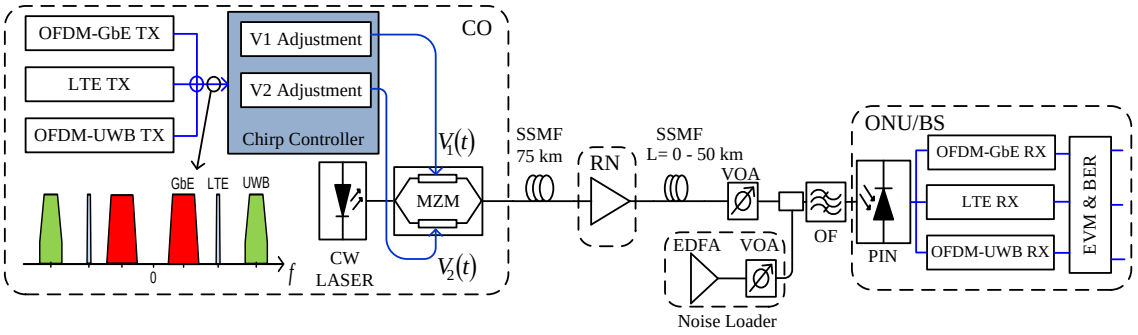

Figure 6.8 - Simulation setup used to simulate the transmission of an OHS through a LR-FTTH with modulation chirp controlled.

In the CO, an EHS $x(t)$ generated by SCM of a custom 16-QAM OFDM-GbE signal, a 16-QAM LTE signal, and an OFDM-UWB signal modulates externally the optical carrier generated by a CW laser emitting at 1550 nm with 5 MHz linewidth, using a DE-MZM. The phase noise of the laser was modeled as a Wiener–Lévy process [118]. The amplitudes of the drive signals $V_1(t)$ and $V_2(t)$, shown in Fig. 6.8, are adjusted in the chirp controller and their values are given by (6.17). A description of how the OFDM signals are generated and demodulated is presented in Appendix B.

The DE-MZM was assumed to provide 25 dB of DC ER and to be lossless. The resulting OHS at the output of the DE-MZM is sent to the customers through a SSMF link modeled as the low-pass equivalent of a linear bandpass system. The SSMF is characterized by an attenuation coefficient of 0.2 dB/km and a chromatic dispersion of 17 ps/(km.nm). After propagation through 75 km of feeder network, at the RN, the optical signal is amplified by a noiseless EDFA to compensate for the losses caused by optical transmission. Then, different fiber transmission segments with 0, 10, 20, 30, and 50 km are considered to simulate different distances from the RN to ONU/BS located at customers premises. These different length segments correspond to transmit distances of 75, 85, 95, 105, 125 km, respectively, from the CO to the ONU/BS. In the noise loading block, a VOA and a EDFA with gain of 15 dB and a noise figure of 4 dB are used to introduce noise in the system and to adjust the OSNR to the desired level. The OSNR is evaluated considering optical noise over the two perpendicular directions of polarization, in a reference optical bandwidth of 0.1 nm (12.5 GHz at 1550 nm).

At the optical receiver, a second-order super-Gaussian OF with 30 GHz FWHM centered at 1550 nm is used to reduce the ASE power, and a PIN photodetector with responsivity of 1 A/W is considered. The ASE noise is modeled as Gaussian noise. The optical power at the input of the PIN photodetector was set to -5 dBm. The thermal

noise of the receiver is not considered, since at the output of the PIN photodetector its effect is insignificant compared with the signal-ASE beating noise [121]. Wireless transmission is not considered, since the goal of this study is to know the impact of modulation chirp on the optical transmission of different OFDM signals through a hybrid LR-FTTH network. Therefore, the photodetected signal is split among three different receivers, to perform OFDM demodulation including removal of CP, serial-to-parallel conversion, DFT, subcarriers equalization, symbol de-mapping and parallel-to-serial conversion, and then the BER is evaluated based on the EVM method applied to the constellation of the signal received at the equalizer output. The performance of the different OFDM signals is assessed in terms the ROSNR at the input of the hybrid ONU/BS to obtain a BER = 10^{-9}. BER estimation based on the EVM method is explained in Appendix C. Furthermore, a BER = 10^{-9} is enough to ensure that the EVM limits of -14.5 dB for QPSK OFDM-UWB and -21.4 dB for 64-QAM LTE signals are respected after optical transmission, as demonstrated in Section C.3 of Appendix C.

The simulation results were produced with Matlab®, considering 14 LTE symbols, 3696 OFDM-GbE symbols, and 3584 OFDM-UWB symbols. In order to select the best *m* to operate the DE-MZM and to have a reference of the performance without fiber transmission, the ROSNR for a BER = 10^{-9} is obtained as a function of *m* for different signals, for an optical B2B configuration, and the results are shown in Fig. 6.9.

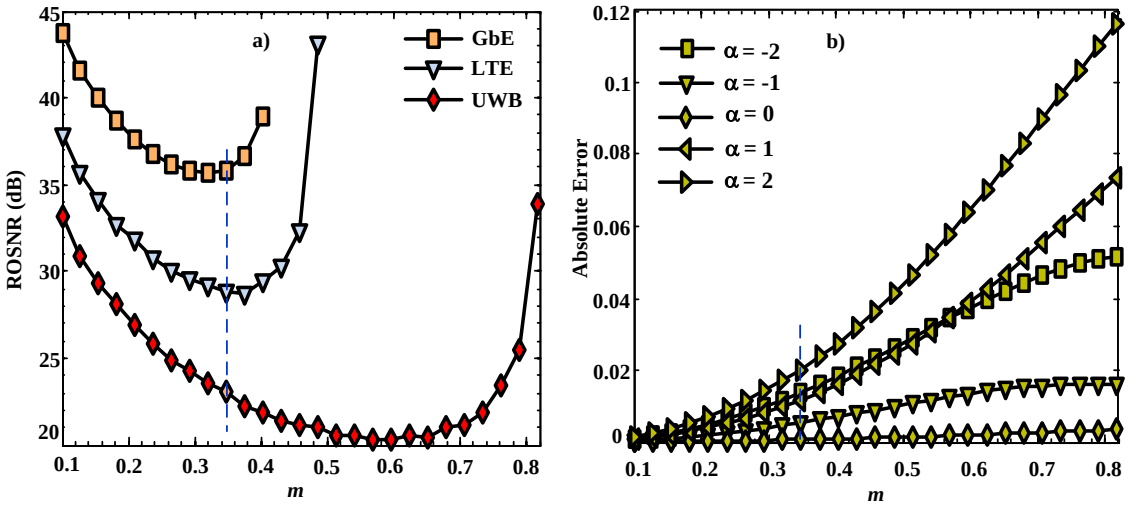

Figure 6.9 – (a) ROSNR for BER = 10^{-9} as a function of *m*; (b) Absolute error between the desired α chirp parameter and the value obtained at the output of the DE-MZM, as a function of *m*.

From the curves presented in Fig. 6.9 a), obtained with the DE-MZM operating in balanced push-pull mode, a modulation index equal to 0.35 is selected, as it represents a good tradeoff between the different ROSNR curves. For *m* = 0.35, the OSNR required

to obtain a BER = 10^{-9} is 35.8 dB, 28.8 dB and 23 dB, for the OFDM-GbE, LTE and UWB signals, respectively.

The ROSNR difference between the UWB and LTE signals for the lower *m* values is due to the different constellation orders, whereas the ROSNR difference between the GbE and LTE signals for the lower *m* values is due to the different electrical drive powers of each OFDM signal. The drive powers estimated on a load of 50 ohms are 4.59 μW, 0.733 μW and 5.77 μW for GbE, LTE and UWB signal, respectively. In order to match the ROSNR curves of LTE and GbE signals, the two signals should have the same PSD. Then, the electrical powers per subcarrier are equal for both OFDM signals and the same SNR per subcarrier is obtained for the lower values of *m*, without the fiber dispersion effect.

The expressions for the amplitudes of the drive signals given by (6.17) were derived for small-signal operation. Therefore, the accuracy of (6.17) is questionable for the *m* value selected. In order to evaluate their accuracy, the absolute error between the desired α chirp parameter value and the value actually obtained at the output of the DE-MZM is calculated for different desired values of the α chirp parameter. The α chirp parameter value at the DE-MZM output is estimated as described in [126], [136]. In Fig. 6.9 b) the absolute error is shown as a function of *m*, for different desired values of α. As can be observed, the maximum absolute error for the *m* value selected is nearly 0.02, which is a negligible error within the range of α values used.

The effect of modulation chirp of a DE-MZM after optical transmission is investigated for different fiber lengths in the distribution network from the RN to the ONU/BS. In Fig. 6.10 a), b) and c), the ROSNR values to have BER = 10^{-9} for GbE, LTE and UWB signals, respectively, are shown as functions of the α chirp parameter for different fiber segments from the RN to the hybrid ONU/BS.

It is apparent from Fig. 6.10 that the controlled negative chirp benefits the performance of all signals, when compared with $\alpha = 0$, at longer distances. It is observed that positive values of α lead to additional dispersion penalty, whereas negative values of α can mitigate the transmission dispersion penalty. However, the reduction of dispersion penalty and the optimum α value are different for the different signals transmitted. The maximum reduction of the dispersion penalty is achieved after transmission through 125 km from the CO to the ONU/BS (50 km from RN to ONU/BS), with dispersion penalty reductions of 1 dB, 1.5 dB and 6 dB for the GbE,

LTE and UWB signals, respectively. The larger dispersion penalty reduction is obtained for the UWB signal, because the dispersion-induced power fading is stronger at the higher subcarrier frequency. The optimum values of α approach 0 as the transmission distance increases. The best values of α to operate de DE-MZM should be -0.2, -0.6 and -1.6, for the GbE, LTE and UWB signals, respectively.

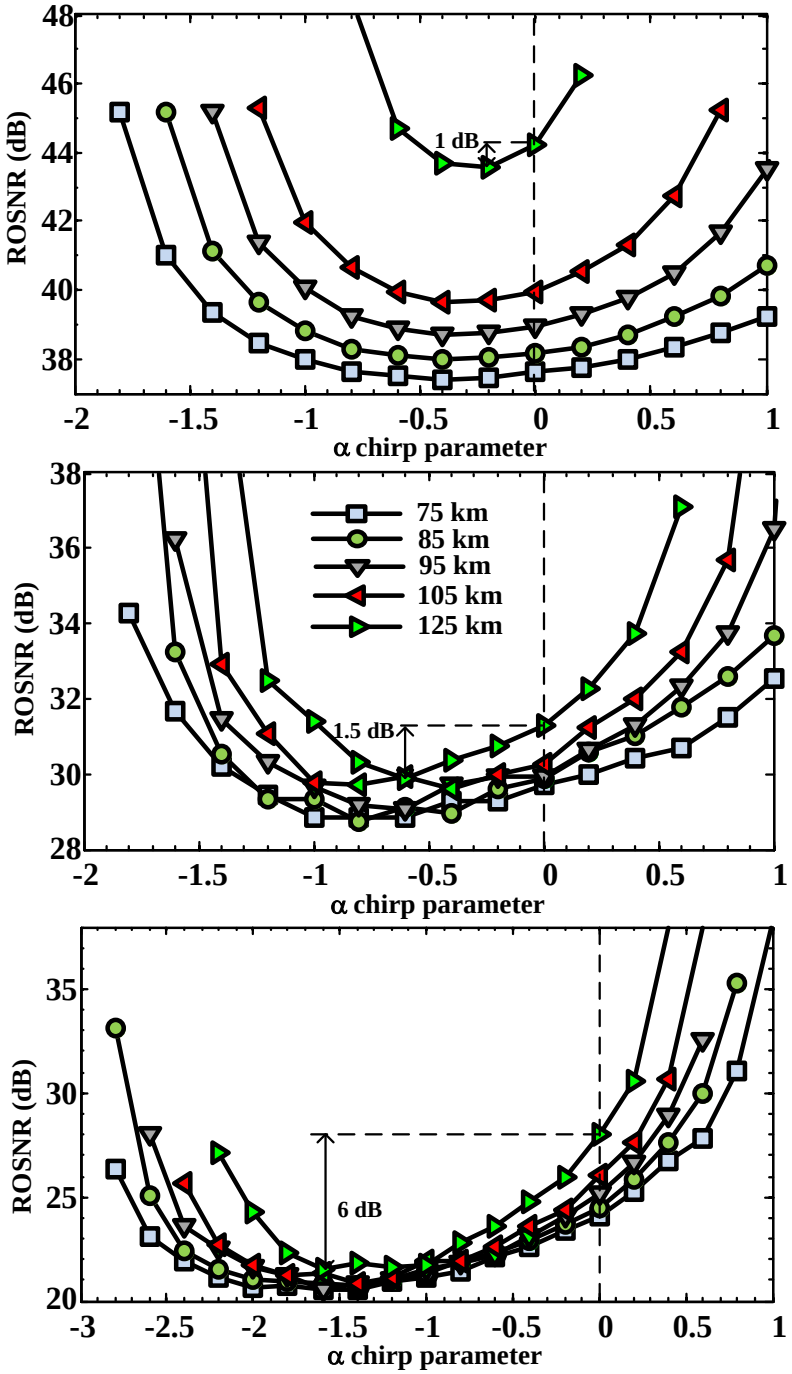

Figure 6.10 - ROSNR for BER = 10^{-9} for different distances from the CO to the ONU, as a function of the chirp parameter, for the following signals: (a) Custom GbE; (b) LTE; and (c) UWB.

Since the DE-MZM only allows setting a single value of α for all signals, a solution is to use the average of the best values for each signal, which in this case study is -0.8. The α chirp parameter value is set at -0.8 and 0 in the DE-MZM located at the CO, and the OSNR penalty as a function of fiber length is estimated. The results obtained are shown in Fig. 6.11. As reference for the OSNR penalty, the OSNR value at the DE-MZM output is considered. The reference OSNR values are the values presented in Fig. 6.9 a) for the selected value of *m*.

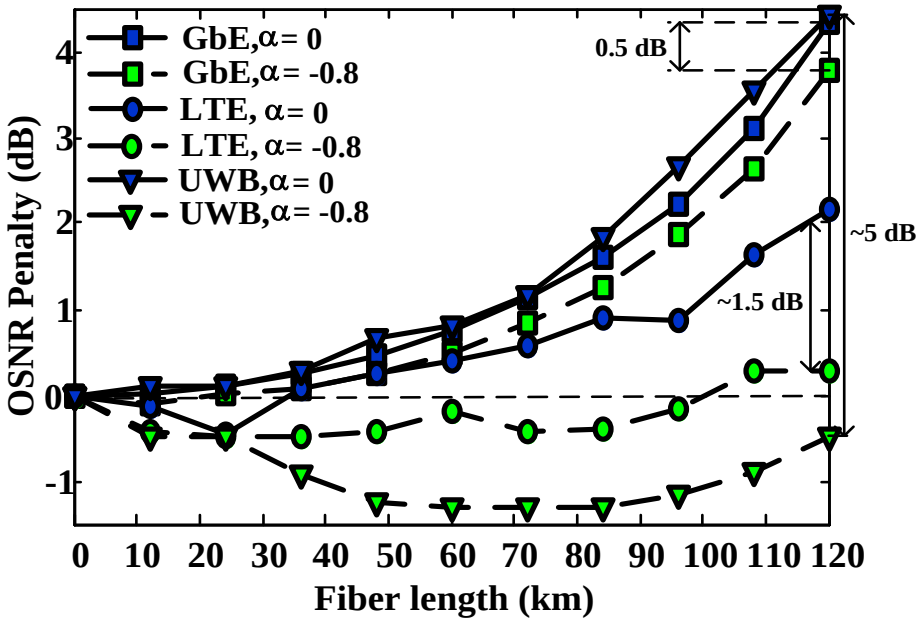

Figure 6.11 - OSNR penalty as a function of fiber length when the DE-MZM is operated with α = -0.8 and chirpless.

From Fig. 6.11 it is concluded that the intensity modulation of the OHS with α = -0.8 allows the transmission of the LTE signal through a fiber length of up to 95 km with negative OSNR penalty, whereas the UWB signal presents negative OSNR penalty for any distance from the CO, in the range considered. On the other hand, the GbE signal presents positive OSNR penalty as the transmission distance from the CO increases, for both values α = -0.8 and α = 0. However, the OSNR penalty is lower by nearly 0.5 dB when negative chirp is considered. For the UWB signal, the OSNR improvement when α = -0.8 compared to α = 0 is nearly 5 dB, whereas for the LTE signal it is nearly 1.5 dB. These results demonstrate that the introduction of controlled negative chirp benefits the performance of services based on any of the OFDM signals considered, after fiber transmission.

The future optical networks will require a sophisticated level of reconfigurability, in order to adapt to dynamic traffic needs and to mitigate system impairments. Optical

modulators with adjustable chirp can exploit the modulation chirp dependencies in order to allow dynamic dispersion compensation, using a real-time network monitoring technique such as proposed in [136].

IMDD systems are largely used in optical access networks due to their simplicity and reduced cost. However, IMDD systems present some drawbacks, such as power fading induced by chromatic dispersion, which occurs after photodetection due to the inherent ODSB spectrum, and low modulation efficiency, since at least 50% of the optical power is wasted in the optical carrier, which does not carry any information.

In this section, it was demonstrated that the introduction of controlled negative modulation chirp in intensity modulation by a DE-MZM mitigates the power fading induced by chromatic dispersion. However, the modulation efficiency improvement and simultaneously the chromatic dispersion mitigation are highly desirable for the next generation optical access networks. In the next section, this point is addressed.

6.4.2 Transmission performance comparison between ODSB and ODSB-RC

In order to improve the modulation efficiency of ODSB signals, inherent to intensity modulation, ODSB-RC modulation [111] has been used, obtained by reducing the power of the optical carrier with an optical notch filter, such as a Fabry-Pérot filter in reflection mode [106] or a narrowband FBG [137]. More recently, a cost-effective method based on biasing the LiNbO3 MZM below its QP, to reduce the power of the optical carrier, has been demonstrated [138].

Up to now, the transmission of optical signals in the presence of modulation chirp has been demonstrated only for intensity modulated signals with full optical carrier, through laser diodes [122], semiconductor optical amplifiers [123], EAMs [124], or DE-MZMs [125], [126].

In Fig. 6.4 it is shown that, inside a bias voltage range around the QP of a DE-MZM, the α chirp parameter components derived can be used to estimate the modulation chirp, whereas they are not valid at the MATP or MITP of the intensity transfer function of the DE-MZM. Unlike the other aforementioned devices, the α chirp parameter of the LiNbO3 DE-MZM given by (6.15) does not depend on the average optical power, *i.e.* power of the optical carrier. This opens the possibility of improving the modulation efficiency of IMDD systems, by employing ODSB-RC modulation, simultaneously with

the control of the modulation chirp to mitigate the power fading induced by chromatic dispersion, as demonstrated in this section.

Figure 6.12 represents schematically a hybrid LR-WDM-PON for a single wavelength transmitted from the OLT located in the CO to the hybrid ONU/BS located at the customer's premises, considering that the separation between wavelengths is enough to allow neglecting the crosstalk between adjacent wavelength channels. In the CO, the optical transmitter based on the DE-MZM has the modulation chirp controlled through the amplitudes of the drive signals, given by (6.17).

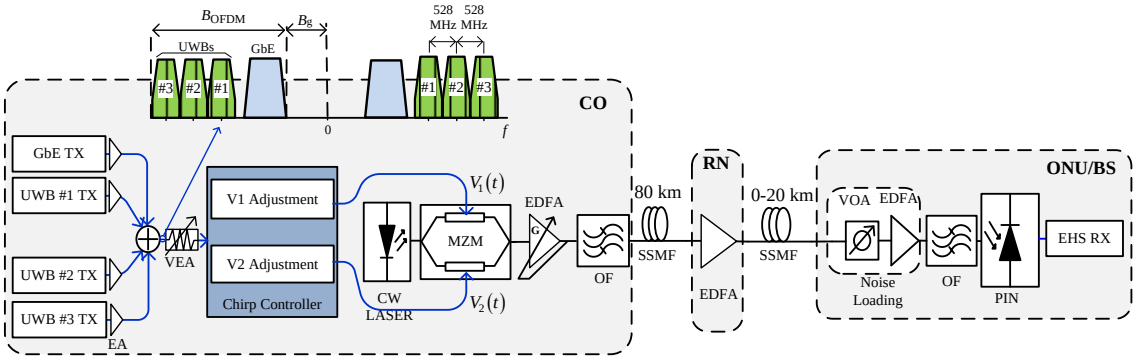

Figure 6.12 - Simulation transmission scheme of an OHS over a hybrid long-reach FTTH network with controlled modulation chirp.

An EHS is created by SCM of four independent OFDM signals: a custom QAM-OFDM-GbE signal with 1 GHz bandwidth, and three independent QPSK-OFDM-UWB signals with 528 MHz bandwidth each.

The three OFDM-UWB signals, UWB #1, UWB #2 and UWB #3, employing QPSK modulation, are up-converted to the frequencies 3.432 GHz, 3.960 GHz and 4.488 GHz, respectively. These three signals perform no frequency hopping, with the three channels at time frequency codes (TFC) TFC5, TFC6 and TFC7, respectively. The subcarriers allocation for each OFDM-GbE symbol is similar to the allocation for the UWB signals. The GbE signal is the only one that is not yet standardized, and thus can be freely transposed in frequency, in order to maximize the B_g between the DC and the lower edge of the GbE signal spectrum and minimize B_{OFDM}, as illustrated in Fig. 6.12. Thus, by allocating a guard band of 100 MHz between the GbE signal and the lower frequency of the UWB signal, the GbE signal is up-converted to the central frequency equal to 2.568 GHz, resulting in a B_{OFDM} = 2.684 GHz and a B_g = 2.068 GHz, which lead to the ratio B_g/B_{OFDM} = 0.7705. Therefore, B_g is insufficient to accommodate all intermodulation distortion products generated upon direct-detection, since it has been shown that B_g should be at least equal to B_{OFDM} [112].

The main parameters used to generate the OFDM signals are presented in Appendix B. The EHS involving four OFDM signals amplified separately modulates externally a CW laser with a linewidth of 5 MHz (conventional DFB laser) emitting at 1550 nm, through a DE-MZM with 25 dB DC ER, half-wave voltage $V_\pi = 5$ V and 6 dB of insertion loss. The phase noise of the CW laser was modeled as a Wiener–Lévy process [118]. The *m* is adjusted through a VEA. The resulting OHS at the output of the DE-MZM is transmitted through SSMF to the customer's premises. When ODSB-RC modulation is employed, biasing the DE-MZM below the QP the modulation excess loss increases. To compensate the losses an EDFA is used, since can be shared between many wavelength channels. The average optical power at the CO output is kept equal for any bias voltage analysed, imposed by the EDFA with controlled gain along with a second-order super-Gaussian OF with 12.5 GHz bandwidth to reduce the ASE power. The SSMF is modeled as the low-pass equivalent of a linear bandpass system, characterized by an attenuation of 0.22 dB/km and a chromatic dispersion parameter $D = 17$ ps/km/nm. After transmission through 80 km of SSMF feeder network, at the RN, the optical signal is amplified by a noiseless EDFA to compensate for the transmission losses. To simulate different locations of the customers relatively to the RN, the OHS is transmitted to the hybrid ONU/BS through fiber segments of length 0 km, 10 km and 20 km.

At the input of the hybrid ONU/BS, a VOA along with along with an EDFA with gain of 15 dB and a noise figure of 4 dB are used to adjust the OSNR of the system, defined in a reference optical bandwidth of 0.1 nm. The OSNR is evaluated considering optical noise over the two perpendicular directions of polarization. In the hybrid ONU/BS, a second-order super-Gaussian OF with 12.5 GHz bandwidth, centered at 1550 nm, is used to reduce the ASE noise power, and a PIN photodetector with responsivity of 0.9 A/W is considered. The ASE noise is modeled as Gaussian noise. The thermal noise of the receiver is not considered, since at the output of the PIN photodetector its effect is negligible, compared with the signal-ASE beating noise [120]. The received EHS is demodulated in the EHS receiver (EHS RX), where each OFDM signal is sent to the respective receiver to perform down-conversion and OFDM demodulation. The OFDM demodulation includes removal of CP, serial-to-parallel conversion, DFT, subcarriers equalization, symbol de-mapping and parallel-to-serial conversion. The performance for each of the received OFDM signals is assessed through the ROSNR for a BER equal to 10^{-9}, estimated by the EVM method applied to

the constellation of the received signal at the equalizer output. This method is presented in Appendix C. Note that a BER = 10^{-9} is enough to ensure that the EVM limit of -14.5 dB after transmission, defined in the standard for QPSK OFDM-UWB signals, is respected.

The simulation results were produced with Matlab®, considering 528 OFDM-GbE and 512 OFDM-UWB symbols. Since the OFDM signals have a spectrum similar to Gaussian noise and different bandwidths, the electrical power of each drive signal is adjusted for a power spectral density equal to -139.6 dB/Hz.

The modulation efficiency of the OHS transmitted was optimized by biasing the DE-MZM below the QP [111]. However, when the DE-MZM is biased below the QP, it operates in the non-linear region of its intensity transfer function, which degrades the transmitted signals due to the generation of harmonics and intermodulation distortion products. To compensate the distortion generated when the DE-MZM is biased below the QP in order to keep constant the performance for all signals, m needs to be decreased. From the study about modulation efficiency optimization, the lowest bias voltage of the DE-MZM is limited by the GbE signal and is equal to -0.8 V_π [111]. Therefore, the bias voltage of -0.8V_π is selected to define the ODSB-RC modulation, as the best value for all signals considered. In order to find the optimum m to drive the DE-MZM in ODSB (V_{bias} = -0.5V_π) and in ODSB-RC (with V_{bias} = -0.8V_π) modulations, the ROSNR as a function of m is evaluated and the result is presented in Fig. 6.13.

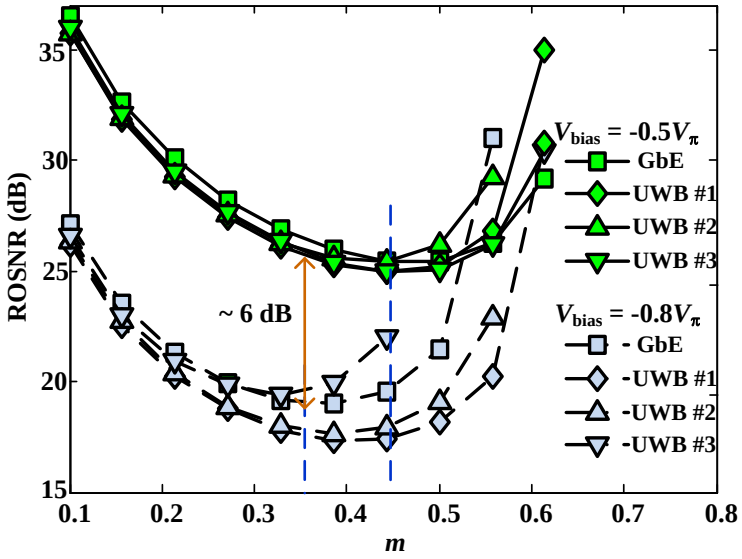

Figure 6.13 - ROSNR for a BER = 10^{-9} as a function of the modulation index for two different bias points of the DE-MZM: -0.5V_π and -0.8V_π.

Biasing the DE-MZM at the QP, all signals present approximately the same ROSNR as m increases (up to $m = 0.5$), since all have the same constellation order and PSD. On the other hand, when the DE-MZM is biased at $-0.8V_\pi$, the GbE and UWB #3 signals exhibit degradation relatively to the other signals, due to spurious spectral components resulting from the nonlinearity of the DE-MZM and the square-law of the direct-detection. The GbE signal is degraded because the ratio B_g/B_{OFDM} is lower than 1, and thus a fraction of the GbE signal is degraded by intermodulation components near DC, after photodetection. When the DE-MZM is biased below the QP, the 2nd harmonic power of the GbE signal at 5.136 GHz increases, affecting the UWB #3 signal centered at 4.488 GHz. Furthermore, in Fig. 6.13 it is observed that the optimum values of m to drive the DE-MZM are approximately 0.35 and 0.45, for the DE-MZM biased at $-0.8\ V_\pi$ and $-0.5\ V_\pi$, respectively. The average OSNR improvement of ODSB-RC ($V_{bias} = -0.8V_\pi$) relative to ODSB with full carrier, for the optimum values of m, among all signals, is about 6 dB.

The drive voltage amplitudes expressed by (6.17) are derived from the small-signal approximation chirp parameter components presented in [126], and depend on the bias point of the DE-MZM. Therefore, it is important to evaluate the accuracy of (6.17) for the optimum values of m, for both ODSB and ODSB-RC modulations. The α chirp parameter value at the DE-MZM output is estimated as described in [136], Figure 6.14 presents the absolute error between the desired α chirp parameter at the output of the DE-MZM and the value obtained as a function of m, for the wired and wireless signals modulated in ODSB-RC and ODSB.

It can be concluded from Fig. 6.14 that, when the DE-MZM is biased at $-0.8V_\pi$, the error of the α chirp parameter desired at the output of the DE-MZM increases, relatively to the error with the DE-MZM biased at $-0.5V_\pi$, due to the increase of the non-linearity of the DE-MZM. Nevertheless, the values of the absolute error obtained for the two different bias voltages are negligible, within the range of values considered. Therefore, the modulation chirp can be controlled with acceptable accuracy for both bias points.

The optimum α chirp parameter values required to obtain the best performance possible are studied for three different distances from the RN to the hybrid ONU/BS: 0, 10, and 20 km.

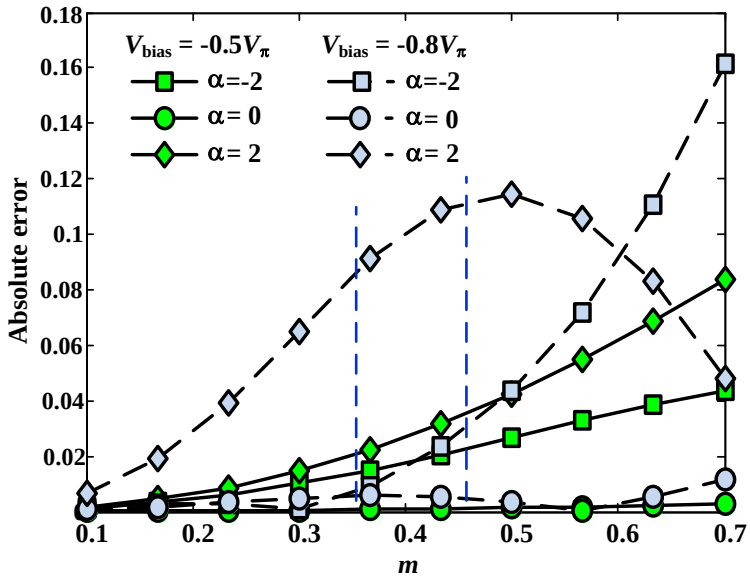

Figure 6.14 - Absolute error between the desired α chirp parameter at the output of the DE-MZM and the value obtained for different bias points of the DE-MZM: -0.5V_π and -0.8V_π.

These correspond to the distances of 80, 90 and 100 km from the OLT to the hybrid ONU/BS. In Fig. 6.15, the ROSNR as a function of the α chirp parameter is presented, for different distances from the CO to the hybrid ONU/BS, with the GbE and UWBs signals modulated in ODSB-RC and ODSB.

From Fig. 6.15 it is concluded that, for ODSB-RC modulation, the introduction of controlled modulation chirp improves the performance for all signals, when compared with $\alpha = 0$. Furthermore, it is observed that, as the central frequency of the OFDM signals increase, the optimum values of α increase towards positive values, demonstrating that positive modulation chirp can also mitigate transmission dispersion penalty. On the other hand, for ODSB modulation, positive values of the α chirp parameter lead to additional dispersion penalty, whereas the negative values of α mitigate the dispersion penalty. Thus, it can be concluded that the reduction of the optical carrier has impact on the optimum values of the α chirp parameter, moving them from negative to positive values. It is observed that the benefits of the introduction of controlled modulation chirp, compared to $\alpha = 0$, are greater for ODSB modulation than for ODSB-RC modulation, mainly because the optimum values of α are more distant from $\alpha = 0$.

The ROSNR curves for the UWB#3 signal, shown in Fig. 6.15 d) for ODSB-RC modulation, exhibit an OSNR penalty compared to ODSB modulation, contrary to what is observed for the other OFDM signals. The reason for this is that the optimum value of

the α chirp parameter for the UWB#3 signal modulated in ODSB-RC is around 0.5, which unfortunately reduces the transmission bandwidth of SSMF, as demonstrated in Fig. 6.7, and consequently the subcarriers of the UWB#3 signal are attenuated.

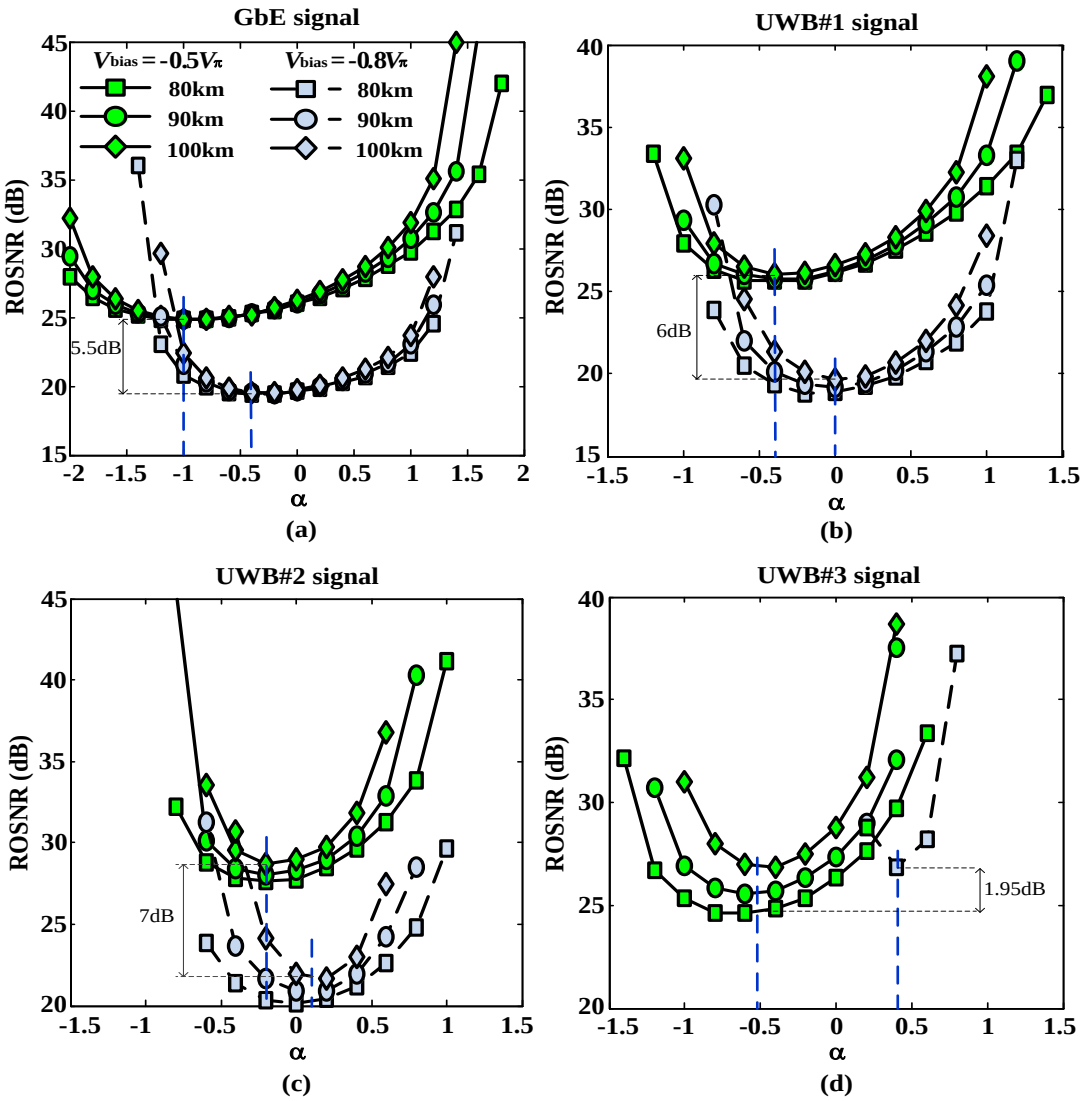

Figure 6.15 – ROSNR for a BER = 10^{-9} for different distances from the CO to the ONU/BS, as a function of the α chirp parameter, for the following signals: (a) GbE signal, (b) UWB#1 signal, (c) UWB#2 signal, (d) UWB#3 signal, all modulated in ODSB-RC (V_{bias}= -0.8V_π) and ODSB (V_{bias}= -0.5V_π).

To better understand the effect of the α chirp parameter on the transmission bandwidth of SSMF, the magnitude of the frequency response in the small-signal regime of a dispersive SSMF link expressed by (6.35) is represented in Fig. 6.16 as a function of frequency for three different values of the α chirp parameter: -0.5, 0 and +0.5. Figure 6.16 shows the frequency response magnitude of a dispersive optical link characterized by D = 17 ps/(km.nm) ,α_f = 0 dB/km and L = 100 km.

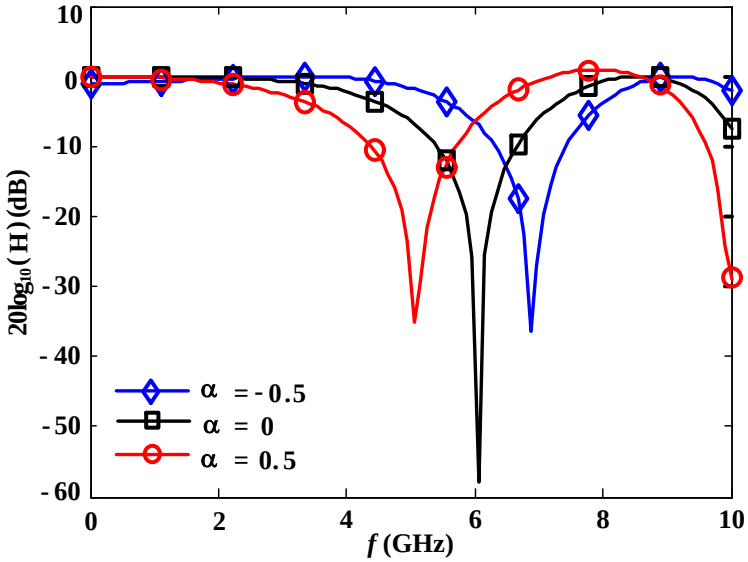

Figure 6.16 - Frequency response magnitude of a dispersive SMF link.

From Fig. 6.16, it is observed that for $\alpha = 0$ the first null in the frequency response occurs around 6 GHz, for $\alpha = -0.5$ around 6.9 GHz, and for $\alpha = 0.5$ around 5 GHz. Thus, for $\alpha = 0.5$ the transmission bandwidth is reduced approximately 1 GHz compared to $\alpha = 0$. The null in the frequency response around 5 GHz for $\alpha = 0.5$ attenuates the subcarriers of the UWB #3 signal centered at 4.488 GHz and with 528 MHz bandwidth, which justifies the OSNR degradation observed in Fig. 6.15 d) for ODSB-RC relative to ODSB modulation. However, this problem can be overcome by changing adaptively the power of the different OFDM signals, using a centralized frequency response compensation at the OLT, such as employed in [53].

6.5 Summary

In this chapter, the effect of modulation chirp on the transmission through SSMF of externally modulated signals based on a DE-MZM was analyzed. The chirp effect of the laser is negligible, since the laser is operated in CW. Therefore, in external modulation based on a DE-MZM the most important modulation chirp is due to the DE-MZM and is studied in detail in this Chapter.

A general expression for the α chirp parameter, decomposed into two parameters related with the two sources of chirp, was presented. The chirp sources, finite ER and drive signals, contribute additively to the total modulation chirp at the output of the DE-MZM. Furthermore, closed form expressions for the amplitude of the drive signals of a

DE-MZM required to control the modulation chirp at its output with accuracy were derived.

The effect of modulation chirp of a DE-MZM was analyzed in both time and frequency domains, for intensity modulated signals. In the time domain, mitigation of the chromatic dispersion effect on the received OFDM signal is analysed, considering a narrow passband OFDM signal. From this analysis it was concluded that driving the DE-MZM with a negative α chirp parameter allows mitigating the chromatic dispersion effect, thereby reducing the power fading induced by chromatic dispersion in IMDD OFDM systems.

From the frequency domain analysis, the frequency response of the SMF transmission was analytically studied, and a closed form expression for the -3dB bandwidth of a SMF transmission system is derived. From this analysis, it was concluded that the bandwidth of a SMF transmission system is strongly dependent on the α chirp parameter and decreases as α increases to positive values. Furthermore, as expected, the bandwidth is reduced for larger fiber transmission lengths.

Finally, chromatic dispersion mitigation for an intensity modulated OHS composed by a custom OFDM-GbE signal, a LTE signal and an OFDM-UWB signal was demonstrated by numerical simulation. Furthermore, the introduction of controlled negative modulation chirp in this intensity modulated OHS lead to negative power penalties after fiber transmission through a long-reach FTTH network, up to specific distances for OFDM-UWB and LTE signals. A performance comparison between ODSB and ODSB-RC was performed, and it was concluded that the benefit of modulation chirp is higher for ODSB than for ODSB-RC, because the reduction of the optical carrier has the effect of moving the optimum α chirp parameter closer to $\alpha = 0$ (chirpless modulation).

7

Conclusions and future work

7.1 Conclusions

A WDM-RoF-PON architecture is considered in this thesis, as a solution for the seamless integration of broadband wired and wireless access networks, referred to as hybrid optical access network. The wireless and wired access networks are used to carry signals with different quality of service specifications, data rates and bandwidths. In order to achieve the integration of wired and wireless access networks into a single shared optical platform in a cost-effective manner, the modulation of different signals in a single wavelength is crucial. Furthermore, for the transmission and delivery of these signals complying with the required quality of service, some challenges have arisen, namely power fading induced by chromatic dispersion and nonlinearities in the electro-optic modulation and upon square-law photodetection.

An optical transmitter scheme based on a z-cut DP-MZM, capable to deliver different wireless services at the MW band and at the 60 GHz MMW band in coexistence with a digital NRZ signal on a single wavelength has been investigated. The wireless signals at MW and MMW band are OTSSB modulated in opposite sides of the optical carrier in a z-cut sub-MZM, whereas in the other z-cut sub-MZM a digital NRZ signal is intensity modulated along with CW sinusoidal signals that emulate optical carriers in the self-heterodyning receivers, for the wireless services in the costumer's

premises. The scheme based on z-cut DP-MZM demonstrated great potential for future converged optical access networks, since it is an integrated modulator that allows modulating wireless signals of all interesting RF bands in coexistence with a BB signal and their delivery in a simple manner. Simulation results indicated that the OFDM wireless signals could be transmitted with high robustness against the power fading induced by chromatic dispersion, because the signals are OTSSB modulated. However, degradation of OFDM signals after 50 km of SSMF transmission has been found to be mainly due to the absence of pilot subcarriers in the OFDM symbols.

Another simpler OSSB transmitter, based on a single DE-MZM, was investigated to transmit signals allocated at the MW band following different standards, through LR-WDM-PONs. A custom 16-QAM OFDM-GbE signal, to provide high speed internet, a 64-QAM LTE signal, to provide enhanced coverage at home through femtocells, and three independent OFDM-UWB signals, to provide multimedia content, were subcarrier multiplexed and used to intensity modulate an optical carrier with a single DE-MZM. To overcome the power fading induced by chromatic dispersion, OSSB modulation based on the filtering method was employed. Nevertheless, due to the nonlinear characteristic of the MZMs, low modulation efficiency is obtained in the intensity modulation. Besides that, in OSSB modulation based on the filtering method a sideband is removed out, which worsens further the modulation efficiency of the OSSB resulting signal. In order to improve the modulation efficiency of the ODSB signal at the output of the DE-MZM, ODSB-RC modulation was used by biasing the DE-MZM below the QP to reduce the optical carrier. However, due to spurious components generated by the DE-MZM and the distortion products from OFDM subcarriers self-beating and beating between different subcarriers of OFDM signals at the quadratic photo-detection, the high constellation OFDM signals close to the DC frequency did not comply with the maximum EVM specified in their standards. To overcome the distortion noise generated by the nonlinearity of the DE-MZM and photodetection, it was proposed to increase the drive power of the OFDM signals more impaired by distortion, which demonstrated to be an effective solution. Furthermore, transmission of the OFDM OSSB hybrid signal up to 130 km with low power penalty has been demonstrated by numerical simulation, which allows concluding that the optimization of the bias voltage and of the OFDM signals drive power applied to the DE-MZM can be performed in an optical B2B configuration.

In order to mitigate the power fading induced by chromatic dispersion in the transmission of wired and wireless signals in LR-PONs, modulation chirp in DE-MZMs has been exploited in thesis. To control electrically the amount of chirp at the output of a DE-MZM, the voltage amplitudes of the drive signals were derived as functions of a chirp parameter, bias voltage and modulation index. Through the drive signals voltage amplitudes determined, the effects of modulation chirp on the received narrowband OFDM signals and on the 3dB bandwidth of SSMF transmission were analytically determined. From that analysis, it was possible to conclude that, for a negative α chirp parameter in intensity modulation with OFDM signals, the nulls in the RF photodetected power appear for larger fiber lengths. On the other hand, a positive α chirp parameter in intensity modulation was found to reduce the 3dB bandwidth of SSMF transmission. Mitigation of power fading induced by chromatic dispersion, for broadband OFDM intensity modulated signals based on modulation chirp, was investigated numerically considering an EHS composed by a 16-QAM OFDM-GbE signal, a 16-QAM LTE signal, and an OFDM-UWB signal. The numerical results indicated that a negative α chirp parameter allows reducing the power fading in any OFDM signal considered, and the optimum value of the α chirp parameter to set in the DE-MZM located in the OLT depends on the fiber length and on the central frequency of the OFDM signals. Finally, a comparison of the mitigation of power penalty induced by SSMF transmission was carried out between ODSB and ODSB-RC modulations, considering as EHS a QPSK OFDM-GbE signal and three independent OFDM-UWB signals. The results indicated that a negative α chirp parameter is more advantageous for ODSB signals than for ODSB-RC, and that a positive α chirp parameter can also be useful to reduce the power fading in ODSB-RC modulated signals.

The general conclusion of this thesis is that the z-cut DP-MZM is an electro-optic modulator with great potential for future hybrid optical networks. Furthermore, OSSB-RC modulation with controlled drive powers, and ODSB, ODSB-RC in a DE-MZM with modulation chirp controlled, have shown the capability to overcome the power fading induced by chromatic dispersion in long-reach hybrid optical access networks.

7.2 Future work

Due to the extensive scope of the work undertaken on the broad field of convergence of wired and wireless access networks, certain areas and potentially interesting directions for future research have been left unexplored. The following topics could be considered:

- Experimental validation of the results presented in the thesis;
- Transmission along LR-WDM-PONs of wired and wireless signals taking into account legacy mobile communications technologies such as GSM and UMTS;
- Uplink transmission considering recovery of the optical carrier from the downstream signal and re-modulation based on reflective modulators such as RSOA and R-EAM;
- During the thesis it was considered only the access to mobile networks through femtocells using 20 MHz LTE signals complying with release 8. However, LTE channels up to 100 MHz in a continuous and non-continuous carrier aggregation, along with MIMO techniques complying with release 10, should be analyzed in coexistence with the other signals considered;
- Energy efficiency in hybrid optical access networks based on WDM-PONs including coherent detection is a research topic of considerable importance.

A

List of publications

A.1 Papers in journal

[J3] Almeida, P. and Silva, H., "OSSB transmitter with modulation efficiency optimized to support OFDM multi-services along hybrid long-reach WDM-PONs" submitted.

[J2] Almeida, Paulo and Silva, Henrique," Investigation of wired and wireless services based on OFDM DSB-RC transmission in the presence of modulation chirp of a DEMZM" *Optics express*, vol.21, no.25, pp.30764-30777, Dec 2013.

[J1] Almeida, Paulo and Silva, Henrique" Impact of Modulation Chirp of a DEMZM on the Transmission of Signals Based on OFDM" *IEEE Photon. Technol. Lett.*, vol.25, no.3, pp.283-286, Feb. 1, 2013.

A.2 Communications

[C10] Almeida, Paulo and Silva, Henrique "Driving a DEMZM to Generate Wired and Wireless OFDM Services in Hybrid Long-reach Optical Access Networks" *Proc International Conf. on Transparent Optical Networks – ICTON2013*, Cartagena, Spain, Vol. -, pp. , July, 2013.

[C9] Almeida, Paulo and Silva, Henrique "Optical Single Sideband Generation Optimized to Support Multi-Services OFDM over Hybrid Long-Reach FTTH Networks" *Proc International Conf. on Transparent Optical Networks – ICTON2013*, Cartagena, Spain, Vol. -, pp. , July, 2013.

[C8] Almeida, Paulo; Silva, Henrique and Medeiros, Maria "Transmission of LTE Signals for Femtocells over Long-reach FTTH networks", Proc. Conf. on Telecommunications – *ConfTele2013*, Castelo Branco, Portugal, Vol. -, pp. 1 - 4, May, 2013.

[C7] Almeida, Paulo and Silva, Henrique "Expressions of the chirp parameter components for intensity modulation with a dual-electrode Mach-Zehnder modulator", Proc *International Conf. on Transparent Optical Networks – ICTON2012*, Coventry, United Kingdom, Vol. -, pp. , July, 2012.

[C6] Almeida, Paulo and Silva, Henrique "Distribution of MB-OFDM UWB and Millimeter-Wave WPAN Signals on Hybrid FTTH Networks," Proc. in *IEEE International Conference on Ultra-Wideband, 2011-ICUWB 2011,* vol., no., pp.1-5, 14-16 Sept.2011.

[C5] Ferreira, Filipe; Pato, Sílvia; Almeida, Paulo; Silva, Henrique and Monteiro, Paulo "Dual Band Signal Generation for Millimeter-wave RoF Systems with Subcarrier Multiplexing," Proc *Conf. on Telecommunications – ConfTele2011*, Lisboa, Portugal, no., vol., pp., 27-19 April, 2011.

[C4] Almeida, Paulo and Silva, Henrique "Multiservices and multiband optical signal generation for hybrid access networks," *International Conference on Optical Network Design and Modeling 2011- ONDM 2011, vol.,no.,pp.1-6*, Bologna, Italy, 8-10 February 2011.

[C3] Ferreira, Filipe; Almeida, Paulo; Antunes, Carlos; and Silva, Henrique "Reconstruction of the non-minimum phase response of chirped fiber Bragg gratings using an adaptive genetic algorithm," in *Proceedings of IEEE Congress on Evolutionary Computation* (IEEE CEC), Barcelona, Spain, 18-23 July 2010.

[C2] Almeida, Paulo; Ferreira, Filipe and Silva, Henrique "Multiband Signals Generation for Hybrid Access Networks Using a Single External Modulator," in Proceedings of Symposium On Enabling Optical Networks and Sensor (SEON), vol., no., pp.1-2, Porto, 25 June 2010.

[C1] Ferreira, Filipe; Almeida, Paulo and Silva, Henrique "Generation of 60 GHz RoF/SCM signals using upconversin and centimeter-wave photonic devices," in *Proceedings of Symposium On Enabling Optical Networks and Sensor* (SEON), vol., no., pp.1-2, Lisbon, 26 June 2009.

A.3 Reports

[R1] Almeida, Paulo; Ferreira, Filipe and Silva, Henrique; "Optical Transmitter for the RoFnet Project Demonstrator", Instituto de Telecomunicações, PTDC/EEA-TEL/71678/2006, June, 2011.

B

Wired and wireless services

B.1 Introduction

In the convergence of wired and wireless access networks to deliver different services, signals with different characteristics and bandwidths / rates are expected to be transmitted through the access networks.

OFDM is well established technology in communications systems, since it is used in different wireless/mobile standards such as IEEE 802.11x WLANs, OFDM-UWB, WiMAX and LTE, as well as in copper wire standards such as digital subscriber lines (DSL) and DVB-T. Recently, the optical OFDM modulation format has been proposed for broadband optical communication systems [139], because it is tolerant to chromatic dispersion and consequently an effective solution to ISI caused by a dispersive optical fiber. Besides that, the spectral efficiency of OFDM is much higher than conventional serial modulation schemes like NRZ, which becomes increasingly important as data rates increase to satisfy the users demand for broadband services.

Thanks to the advance in digital-signal-processing technology, OFDM-PON has been envisioned as a prominent modulation/multiplexing technology for access networking. Furthermore, according to the FSAN group [140] OFDM-PON is a candidate for NG-PON2 [141], for which a standard is not yet defined.

In this appendix, the main characteristics of the OFDM-UWB signals following ECMA-368 standard [100], LTE signals complying with the release 8 [113], and a proposal for a possible OFDM-GbE signal are described. The structures of the

transmitter and receiver and the main parameters required to generate OFDM signals following the different standards considered are briefly described.

The NRZ modulation format is still the most widely deployed modulation format in the optical access networks, currently, because it is easily generated with few components. Therefore, the generation of NRZ modulation format is also considered.

The remainder of this appendix is organized as follows. First of all, in Section B.2 general structures for OFDM transmitter and receivers valid for any wireless signal are introduced. In Section B.2.1.1 the generation of the OFDM-UWB signals is described and the main parameters required to generate the OFDM-UWB signals are identified. Afterwards, the OFDM-UWB receiver is described in Section B.2.1.2. The transmitter and receiver for LTE signals following the release 8 are described in Sections B.2.2.1 and B.2.2.2. Finally, in Section B.3 the wired services are addressed. In Section B.3.1, the different types of optical OFDM systems are introduced and the specification of complex-valued OFDM signals candidate to the standardization of OFDM-GbE signals are presented. At the end of the appendix a summary about the systems discussed is presented.

B.2 Wireless services

Figure B.1 shows the block diagram of the OFDM transmitter and receiver used to simulate the modulation and demodulation of OFDM signals. The structure presented in Fig. B.1 is a generic structure for complex-valued baseband OFDM transmitter and receiver.

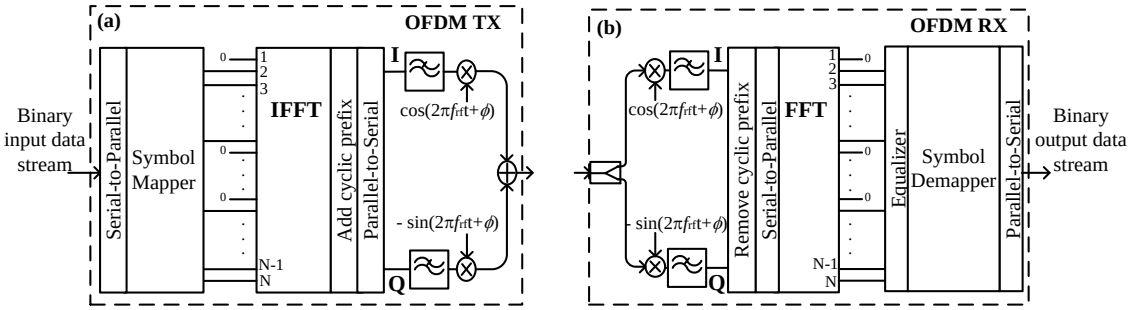

Figure B.1 –Block diagram of the: (a) OFDM transmitter and (b) respective OFDM receiver.

B.2.1 OFDM-UWB signals

B.2.1.1 OFDM-UWB transmitter

The OFDM-UWB signal is generated according to the specification in the ECMA-368 standard [100]. The binary data stream at the input of the transmitter is converted into

N_d parallel binary data streams by the serial-to-parallel block. These N_d binary data streams are applied to a QPSK symbol mapper, where Gray encoding is performed and its outputs feed the inverse fast Fourier transform (IFFT) block to modulate the orthogonal subcarriers in parallel.

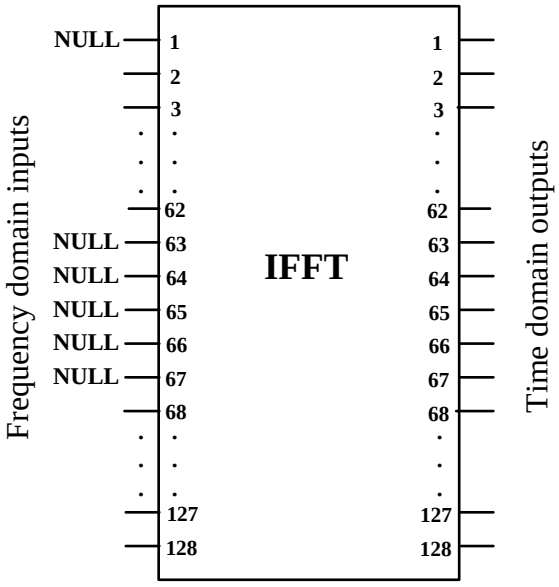

Figure B.2 – Inputs and outputs of IFFT.

The inputs of the IFFT block, referred to as logical subcarriers, are allocated for each OFDM symbol taking account the Fig.B.1 and Fig. B.2 and the values of the main parameters gathered in Table B.1.

Table B.1- Main parameters to generate an OFDM-UWB signal following ECMA-368 standard.

Parameter description	**Value**
Sampling frequency (f_s)	528 MHz
Total number of subcarriers / IFFT size (N)	128
Number of data subcarriers (N_d)	100
Number of pilot subcarriers (N_p)	12
Number of guard subcarriers (N_g)	10
Subcarrier frequency spacing (Δf)	4.125 MHz ($=f_s/N$)
IFFT and FFT time period (T)	242,42 ns ($=1/\Delta f$)
Number of samples in zero-padded suffix (N_{zps})	37
Time duration zero-padded suffix (T_{zps}/T_{cp})	N_{zps}/f_s
Symbol interval (T_s)	312.5 ns ($=T+T_{zps}$)

The total number of subcarriers used is 122 ($N_d+N_p+N_g$) and they are set to the free inputs shown in Fig. B.2. Six logical subcarriers are set to null. The subcarrier falling at DC, 1st subcarrier, is set to null to avoid difficulties in digital-to-analog-converters and analog-to-digital-converters. The DC subcarrier corresponds to the central frequency of

the OFDM signal band after up-conversion, which is the central frequency of the wireless signal radiated.

For each OFDM symbol there are 10 subcarriers, 5 on each edge of the occupied frequency band, allocated as guard subcarriers. The objectives of the guard subcarriers are to relax the specifications of analog transmit and analog receive LPFs, or to improve the performance. Considering the logical subcarriers in the interval [1, *N*], such as represented in Fig. B.2, the guard logical subcarriers are set to the inputs 57, 58, 59, 60, 61 and 67, 68, 69, 70, 71. The data on these subcarriers are created by copying over the five nearest edge data subcarriers of the OFDM symbol.

Furthermore, 12 subcarriers in all OFDM symbols are pilot subcarriers dedicated to allow coherent detection and to provide robustness against frequency offsets and phase noise. These pilot subcarriers are set to the logical subcarriers 5, 15, 25, 35, 45, 55, 73, 83, 93, 103, 113, 123.

In each OFDM symbol, 37 zero-padded samples are added to the orthogonal modulated subcarriers at the output of the IFFT block, to provide robustness against multi-path fading and ISI, and guard time for switching between two sub-bands. Afterwards, the samples are converted from parallel-to-serial, and converted to analog using an ideal DAC. The in-phase (I) and quadrature (Q) components are low pass filtered by an interpolation filter [143] and up-converted by two quadrature RF carriers to the central frequency of each channel.

The time duration of an OFDM-UWB symbol in one sub-band is defined as 312.5 ns. A 9.5 ns guard interval is sufficient for a safe switching between two sub-bands, and a zero-padded 60.6 ns interval provides robustness against multi-path and reduces the power needs.

The whole radio spectrum of 3.1-10.6 GHz for OFDM-UWB is divided into 14 bands with a bandwidth of 528 MHz for each band [100], according to Fig. B.3. These 14 channels are organized in six groups, and the central carrier frequency of each channel is given by $2904 + 528n_b$ MHz, with the band number $n_b = 1, 2,\ldots,14$. Each group has three channels except group five, which has only two channels. Group 1 is mandatory and other groups are optional. Currently most of the devices available in the market [144], [145] work in the band group #1, comprising the three first UWB channels from 3.1 to 4.8 GHz listed in Table B.2.

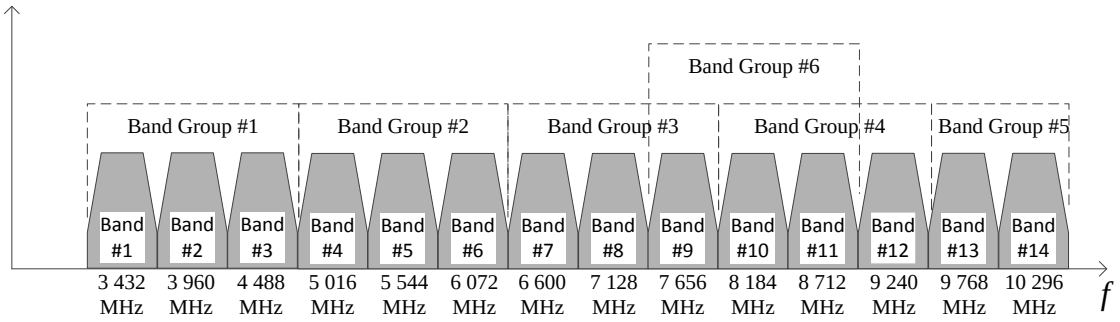

Figure B.3 - Band allocation for multi-band OFDM-UWB [100].

Table B.2 – Detailed frequency information of the band group #1 of ECMA-368 standard.

Band group	**Band ID (n_b)**	**Lower frequency (MHz)**	**Central frequency (MHz)**	**Upper frequency (MHz)**
1	1	3168	3432	3696
	2	3696	3960	4224
	3	4224	4488	4752

In order to enable the operation of multiple OFDM-UWB systems (piconets) at the same time, the OFDM symbols can hop across channels inside each band group, but they cannot hop between groups. A hopping sequence is called a TFC and occurs between OFDM symbol-to-symbol transitions in a predefined order. The structure of the transmitter is very similar to that of a conventional wireless OFDM physical layer subsystem, except that the carrier frequency is changed based on the time-frequency interleaving pattern. Each band group supports 10 TFCs [100].The possible TFCs for band group #1 are gathered in Table B.3.

Table B.3 – Time-frequency codes and preamble patterns for band group #1.

TFC Number	**Base Sequence/Preamble**	**Band_ID (n_b) for TFC**					
1	1	1	2	3	1	2	3
2	2	1	3	2	1	3	2
3	3	1	1	2	2	3	3
4	4	1	2	3	3	2	2
5	5	1	1	1	1	1	1
6	6	2	2	2	2	2	2
7	7	3	3	3	3	3	3
8	8	1	2	1	2	1	2
9	9	1	3	1	3	1	3
10	10	2	3	2	3	2	3

Figure B.4 shows one realization of the transmitted RF signal using three frequency bands, where the first symbol is transmitted on band #1, the second symbol is transmitted on band #2, the third symbol is transmitted on band #3, the fourth symbol is

transmitted on band #1 again, and so on. In addition, it is apparent from Fig. B.4 that the symbol is created by appending a zero-padded suffix to the IFFT output, or equivalently, to the useful OFDM symbol. The zero-padded suffix serves two purposes: it provides robustness against multi-path fading and ISI, and it provides a time window (a guard interval) to allow sufficient time for the transmitter and receiver to switch between the different sub-bands.

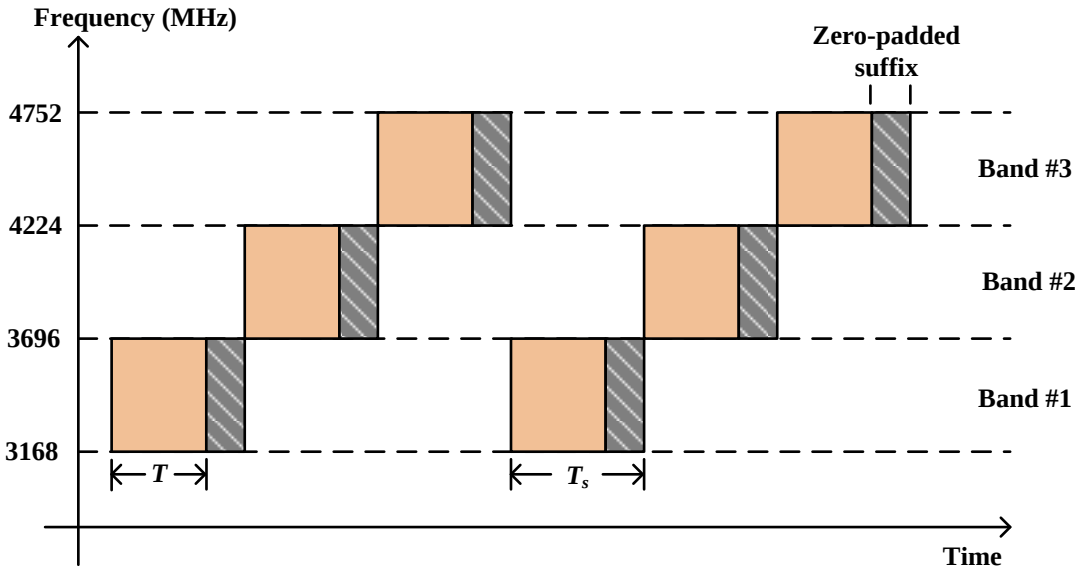

Figure B.4 – Example of time-frequency interleaving following the TFC 1.

An easy way to simulate an OFDM-UWB transmission system operating at the mandatory three lower frequency bands is to assume the TFC equal to 5, 6 or 7 and multiplex the three frequency bands by frequency division multiplexing. In these three TFCs frequency hopping across channels does not occur.

B.2.1.2 OFDM-UWB receiver

The OFDM receiver shown in Fig. B.1 b) performs the reverse operations of the transmitter, with the additional insertion of a channel equalizer after the fast Fourier transform (FFT) block.

At the input of the OFDM receiver, the OFDM-UWB signal is down-converted to baseband by two quadrature RF carriers, and then the I and Q components are low-pass filtered to remove the undesirable spurious spectral components. Normally, these low-pass filters have the same characteristics as the LPFs used in the transmitter. The two baseband components are converted to the digital domain through ideal synchronized ADCs, and 37 zero-padded samples are removed. Afterwards, the samples are converted from serial to parallel and applied to the FFT block to demodulate the orthogonal subcarriers. The FFT outputs that correspond to null and guard subcarriers are

discarded, whereas the pilot subcarriers are extracted to estimate the frequency response of the channel. From the estimated channel frequency response, the frequency transfer function of the equalizer is determined to compensate for the amplitude and phase distortion induced by the transmission channel. The data subcarriers are equalized and sent to the QPSK symbol demapper that performs the demapping of symbol into bits. Finally, the stream of bits is converted from parallel to serial in order to obtain the output binary stream.

B.2.2 LTE signals

In this section, the LTE transmitter and receiver operation in radio frequency division duplex (FDD) mode is described, as proposed in the LTE release 8 standard [113]. The structure for FDD (type 1) of downlink and uplink transmissions is organized into radio frames with 10 ms, consisting of 10 sub-frames of 1 ms and 20 slots of 0.5 ms, such as shown in Fig. B.5. Uplink and downlink transmissions are separated in the frequency domain. Here, only the downlink modulation and demodulation is considered.

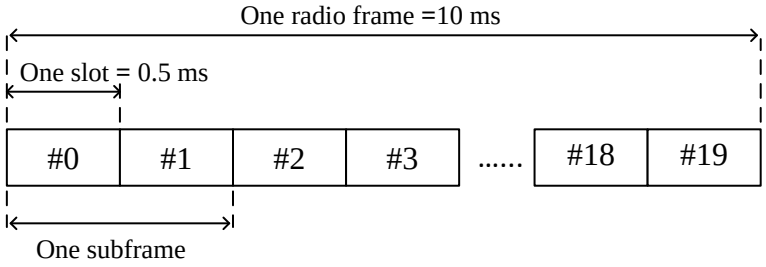

Figure B.5 – Radio frame structure for LTE systems in FDD mode [142].

B.2.2.1 LTE Transmitter

A block diagram of the LTE transmitter is presented in Fig. B.1 a). A binary input data stream is converted from serial to parallel and the bits are then mapped into QPSK, 16-QAM or 64-QAM depending on the data rate required, on the distance from the user device to the transmitter antenna, and on the channel quality. Gray encoding is performed by the symbol mapper block, and its outputs feed the IFFT block to modulate orthogonal subcarriers in parallel. At the input of the IFFT block, the subcarriers are allocated in accordance with a time-frequency grid divided into resource blocks, such as illustrated in Fig. B.6.

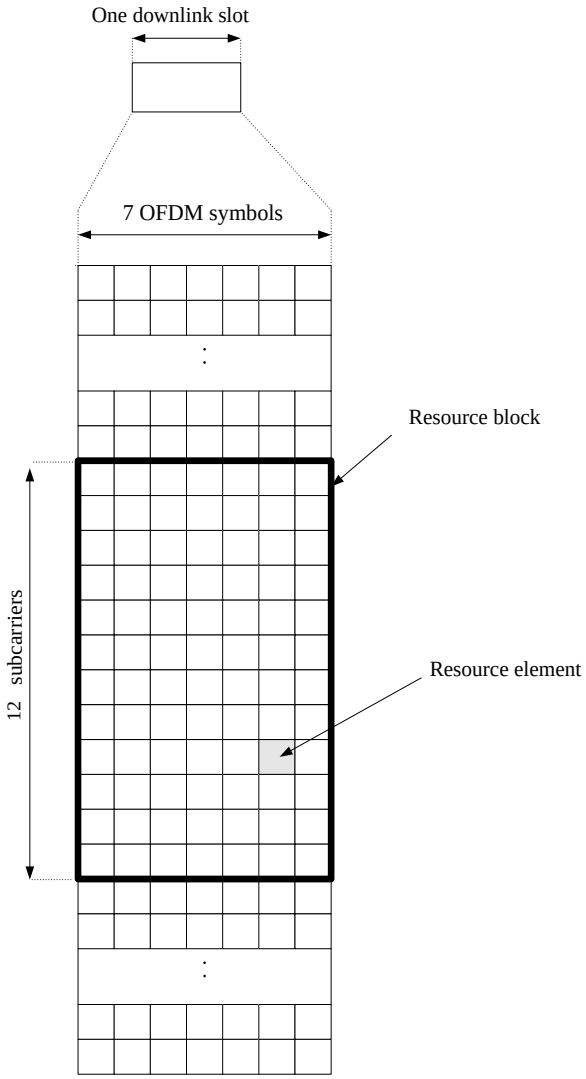

Figure B.6 – Downlink resource grid within a slot, for normal cyclic prefix.

As represented in Fig. B.6, each resource block has the duration of a slot in the time axis and includes 12 subcarriers in the frequency axis. Each sub-frame is divided in two slots of 0.5 ms. Each slot has 7 or 6 OFDM symbols, depending on whether the CP is normal or extended, respectively. The normal CP is used in urban cells and high data rate applications, while the extended CP is used in very large cells (e.g. rural areas, low data rate applications). Two of the 6/7 OFDM symbols are OFDM symbols containing pilot subcarriers equally spaced between data subcarriers. The downlink pilot subcarriers are inserted within the first and third last OFDM symbols of each slot, with a frequency domain spacing of six subcarriers. The arrangement of the pilot subcarriers is shown in Fig. B.7, in two consecutive resource blocks in the time axis, for a single-input single-output LTE system.

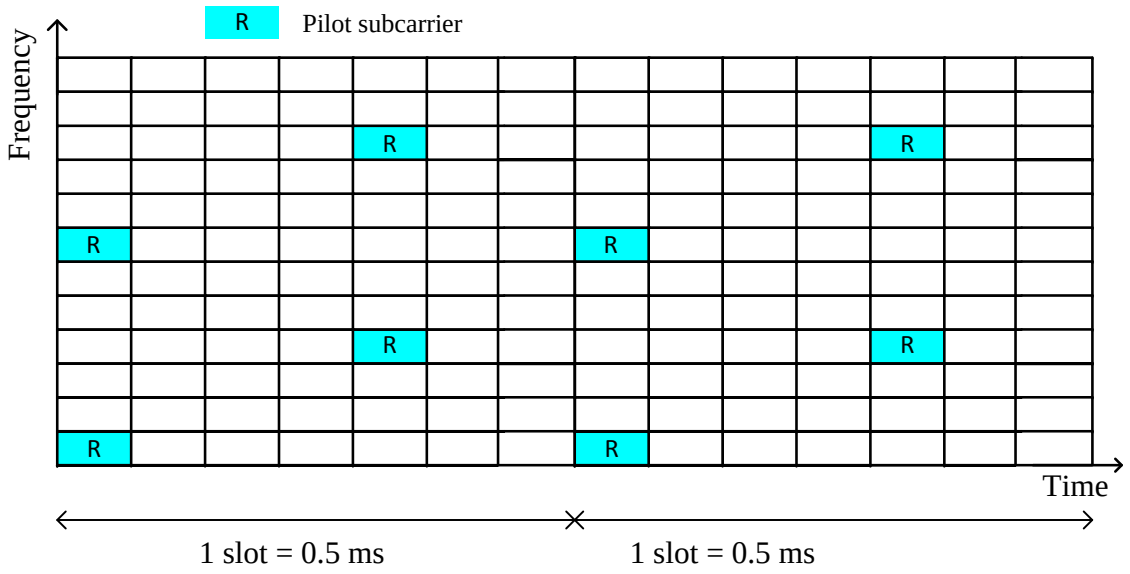

Figure B.7 - Mapping of downlink pilot subcarriers for a single antenna and normal CP.

Guard subcarriers set to null are added to relax the requirements of the filters located at the transmitter and receiver. The number of data subcarriers (N_d), as well as of pilot subcarriers (N_p) and guard subcarriers (N_g), depends on the channel bandwidth considered. The channel bandwidths of 5 MHz and 10 MHz are currently the channel bandwidths most commonly used in practice. Flexile channel bandwidths of 1.4 MHz, 3 MHz, 5 MHz, 15 MHz and 20 MHz are standardized, but in this paper only the bandwidths higher than 5 MHz are considered. The reason for this is twofold: on one hand the mobile operators are installing these bandwidths, and on the other hand these are the bandwidths for which the worse performance is expected. The parameters used in the modulation of the LTE OFDM signals only for bandwidths higher or equal to 5 MHz, in accordance to the downlink physical layer specified in the standard [105], [113], are gathered in Table B.4.

Table B.4 – Main LTE downlink physical layer parameters for FDD mode.

Channel bandwidth (B_{Ch}) [MHz]	5	10	15	20
Subframe duration [ms]	1			
Slot [ms]	0.5			
Subcarrier spacing [kHz]	15			
Sampling frequency [MHz]	7.68	15.36	23.36	30.72
FFT size (N)	512	1024	1536	2048
Occupied subcarriers (DC+N_d+N_p)	301	601	901	1201
Guard subcarriers (N_g)	211	423	635	847
Number of resource blocks	25	50	75	100
Occupied channel bandwidth [MHz]	4.515	9.015	13.515	18.015
OFDM Symbols/slot	7/6(Normal/Extended CP)			

Normal CP [μs]	5.2 (first symbol)/ 4.69 (six following symbols)
Extended CP [μs]	16.67

The first subcarrier (DC subcarrier) of the IFFT block corresponds to the RF central frequency of the transmitting station and is set to null in order to simplify DAC and ADC operations. The DC sub-carrier is not used, as well as guard subcarriers on either side of the channel band. An extended or normal CP is added to the outputs of the IFFT block, depending on the impulse response of the wireless channel. The CP here is a duplication of a fraction of each symbol end. After that, the outputs are converted from parallel to serial and converted to analog using an ideal DAC. The I and Q components are low pass filtered by an interpolation filter and up-converted by two quadrature RF carriers to 2.6 GHz, that corresponds to the E-UTRA band 7 (downstream 2.62-2.69 GHz). However, other bands are specified in LTE standard [145].

B.2.2.2 LTE Receiver

The LTE receiver is represented by the block diagram in Fig. B.1 b). The received signal is low pass filtered to remove undesired components, and then is converted to the digital domain using an ideal ADC. After removal of the CP added at the transmitter side, serial-to-parallel conversion is performed. The resulting signal is converted back to the frequency domain through the FFT block. The outputs of the FFT block are fed to the equalizer block, where the frequency response of the channel is estimated using the pilot subcarriers. The channel response is estimated within each sub-frame using the pilot subcarriers, and the frequency response for all frequencies of the OFDM signal is determined through interpolation. From the channel frequency response, the frequency transfer function of the equalizer is obtained as the inverse of the channel frequency response, designed as Zero-Forcing equalization. The logical subcarriers are multiplied by the transfer function of the equalizer in order to minimize the ISI. The equalized symbols are sent to the demapper block, where the recovered symbols are decoded into data bits, which are converted from parallel-to-serial in order to obtain the recovered binary output data stream.

B.3 Wired services

B.3.1 Complex-valued OFDM-GbE signals

Basically, there are three types of optical OFDM modulations. The first one is IMDD OFDM modulation and is the simplest way of transmitting an OFDM signal [139]. In the next generation PON systems, the IMDD approach allied to simple digital signal processing techniques can represent a significant advantage in terms of costs, thanks to its simplicity and the ease of implementation with mature optical components.

In the second type of OFDM modulation, known as coherently-detected OFDM (CO-OFDM), the information can be transmitted on the intensity and phase of the optical carrier using an optical IQ modulator [146]. This approach needs more complex optical design, if compared to IMDD systems, and this may represent a serious limitation for the subscriber premises equipment.

Finally, in the last type of OFDM modulation, called all-optical OFDM, the subcarriers are directly created and transmitted in the optical domain. All-optical OFDM holds the records in terms of throughput of optical OFDM systems [147]. At the present time, the all-optical OFDM approach is only considered for long-haul networks.

In IMDD OFDM systems, the electrical OFDM signal needs to be purely real-valued, since it uses only intensity variations of the light to transmit the information. Two methods can be used to generate a real-valued OFDM signal:

- The first one consists in electrically up-converting the complex baseband signal generated at the output of the OFDM modulator to a central frequency f_{rf} through I/Q mixing. In this scheme, one DAC for the quadrature component and one DAC for the in-phase component of the OFDM time-domain signal are required.
- The second way of generating the real-valued OFDM signal is in digital domain, through the Hermitian symmetry of the inputs of the IFFT block. The Hermitian symmetry condition creates a real-valued baseband OFDM signal by imposing an IFFT with $2(N_d + 1)$ inputs, with symbols given by [148]:

$$\begin{cases} a_k = a^*_{2(N_d+1)-k} \\ a_0 = a_{Nd+1} = 0 \end{cases}, k = 1, 2, ..., N_d \tag{B.1}$$

where N_d is the number of data subcarriers, without considering the DC subcarrier. One of the advantages of this approach over the electrical up-conversion is that the system will not suffer from any kind of I/Q unbalancing, neither on the transmitter nor on the

receiver side. However, its main drawback is the spectral efficiency reduction of the signal, since half the inputs of the IFFT are not used to carry useful information.

Due to this reason, the complex-valued OFDM signals and electrical up-conversion approach is used to carry the Gigabit Ethernet information through optical transmission. Therefore, the structure of the transmitter and receiver are shown in Fig. B.1 a) and b), respectively. The proposal for the modulation and demodulation of the OFDM-GbE signals has the same operation principle of the OFDM-UWB signals, and the main parameters required in the modulated signal generation are gathered in Table B.5.

Table B.5 – Main parameters required to generate the OFDM-GbE signal.

Nominal bandwidth [GHz]	**1**	**2**
Sampling frequency *f*s [GHz]	1.056	2.112
FFT/IFFT size (N)	256	512
Number of data subcarriers (N_d)	216	434
Number of pilot subcarriers (N_p)	24	48
Number of guard subcarriers (N_g)	15	29
Cyclic prefix number of samples (N_{cp})	64	128

Regarding the constellation employed for the OFDM-GbE signals, QPSK, QAM, 16-QAM and 64-QAM can be used, since a standard is not yet defined at this moment.

B.3.2 Non-return-to-zero signal

NRZ is a frequently used modulation format, since it is straightforward to generate with few components. The main functional blocks required to generate an NRZ signal are represented in Fig. B.8.

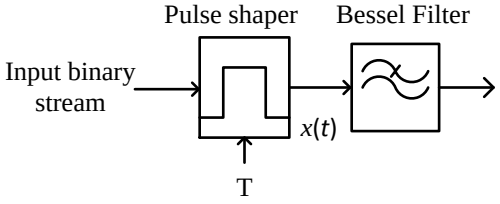

Figure B.8 - Block diagram to generate a bipolar NRZ signal.

After the pulse shaper, the generated waveform $x(t)$ can be written in the form:

$$x(t) = \sum_{k=-\infty}^{+\infty} a_k \, p(t - kT_s) \tag{B.2}$$

where a_k is the k-th symbol, $p(t)$ is the pulse shape, and T_s is the symbol duration. For a binary NRZ signal, $a_k = 1$ when the pulse shaper input bit is '1' and $a_k = -1$ when the input bit is '0'. Considering rectangular pulse shapes given by $p(t) = u(t)-u(t-T_s)$, where $u(t)$ is the step function, in order to limit the spectrum of the NRZ signal at the output of

the pulse shaper the signal is normally filtered by a Bessel LPF to smooth the transitions between sates.

B.4 Quality requirements

The quality of the wireless signals is defined in terms of the EVM measured at the output of the transmitter in the base station. The EVM is a measure of the difference between the ideal symbols and the measured symbols after the equalization. This difference is called the error vector. The EVM is defined as the square root of the ratio between the mean error vector power and the mean reference power, expressed in percentage or in decibels. In Appendix C it is explained how the EVM is determined from the received signal constellation.

The measured/estimated EVM values should be better than the EVM limits defined in the respective standards, presented in tables B.6 and B.7 for OFDM-UWB and LTE signals.

Table B.6 – EVM requirements for OFDM-UWB signals [100].

Modulation scheme	Required EVM [%]	Required EVM* [dB]
QPSK, data rate up 200Mbit/s	18.84	-14.5

Table B.7 – EVM requirements for LTE signals [145].

Modulation scheme	Required EVM [%]	Required EVM* [dB]
QPSK	17.5	-15.13
16QAM	12.5	-18.06
64QAM	8	-21.94

*$20\times\log_{10}$(EVM)

The signal quality required for the OFDM-GbE signal is defined in terms of BER. For the state-of-the-art FEC limit (BER = 2×10^{-3}), in order to have an operational margin, BER = 10^{-4} typically has been chosen as the performance criterion [149], [150].

B.5 Summary

In a converged access network, signals with different characteristics carry information of the different services to the final users. In this appendix, the physical layer main characteristics for the modulation and demodulation of LTE and OFDM-UWB signals are presented. A proposed specification of the main parameters for modulation and demodulation of OFDM signals to carry 1 Gbit/s Ethernet information is presented.

Furthermore, the structure of the transmitter and the receiver is equal for both wireless and wired signals, which enables the integration of all transmitters and receivers in a single chip.

C

Relationship between EVM, SNR and BER

C.1 Introduction

Measuring the quality of signals is one of the most important tasks in the evaluation of any communication system. A variety of performance measures are available, being the BER the most conclusive in digital communication systems. However, BER is sometimes difficult to quantify, especially in simulations and off-line estimation, due to the processing time required.

In wireless communication systems, especially when QAM formats are used, BER and EVM are two primary specifications that determine the performance of the wireless systems in terms of transmitted and received symbols corresponding to a given digital modulation scheme.

In optical communication systems, the OOK intensity modulation is the the most employed modulation format. In these systems, a variety of performance measures are available, namely the shape of the eye diagram, the OSNR, and the *Q*-factor. In order to estimate BER from the Q factor, marks and spaces in the detected photocurrent are assumed to be disturbed by additive white Gaussian noise, the probability density of which is fully described by its mean and variance. Thanks to the advance in digital-signal-processing technology, OFDM has been envisioned as a prominent modulation/multiplexing technique to be employed in different communication systems, such as RoF access networks [151], metro networks [152] and long-haul transmission systems [153].

Four approaches have been used to calculate the BER in the simulation of optical OFDM systems: Monte Carlo simulation, semi-analytical approaches, analytical methods (see references in [154]), and through EVM considering the received OFDM signal corrupted only by Gaussian noise [95], [155]. The latter method is the most employed to estimate the performance of OFDM signals transmitted over optical fiber, because it is the simplest method. Therefore, a method to estimate the BER as a function of EVM is presented here.

The remainder of this appendix is organized as follows. In Section C.2, the error vector magnitude calculated as an average of the EVM for different subcarriers is presented. The relationship between EVM, SNR and BER is explained in Section C.3 and the model of BER as a function of the root mean square value of the EVM is presented and validated with another model proposed in the literature. Finally a summary of this appendix is presented in Section C.4.

C.2 Error vector magnitude

EVM is a measure of the difference between the measured (received) symbols and reference symbols of a noiseless and non-distorted constellation. This difference is called the error vector, as illustrated in Fig. C.1. The EVM is defined as the square root of the ratio between the mean error vector power and the mean reference power, expressed in decibels or in percentage. EVM measurements are often performed in real-time VSAs, or other instruments that capture a time record and internally perform a FFT to enable frequency domain analysis.

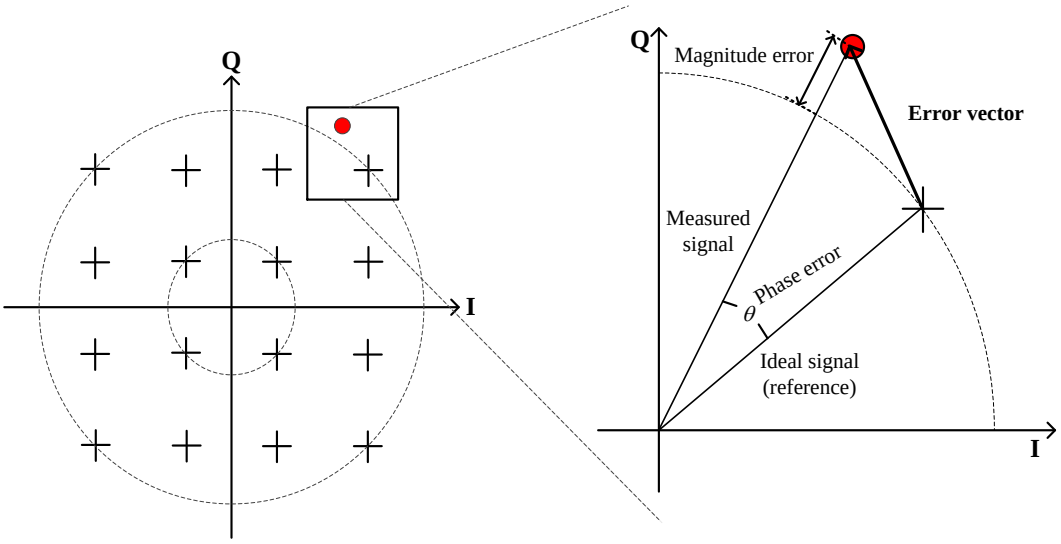

Figure C.1 – Normalized constellation diagram for 16-QAM and representation of reference and measured symbols and the corresponding error vector.

To allow direct calculation of EVM, normalization of the constellations is required to find the EVM by comparing an ideal symbol value with one that is measured. The normalization is such that the mean-square amplitude of all possible symbols in the constellation is one [156].

Consider a received OFDM signal with N_s OFDM symbols (typically a large number of symbols) at equalizer output, with the guard symbols and pilot subcarriers discarded, before the parallel-to-serial conversion. Each OFDM symbol has N_d data subcarriers, such as depicted in Fig. C.2. The higher frequency subcarriers are attenuated by the optical and electrical filters of the optical transmission system, reducing the SNR of each subcarrier, which causes an increase of BER for the higher frequency subcarriers [153]. Hence, the EVM should be determined as the average over all N_d data subcarriers of the EVM of each subcarrier.

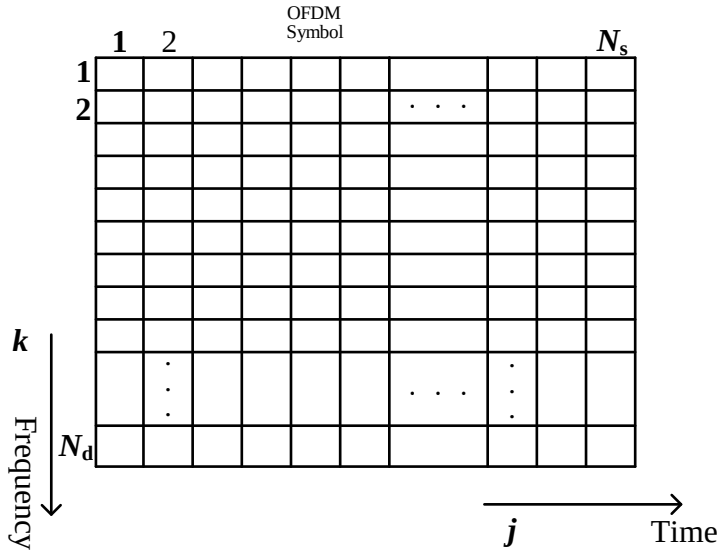

Figure C.2 - Time-frequency grid of the OFDM symbols.

The root mean square EVM for the k^{th} subcarrier, is given by [155]:

$$EVM_{RMS}[k] = \sqrt{\frac{\sum_{j=1}^{N_s} \left| s_o^{(j)}[k] - s_i^{(j)}[k] \right|^2}{\sum_{j=1}^{N_s} \left| s_i^{(j)}[k] \right|^2}}, \tag{C.1}$$

with $k = 1, 2, \ldots, N_d$. The resulting terms in the numerator inside the square root are the normalized error vector powers due to noise or/and distortion on the received symbols, whereas the resulting terms in the denominator inside the square root are normalized powers of the symbols of the ideal constellation.

The RMS EVM of the OFDM signal over N_d symbols is given by:

$$EVM_{RMS} = \sqrt{\frac{1}{N_d}\sum_{k=1}^{N_d} EVM_{RMS}^2[k]} \tag{C.2}$$

where $s_i^{(j)}[k]$ and $s_o^{(j)}[k]$ are the ideal and obtained (received) symbols at the equalizer output, corresponding to the j^{th} OFDM symbol of the k^{th} subcarrier.

C.3 Relationships between EVM, SNR and BER

In a multi-level communication system, the symbol errors can arise from two different effects: noise and distortion on the amplitude and phase of the received data symbols. For a communication system with additive white Gaussian noise channel, the error power terms in (C.1) are noise power terms, and then the ratio of the normalized noise power to the normalized signal power of in the ideal constellation can be related with the SNR in the following form [95]:

$$EVM_{RMS} \approx \left(\frac{Noise\ \text{power}}{Signal\ \text{power}}\right)^{\frac{1}{2}} = \left(\frac{N_0}{E_s}\right)^{\frac{1}{2}} = \left(\frac{1}{SNR}\right)^{\frac{1}{2}}, \tag{C.3}$$

where N_0 is the unilateral noise power spectral density and E_s is the average symbol energy. (C.3) expresses the relationship between EVM and SNR for Gaussian noise channels. The average symbol error probability for an M-QAM modulation constellation with $M = 2^{2n}$, where n is an integer, as a function of E_s/N_0 [157], is given by:

$$P_e \cong 2\left(1-\frac{1}{\sqrt{M}}\right) erfc\left(\frac{3}{2(M-1)}\frac{E_s}{N_0}\right) \tag{C.4}$$

Using Gray mapping, for large SNRs the following well-known relation can be applied:

$$BER[k] = \frac{P_e}{\log_2 M} = 2\left(1-\frac{1}{\sqrt{M}}\right) erfc\left(\frac{3}{2(M-1)}\frac{1}{EVM_{RMS}^2[k]}\right) \tag{C.5}$$

where *erfc*(.) is the complementary error function. The $EVM_{RMS}[k]$ is calculated by (C.1). Due to the different attenuations on the received subcarriers with different frequencies, similarly to the EVM, the BER of a received OFDM signal should be determined as the average over all data subcarriers of the BER values of each subcarrier. Then:

$$BER = \frac{1}{N_d}\sum_{k=1}^{Nd} BER[k] \tag{C.6}$$

Equation (C.5) is simpler than the equation presented in [155] for BER as a function of the EVM_{RMS}. To validate equation (C.5), the BER is shown in Fig. C.3 as a function of EVM_{RMS} obtained with (C.5), overlapped with the BER given by reference [155], for different values of M.

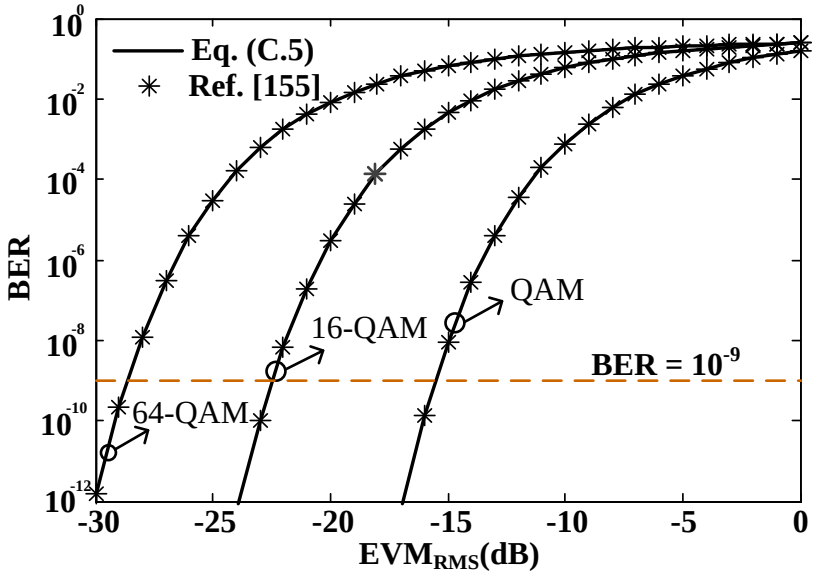

Figure C.3 – Comparison of two different models to relate EVM with BER.

From Fig. C.3 it can be concluded that the model derived for the relationship between BER and EVM and expressed by (C.5) is in excellent match with the model presented in [155].

A comparison between four methods to estimate BER is presented in [155], and it has been shown that the BER estimation by the EVM method shows a good accuracy for modulation indexes lower or equal to 35%. For higher modulation indexes and with fiber chromatic dispersion, the EVM method to estimate BER has been demonstrated to be conservative, since it provides higher values of BER than the other methods.

C.4 Summary

Performance assessment of transmitted signals is an important procedure to evaluate any communication system. In this appendix, the EVM measure typically specified in wireless standards is presented and its relationship with SNR and BER is shown. The relationship between EVM, SNR and BER is especially important to estimate the

performance of OFDM signals transmitted over optical fiber, because it is a ratio of two mean powers and is insensitive to the constellation geometry.

D

Remote heterodyning in OFDM RoF systems

D.1 Introduction

The MMW band has attracted much attention due to the worldwide availability of a license-free 7 GHz band around 60 GHz for multi-gigabit per second wireless communications, which makes this MMW band very attractive for wireless transmission of high-definition multimedia content and broadband wireless access. However, the wireless transmission in this band has some drawbacks, such as high propagation attenuation and cost of the components required to build the transmitter. In order to distribute the wireless signals, RoF technology has been considered a promising solution, since the optical fiber has low attenuation and huge bandwidth, enabling optical transport of MMW signals along large distances. To simplify and reduce the cost of the optical transmitters in RoF systems, some techniques have been proposed in the literature, and were summarized in [80]. The up-conversion of broadband signals to the MMW band is usually achieved by heterodyning two optical spectral components in a high-speed photodiode.

The method of heterodyning two unlocked lasers with different linewidths, in which one is externally modulated and the other is un-modulated, has been proven to be the simplest method to generate modulated MMW signals [158], [159]. As no locking scheme is used for the lasers, the complexity of the system is shifted to the receiver, in the demodulation of the received signals.

The main advantage of the method resides in its simplicity, whereas drawbacks come in the form of the resulting linewidth of the MMW carrier signal. In the case of uncorrelated heterodyning of two laser sources, there is complete decorrelation of the laser spectral lines, and thus the resulting MMW carrier signal will have a linewidth equivalent to the sum of the lasers linewidths [158]. Two incoherent demodulators have been demonstrated in [158]: self-homodyne and envelope detection. Envelope detection is preferred over self-homodyning because it is cheaper and has been shown to provide better sensitivity [159].

In this appendix, expressions are derived for the MMW OFDM-UWB and MW OFDM-UWB signals obtained after transmission through a RoF system based on the heterodyne mixing in a broadband photodiode of a phase shifted OSSB OFDM-UWB signal with an uncorrelated signal emitted by a free-running CW laser. Furthermore, a particular case is addressed, in which the two lasers are phase-locked.

The remainder of this appendix is structured as follows. In Section D.2, general expressions for remote heterodyning in RoF systems are derived. In Section D.2.1, the particular case of phase-locked lasers is addressed, to investigate the impact of an optical phase shift at the output of an OSSB modulator, generated by a phase modulator driven by a DC voltage, on the EVM performance of the OFDM signals in the different bands. Finally, a summary of this appendix is drawn in Section D.3.

D.2 Theoretical analysis

Fig. D.1 shows the general scheme of heterodyning an OSSB plus carrier OFDM-UWB signal with a free-running LO laser in a broadband photodiode to generate the OFDM-UWB signal at the MMW band and a copy of the OFDM-UWB signal at the MW band.

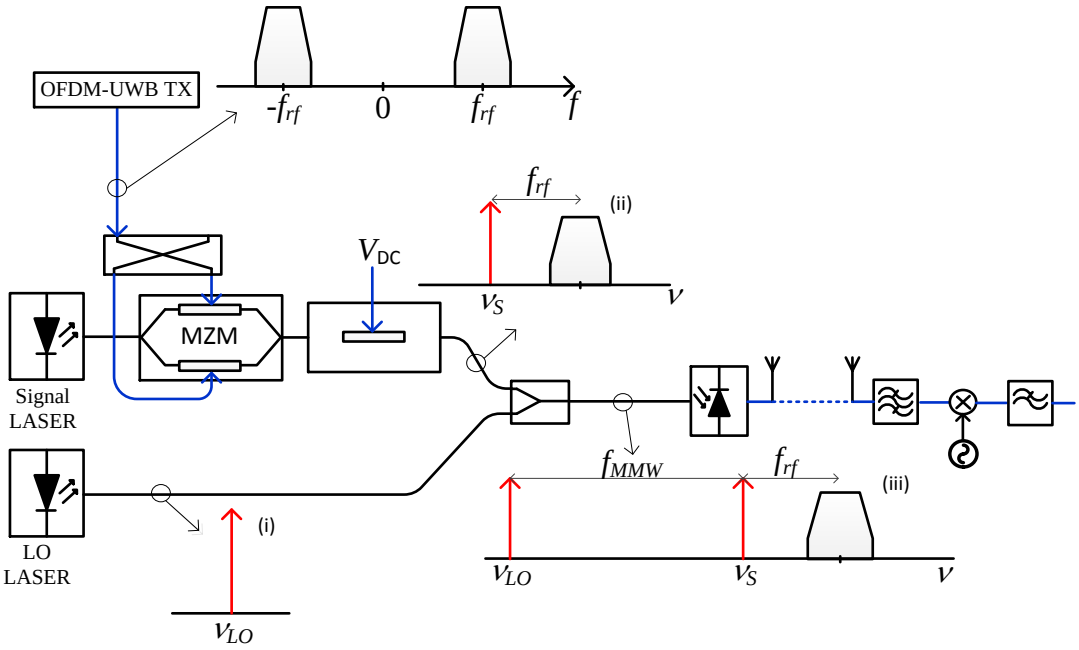

Figure D.1 – General setup of MMW OFDM-UWB signal generation based on remote heterodyning in a broadband photodiode.

Without loss of generality, an OFDM-UWB signal is considered as drive signal, with the characteristics presented in Appendix B.

The *k*-th OFDM symbol $s_{OFDM}^{k}(t)$ is generated through IFFT with coefficients C_n, which consist of data symbols, pilots, or guard symbols [103]:

$$s_{OFDM}^{k}(t) = \sum_{n=-N/2+1}^{N/2} C_n e^{j2\pi n\Delta f(t-T_{CP})}, \; t \in [T_{CP}, T+T_{CP}], \; otherwise \; 0 \qquad (D.1)$$

where $N = 128$ is the total number of subcarriers (IFFT/FFT size) used, $\Delta f = f_s/N = 4.125$ MHz is the subcarrier frequency separation, n is the subcarrier number, $T_{CP} = 60.61$ ns is the cyclic prefix duration, and $T = 1/\Delta f = 242.42$ ns is the IFFT/FFT period. Considering the *k*-th OFDM symbol in the analysis, the OFDM signal after RF up-conversion is expressed by:

$$\begin{aligned} x^k(t) &= \Re_e\left\{s_{OFDM}^{k}(t) V_{RF}^{tx} e^{j\left(2\pi f_{rf} t + \phi_{RF}^{tx}(t)\right)}\right\} \\ &= \Re_e\left\{V_{RF}^{tx} \sum_{n=-N/2+1}^{N/2} |C_n| e^{j\theta_n} e^{j2\pi n\Delta f(t-T_{CP})} e^{j\left(2\pi f_{rf} t + \phi_{RF}^{tx}(t)\right)}\right\} \\ &= V_{RF}^{tx} \sum_{n=-N/2+1}^{N/2} |C_n| \cos\left[2\pi f_{rf} t + 2\pi n\Delta f(t-T_{CP}) + \theta_n + \phi_{RF}^{tx}(t)\right], \end{aligned} \qquad (D.2)$$

where f_{rf} and $\phi_{RF}^{tx}(t)$ are the frequency and phase noise of the transmitter RF carrier. In addition, V_{RF}^{tx} is the amplitude of the transmitter RF carrier. $C_{\text{n}} = |C_{\text{n}}|e^{j\theta n}$ are QPSK modulated symbols, and $\Re_e\{.\}$ is the real part of the enclosed quantity.

For OSSB modulation, the phase shift method is used, employing a DE-MZM biased at the QP, with the modulating signal $x^k(t)$ and its Hilbert transform $x_h^k(t)$ applied to different electrodes.

The analysis of OSSB modulation can be simplified through the use of the analytic signal $x_a^k(t)$, expressed by:

$$\begin{aligned} x_a^k(t) &= x^k(t) + jx_h^k(t) \\ &= V_{RF}^{tx}\sum_{n=-N/2+1}^{N/2}|C_n|\cos\left[2\pi f_{rf}t + 2\pi n\Delta f\left(t-T_{CP}\right)+\theta_n+\phi_{RF}^{tx}(t)\right] \\ &+ jV_{RF}^{tx}\sum_{n=-N/2+1}^{N/2}|C_n|\sin\left[2\pi f_{rf}t + 2\pi n\Delta f\left(t-T_{CP}\right)+\theta_n+\phi_{RF}^{tx}(t)\right] \\ &= V_{RF}^{tx}\sum_{n=-N/2+1}^{N/2}|C_n|e^{j\left(2\pi f_{rf}t+2\pi n\Delta f\left(t-T_{CP}\right)+\theta_n+\phi_{RF}^{tx}(t)\right)} \end{aligned} \tag{D.3}$$

The signal laser is operated in CW, and the emitted optical signal is externally modulated in OSSB by a DE-MZM. The optical field at the laser output can be expressed by:

$$E_{in}(t) = E_{in}e^{j\left(w_s t+\phi_s(t)\right)} \tag{D.4}$$

and, in a similar way, the optical field at the output of the second laser (LO laser), in the presence of phase noise, can be expressed as:

$$E_{LO}(t) = E_{LO}e^{j\left(w_{LO}t+\phi_{LO}(t)\right)}, \tag{D.5}$$

where E_{in} and E_{LO} are amplitudes of the optical fields emitted by the signal laser and LO laser, respectively. $w_{\text{s}} = 2\pi\nu_{\text{s}}$ and $w_{LO} = 2\pi\nu_{\text{LO}}$ are the angular frequencies of the two lasers, with the respective phase noise terms $\phi_{\text{s}}(t)$ and $\phi_{\text{LO}}(t)$. In accordance with Fig. D.1, the laser frequency separation $\nu_{\text{LO}} - \nu_{\text{s}} = f_{\text{MMW.}}$

Assuming a DE-MZM with flat frequency response and negligible insertion loss, operated in the small-signal regime, the OSSB plus carrier modulated optical field at the output of the DE-MZM can be approximated by:

$$E_{out}(t) \cong E_{in}(t) + E_{in}(t)s_a^k(t), \tag{D.6}$$

and the resulting optical field at the output of the phase modulator is given by:

$$E_{PM}(t) = e^{j\frac{\pi}{V_\pi}V_{DC}} E_{out}(t) = e^{j\phi_0} E_{out}(t). \tag{D.7}$$

where $\phi_0 = \pi V_{DC}/V_\pi$. The two optical signals $E_{PM}(t)$ and $E_{LO}(t)$ are combined in a 3dB optical coupler/Y-junction, producing an optical signal spectrum similar to that shown in the inset (iii) of Fig. D.1, neglecting any spectral spurious component and the linewidth of the lasers. Likewise, the optical signal spectra of the $E_{LO}(t)$ and $E_{PM}(t)$ signals are shown in the insets (i) and (ii) of Fig. D.1, respectively. For simplicity, fiber transmission is neglected in this analysis. The photocurrent, $i(t)$, generated at the output of the broadband photodiode, is given by:

$$\begin{aligned} i(t) &= \Re\left\{\left(E_{PM}(t) + E_{LO}(t)\right)\left(E_{PM}(t) + E_{LO}(t)\right)^*\right\} \\ &= i_{DC} + i_{IMD2}(t) + i_{S-MW}(t) + i_{LO}(t) + i_{S-MMW}(t) \end{aligned} \tag{D.8}$$

where $\Re$ is the responsivity of the photodiode and the superscript * denotes the complex conjugation operation. A sketch of the electrical spectrum of the photocurrent is shown in Fig. D.2.

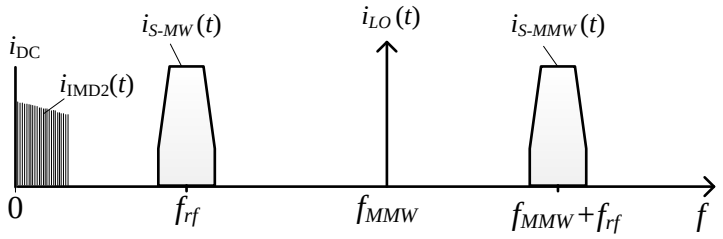

Figure D.2 – Sketch of the electrical spectrum at the output of the high-speed photodiode.

The first term of (D.8) is the photocurrent DC component, and given by:

$$i_{DC} = \Re\left(|E_s|^2 + |E_{LO}|^2 + \left(V_{RF}^{tx}\right)^2 \sum_{n=-N/2+1}^{N/2} |C_n|^2\right) \tag{D.9}$$

The IMD2 product terms present in the photocurrent are:

$$i_{IMD2}(t) = \Re|E_s|^2 \left(V_{RF}^{tx}\right)^2 \left[\sum_{l=-N/2+1}^{N/2} |C_l| e^{j\varphi_l} \sum_{\substack{j=-N/2+1 \\ j\neq l}}^{N/2} |C_j| e^{-j\varphi_j}\right] \tag{D.10}$$

with $\varphi_i(t) = w_{rf}t + 2\pi i \Delta f\left(t - T_{CP}\right) + \theta_i + \phi_{RF}^{tx}(t) \quad i = l, j.$ The photocurrent signal component located at the MW band is expressed by:

$$\begin{aligned} i_{s-MW}(t) &= 2\Re|E_s|^2 V_{RF}^{tx} \sum_{n=-N/2+1}^{N/2} |C_n| \cos\left[w_{rf}t + 2\pi n \Delta f\left(t - T_{CP}\right) + \theta_n + \phi_{rf}^{tx}(t)\right] \\ &= 2\Re|E_s|^2 x^k(t) \end{aligned} \tag{D.11}$$

The LO photocurrent located at frequency f_{MMW} is given by:

$$i_{LO}(t)=2\Re E_{LO}E_s\cos\left[\left(w_s-w_{LO}\right)t+\left(\phi_s(t)-\phi_{LO}(t)\right)+\phi_o\right] \tag{D.12}$$

whereas the photocurrent signal component located in the MMW band is given by:

$$\begin{aligned} i_{s-MMW}(t)=2\Re E_{LO}E_sV_{RF}^{tx}\sum_{n=-N/2+1}^{N/2}|C_n|\cos\Big[&\left(\left(w_s-w_{LO}\right)+w_{rf}\right)t \\ &+2\pi n\Delta f\left(t-T_{CP}\right)+\theta_n \\ &+\phi_{RF}^{tx}(t)+\left(\phi_s(t)-\phi_{LO}(t)\right)+\phi_o\Big]. \end{aligned} \tag{D.13}$$

The photocurrent $i(t)$ is filtered by an ideal band-pass filter centered at the frequency $f_{MMW}+f_{rf}$, with bandwidth larger than the signal bandwidth, as shown in Fig.D.1. This band-pass filter removes the undesired spectral components. Considering the LO signal in the OFDM receiver expressed by:

$$V^{tx}(t)=V_{RF}^{rx}\cos\left(\left(\left(w_s-w_{LO}\right)+w_{rf}\right)t+\phi_{RF}^{rx}(t)\right), \tag{D.14}$$

the signal at the output of the mixer can be expressed by:

$$\begin{aligned} x_{down}(t)=&\frac{V_{rec}}{2}\sum_{n=-N/2+1}^{N/2}|C_n|\cos\Big[2\pi n\Delta f\left(t-T_{CP}\right)+\theta_n+\left(\phi_s(t)-\phi_{LO}(t)\right) \\ &\qquad+\left(\phi_{rf}^{tx}(t)-\phi_{rf}^{rx}(t)\right)+\phi_o\Big] \\ &+\frac{V_{rec}}{2}\sum_{n=-N/2+1}^{N/2}|C_n|\cos\Big[2\left(\left(w_s-w_{LO}\right)+w_{rf}\right)t+2\pi n\Delta f\left(t-T_{CP}\right)+\theta_n \\ &\qquad+\left(\phi_s(t)-\phi_{LO}(t)\right)+\left(\phi_{rf}^{tx}(t)-\phi_{rf}^{rx}(t)\right)+\phi_o\Big] \end{aligned} \tag{D.15}$$

with $V_{rec}=2\Re E_{LO}E_sV_{RF}^{tx}V_{RF}^{rx}$. The signal at the output of an ideal LPF is then given by:

$$\begin{aligned} x_{rec}(t)=&\frac{V_{rec}}{2}\sum_{n=-N/2+1}^{N/2}|C_n|\cos\Big[2\pi n\Delta f\left(t-T_{CP}\right)+\theta_n+\left(\phi_s(t)-\phi_{LO}(t)\right)\Big] \\ &\qquad+\left(\phi_{rf}^{tx}(t)-\phi_{rf}^{rx}(t)\right)+\phi_o\Big] \end{aligned} \tag{D.16}$$

D.2.1 Particular case – phase-locked lasers

Assuming that the two lasers of the Fig. D.1 are phase-locked with a frequency separation equal to f_{MMW} = 60 GHz, the expressions derived in the previous section are simplified by considering $\phi_s(t) = \phi_{LO}(t)$. In order to further simplify the analysis, the LOs of the up-conversion and down-conversion in the transmitter and receiver are also assumed phase-locked, that is $\phi_{rf}^{tx}(t)=\phi_{rf}^{rx}(t)$. Under these conditions, (D.13) is simplified to:

$$x_{rec}(t) = \frac{V_{rec}}{2} \sum_{n=-N/2+1}^{N/2} |C_n| \cos\left[2\pi n \Delta f \left(t - T_{CP}\right) + \theta_n + \phi_o\right] = \frac{V_{rec}}{2} \Re_e \left\{ s_{OFDM}^k (t) e^{j\phi_o} \right\}. \quad \text{(D.17)}$$

By examination of (D.13) and (D.17), it is observed that the MMW OFDM-UWB signal, after down-conversion to the baseband, depends on the optical phase shift induced by the DC voltage applied to the phase modulator. Thus, all complex-valued baseband subcarriers are affected by the same phase shift, which depends linearly on the DC voltage V_{DC}.

A simulation study was carried out, to examine the effect of the optical phase shift induced by the DC voltage applied to the optical phase modulator on the EVM performance of the received OFDM-UWB signal at the MMW band and a copy located at the MW band.

As OFDM signal, the 1st OFDM-UWB channel defined in the ECMA-368 standard is considered. More details about the characteristics of the OFDM-UWB signal and how it is generated and demodulated are presented in Appendix B. The central frequency of the OFDM-UWB signal is f_{rf} = 3.432 GHz, which corresponds to the first channel of the OFDM-UWB standard. In the OSSB modulation based on the phase-shift method, the Hilbert transform of the OFDM-UWB signal is obtained considering an ideal Hilbert transformer (the negative frequencies of the signal are phase-advanced by 90 degrees, and the positive frequencies are phase-delayed by 90 degrees).

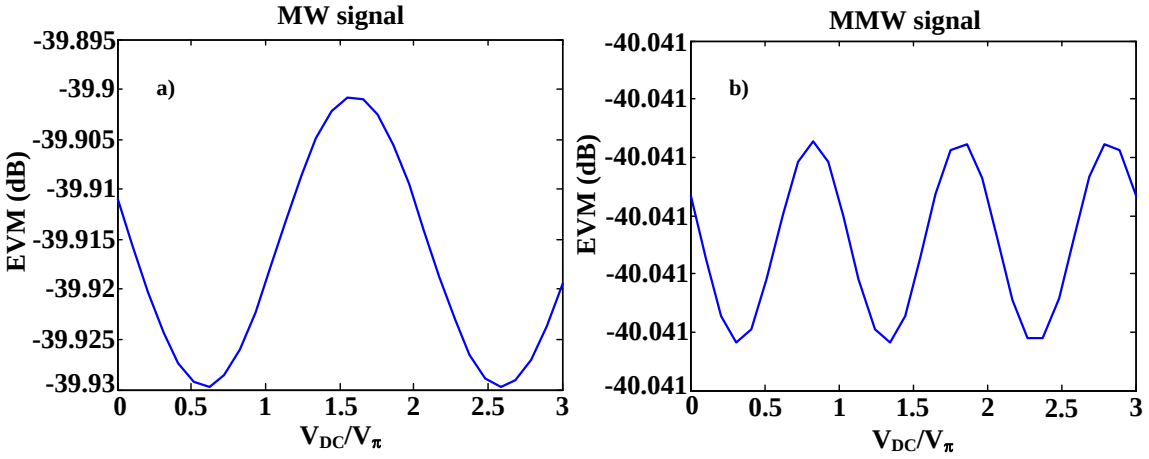

Figure D.3 – EVM as a function of the DC voltage considering OFDM receivers with equalizer active: a) MW OFDM-UWB signal; b) MMW OFDM-UWB signal.

The DE-MZM is considered ideal, as well as the phase modulator, and both with a half-wave voltage V_π= 5 V.

From Fig. D.3 it can be concluded that the EVM variation when V_{DC} increases from 0 to V_{π} is negligible, for both MW OFDM-UWB and MMW OFDM-UWB signals. The MW OFDM-UWB signal is the result of the self-heterodyning of the OSSB plus carrier signal. All optical spectral components of the OSSB signal suffer the same optical phase shift, and thus the optical phase shift is canceled in the self-heterodyning process. However, the MMW OFDM-UWB signal is the result of heterodyning of the optical OFDM-UWB sideband shown in the inset (ii) of Fig. D.1 with the un-modulated CW optical signal, $E_{LO}(t)$. Therefore, as the optical phase shift only affects the OFDM-UWB optical sideband, the optical phase shift is not canceled in the heterodyning with the un-modulated CW signal, being instead translated into the electrical domain, as is expressed in (D.13) and (D.17). Therefore, the variation of the optical phase shift through the voltage V_{DC} forces the signal constellation to be rotated around the origin. The rotation of the constellation increases the Euclidian distance between the ideal constellation and the obtained one, and in this way the EVM. Nevertheless, the constellation rotation can be compensated simply by a single tap frequency-domain equalizer in the OFDM-UWB receivers, as shown in Fig. D.3 b).

In order to demonstrate that a single tap frequency-domain equalizer can compensate any phase shift induced in the optical domain by a DC voltage in a phase modulator, the same study shown in Fig. D.3 was performed but with the equalizer in the OFDM-UWB receivers disabled. In Fig. D.4, the EVM for the MW and MMW OFDM-UWB signals is shown as a function of the DC voltage, when the frequency-domain equalizer is disabled.

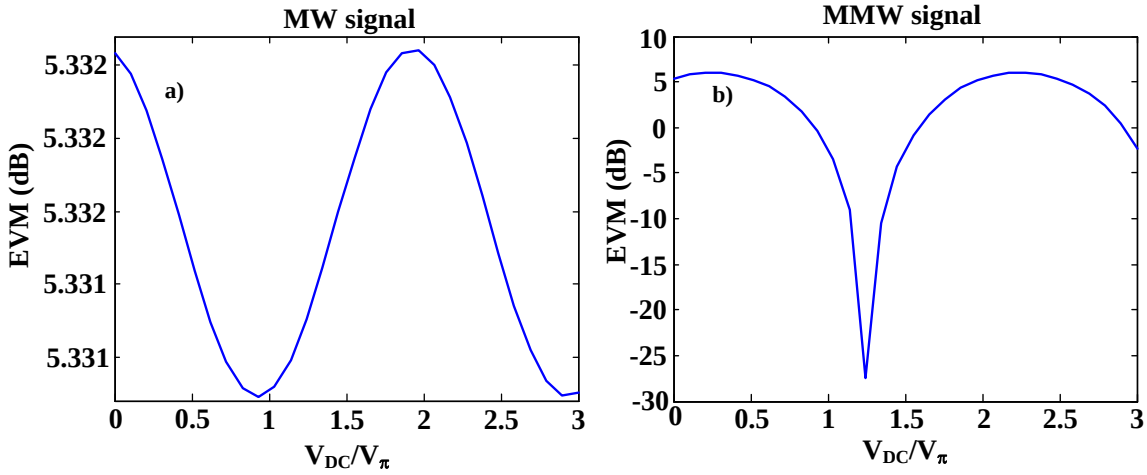

Figure D.4 - EVM as a function of the DC voltage considering OFDM receivers with equalizer disabled: a) MW OFDM-UWB signal; b) MMW OFDM-UWB signal.

Comparing Fig. D.4 a) with Fig. D.3 a), it is concluded that the absence of the equalizer increases the EVM, but the EVM variation as V_{DC} increases from 0 to V_{π} is the same. For

$V_{DC} = 0$ the phase shift induced by the DC voltage is null. The reason of EVM increasing when $V_{DC} = 0$ is because the amplitude equalization is not performed and furthermore the different phase shift introduced by electrical filters on different subcarriers are also not equalized.

Figure D.4 b) demonstrates the importance of the equalizer in the OFDM-UWB receivers. For $V_{DC} = 0$ the EVM values obtained for the MMW OFDM-UWB signal are nearly equal to the EVM values obtained for MW OFDM-UWB signal. However, as V_{DC} increases from 0 up to $1.3V_{\pi}$, the demodulation of the orthogonal subcarriers in the FFT block becomes much more coherent, and then the EVM reaches a minimum. For higher values of V_{DC} the EVM increases up to a maximum and decreases again in a periodical from.

D.3 Summary

In this appendix, general expressions for remote heterodyning of a phase shifted OFDM-UWB OSSB plus carrier signal with an uncorrelated CW laser, for an optical back-to-back configuration, are derived. The impact of a phase modulator at the output of the OSSB modulator, driven with a DC voltage, on the EVM of the received OFDM-UWB signal in the MW and MMW bands was examined by numerical simulation. It was concluded that the optical phase shift has impact on the MMW OFDM signal mainly when equalization in the frequency-domain is not active.

References

[1] The Zettabyte Era - Trends and Analysis, Available online: **http://www.cisco.com/en/US/solutions/collateral/ns341/ns525/ns537/ns705/ns827/VNI_Hyperconnectivity_WP.html**, January 2014.

[2] The connected television debate in OECD countries, Available online: **http://oecdinsights.org/2014/01/23/the-connected-television-debate-in-oecd-countries/**, 24 January 2014.

[3] FTTH/B Panorama European Union (36) at December 2010, Fiber to the Home Council Europe. Available online: http://www.ftthcouncil.eu/documents/Reports/Market_Data_December_2010.pdf, January 2014.

[4] Fiber to the Home Council United States, Available online: http://www.ftthcouncil.org/sites/ftthcouncil.org/files/BBP_2010_Primer.pdf, January 2014

[5] Ericson "Ericson mobility report – on the pulse of the networked society", Ericson report, Nov. 2012.

[6] Cisco Visual Networking Index: Global Mobile Data Traffic Forecast Update, 2012–2017, Available Online: http://www.cisco.com/en/US/solutions/collateral/ns341/ns525/ns537/ns705/ns827/white_paper_c11-520862.html, January 2014

[7] 3rd Generation Partnership Project, Available online: http://www.3gpp.org/, January 2014.

[8] Wikipedia, 5G, Available online: http://en.wikipedia.org/wiki/5G, January 2014

[9] European METIS project, Available online: https://www.metis2020.com/, January 2014.

[10] Rappaport, T.S.; Shu Sun; Mayzus, R.; Hang Zhao; Azar, Y.; Wang, K.; Wong, G.N.; Schulz, J.K.; Samimi, M. and Gutierrez, F., "Millimeter Wave Mobile Communications for 5G Cellular: It Will Work!," *IEEE Access*, vol.1, no., pp.335,349, 2013.

[11] Al-Raweshidy, H. and komaki, S. "Radio over Fiber Technologies for Mobile Communications networks," Artech House, Inc, 2002.

[12] Sauer, M.; Kobyakov, A. and George, J., "Radio Over Fiber for Picocellular Network Architectures," *Journal of Lightwave Technology*, vol.25, no.11, pp.3301-3320, Nov. 2007.

[13] Chun-Ting Lin; Chen, J.; Peng-Chun Peng; Cheng-Feng Peng; Wei-Ren Peng; Bi-Shiou Chiou and Sien Chi, "Hybrid Optical Access Network Integrating Fiber-to-the-Home and Radio-Over-Fiber Systems," *IEEE Photonics Technology Letters*, vol.19, no.8, pp.610-612, April, 2007.

[14] FSAN, URL: http://www.fsan.org/, January 2014

[15] Maria C.R. Medeiros, Ricardo Avó, Paula. Laurêncio, N.S. Correia, Alvaro. Barradas, Henrique J.A. da Silva, Izzat Darwazeh, Jonh E. Mitchell and Paulo M.N. Monteiro, 'RoFnet-Reconfigurable Radio over Fiber Network Architecture Overview' *Journal of Telecommunications and Information Technology*, 1, pp. 38 – 43, Dec. 2009.

[16] Lim, C., Nirmalathas, A., Attygalle, M., Novak, D. and Waterhouse, R., "On the merging of millimeter-wave fiber-radio backbone with 25-GHz WDM ring networks," *Journal of Lightwave Technology*, vol.21, no.10, pp. 2203- 2210, Oct. 2003.

[17] Li, G. L.; Yu, P.K.L., "Optical intensity modulators for digital and analog applications," *Journal of Lightwave Technology*, vol.21, no.9, pp.2010-2030, Sept. 2003.

[18] Kjebon, O., Schatz, R., Lourdudoss, S., Nilsson, S., Stalnacke, B. and Backbom, L.,"30 GHz direct modulation bandwidth in detuned loaded InGaAsP DBR lasers at 1.55 μm wavelength," *Electronics Letters*, vol.33, no.6, pp.488-489, 13 Mar 1997.

[19] Schmuck, H. "Comparison of optical millimetre-wave system concepts with regard to chromatic dispersion," *Electronics Letters*, vol.31, no.21, pp.1848-1849, 12 Oct 1995.

[20] Smith, G.H., Novak, D. and Ahmed, Z., "Overcoming chromatic-dispersion effects in fiber-wireless systems incorporating external modulators," *IEEE Transactions on Microwave Theory and Techniques*, vol.45, no.8, pp.1410-1415, Aug 1997.

[21] Pastor, D., Capmany, J., Ortega, D., Tatay, V., Marti, J., "Design of apodized linearly chirped fiber gratings for dispersion compensation," *Journal of Lightwave Technology*, vol.14, no.11, pp.2581-2588, Nov. 1996.

[22] Payne, D. and Stern, J. "Transparent single-mode fiber optical networks," *Journal of Lightwave Technology*, vol.4, no.7, pp. 864-869, Jul. 1986.

[23] Larsen, C.P.; Gavler, A. and Wang, K. "Comparison of active and passive optical access networks," *2010 9th Conference on Telecommunications Internet and Media Techno Economics (CTTE)*, vol., no., pp.1-5, 7-9 June 2010.

[24] Koonen, T. "Fiber to the Home/Fiber to the Premises: What, Where, and When?," *Proceedings of the IEEE*, vol.94, no.5, pp.911-934, May 2006.

[25] ITU-T, Study group 15, Available online: http://www.itu.int/en/ITU-T/studygroups/2013-2016/15/Pages/default.aspx, January 2014.

[26] ITU-T, "Recommendation G.983.1," Available online: http://www.itu.int/rec/T-REC-G.983.1-200501-I/en.

[27] ITU-T, "Recommendation G.984.1," Available online: http://www.itu.int/rec/T-REC-G.984.1/en.

[28] ITU-T, "Recommendation G.987," Available online: http://www.itu.int/rec/T-REC-G.987-201206-P/en.

[29] Huawei. "Next-generation PON evolution", 2010, Available online: http://www.huawei.com/en/static/HW-077443.pdf

[30] IEEE, "802.3ah-2004 - IEEE Standard for Information technology-Local and metropolitan area networks," Available online: http://standards.ieee.org/findstds/standard/802.3ah-2004.html.

[31] IEEE, "802.3av-2009 - IEEE Standard for Information technology-Local and metropolitan area networks," Available online: http://web.archive.org/liveweb/http://standards.ieee.org/findstds/standard/802.3av-2009.html.

[32] P. Chanclou, A. Cui, F. Geilhardt, H. Nakamura and D. Nesset, "Network operator requirements for the next generation of optical access networks," *IEEE Network*, vol. 26, no. 2, pp. 8-14, March-April 2012.

[33] Shea, D.P. and Mitchell, J.E. "Architecture to integrate multiple PONs with long reach DWDM backhaul," *IEEE Journal* on Selected *Areas* in *Communications*, vol.27, no.2, pp.126-133, Feb. 2009.

[34] Lazaro, J.A., Prat, J., Chanclou, P., Beleffi, G.M.T., Teixeira, A., Tomkos, I., Soila, R., Koratzinos, V., "Scalable Extended Reach PON," *in Conference on Optical Fiber communication OFC2008.*, 24-28 Feb. 2008.

[35] Andrade, M.D.; Kramer, G.; Wosinska, L.; Jiajia Chen; Sallent, S.; Mukherjee, B., "Evaluating strategies for evolution of passive optical networks," *IEEE Communications Magazine*, vol.49, no.7, pp.176-184, July 2011.

[36] N. Cvijetic, "OFDM for Next-Generation Optical Access Networks," *Journal of Lightwave Technology*, vol. 30, no. 4, pp. 384-398, February 2012.

[37] Kanonakis, K., Tomkos, I., Pfeiffer, T., Prat, J. and Kourtessis, P., "ACCORDANCE: A novel OFDMA-PON paradigm for ultra-high capacity converged wireline-wireless access networks," *12th International Conference on Transparent Optical Networks ICTON 2010*, vol., no., pp.1-4, July 2010.

[38] European ACCORDANCE project: Available online: http://www.ict-accordance.eu/ , January 2014.

[39] Milosavljevic, M., Kourtessis, P. and Senior, J.M. "Transparent wireless transmission over the ACCORDANCE optical/wireless segment," *2010 7th International Symposium on Communication Systems Networks and Digital Signal Processing (CSNDSP)*, vol., no., pp.138-142, July 2010.

[40] Kanonakis, K., Tomkos, I., Krimmel, H., Schaich, F., Lange, C., Weis, E., Leuthold, J., Winter, M., Romero, S., Kourtessis, P., Milosavljevic, M., Cano, I.N. and Prat, J. "An OFDMA-based optical access network architecture exhibiting ultra-high capacity and wireline-wireless convergence," *IEEE Communications Magazine*, vol.50, no.8, pp.71-78, Aug. 2012.

[41] G. Townsend and P. Talli, "Hybrid DWDM-TDM Long-Reach PON for Next-Generation Optical Access," *Journal of Lightwave Technology*, vol. 24, no. 7, pp. 2827-2834, July 2006.

[42] K. Wakayama, C. Hasegawa, D. Ishii and N. Yamanaka, "Evaluation of Prototype for 10Gbps Active Optical Access System," *15th OptoElectronics and Communications Conference OECC2010*, No. 8A4-3, pp. 436-437, July 2010.

[43] European SODALES project, Available online: http://www.fp7-sodales.eu/, January 2014.

[44] Bock, C., Figuerola, S., Parker, M.C., Quinlan, T. and Walker, S.D., "Convergent radio and fibre access architectures using low-energy systems," *14th International Conference on Transparent Optical Networks (ICTON)*, 2012, vol., no., pp.1,7, 2-5 July 2012.

[45] ITU-T, http://www.itu.int/md/R12-SG05-C-0086/en

[46] Bock, C.; Figuerola, S.; Parker, M.C.; Walker, S.D.; Mendes, T.; Marques, V.; Jungnickel, V.; Habel, K.; Levi, D., "Convergent radio and fibre architectures for high-speed access," *15th International Conference on Transparent Optical Networks (ICTON)*, 2013, vol., no., pp.1-4, June 2013

[47] Davide Visani, Giovanni Tartarini, Pier Faccin, Luigi Tarlazzi, "Cost-effective radio over fiber system for multi service wireless signal," *Optics Communications*, Vol.284, no.12, 1 June 2011.

[48] Guo, Y.X.; Yee, M.L.; Luo, B.; Ong, L.C.; Zhou, M.-T.; Harada, H.; "Hybrid 60 GHz and 2.4 GHz WLAN radio-over-fiber system for efficient broadband signal distribution," *Asia-Pacific, Microwave Conference, 2008. APMC 2008.*, vol., no., pp.1-4, 16-20 Dec. 2008.

[49] European FIVER project, Online available: http://www.ict-fiver.eu/, January 2014.

[50] Llorente, R.; Morant, M.; Quinlan, T.; Medina, N. and Walker, S., "Optical architectures evaluation for triple-play distribution in FIVER project," *in Future Network & Mobile Summit (FutureNetw), 2011*, vol., no., pp.1,8, 15-17 June 2011.

[51] Llorente, R., Morant, M., Martinez, F., Alves, T., Cartaxo, A., Quinlan, T., Walker, S.; Rodrigues, C., Herrera, J., Cluzeaud, P., Schmidt, A., Sambaraju, R., Rico, E., Piesiewicz, R. and Herman, M., "Impairment compensation in long-reach integrated optical-wireless PON," *in Future Network & Mobile Summit (FutureNetw), 2012*, vol., no., pp.1,9, 4-6 July 2012.

[52] M. Morant, T. Quinlan, R. Llorente and S. Walker, "Full standard triple-play bi-directional and full-duplex CWDM transmission in passive optical networks", *in optical fiber communications conference OFC2011*, paper OWB3, March 2011

[53] T. Alves, M. Morant, A. Cartaxo and R. Llorente "Transmission of OFDM wired-wireless quintuple-play services along WDM LR-PONs using centralized broadband impairment compensation", *Optics Express*, vol. 20, pp.13748 - 13761, 2012.

[54] Llorente, R., Morant, M., Pellicer, E., Herman, M., Nagy, Z., Alves, T., Cartaxo, A., Herrera, J., Correcher, J., Quinlan, T., Walker, S., Rodrigues, C., Cluzeaud, P., Schmidt, A., Piesiewicz, R. and Sambaraju, R., "On-the-field demonstration of quintuple-play service provision in long-reach OFDM-based WDM-PON

access networks," *in 39th European Conference and Exhibition on Optical Communication, ECOC 2013*, vol., no., pp.1,3, 22-26 Sept. 2013.

[55] Huawei, TWDM-PON the solution of choice for NG-PON, Available online: http://www.huawei.com/en/about-huawei/publications/communicate/hw 201329.htm

[56] Ali Razmtouz, Kai Habel, Christoph Kottke, Christian Ruprecht, and Werner Rosenkranz, "Initial ranging scheme based on interpolated Zadoff-Chu sequences for OFDMA-PON," *Optics Express* **22**, pp.3669-3674, Feb. 2014.

[57] Jingjing Zhang, and Ansari, N., "Design of WDM PON With Tunable Lasers: The Upstream Scenario," *Journal of Lightwave Technology*, vol.28, no.2, pp.228-236, Jan.15, 2010.

[58] Wong, E., Ka Lun Lee, and Anderson, T.B., "Directly Modulated Self-Seeding Reflective Semiconductor Optical Amplifiers as Colorless Transmitters in Wavelength Division Multiplexed Passive Optical Networks," *Journal of Lightwave Technology*, vol.25, no.1, pp.67-74, Jan. 2007.

[59] Chul Han Kim, "Performance evaluation of reflective electro-absorption modulator based optical source using a broadband light seed source for colorless WDM-PON applications," *Optics Express* 21, 12914-12919 (2013).

[60] Smith, G.H., Novak, D. and Lim, C."A millimeter-wave full-duplex fiber-radio star-tree architecture incorporating WDM and SCM,"*IEEE Photonics Technology Letters*, vol.10, no.11, pp.1650-1652, Nov. 1998.

[61] Pareit, Daan, Lannoo, Bart, Moerman, Ingrid and Demeester, Piet, "The History of WiMAX: A Complete Survey of the Evolution in Certification and Standardization for IEEE 802.16 and WiMAX," *IEEE Communications Surveys & Tutorials*, vol.14, no.4, pp.1183-1211, Fourth Quarter 2012.

[62] T. Kawanishi, T. Sakamoto, and M. Izutsu, "High-speed control of lightwave amplitude, phase, and frequency by use of electrooptic effect," *IEEE Journal of Selected Topics in Quantum Electronics*, vol. 13, no. 1, pp. 79–91,Jan./Feb. 2007.

[63] Tetsuya Kawanishi, Takahide Sakamoto, Tetsuya Miyazaki, Masayuki Izutsu, Takahisa Fujita, Shingo Mori, Kaoru Higuma, and Junichiro Ichikawa, "High-speed optical DQPSK and FSK modulation using integrated Mach-Zehnder interferometers," *Optics Express* vol.14, pp.4469-4478,2006.

[64] Wooten, E.L., Kissa, K.M., Yi-Yan, A., Murphy, E.J., Lafaw, D.A., Hallemeier, P.F., Maack, D., Attanasio, D.V., Fritz, D.J., McBrien, G.J., Bossi, D.E., "A review of lithium niobate modulators for fiber-optic communications systems," *IEEE Journal of Selected Topics in Quantum Electronics*, vol.6, no.1, pp.69,82, Jan.-Feb. 2000.

[65] K. Prosyk, A. Ait-Ouali, C. Bornholdt, T. Brast, M. Gruner, M. Hamacher, D. Hoffmann, R. Kaiser, R. Millett, K. Velthaus, and I. Woods, "High Performance 40GHz InP Mach-Zehnder Modulator," *in Optical Fiber Communication Conference*, OFC2012, paper OW4F.7.

[66] R. Spickermann, S. R. Sakamoto, M. G. Peters and N. Dagli "GaAs/AlGaAs Travelling Wave Electro-Optic Modulator with an Electrical Bandwidth > 40 GHz", *Electronics. Letters*, vol. 32, no. 12,pp. 1095 -1096 1996.

[67] Huang, H., Nuccio, S. R., Yue, Y., Yang, J., Ren, Y., Wei, C., Yu, G., Dinu, R., Parekh, D., Chang-Hasnain, C. J., Willner, A. E., "Broadband Modulation Performance of 100-GHz EO Polymer MZMs," *Journal of Lightwave Technology*, vol.30, no.23, pp.3647-3652, Dec.1, 2012.

[68] Ling Liao, Dean Samara-Rubio, Michael Morse, Ansheng Liu, Dexter Hodge, Doron Rubin, Ulrich Keil, and Thorkild Franck, "High speed silicon Mach-Zehnder modulator," *Optics Express* 13, 3129-3135 (2005).

[69] Walklin, S. and Conradi, J., "Effect of Mach-Zehnder modulator DC extinction ratio on residual chirp-induced dispersion in 10-Gb/s binary and AM-PSK duobinary lightwave systems," *IEEE Photonics Technology Letters*, vol.9, no.10, pp.1400-1402, Oct. 1997.

[70] J. Park, W. V. Sorin, and K. Y. Lau, "Elimination of fiber chromatic dispersion penalty on 1550 nm millimeter-wave optical transmission," *Electronics Letters.*, Vol. 33, pp. 512–513, Mar. 1997.

[71] M. Sieben, J. Conradi, and D. Dodds, "Optical single sideband transmission at 10 Gb/s using only electrical dispersion compensation," *Journal of Lightwave Technology*, vol. 17, no. 10, pp. 1742-1749, Oct. 1999.

[72] D. Fonseca, A. Cartaxo, and P. Monteiro, "Optical single sideband transmitter for various electrical signaling formats", *Journal of Lightwave Technology*, Vol. 24, No. 5, pp. 2059-2069, May 2006.

[73] J. Conradi, “Bandwidth-efficient modulation formats for digital fiber transmission systems”, in *Optical Fiber Telecommunications IV B*, Academic Press, New Jersey, pp. 862-901, 2002.

[74] Marple, S.L., Jr., "Computing the discrete-time “analytic” signal via FFT," *IEEE Transactions on Signal Processing*, vol.47, no.9, pp.2600-2603, Sep 1999.

[75] Y. Zhu, P. A. Gamage, K.-L. Lee, C. Lim, and E.Wong, “Optical-wireless integration incorporating optical tandem single sideband modulation format,” in *Proc. Opto-Electronics Communication Conference (OECC2008)*, 2008, pp.1–2.

[76] Gamage, P.A., Nirmalathas, A., Lim, C., Wong, E., Novak, D. Waterhouse, R., "Performance Comparison of Directly Modulated VCSEL and DFB Lasers in Wired-Wireless Networks," *IEEE Photonics Technology Letters*, vol.20, no.24, pp.2102,2104, Dec.15, 2008.

[77] José A. P. Morgado, Daniel Fonseca, and Adolfo V. T. Cartaxo, "Experimental study of coexistence of multi-band OFDM-UWB and OFDM-baseband signals in long-reach PONs using directly modulated lasers," *Optics Express* **19**, 23601-23612 (2011)

[78] Alves, T.M.F., Morant, M., Cartaxo, A.V.T. and Llorente, R., "Wired-Wireless Services Provision in FSAN NG-PON2 Compliant Long-Reach PONs: Performance Analysis," *in optical fiber communications conference OFC2013*, March 2013, paper OM3D.3.

[79] Alves, T.M.F., Morant, M., Cartaxo, A.V.T. and Llorente, R., "Design of directly modulated long-reach PONs reaching 125 km for provisioning of hybrid wired-wireless quintuple-play service," *IEEE/OSA Journal of Optical Communications and Networking*, vol.5, no.8, pp.848-857, Aug. 2013

[80] Zhensheng Jia, Jianjun Yu, Ellinas, G. and Gee-Kung Chang;" Key Enabling Technologies for Optical–Wireless Networks: Optical Millimeter-Wave Generation, Wavelength Reuse, and Architecture," *Journal of Lightwave Technology*, vol.25, no.11, pp.3452-3471, Nov. 2007.

[81] Martinez, A., Polo, V., Marti, J., "Simultaneous baseband and RF optical modulation scheme for feeding wireless and wireline heterogeneous access networks," *IEEE Transactions on Microwave Theory and Techniques*, vol.49, no.10, pp.2018,2024, Oct 2001.

[82] K. Ikeda, T. Kuri, and K. Kitayama, “Simultaneous three-band modulation and fiber-optic transmission of 2.5-Gb/s baseband, microwave and 60-GHz-band

signals on a single wavelength," *Journal of Lightwave Technology*, vol. 21, no. 12, pp. 3194-3202, Dec. 2003.

[83] Z. Jia, J. Yu, Y.-T. Hsueh, A. Chowdhury, H.-C. Chien, J. A. Buck, and G.-K. Chang, "Multiband signal generation and dispersion-tolerant transmission based on photonic frequency tripling technology for 60-GHz radio-over-fiber systems," *IEEE Photonics Technology Letters*, vol.20, no. 17, pp. 1470–1472, Sep. 1, 2008.

[84] Chun-Ting Lin, Chen, J., Peng-Chun Peng, Cheng-Feng Peng, Wei-Ren Peng, Bi-Shiou Chiou and Sien Chi, "Hybrid Optical Access Network Integrating Fiber-to-the-Home and Radio-Over-Fiber Systems," *IEEE Photonics Technology Letters*, vol.19, no.8, pp.610-612, April15, 2007.

[85] C. Qingjiang, F. Hongyan, and S. Yikai, "Simultaneous generation and transmission of downstream multiband signals and upstream data in a bidirectional radio-over-fiber system," *IEEE Photonics Technology Letters*, vol. 20, no. 3, pp. 181–183, Feb. 1, 2008.

[86] Po-Tsung Shih, Chun-Ting Lin, Wen-Jr Jiang, Yu-Hung Chen, Chen, J. and Sien Chi, "Hybrid Access Network Integrated With Wireless Multilevel Vector and Wired Baseband Signals Using Frequency Doubling and No Optical Filtering," *IEEE Photonics Technology Letters* , vol.21, no.13, pp.857,859, July1, 2009.

[87] C. W. Chow, S. P. Huang, L. G. Yang, and C. H. Yeh, "Extended-reach access network with downstream radio-over-fiber (RoF) signal and upstream NRZ signal using orthogonal-WDM," *Optics Express* 20, 16757-16762 (2012).

[88] Griffin, R.A., Lane, P.M., and O'Reilly, J.J., "Dispersion-tolerant subcarrier data modulation of optical millimetre-wave signals," *Electronics Letters*, vol.32, no.24, pp.2258-2260, 21 Nov 1996.

[89] C. W. Chow and Y. H. Lin, "Convergent optical wired and wireless long-reach access network using high spectral-efficient modulation," *Optics Express* 20, 9243-9248 (2012).

[90] Almeida, P., Ferreira, F., and Silva, H. "Multiband signals generation for hybrid access networks using a single external modulator," *in Symposium On Enabling Optical Networks and Sensor-SEON* 2010, vol., no., pp.1-2, Porto, 25 June 2010.

[91] Almeida, P. and Silva, H. "Multiservices and multiband optical signal generation for hybrid access networks," *15th International Conference on Optical Network Design and Modeling - ONDM2011*, 2011, vol., no., pp.1-6, 8-10 Feb. 2011.

[92] C. Lim, A. Nirmalathas, D. Novak, R. Waterhouse, and G. Yoffe, "Millimeter-wave broadband fiber-wireless system incorporating baseband data transmission over fiber and remote LO delivery," *Journal of Lightwave Technology*, vol. 18, no. 10, pp. 1355-1363, Oct 2000.

[93] T. Erdogan, "Fiber Grating Spectra," *Journal of Lightwave Technology*, Vol. 15, no. 8, pp. 1277-1294, Aug.1997.

[94] Marcuse, D., "Calculation of bit-error probability for a lightwave system with optical amplifiers and post-detection Gaussian noise," *Journal of Lightwave Technology*, vol.9, no.4, pp.505-513, Apr. 1991.

[95] Shafik, R.A., Rahman, S., AHM Razibul Islam, "On the Extended Relationships Among EVM, BER and SNR as Performance Metrics," in *Proc. ICECE06*, Dec. 2006.

[96] Ferreira, F., Pato, S., Almeida, P., Silva, H. and Monteiro, P." Dual band signal generation for millimeter-wave RoF systems with subcarrier multiplexing," *Proc Conf. on Telecommunications – ConfTele 2011*, Lisboa, Portugal, no., vol., pp., 27-19 April, 2011.

[97] Lim, C., Nirmalathas, A., Ka-Lun Lee, Novak, D. and Waterhouse, R. "Intermodulation Distortion Improvement for Fiber–Radio Applications Incorporating OSSB+C Modulation in an Optical Integrated-Access Environment," *Journal of Lightwave Technology*, vol.25, no.6, pp.1602-1612, June 2007.

[98] Shieh, W., Athaudage, C. "Coherent optical orthogonal frequency division multiplexing," *Electronics Letters*, vol.42, no.10, pp.587-589, 11 May 2006.

[99] Almeida, P. and Silva, H. "Distribution of MB-OFDM UWB and Millimeter-Wave WPAN Signals on Hybrid FTTH Networks," *Proc. in IEEE International Conference on Ultra-Wideband, 2011-ICUWB 2011*, vol., no., pp.1-5, 14-16 Sept.2011.

[100] ECMA,"Standard ECMA-368: High rate ultra-wideband PHY and MAC standard,"3rd edition, Geneva, ECMA International, Dec. 2008.

[101] W. Shieh, H. Bao, and Y. Tang, "Coherent optical OFDM: theory and design," *Opt. Express* 16, 841-859 (2008)

[102] ECMA, "Standard ECMA-387: High Rate 60 GHz PHY, MAC and HDMI PAL,"2sd edition, Geneva, ECMA International, Dec. 2010.

[103] M. Sakib, B. Hraimel, X. Zhang, M. Mohamed, W. Jiang, K. Wu and D. Shen "Impact of optical transmission on multiband OFDM ultra-wideband wireless system with fiber distribution", *Journal of Lightwave Technology*, vol. 27, no. 18, pp.4112 -4123 2009.

[104] Kanesan, T.; Ng, W.P.; Ghassemlooy, Z. and Lu, C., "Theoretical and experimental design of an alternative system to 2×2 MIMO for LTE over 60 km directly modulated RoF link," *IEEE Global Communications Conference (GLOBECOM), 2012*, vol., no., pp.2959-2964, 3-7 Dec. 2012

[105] Almeida, P., Silva, H. and Medeiros, M.C. "Transmission of LTE Signals for Femtocells over Long-reach FTTH networks," *in Conference on Telecommunications – ConfTele2013*, Castelo Branco, Portugal, May, 2013.

[106] Hui, Rongqing; Benyuan Zhu; Renxing Huang; Allen, C.T.; Demarest, K.; Richards, D., "Subcarrier multiplexing for high-speed optical transmission," *Journal of Lightwave Technology*, vol.20, no.3, pp.417,427, Mar 2002.

[107] C. Lim, M. Attygalle, A. Nirmalathas, D. Novak, and R. Waterhouse, "Analysis of optical carrier-to-sideband ratio for improving transmission performance in fiber-radio links," *IEEE Transactions on Microwave Theory and Techniques* ,vol.54, no.5, pp.2181–2187, May 2006.

[108] Hraimel, B., X. Zhang, Y. Pei, K.Wu, T. Liu, T. Xu, and Q. Nie "Optical single-sideband modulation with tunable optical carrier to sideband ratio in radio over fiber systems," *Journal of Lightwave Technology*, vol. 29, no. 5, pp.775-781, March 2011.

[109] Lowery, A.J.; Du, L. and Armstrong, J., "Orthogonal Frequency Division Multiplexing for Adaptive Dispersion Compensation in Long Haul WDM Systems," *in Proc. OFC 2006*, March 2006.

[110] W. Hu, K. Inagaki, T. Tanaka, T. Ohira, and A. Xu, "High SNR 50 GHz radio-over-fibre uplink system by use of low biased Mach–Zehnder modulator technique," *Electronics Letters*, vol. 42, p. 550, 2006.

[111] Almeida, P. and Silva, H.," Investigation of wired and wireless services based on OFDM DSB-RC transmission in the presence of modulation chirp of a DEMZM" *Optics express*, vol.21, no.25, pp.30764-30777, Dec 2013.

[112] Ali, A.; Leibrich, J. and Rosenkranz, W." Spectral Efficiency and Receiver Sensitivity in Direct Detection Optical-OFDM," *in optical fiber communication conference OFC 2009*, March 2009.

[113] LTE, Evolved Universal Terrestrial Radio Access (E-UTRA), "Physical channels and modulation," (3GPP TS 36.211 version 8.9.0 Release 8), ETSI, Jan. 2010.

[114] Almeida, P. and Silva, H., "Optical single sideband generation optimized to support multi-services OFDM over hybrid long-reach FTTH networks," *15th International Conference on Transparent Optical Networks (ICTON), 2013*, vol., no., pp.1-4, 23-27 June 2013.

[115] Almeida, P. and Silva, H., "OSSB transmitter with modulation efficiency optimized to support OFDM multi-services along hybrid long-reach WDM-PONs" submitted.

[116] G. Chang, A. Chowdhury, Z. Jia, H. Chien, M. Huang, J. Yu, and G. Ellinas, "Key technologies of WDM-PON for future converged optical broadband access networks [Invited]," *IEEE/OSA Journal of Optical Communications and Networking*, vol. 1, no. 4, pp. C35–C50, Sept. 2009.

[117] Chi-Wai Chow, Chien-Hung Yeh, Chia-Hsuan Wang, Fu-Yuan Shih, Ci-Ling Pan, and Sien Chi, "WDM extended reach passive optical networks using OFDM-QAM," *Optics. Express, vol* 16, pp.12096-12101, 2008.

[118] Tomba, L., "On the effect of Wiener phase noise in OFDM systems," *IEEE Transactions on Communications*, vol.46, no.5, pp.580-583, May 1998.

[119] Wei, J. L., Sanchez, C., Hugues-Salas, E., Spencer, P.S. and Tang, J. M., "Wavelength-offset filtering in optical OFDM IMDD systems using directly modulated DFB lasers," *Journal of Lightwave Technology*, vol.29, no.18, pp.2861-2870, Sept.15, 2011.

[120] Peng,W., Feng,K., Willner,A.E., and Chi,S. "Estimation of the bit error rate for direct-detected OFDM signals with optically preamplified receivers," *Journal of Lightwave Technology*, vol.27, no.10, pp.1340-1346, May15, 2009.

[121] Lowery, A.J. "Amplified-spontaneous noise limit of optical OFDM lightwave systems" *Optics Express*, vol. 16, pp. 860-865, Jan. 2008.

[122] Silva, H.; Fyath, R.; O'Reilly, J., "Sensitivity degradation with laser wavelength chirp for direct-detection optical receivers," *IEE Proceedings J - Optoelectronics*, vol. 136, no. 4, pp.209-218, Aug. 1989.

[123] J. L. Wei, E. Hugues-Salas, R. P. Giddings, X. Q. Jin, X. Zheng, S. Mansoor, and J. M. Tang, "Wavelength reused bidirectional transmission of adaptively

modulated optical OFDM signals in WDM-PONs incorporating SOA and RSOA intensity modulators," *Optics Express* 18, pp.9791-9808, 2010.

[124] Dar-Zu Hsu, Chia-Chien Wei, Hsing-Yu Chen, Jyehong Chen, Maria C. Yuang, Shih-Hsuan Lin, and Wei-Yuan Li "21 Gb/s after 100 km OFDM long-reach PON transmission using a cost-effective electro-absorption modulator," *Optics Express*, vol. 18, pp.27758-27763, Dec 2010.

[125] Gnauck, A.H., Korotky, S.K., Veselka, J.J., Nagel, J., Kemmerer, C.T., Minford, W.J. and Moser, D.T., "Dispersion penalty reduction using an optical modulator with adjustable chirp," *IEEE Photonics Technology Letters*, vol.3, no.10, pp.916-918, Oct. 1991.

[126] Almeida, P. and Silva, H., "Expressions of the chirp parameter components for intensity modulation with a dual-electrode Mach-Zehnder modulator," in *14th International Conference on Transparent Optical Networks (ICTON), 2012*, vol., no., pp.1-4, 2-5 July 2012.

[127] Almeida, P. and Silva, H. "Impact of the Modulation Chirp of a DEMZM on the Transmission of Signals Based on OFDM," *IEEE Photonics Technology Letters*, vol.25, no.3, pp.283-286, Feb., 2013.

[128] Kanesan, T., Ng, W.P., Ghassemlooy, Z., Perez, J., "Optimization of Optical Modulator for LTE RoF in Nonlinear Fiber Propagation," *IEEE Photonics Technology Letters,* vol.24, no.7, pp.617,619, April, 2012

[129] Koyama, F. and Iga, K., "Frequency chirping in external modulators," *Journal of Lightwave Technology*, vol.6, no.1, pp.87-93, Jan. 1988.

[130] Hoon Kim and Gnauck, A.H.,"Chirp characteristics of dual-drive Mach-Zehnder modulator with a finite DC extinction ratio," *IEEE Photonics Technology Letters*, vol.14, no.3, pp.298-300, Mar 2002.

[131] Jichai Jeong and Park, Y.K. "Accurate determination of transient chirp parameter in high speed digital lightwave transmitters," *Electronics Letters*, vol.33, no.7, pp.605-606, Mar. 1997.

[132] Schiess, M. and Carlden, H."Evaluation of the chirp parameter of a Mach-Zehnder intensity modulator," *Electronics Letters*, vol.30, no.18, pp.1524-1525, Sep 1994.

[133] G. P. Agrawal, "Fiber-Optic Communication Systems," 3rd ed. NJ, 2002.

[134] Nguyen, L.V.T., Hunter, D.B., "A photonic technique for microwave frequency measurement," *IEEE Photonics Technology Letters*, vol.18, no.10, pp.1188-1190, May 2006.

[135] F. Devaux, Y. Sorel, and J. F. Kerdiles, "Simple measurement of fiber dispersion and of chirp parameter of intensity modulated light emitter," *Journal of Lightwave Technology* 11, 1937-1940 (1993).

[136] Dennis, T. and Williams, P.A. "Chirp Characterization of External Modulators With Finite Extinction Ratio Using Linear Optical Sampling," *IEEE Photonics Technology Letters*, vol.22, no.9, pp.646-648, May 2010.

[137] M. Attygalle, C. Lim, G. J. Pendock, A. Nirmalathas, and G. Edvell,"Transmission improvement in fiber wireless links using fiber Bragg gratings," *IEEE Photonics Technology Letters*, vol.17, no.1, pp.190-192, 2005.

[138] J. Leibrich, A. Ali, H. Paul, W. Rosenkranz, and K. D. Kammeyer "Impact of modulator bias on the OSNR requirement of direct-detection optical OFDM," *IEEE Photonics Technology Letters*, vol.21, no.15, pp.1033-1035, 2009.

[139] Jean Armstrong "OFDM for Optical Communcations" *Journal of Ligthwave Technology*, vol.27, no.3, Feb. 2009.

[140] http://www.fsan.org/news/

[141] PT inovação white paper,"Evolution of FTTH networks for NG-PON2", July 2013.

[142] Sanjit K Mitra,"Digital Signal Processing: A Computer-Based Approach", McGraw-Hill Education, 4th edition, Sep 13, 2010.

[143] Wisair "Wisair Wireless USB products" info available at: http://www.wisair.com/products/wireless-usb-solutions/wusb-dongle-set/

[144] Iogear "Wireless USB Hub and Adapter" info available at: http://www.iogear.com/print.php?loc=product_pdf&printv=1&Item=GUWH104KIT , 19th Septembre, 2013.

[145] LTE, Evolved Universal Terrestrial Radio Access (E-UTRA),"Base Station (BS) radio transmission and reception," (3GPP TS 36.211 version 8.13.0 Release 8), ETSI, July. 2012.

[146] Jansen, S.L., Morita, I., Schenk, T. C W, Takeda, N., and Tanaka, H., "Coherent Optical 25.8 Gbps OFDM Transmission Over 4160 km SSMF," *Journal of Lightwave Technology*, vol.26, no.1, pp.6-15, Jan.1, 2008.

[147] D. Hillerkuss *et al.* “26 Tbit/s Line-rate Super-channel Transmission Utilizing All-optical Fast Fourrier Transform Processing”. *Nature Photonics* 5, pp.364–371, May 2011.

[148] S. C. J. Lee, F. Breyer, S. Randel, M. Schuster, J. Zeng, F. Huiskens, H. P. A. van den Boom, A. M. J. Koonen, and N. Hanik, “24-Gb/s transmission over 730 m of multimode fiber by direct modulation of 850-nm VCSEL using discrete multi-tone modulation,” *in optical fiber communication conference OFC2007*, 2007, PDP6.

[149] Yu-Min Lin and Po-Lung Tien, "Next-generation OFDMA-based passive optical network architecture supporting radio-over-fiber," *IEEE Journal on Selected Areas in Communications*, vol.28, no.6, pp.791-799, Aug. 2010.

[150] Laurent Schmalen, Adriaan J. de Lind van Wijngaarden, and Stephan ten Brink “Forward Error Correction in Optical Core and Optical Access Networks” *Bell Labs Technical Journal*, vol.18, no.3, pp. 39–66, Nov. 2013.

[151] Mitchell, J.E., "Performance of OFDM at 5.8 GHz using radio over fibre link," *Electronics Letters*, vol.40, no.21, pp.1353-1354, 14 Oct. 2004.

[152] Hewitt, D.F.and Skafidas, E., "Performance and applications of Gigabit OFDM over optical fibre systems in metro and access networks," *in European Conference on Optical Communications, 2006 - ECOC 2006*, vol., no., pp.1-3, 24-28, Sept. 2006.

[153] B. J. Schmidt, A. J. Lowery, and J. Armstrong, "Experimental demonstrations of 20 Gbit/s direct-detection optical OFDM and 12 Gbit/s with a colorless transmitter," *in optical fiber communication conference OFC2007*, paper PDP 18.

[154] Alves, T., and Cartaxo, A.,”Semi-analytical approach for performance evaluation of direct-detection OFDM optical communication systems”, *Optics Express*, Vol. 17, No. 21, pp. 18714-18729, 2009.

[155] Alves, T., and Cartaxo, A., “Analysis of methods of performance evaluation of direct-detection OFDM communication systems”, *Fiber and Integrated Optics*, Vol. 29, No. 3, pp. 170-186, 2010.

[156] M.D. McKinley, K.A. Remley, M. Myslinski, J.S.Kenney, D. Schreurs, and B. Nauwelaers, “EVM calculation for broadband modulated signals,” in *64th ARFTG Conf. Dig, 2004*, pp. 45–52.

[157] D. Guimarães “Passband digital transmission” *in Digital Transmission - A simulation aided introduction with VisSim/Comm. Springer*, pp.430-602, 2009.

[158] Insua, I.G., Plettemeier, D. and Schaffer, C.G. "Simple Remote Heterodyne Radio-Over-Fiber System for Gigabit Per Second Wireless Access," *Journal of Lightwave Technology*, vol.28, no.16, pp.2289-2295, Aug.15, 2010.

[159] Omomukuyo, O., Thakur, M.P. and Mitchell, J.E., "Simple 60-GHz MB-OFDM Ultrawideband RoF System Based on Remote Heterodyning," *IEEE Photonics Technology Letters*, vol.25, no.3, pp.268-271, Feb.1, 2013.